TESIS DOCTORAL

THE GREATWALL-ENDOSULFINE-PP2A/B55 PATHWAY IN *Schizosaccharomyces pombe*: REGULATORY MECHANISMS AND ROLES IN CELL DIFFERENTIATION AND AGEING

NATALIA GARCÍA BLANCO

CSIC-UNIVERSIDAD DE SALAMANCA

INSTITUTO DE BIOLOGÍA FUNCIONAL Y GENÓMICA

2021

CSIC
CONSEJO SUPERIOR DE INVESTIGACIONES CIENTÍFICAS

VNiVERSiDAD D SALAMANCA
CAMPUS DE EXCELENCIA INTERNACIONAL

INSTITUTO DE BIOLOGÍA FUNCIONAL Y GENÓMICA

ibfg

Tesis Doctoral

The Greatwall-Endosulfine-PP2A/B55 pathway in *Schizosaccharomyces pombe*: regulatory mechanisms and roles in cell differentiation and ageing

Natalia García Blanco

Universidad de Salamanca – CSIC
Instituto de Biología Funcional y Genómica

2021

CSIC
CONSEJO SUPERIOR DE INVESTIGACIONES CIENTIFICAS
VNiV ERSiDAD D SALAMANCA
CAMPUS D EXCE LENCIA INTERNACIONAL

INSTITUTO DE BIOLOGÍA FUNCIONAL Y GENÓMICA
ibfg

Universidad de Salamanca – CSIC
Instituto de Biología Funcional y Genómica

El **Dr. D. Francisco del Rey Iglesias**, Catedrático del Departamento de Microbiología y Genética de la Universidad de Salamanca,

CERTIFICA:

Que la memoria titulada "The Greatwall-Endosulfine-PP2A/B55 pathway in *Schizosaccharomyces pombe*: regulatory mechanisms and roles in cell differentiation and ageing" presentada por la graduada Dª. Natalia García Blanco para optar al grado de Doctora en Biología por la Universidad de Salamanca, ha sido realizada bajo la dirección del Dr. D. Sergio Moreno Pérez en el Centro Mixto de Biología Funcional y Genómica, CSIC-Universidad de Salamanca.

Y para que así conste, firma el siguiente certificado en Salamanca,

A 18 de marzo de 2021

Fdo. Francisco del Rey Iglesias

directoribfg@usal.es, direccion.ibfg@csic.es
http://www.ibfg.usal-csic.es

C/ Zacarías González, 2
37007 Salamanca. ESPAÑA
TEL.: 923 294900; FAX: 923 224876

CSIC
CONSEJO SUPERIOR DE INVESTIGACIONES CIENTÍFICAS
VNiVERSiDAD D SALAMANCA
CAMPUS DE EXCELENCIA INTERNACIONAL

INSTITUTO DE BIOLOGÍA FUNCIONAL Y GENÓMICA
ibfg

Universidad de Salamanca – CSIC
Instituto de Biología Funcional y Genómica

El **Dr. D. Sergio Moreno Pérez**, Profesor de Investigación del Consejo Superior de Investigaciones Científicas,

CERTIFICA:

Que la memoria titulada "The Greatwall-Endosulfine-PP2A/B55 pathway in *Schizosaccharomyces pombe*: regulatory mechanisms and roles in cell differentiation and ageing" presentada por la graduada Dª. Natalia García Blanco para optar al grado de Doctora en Biología por la Universidad de Salamanca, ha sido realizada bajo la dirección del Dr. D. Sergio Moreno Pérez en el Centro Mixto de Biología Funcional y Genómica, CSIC-Universidad de Salamanca.

Y para que así conste, firma el siguiente certificado en Salamanca,

A 18 de marzo de 2021

Fdo. Sergio Moreno Pérez

directoribfg@usal.es, direccion.ibfg@csic.es
http://www.ibfg.usal-csic.es

C/ Zacarías González, 2
37007 Salamanca. ESPAÑA
TEL.: 923 294900; FAX: 923 224876

A mi madre. Sin ti no hubiera sido posible.
A mi padre. Tu recuerdo impregna todas estas páginas.

Agradecimientos

Esta memoria simboliza el fin de una etapa. No me refiero al cierre de un capítulo laboral, sino al fin de un periodo de mi vida. Periodo fuertemente ligado a Salamanca, ciudad que no me vio nacer pero que ha sido testigo de mi crecimiento, de mis amores y mis desamores, de esas amistades que se fueron y de las que se quedaron, de mis llantos y mis risas, del nacimiento de mi hermano y, en definitiva, de mi vida hasta ahora. Llegamos aquí cuando tenía tan solo 6 años. Hoy tengo 27. 21 años llevo en esta hermosa y risueña ciudad. ¡Aún no me he ido de aquí y ya te echo de menos, Salamanca! Sentimiento que comparto con muchos otros, pues ya escribía Cervantes en su Licenciado de Vidriera allá por el siglo XVII "Salamanca, que enhechiza la voluntad de volver a ella a todos los que de la apacibilidad de su vivienda han gustado". ¡Y cómo me has hechizado! Pero no te preocupes, afortunadamente, te visitaré con frecuencia y disfrutaré de ese color dorado de tus fachadas. Gracias Salamanca, aquí he sido muy feliz.

Este fin de etapa es tan solo el comienzo de otra nueva aventura. Aventura que comenzaré con la misma ilusión con la que inicié mi camino hacia el doctorado. Por suerte, no he estado sola durante mi periplo doctoral, sino que muchas personas han compartido esta experiencia conmigo y gracias a ellas hoy me encuentro al final del trayecto.

Debo empezar mis agradecimientos por mis compañeros de laboratorio. Gracias por hacer mi día a día más ameno. En especial, a Livia. Gracias por tu tiempo, tu paciencia y tu conocimiento, sin duda eres una gran científica. También a Anaé, sin ella el laboratorio no es el mismo. Eres una gran persona, echaré de menos tu compañía. Dani (González) gracias por compartir conmigo esta última parte de mi doctorado y por alegrar mis días. Te deseo mucha suerte. Celia, a ti también te deseo mucha suerte, la burocracia de la FPU es desesperante, lo sé, pero no te desanimes por ello.

A mi director de tesis, Sergio, me gustaría darle las gracias por animarme a solicitar la FPU y por acogerme en su laboratorio como estudiante de máster. He aprendido mucho durante este tiempo, gracias por esta oportunidad.

De esta aventura no solo me llevo la experiencia y el título, sino también a personas maravillosas. A Irene y Alicia las conocí en el laboratorio. Me acuerdo de esos primeros encuentros. He de reconocer que la primera impresión no fue muy acertada. Alicia, pensé que eras demasiado seria, luego descubrí que solo al principio. Decirte que eres una persona maravillosa y que me siento tremendamente afortunada de haber realizado la tesis junto a ti. Sé que ya nada será igual, nunca tendré una compañera de trabajo como tú. Irene, en esa primera impresión recuerdo sobre todo llamar desayuno a lo que yo llamaba café. ¡Creo que todavía no estoy recuperada de aquello! Irene, eres increíble, emites tanta luz que iluminas todo lo que te rodea. Chicas, habéis marcado mi vida estos últimos años. Me llevo dos amigas, dos grandes amigas que me acompañaran durante toda mi vida. Por cierto, hay que hacer otro viaje, fue demasiado especial para hacer solo uno.

Otra persona relacionada con el laboratorio es Dani (García). Dani te echo de menos, el laboratorio no es lo mismo sin ti. Eres una gran persona, te mereces todo lo bueno que te pase. Gracias por alegrarme los días en el lab y fuera de él. Ojalá pueda ir a verte a Francia.

Me gustaría también dar las gracias a las personas que hicieron de mi estancia en Nashville una maravillosa experiencia. El problema es que estas no saben español, así que permitidme cambiar de idioma. I would like to thank Kathy for giving me the opportunity to work

in her lab. Those three months were wonderful. I will always cherish that time in Nashville. Kathy, you are an incredible mentor, a unique scientist and an inspiring role model for women in science. Thanks to everyone in Kathy's lab, especially to Alaine, Sierra, Emma, Josh, Liping and Jun-Song. Working with you was a blast.

No puedo olvidarme de todos aquellos que sin estar relacionados con el laboratorio también han ayudado a que yo llegara donde estoy hoy. Vosotros sois los que me dais fuerza para afrontar todos los baches del camino.

Empezaré por mi grupo de amigos. Gracias a todos, sobre todo por soportar mis quejas, ya sabéis que yo me quejo y me desinflo, lo llaman mecanismo de defensa. María T, mi pepito grillo, ¿qué decir que no haya dicho ya? Gracias por caminar a mi lado estos años y los anteriores, sin ti no sé si hubiera llegado al final. No he visto persona más buena que tú. Noe, lo tuyo es hacer reír a la gente. Aunque yo sea la mayor crítica de tus chistes, los echo de menos. Sigue adelante, como siempre has hecho, tú puedes. Gracias por todo. Gracias a Sira y a Óscar, pues también habéis sido indispensables estos años. A mis chicas de la Uni, Laura y Ana, gracias. ¡Cuánto os echo de menos! María F, media vida juntas (y lo que nos queda). Gracias por estar siempre ahí. ¡Qué ganas de seguir sumando momentos juntas! Eres la mejor. Al resto de chicas VIP del Pezón, gracias por todos estos años y por todas esas risas, bailes, paseos y quedadas.

A mi familia le debo agradecer muchas cosas, si soy la que soy y estoy donde estoy es por vosotros. La convivencia suele sacar el lado más feo de cada uno, y vosotros habéis visto el mío varias veces. Gracias por todo lo que me habéis dado. Gracias por creer siempre en mí y animarme a cumplir mis sueños. A mi hermana Lore, que está un poco loca, gracias por toda mi infancia. Eres la pequeña, pero siempre me has defendido y apoyado. Desde que te fuiste, nuestra habitación está demasiado silenciosa. También más recogida. Gracias por pensar que soy la mejor en lo que hago. No puedo esperar a ver la gran mujer en la que te convertirás. A mi hermano Hugo, Huguito para mí, gracias por llenar la casa de vida. Te echaré mucho de menos, ya sabes que eres mi punto débil. Mamá, no tendría palabras suficientes para agradecerte todo lo que has hecho por mí. No hay madre mejor que tú. Toda la vida has luchado por sacarnos adelante. Madre y padre a la vez, no debe ser fácil, pero puedes estar tranquila, gracias a ti somos buena gente. ¡Ay, mamá, cuántas veces he llegado llorando a casa! Y tú siempre me has animado a seguir y a no rendirme. El mérito de estar donde estoy hoy, al final del doctorado, es tuyo. Y el resto de los que vengan también. Te echaré mucho de menos ahora que emprendo camino a Madrid. A mis abuelos maternos, les debo mucho. El amor por la naturaleza, la vida sencilla, el amor incondicional... son algunas de las cosas que me habéis enseñado. Gracias por todo. Y por último, gracias también a mi familia de Vigo.

Si has llegado hasta el final de esta larga parrafada de gracias, puede que te estés preguntando sobre cierta personita importante para mí. La he reservada para la parte final, pues ocupa un lugar muy especial en mi corazón. Para ti, amor, las gracias las elevo al cuadrado. Guille, mi compañero de vida, hoy no estaría aquí sin tu ayuda. Si hay alguien a quien le he dado la tabarra con la tesis, la ciencia y el laboratorio, ese eres tú. Gracias por tu paciencia y tu comprensión. Gracias por creer en mí. Pero, sobre todo, gracias por haber estado y estar siempre a mi lado. Cariño, tu amor me hace crecer. Contigo soy mejor persona y contigo voy al infinito.

A todos, muchas gracias, porque este trabajo no hubiera sido posible sin vosotros.

Index

List of figures and tables

Abbreviations

2D LC-MS/MS	Two-dimensional liquid chromatography tandem mass spectrometry
4EBP	eIF4E binding protein
AMPK	AMP-activated protein kinase
ATF4	Activating transcription factor 4
ATP	*Adenosine triphosphate*
BSA	Bovine serum albumin
BME	2-ß-Mercaptoethanol
CAPS	N-cyclohexyl-3-aminopropanesulfonic acid
CKI	Casein protein I
CKII	Casein protein II
CLS	Chronological lifespan
ClonNAT	Nourseothricin
CDK	Cyclin-dependent kinase
DAPI	4,6-diamidino-2-fenilindol
DMSO	Dimethyl sulfoxide
DNA	Deoxyribonucleic acid
DTT	Dithiothreitol
EDTA	Ethylenediaminetetraacetic acid
FACS	Fluorescence-activated cell sorting
FOA	5-Fluoroorotic acid
G-418	Geneticin
GAP	GTPase-activating protein
GEF	Guanine nucleotide exchange factor
GSK3	*Glycogen synthase kinase 3*
GTP	Guanosine triphosphate
GZE	G-zero essential
HAT	Histone acetyltransferase
HDAC	Histone deacetylase
HULC	Histone H2B ubiquitin ligase complex
HIF1α	Hypoxia-inducible factor 1-α
Igf	Insulin-like growth factor
Ino80 complex	Inositol-requiring mutant 80 ATP-dependent chromatin-remodelling complex
IPTG	Isopropyl ß-D-1-thiogalactopyranoside
KAT	Lysine acetyltransferase
kb	Kilobase
LB	Luria-Bertani medium

LiAc	Lithium acetate
MBF	MluI cell Cycle Box (MCB) Binding Factor
mLst8	Mammalian lethal with Sec13 protein 8
MEA	Malt extract agar
MM	Minimal medium
MM-FOA	Minimal medium with FOA
MM-N	Minimal medium without nitrogen
MMF	Minimal medium with phenylalanine
NHEJ	Non-homologous end joining
NP-40	Nonyl phenoxypolyethoxylethanol
OD	Optical density
ORF	Open reading frame
pb	Base pairs
PBS	Phosphate-buffered saline
PCR	Polymerase chain reaction
PEG	Polyethylene glycol
PHLPP	PH domain leucine-rich repeat protein phosphatase
PI3K	Phosphoinositide 3-kinase
PIKK	Phosphatidylinositol kinase-related protein kinase
PKA	Protein kinase A
PKC	Protein kinase C
PMSF	Phenylmethylsulfonyl fluoride
PP2A	Protein phosphatase type 2A
Rag	Ras-related GTPases
Raptor	Regulatory protein associated with mTOR
Rheb	Ras-homolog enriched in brain
Rictor	Rapamycin insensitive companion of mTOR
RLS	Replicative lifespan
RNA	Ribonucleic acid
RNAi	RNA interference
RSC complex	Remodelling the Structure of Chromatin complex
S6K1	p70S6 kinase
SAGA complex	Spt-Ada-Gcn5 acetytransferase complex
SEA complex	Seh1-associated complex
SDS	Sodium dodecyl sulfate
SGK1	Serum/Glucocorticoid regulated kinase 1
SIR2	Silent Information Regulator 2
SWI/SNF complex	SWItch/Sucrose Non-Fermentable complex

TAE	Tris-acetate EDTA buffer
TB	Terrific Broth medium
TBS	Tris-buffered saline
TCA	Trichloroacetic acid
TE	Tris-EDTA buffer
TFEB	Transcription factor EB
TFIID	Transcription factor IID
TFIIF	Transcription factor IIF
TOR	Target of rapamycin
TORC1	Target of Rapamycin complex 1
TORC2	Target of Rapamycin complex 2
TSC	Tuberous Sclerosis Complex
ULK1	Unc-51 like autophagy activating kinase 1
UV	Ultraviolet
YES	Yeast extract with supplements

Resumen

El crecimiento celular está normalmente acoplado a la división celular para dar lugar a un órgano u organismo de un tamaño determinado. Cuando las células proliferan, mantienen un tamaño constante y la división celular se produce cuando la masa celular se duplica. No obstante, el tamaño celular está modulado por las condiciones nutricionales (Fantes and Nurse, 1977). En medios ricos en nutrientes, la tasa de crecimiento es elevada y el tamaño celular aumenta. Por el contrario, en ambientes nutricionales pobres, las células reducen la síntesis de macromoléculas y disminuyen de tamaño.

La progresión por el ciclo celular está controlada por los complejos CDK/Ciclina. Las oscilaciones en su actividad dependen de los niveles y de la especificidad de la Ciclina (Bloom and Cross, 2007; Loog and Morgan, 2005), y activan la transición por las distintas fases del ciclo celular (Nurse, 1990). Sin embargo, múltiples estudios recientes han puesto de manifiesto la importancia de las proteínas fosfatasas en el control del ciclo celular (Cundell et al., 2013, 2016; Domingo-Sananes et al., 2011; Grallert et al., 2015; Mochida and Hunt, 2012). De hecho, el equilibrio entre la actividad CDK/Ciclina y las fosfatasas que la contrarrestan determina el estado de fosforilación de los sustratos de los complejos CDK/Ciclina (Cundell et al., 2016). En metazoos, la proteína fosfatasa PP2A/B55 juega un papel esencial en la progresión del ciclo celular, ya que antagoniza la fosforilación de las dianas de CDK/Ciclina (Mochida et al., 2009). En concreto, la entrada en mitosis es el resultado del balance entre la actividad quinasa del complejo Cdk1/CiclinaB y la actividad fosfatasa de PP2A/B55 (Glover, 2012; Lorca and Castro, 2013). Durante la interfase, PP2A/B55 promueve la activación de Wee1 (Mueller et al., 1995) y la inhibición de Cdc25 (Pal et al., 2008), asegurando que los niveles de Cdk1/CiclinaB se mantienen bajos en G2, y, por tanto, evitando que las células entren en mitosis (Mochida et al., 2009). En la transición G2/M, la inhibición de PP2A/B55 permite que los niveles de actividad Cdk1/CiclinaB aumenten y se desencadene, así, el inicio de la mitosis. El módulo Greatwall-Endosulfina es el responsable de inactivar PP2A/B55 al final de la fase G2 (Glover, 2012; Lorca and Castro, 2013). Greatwall es una serina/treonina quinasa que fosforila a Endosulfina, promoviendo su interacción con PP2A/B55 y la inactivación de esta fosfatasa (Gharbi-Ayachi et al., 2010; Mochida et al., 2010). Curiosamente, el complejo Cdk1/CiclinaB regula la actividad del módulo Greatwall-Endosulfina en animales. En la fase G2 tardía, Greatwall es fosforilado por Cdk1/CiclinaB, lo que promueve su autofosforilación y activación completa (Blake-Hodek et al., 2012; Vigneron et al., 2011). Una vez activo, Greatwall fosforila a Endosulfina, lo cual favorece que Endosulfina interaccione e inhiba al complejo fosfatasa PP2A/B55. Como consecuencia, la actividad Cdk1/CiclinaB se dispara, los sustratos mitóticos se fosforilan y comienza la mitosis.

La quinasa TOR posee una función central en la regulación del crecimiento celular y la proliferación en los organismos eucariotas. Esta serina/treonina proteína quinasa se ensambla en dos complejos proteicos, el Complejo TOR 1 (TORC1) y el complejo TOR 2 (TORC2), cuyas funciones están conservadas a lo largo de la evolución. TORC1 controla el crecimiento y es activado por nutrientes, factores de crecimiento y hormonas. Para estimular el crecimiento celular, TORC1 promueve procesos anabólicos, como la biosíntesis de proteínas, la biogénesis de ribosomas o la transcripción; e inhibe procesos catabólicos, como la autofagia y la diferenciación celular (Alvarez and Moreno, 2006; Matsuo et al., 2007; Saxton and Sabatini, 2017; Uritani et al., 2006). Por su parte, TORC2 desempeña una gran variedad de funciones celulares, desde la regulación del citoesqueleto de actina, la endocitosis, la biosíntesis de lípidos, la respuesta a daño en el ADN y a distintos tipos de estrés, la citoquinesis, el silenciamiento génico, el mantenimiento de los telómeros y la diferenciación celular (revisado en Eltschinger and Loewith, 2016; Gaubitz et al., 2015; Weisman, 2016).

En levaduras, el módulo Greatwall-Endosulfina conecta el crecimiento celular con el ciclo celular al modular la actividad de la fosfatasa PP2A/B55. En *S. cerevisiae*, Greatwall y Endosulfina son reguladas negativamente por PKA y TORC1 (Pedruzzi et al., 2003). La actividad

de este módulo es necesaria para la expresión de genes meióticos y para la supervivencia en la fase G_0 (Pedruzzi et al., 2003; Reinders et al., 1998; Talarek et al., 2010; Vidan and Mitchell, 1997). Por el contrario, en *S. pombe*, solo TORC1 regula negativamente el módulo Greatwall-Endosulfina (Chica et al., 2016). En medios ricos en nutrientes, la actividad de TORC1 es elevada, potenciando la inhibición de Greatwall y con ello la activación de PP2A/B55. Niveles altos de PP2A/B55 contrarrestan la activación de Cdk1/CiclinaB y las células entran en mitosis con un tamaño grande. Sin embargo, en medios pobres, la actividad de TORC1 cae, Greatwall se activa y fosforila a Endosulfina, que a su vez inhibe a PP2A/B55, permitiendo la activación prematura de Cdk1/CiclinaB y la entrada en mitosis con menor tamaño. En la levadura de fisión, el módulo Greatwall-Endosulfina controlan el tamaño de división celular (Chica et al., 2016), la entrada en quiescencia (Aono et al., 2019) y la respuesta transcripcional necesaria para la diferenciación sexual (Laboucarié et al., 2017; Martín et al., 2017).

En esta Tesis Doctoral, se han estudiado los mecanismos moleculares implicados en la regulación de la ruta de Greatwall-Endosulfina-PP2A/B55 y su función en *Schizosaccharomyces pombe*. En particular, la Tesis se centra en: (1) examinar la implicación de la ruta en la regulación del bloqueo en la fase G1 en ausencia de nitrógeno, (2) diseccionar su papel en la respuesta de diferenciación sexual, (3) analizar su función en la regulación del envejecimiento celular, (4) caracterizar los cambios de fosforilación que regulan la actividad de Endosulfina, (5) e identificar posibles nuevas dianas de las proteínas Endosulfina y B55.

Los resultados obtenidos en este proyecto se engloban en cuatro grandes apartados. En primer lugar, la ruta de Greatwall-Endosulfina-PP2A/B55 juega un papel crucial en la regulación de la respuesta celular de la levadura de fisión a la falta de nitrógeno. Greatwall y Endosulfina regulan negativamente la actividad de PP2A/B55, permitiendo la reducción del tamaño celular, el bloqueo en G1 y diferenciación sexual en ausencia de nitrógeno. En segundo lugar, el módulo Greatwall-Endosulfina promueve la entrada en la fase G_0, la supervivencia celular y la correcta dinámica de la cromatina durante la quiescencia. La inactivación de PP2A/B55 mediada por Greatwall y Endosulfina es necesaria para la supervivencia celular en la fase G_0 inducida por la falta de nitrógeno. En tercer lugar, varias quinasas fosforilan a Endosulfina *in vivo*, incluidas Cdk1 y PKA. La fosforilación de las serinas 31, 89, 102 y 118 de Endosulfina llevada a cabo por Cdk1/CiclinaB promueve la actividad de Endosulfina en medio rico en nitrógeno. Por último, los interactomas de Endosulfina y B55 muestran múltiples interacciones con otras proteínas. En concreto, B55 interacciona con varios complejos de proteínas involucrados tanto en la condensación y remodelación de la cromatina, como en la modificación de histonas, lo que apoya la hipótesis de que PP2A/B55 participa en la regulación del silenciamiento de la cromatina durante la entrada en quiescencia.

Introduction

1. *Schizosaccharomyces pombe* as a model organism

Saccharomyces cerevisiae and *Shizosaccharomyces pombe* diverged approximately 350 million years ago (Hoffman et al., 2015; Sipiczki, 2000). Both yeasts have long been used as model organisms in molecular and cell biology since most cellular processes are also conserved in higher eukaryotes.

Although 75% of their genes are functional orthologues (Dixon et al., 2008), some features of budding and fission yeast biology differ. *Saccharomyces cerevisiae* cells are round, normally diploid and divide by budding. Moreover, since budding yeast has a long G1 cell-cycle phase, cell growth and cell cycle are regulated mainly in this phase. By contrast, *S. pombe* cells are rod-shaped, grow by cell elongation and divide by medial fission. In addition, only zygotes are diploids as conjugation and meiosis are coupled. Interestingly, *S. pombe* and metazoans share some molecular characteristics (Wood et al., 2002). Regulation of the G2/M transition, the structure of centromeres and DNA replication origins are similar to those of higher eukaryotes (Wood et al., 2002; reviewed in Sunnerhagen, 2002). Like in animal cells, the RNA interference (RNAi) pathway also controls gene expression in *S. pombe*. Additionally, 43% of the fission yeast genes have introns.

In the last decades, *S. pombe* has become a highly popular organism to investigate a myriad of biological processes. Specifically, fission yeast has been key in the studies of morphogenesis and cell polarity (Brunner and Nurse, 2000), cell-cycle regulation (Moser and Russell, 2000) and chromatin dynamics (Allshire and Ekwall, 2015).

2. Cell cycle

The cell cycle, or cell-division cycle, is the orderly sequence of events that drive cell growth and cell division to give rise two daughter cells from a mother cell. Hence, it is the mechanism by which organisms spread. In unicellular organisms, each cell cycle produces a new individual, whereas, in multicellular species, each new organism requires a complex set of cell-division cycles.

In eukaryotic cells, the cell cycle consists of four phases: two gap phases (G1 and G2), an S phase, where DNA replication occurs, and the M phase or mitosis. G1 is located between the end of mitosis and the beginning of DNA synthesis, whereas G2 is placed between DNA replication and mitosis. In G1, the cell resumes its biosynthetic activities and prepares for DNA duplication. By contrast, during G2, the cell grows and prepares for cell division. G1, G2 and S phases are collectively known as interphase.

Mitosis constitutes the last event of the cell cycle and is divided into four stages: prophase, metaphase, anaphase and telophase. During prophase, which takes places after G2, chromosome condensation occurs. Animals cells undergo an open mitosis, and therefore, the nuclear envelope also breaks down during prophase. Conversely, in fungi, the nuclear envelope remains intact, and chromosome division occurs within the nucleus (De Souza and Osmani, 2007). Although, recent data in fission yeast shows that mitosis requires local disassembly of the nuclear envelope (Dey et al., 2020). In metaphase, chromosomes align along the equatorial plane or metaphase plate due to the attachment of the mitotic spindle to kinetochores. The mitotic spindle consists of microtubules nucleated from the centrosome in metazoan, or the spindle pole body (SPB) in fungi. During anaphase, sister chromatids are separated and pulled to opposites poles of the cell owing to cohesin cleavage and shortening of the mitotic spindle. Finally, in telophase, the nuclear envelope is reformed, and the cytoplasm is divided between the two daughter cells in a process called cytokinesis.

Meiosis is a complex variation on the mitotic cell cycle. This non-canonical cycle produces cells with half the number of chromosomes of the mother cell. In the meiotic cell cycle, the mother cell undergoes one cycle of DNA replication, also known as pre-meiotic S phase, followed by two rounds of nuclear division called Meiosis I and Meiosis II. During the first meiotic division, homologous chromosomes pair and exchange genetic material in a process known as homologous recombination, increasing genetic diversity. In Meiosis I, homologous chromosomes are separated, whereas in Meiosis II sister chromatids segregate generating four haploid cells (reviewed in Watson et al., 2015).

2.1. *Schizosaccharomyces pombe* life cycle

Schizosaccharomyces pombe, commonly known as fission yeast, is a unicellular eukaryotic organism that divides by binary fission. During cytokinesis, a cell septum is laid down across the middle of the cell (Fantes, 1977), that is then cleaved, separating the two daughter cells. *S. pombe* genome is 13.8 Mb and contains three chromosomes (Wood et al., 2002). Like in other eukaryotes, cell growth and cell division are coupled. During growth, fission yeast cells increase in cell length until they reach the necessary size to divide. Moreover, cell size depends on the nutritional environment. In rich media, which is the standard laboratory condition, *S. pombe* cells are 3 to 4 µm wide and initiate mitosis when they are 14 µm long (Fantes and Nurse, 1977).

Most laboratories grow *S. pombe* in nutrient-rich media, where cells divide with a large size after a long G2 (Nurse, 1975). In these media, G1 is short, and DNA replication begins before cytokinesis ends (Figure 1) since cell size exceeds the threshold required to enter S phase (Nasmyth et al., 1979). Consequently, fission yeast cells remain most of their cell cycle with two copies of the genetic material despite being haploids. However, *S. pombe* can also proliferate in poor nutritional environments. In nitrogen-poor media, fission yeast cells shorten G2 and enter mitosis with a reduced cell size (approximately 10 µm) (Figure 1). In these conditions, G1 is extended in order to maintain cell size homeostasis, and cells proliferate with slower cell cycles (Chica et al., 2016; Fantes, 1977; Nurse and Thuriaux, 1977; Pérez-Hidalgo and Moreno, 2016; Sveiczer and Horváth, 2017). Furthermore, as S phase occurs after the completion of cytokinesis, cells with one copy (1C) or two copies (2C) of DNA can be observed (Figure 1).

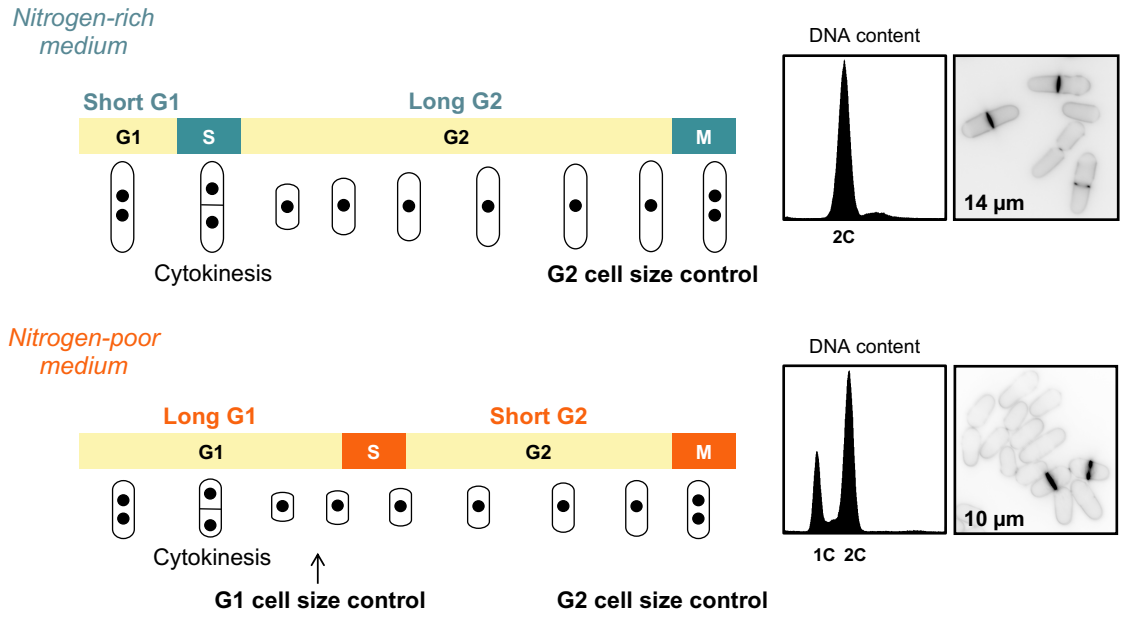

Figure 1. Nitrogen regulates the *S. pombe* cell cycle. In nitrogen-rich media, fission yeast cells are large. Fluorescence-activated cell sorting (FACS; DNA content) profile of ethanol-fixed cells stained with propidium iodide shows a single 2C cell population since septation occurs during DNA replication (**Top**). In

nitrogen-poor media, cells are small and extend G1 before undergoing DNA replication. As cytokinesis occurs before S phase, the FACS profile shows 1C and 2C cell populations (**Bottom**).

Under glucose starvation, *S. pombe* cells stop cell growth and arrest in G2 (Costello et al., 1986). By contrast, in the absence of nitrogen, they undergo two rounds of cell division, which results in a reduction in cell size and G1 arrest (Figure 2). If these G1 arrested cells meet a partner of the opposite mating type or can switch mating type (homothallic h^{90}), they initiate the sexual differentiation response (Nurse and Bissett, 1981). During this process, cells conjugate to give rise to a zygote that, after meiosis, will form an ascus with four haploid spores. These spores will remain in a dormant state until the nutritional environment is favourable to enter the vegetative cycle (Petersen et al., 1995). Otherwise, if cells are heterothallic, they enter a differentiated G_0-like state, called quiescence (Su et al., 1996). Quiescent cells will resume proliferation when nitrogen is added to the medium (Mochida and Yanagida, 2006; Su et al., 1996).

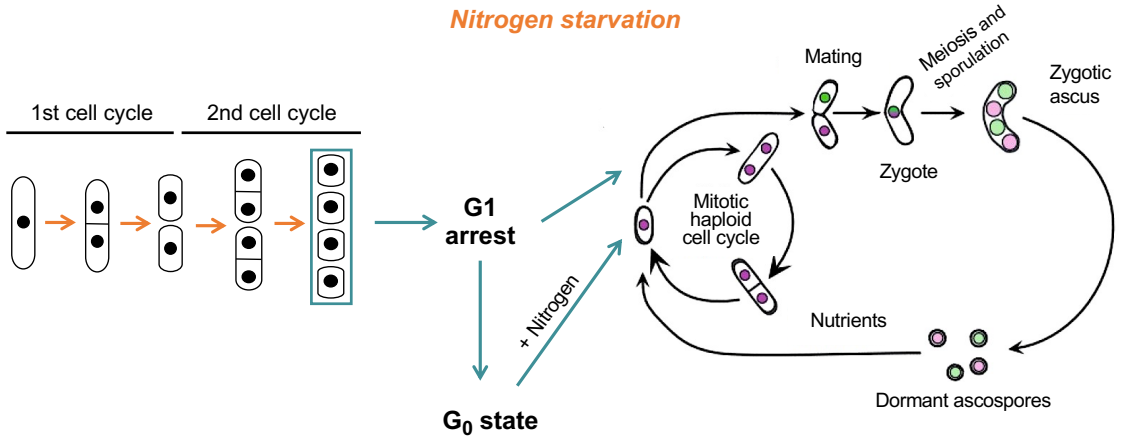

Figure 2. *S. pombe* cell cycle under nitrogen starvation. When nitrogen is removed from the medium, fission yeast cells divide twice and arrest in G1. In the presence of cells of the opposite mating type, cells conjugate, undergo karyogamy, meiosis and sporulation to produce four haploid spores. However, if cells are heterothallic, they enter quiescence, also called G_0.

2.2. Regulation of the cell cycle

2.2.1. Checkpoints

To ensure that cell-cycle events occur in an orderly and accurate manner, cells possess control mechanisms that promote or halt or delay cell-cycle progression depending on internal and external cues. These monitoring systems are called checkpoints and operate at the end of G1, during G2 or at the metaphase/anaphase transition (Hartwell and Weinert, 1989).

The G1 checkpoint, also known as Start in yeast and the Restriction point in animal cells, operates before S phase entry. Cells become committed to cell division and monitor external and internal parameters, such as nutritional conditions, DNA damage, cell size or energy levels. If these requirements are met, CDK activity increases, promoting entry into S phase. Conversely, if the environment is not favourable, cells either delay G1 progression or enter G_0 until conditions improve.

At the G2/M transition, cells assess cell size, monitor energy levels and check that chromosomes have been completely replicated and that there is no DNA damage. If the checkpoint detects errors in DNA, mitotic entry is delayed, and cells activate DNA repair mechanisms.

The M-phase checkpoint occurs at the metaphase to anaphase transition. This checkpoint is also known as the spindle assembly checkpoint (**SAC**) since it checks whether all

the sister chromatids are properly attached to the mitotic spindle. This is a crucial step to ensure an accurate chromosome segregation.

2.2.2. CDK/cyclin complexes

Cell-cycle progression is driven by the periodic activation and inactivation of Cyclin-dependent kinase (**CDK**)/Cyclin complexes (Nurse, 1990). CDKs are serine/threonine protein kinases and constitute the catalytic subunit of the complex, whereas cyclins are the regulatory subunit. Cyclins bind to CDKs, inducing a large conformational change that activates the kinase activity of the CDK (Jeffrey et al., 1995).

Oscillations in the activity of CDK/Cyclin complexes depend on cyclin specificity and cyclin levels (Bloom and Cross, 2007; Loog and Morgan, 2005), and define the transition between cell-cycle phases (Nurse, 1990). CDK/Cyclin activity peaks at mitosis, decreases during anaphase, is low in G1, rises in late G1 to trigger S phase entry, and continues to increase during G2 to induce entry into mitosis (Coudreuse and Nurse, 2010; Moreno et al., 1989) (Figure 3). The phosphorylation status of the CDK, which is regulated in response to the nutritional environment, cell size and checkpoint activation, also influences the activity of CDK/Cyclin complexes (Morgan, 1997). Moreover, there are specific regulators of these complexes that activate or repress CDK activity (Figure 3).

In metazoans, cell cycle is regulated by several CDKs, whereas yeast cell-cycle is only driven by one CDK, Cdc2 in *S. pombe* and Cdc28 in *S. cerevisiae* (Malumbres, 2014; Uhlmann et al., 2011) (Table 1). In fission yeast, Cdc2 interacts with four cyclins, Cig1, Cig2, Puc1 and Cdc13 (Table 1). Cig1 and Puc1 regulate G1 progression (Bueno et al., 1991; Martín-Castellanos et al., 1996, 2000), Cig2 controls primarily G1/S transition and S phase (Mondesert et al., 1996), and Cdc13 is important mainly for mitosis (Hagan et al., 1988). Moreover, it has been shown that the Cdc2-Cdc13 complex can be the primary regulator of the fission yeast cell cycle by promoting both S phase and mitosis (Coudreuse and Nurse, 2010; Martín-Castellanos et al., 2000).

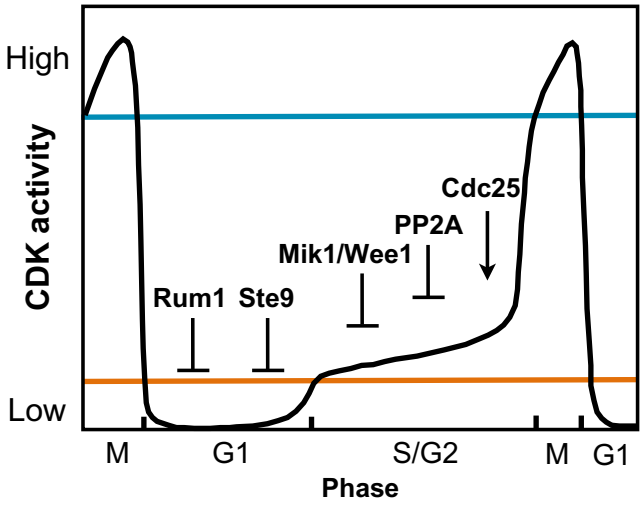

Figure 3. Quantitative model of the CDK activity and some CDK positive and negative regulators in *S. pombe*. Rum1 and Ste9 maintain low levels of CDK activity during G1 (orange line). At the G1/S transition, the formation of the Cdk1/ClyclinB complex slightly increases CDK activity. However, Mik1, Wee1 and PP2A ensure that Cdk1/ClyclinB activity remains repressed. As G2 progresses, Mik1, Wee1 and PP2A are inhibited, and Cdc25 promotes CDK activity until it reaches maximum levels at mitosis (blue line). Modified from Coudreuse and Nurse, 2010.

Table 1. CDK/Cyclin complexes in yeast and mammals. Adapted from Malumbres, 2014; Uhlmann et al., 2011.

Phase	*S. cerevisiae*		*S. pombe*		Mammals	
	Cyclin	**CDK**	**Cyclin**	**CDK**	**Cyclin**	**CDK**
G1	Cln3	Cdc28	Puc1, Cig1	Cdc2	Cyclin D	Cdk4,6
G1/S	Cln1,2	Cdc28	Cig2, Cdc13	Cdc2	Cyclin E	Cdk2
S	Clb5,6	Cdc28	Cig2, Cdc13	Cdc2	Cyclin A	Cdk2
M	Clb1,2,3,4	Cdc28	Cdc13	Cdc2	Cyclin B	Cdk1

2.2.3. PP2A: a protein phosphatase that counteracts CDK/cyclin activity

Reversible protein phosphorylation constitutes a key regulatory mechanism in cell biology (Hunter, 1995). Protein phosphatase type 2A (**PP2A**) is a serine/threonine phosphatase that dephosphorylates their substrates in a single step using a metal-activated water molecule or hydroxide ion (Barford et al., 1998). PP2A plays an essential role in the control of multiple cellular processes including cell growth, cell differentiation, DNA damage response and mitotic progression (reviewed in Wurzenberger and Gerlich, 2011). In fission yeast, PP2A regulates cytokinesis (Goyal and Simanis, 2012; Jiang and Hallberg, 2001; Lahoz et al., 2010), morphogenesis (Kinoshita et al., 1996), chromosome segregation (Kitajima et al., 2006) and mitotic progression (Chica et al., 2016; Grallert et al., 2015; Kinoshita et al., 1990).

The PP2A protein phosphatase is a heterotrimer that consists of a catalytic (C) and a scaffold (A) subunits that interact with different regulatory subunits (B) (Xing et al., 2006; Xu et al., 2006). Two C subunits, α and β, two A subunits, α and β, and four families of B subunits, B55/B, B56/B, B" (PR72) and B"' (PR93), have been identified in human cells (Eichhorn et al., 2009). In *S. pombe*, *ppa1+* and *ppa2+* genes encode the catalytic subunits of the PP2A protein phosphatase (Kinoshita et al., 1990), *paa1+* gene encode the scaffold subunit, and *pab1+*, *par1+* and *par2+* the regulatory subunits (Jiang and Hallberg, 2000; Kinoshita et al., 1996). PP2A activity depends on the associated regulatory subunit and on the phosphorylation and methylation status of the catalytic subunit (Janssens and Goris, 2001).

Recently, multiple studies have highlighted the function of protein phosphatases in cell-cycle control (Cundell et al., 2013, 2016; Domingo-Sananes et al., 2011; Grallert et al., 2015; Mochida and Hunt, 2012). The balance between CDK/Cyclin kinase activity and its counteracting phosphatases determines the phosphorylation status of CDK/Cyclin substrates (Cundell et al., 2016). In metazoans and fission yeast, PP2A/B55 phosphatase complex plays a vital role in cell-cycle progression as it is the main antagonist of CDK/Cyclin phosphorylation (Mochida et al., 2009). CDK/Cyclin and PP2A/B55 activities oscillates during the cell cycle with opposite phases (Mochida and Hunt, 2012; Mochida et al., 2009, 2010). CDK/Cyclin activity is low in G1 and high from late G2 to metaphase (Figure 4). By contrast, PP2A/B55 activity remains high during interphase and decreases in metaphase (Figure 4). Furthermore, substrate-specific CDK/cyclin activity also drives the temporal order of the cell cycle (Swaffer et al., 2016). Remarkably, the properties of CDK/Cyclin substrates contribute to define the phosphorylation timing. Consequently, good substrates are more sensitive to CDK activity, becoming phosphorylated early in the cell cycle, while poor substrates tend to be phosphorylated later, with higher CDK/Cyclin activity (Swaffer et al., 2016). Specifically, the identity of the phosphorylated residue and its surrounding amino acid sequence influence the phosphorylation order of the CDK/Cyclin substrates. Hence, CDKs prefer serine residues, whereas PP2A/B55 phosphatase prefers threonines. As a consequence, serines tend to be phosphorylated early in the cell cycle compared to threonine residues (Godfrey et al., 2017; Kamenz and Ferrell, 2017).

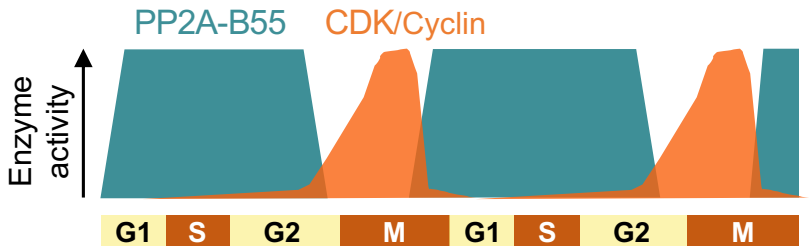

Figure 4. CDK/Cyclin and PP2A/B55 activities oscillate throughout the cell cycle with opposite phases. CDK/Cyclin activity (orange) is low in G1, rises during DNA replication, and peaks in metaphase. Conversely, PP2A/B55 activity (blue) is high during interphase and drops in mitosis. Adapted from Mochida and Hunt, 2012.

2.2.4. Regulation of the G2/M transition

The phosphorylation of multiple CDK/Cyclin substrates brings about entry into M phase (Moreno et al., 1989). In early G2, Wee1 kinase phosphorylates Cdk1 on the tyrosine 15 (Cdk1-Y15) residue, inactivating the Cdk1/CyclinB complex (Gould and Nurse, 1989). However, Wee1 activity is opposed by Cdc25 phosphatase that dephosphorylates Cdk1-Y15, and whose levels increase throughout G2 (Coleman and Dunphy, 1994; Moreno et al., 1990). At the G2/M transition, Cdk1/CyclinB phosphorylates Wee1 and Cdc25, triggering Wee1 inhibition and Cdc25 activation, shifting the Wee1-Cdc25 balance towards Cdc25 dephosphorylation of Cdk1-Y15. This results in full activation of the Cdk1/CyclinB complex and entry into mitosis.

Entry into mitosis is also regulated by the PP2A/B55 phosphatase complex (Mochida et al., 2009). During interphase, PP2A/B55 controls Cdk1-Y15 phosphorylation since it promotes the dephosphorylation of Wee1, and its consequent activation (Mueller et al., 1995), and of Cdc25, and its inhibition (Pal et al., 2008) (Figure 5). By regulating Cdk1-Y15 phosphorylation, PP2A/B55 ensures that Cdk1/CyclinB activity levels are low in G2, preventing cells from entering mitosis (Mochida et al., 2009). Importantly, PP2A/B55 is inhibited at the G2/M transition, allowing full activation of Cdk1/CyclinB and therefore, mitotic entry. PP2A/B55 inhibition is carried out by the Greatwall-Endosulfine module (Glover, 2012; Lorca and Castro, 2013). Greatwall, also known as Mastl in mammals, Rim15 in *S. cerevisiae* and Ppk18 and Cek1 in fission yeast, is a serine/threonine kinase of the AGC family of protein kinases (Blake-Hodek et al., 2012; Vigneron et al., 2011). Greatwall phosphorylates Endosulfine, two proteins in metazoans, (ENSA and ARPP-19) and in *S. cereivisiae* (Igo1 and Igo2), and a single protein in *S. pombe* (Igo1), promoting its interaction with PP2A/B55 and the inactivation of the phosphatase complex (Gharbi-Ayachi et al., 2010; Mochida et al., 2010). Interestingly, the Greatwall-Endosulfine pathway is subjected to Cdk1/CyclinB regulation (Figure 5). In the metazoan late G2, Cdk1/CyclinB phosphorylates Greatwall, promoting Greatwall autophosphorylation and full activation (Blake-Hodek et al., 2012; Vigneron et al., 2011). Active Greatwall triggers phosphorylation of Endosulfine that binds to and inhibits the PP2A/B55 phosphatase complex. Hence, Cdk1/Cyclin B inhibition by Wee1 is relieved, mitotic substrates are phosphorylated and mitosis begins.

3. Cell growth

3.1. TOR

Cell growth (mass accumulation) is normally coupled to cell cycle. Proliferating cells normally maintain a constant size, and cell division occurs when cell mass doubles. Nevertheless, cell size is modulated by nutrients (Fantes and Nurse, 1977). In nutrient-rich media, cells sustain a high rate of macromolecular synthesis, which promotes growth and increases cell size. By contrast, when nutrients are scarce, cells decrease macromolecular synthesis and reduce cell size.

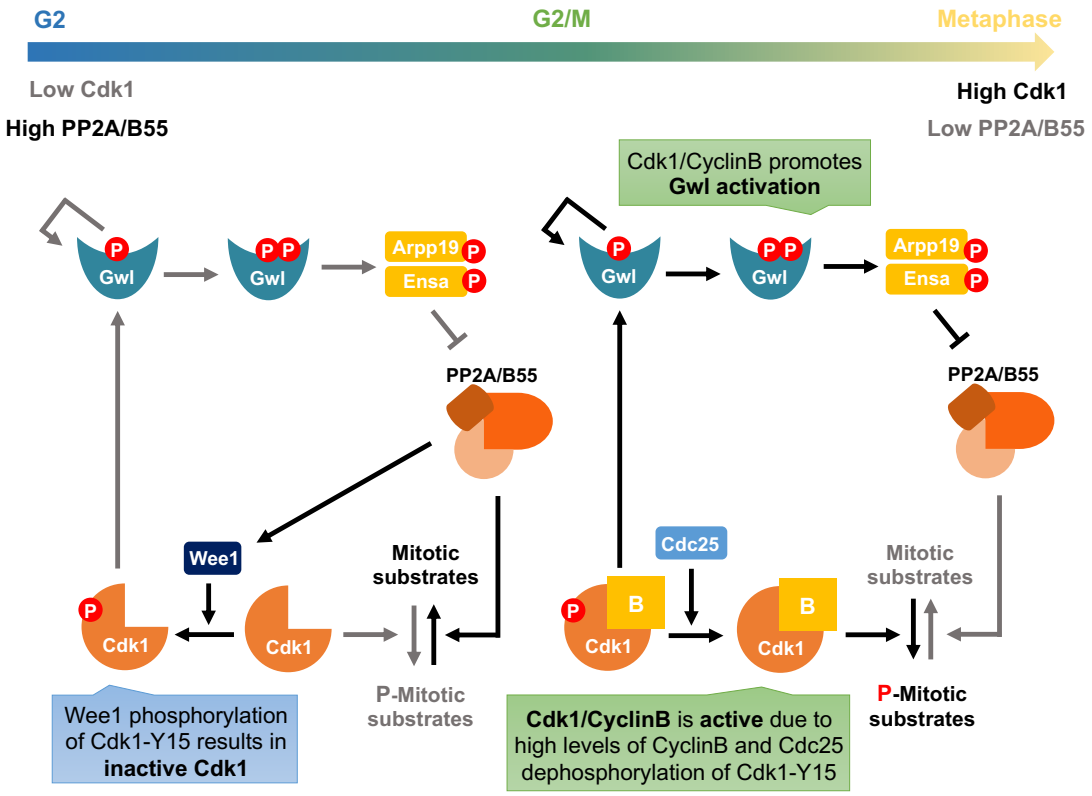

Figure 5. Regulation of the mitotic entry. In early G2, PP2A/B55 phosphatase promotes Wee1 inhibitory phosphorylation of Cdk1 on Y15 residue. This together with low levels of CyclinB keeps Cdk1 inactive. PP2A/B55 also dephosphorylates mitotic substrates, antagonising Cdk1/CyclinB activity and preventing entry into mitosis. As G2 progresses, Cdk1/CyclinB activity rises due to increased levels of CyclinB and Cdc25 phosphatase, and triggers PP2A/B55 inhibition by the Greatwall-Endosulfine module. Low PP2A/B55 levels lead to full activation of Cdk1/CyclinB, and cells enter mitosis. Modified from García-Blanco et al., 2019.

The highly conserved Target of Rapamycin (TOR) kinase plays a key role in controlling cell growth and proliferation in eukaryotes. TOR was first identified in yeast by isolating rapamycin-resistant mutants (Heitman et al., 1991; Cafferkey et al., 1993; Kunz et al., 1993). Shortly afterwards, biochemical studies identified the mammalian TOR (mTOR) and revealed that rapamycin forms a complex with the peptidyl-prolylisomerase FKBP12 that binds to and inhibits TOR (Brown et al., 1994; Sabatini et al., 1994; Sabers et al., 1995). Rapamycin is a lipophilic macrolide produced by *Streptomyces hygroscopicus* with remarkable antifungal, immunosuppressive, and antitumor properties (Eng et al., 1984; Martel et al., 1977; Vézina and Kudelski, 1975).

TOR is a member of the phosphatidylinositol kinase-related protein kinase (PIKK) family. This serine/threonine kinase assembles into two multiprotein complexes, TOR Complex 1 (TORC1) (Table 2) and TOR complex 2 (TORC2) (Table 3), whose functions are conserved throughout evolution. Briefly, while TORC1 controls cell growth and metabolism, TORC2 regulates cell proliferation and survival (Eltschinger and Loewith, 2016; Weisman, 2016). In mammalian cells, a single mTOR protein acts as the catalytic subunit of both mTORC1 and mTORC2 complexes. mTOR binds to Raptor (regulatory associated protein with mTOR) and mLST8 (mammalian lethal with Sec13 protein 8) (Hara et al., 2002; Kim et al., 2002, 2003). mTORC2 also consists of mTOR and mLST8. However, instead of Raptor, it contains **Rictor** (rapamycin insensitive companion of mTOR) (Jacinto et al., 2004; Sarbassov et al., 2004). Conversely, yeast cells contain two TOR kinases, Tor1 and Tor2. In budding yeast, the catalytic subunit of TORC1 can be either Tor1 or Tor2, whereas TORC2 only contains Tor2 (Loewith et

al., 2002). In *S. pombe*, the nomenclature can be misleading, since Tor2 is found in TORC1 complex and Tor1 in TORC2 (Alvarez and Moreno, 2006; Matsuo et al., 2007; Weisman and Choder, 2001). The Raptor orthologue is Kog1 in *S. cerevisiae* and Mip1 in *S. pombe*, while Avo3 and Ste20 are Rictor orthologues, and Lst8 and Wat1 are mLST8 orthologues, respectively (reviewed in Weisman, 2016).

Table 2. TORC1 subunits in *S. cerevisiae*, *S. pombe* and mammals. Adapted from Weisman, 2016 and Pérez-Hidalgo and Moreno, 2017.

	S. cerevisiae	***S. pombe***	**Mammals**
TORC1	Tor1 or Tor2	Tor2	mTOR
	Kog1	Mip1	Raptor
	Lst8	Wat1	mLST8
	Tco89	Tco89	-
	-	-	Deptor
	-	-	PRAS40

Table 3. TORC2 subunits in *S. cerevisiae*, *S. pombe* and mammals. Adapted from Weisman, 2016 and Pérez-Hidalgo and Moreno, 2017.

	S. cerevisiae	***S. pombe***	**Mammals**
TORC2	Tor2	Tor1	mTOR
	Avo3	Ste20	Rictor
	Avo1	Sin1	mSIN1
	Bit61	Bit61	Protor
	Lst8	Wat1	mLST8
	-	-	Deptor

The TOR signalling pathway senses and integrates different environmental inputs, including nutrients and growth factors, in order to control growth and organismal physiology. Numerous studies have established a central role for TOR signalling in the regulation of many major cellular processes, from protein synthesis to autophagy (reviewed in Laplante and Sabatini, 2012; Saxton and Sabatini, 2017). They have also shown that TOR dysfunction is involved in many pathological conditions, such as cancer or type II diabetes (reviewed in Laplante and Sabatini, 2012; Saxton and Sabatini, 2017), and in the ageing process (reviewed in Blagosklonny and Hall, 2009).

3.1.1. TORC1

TORC1 is the master regulator of cell growth, and it is activated by nutrients, growth factors and hormones. To stimulate cell growth, TORC1 promotes anabolic processes, such as protein and lipid synthesis, ribosome biogenesis or transcription; and inhibits catabolic processes, including autophagy and the differentiation response (Alvarez and Moreno, 2006; Uritani et al., 2006; Matsuo et al., 2007; Saxton and Sabatini, 2017).

Upstream of TORC1: regulation of TORC1

In yeasts, TORC1 is regulated in response to nitrogen and amino acids availability, becoming active when these nutrients are plentiful, and inactive if they are scarce, as well as to various type of stresses (Loewith and Hall, 2011). By contrast, in mammals, TORC1 also

responds to growth factors, and energy and oxygen levels (Saxton and Sabatini, 2017) (Figure 6). TORC1 activation is carried out by a two-step mechanism that involves two GTPases: the Rag (Ras-related GTPases) family and the Rheb (Ras-homologue enriched in brain GTPase). Rag GTPases (Gtr1 and Gtr2) are conserved in both *S.cerevisiae* and *S. pombe*. However, Rheb (Rhb1) is only present in the fission yeast (Saxton and Sabatini, 2017).

In mammals, the Rag GTPase family consists of RagA, RagB, RagC and RagD (Sekiguchi et al., 2001). Rags are found as heterodimers of RagA or RagB with RagC or RagD that locate on the lysosomal surface when interacting with the Ragulator complex (Sancak et al., 2010) (Figure 6, left). Amino acids stimulation triggers the binding of guanosine triphosphate (GTP) to RagA and RagB, allowing Rag heterodimers to bind to Raptor and recruit mTORC1 to the lysosomal membrane (Sancak et al., 2010). Once mTORC1 is translocated to the lysosomal membrane, it is activated by Rheb (Long et al., 2005). mTORC1 senses both cytosolic and intra-lysosomal amino acid concentration. Rag activity is modulated by lysosomal amino acids through a mechanism involving the lysosomal v-ATPase, that promotes the guanine nucleotide exchange factor (GEF) activity of Ragulator towards Rag A or RagB (Zoncu et al., 2011; Bar-Peled et al., 2012). Conversely, mTORC1 detects cytosolic leucine and arginine through the GATOR1-GATOR2-Rag pathway (Bar-Peled et al., 2013). The KICSTOR complex tethers GATOR1 to the lysosomal membrane (Wolfson et al., 2017), where it downregulates mTORC1 by acting as a GTPase-activating protein (GAP) for RagA or RagB (Bar-Peled et al., 2013). However, GATOR2 is a positive regulator of mTORC1, since it inhibits GATOR1. In the absence of leucine and arginine, Sestrin2 and CASTOR1 bind to and inhibit GATOR2, promoting mTORC1 downregulation (Chantranupong et al., 2014, 2016; Parmigiani et al., 2014; Saxton et al., 2016). Furthermore, growth factors and energy levels also control mTORC1 activity as they inhibit the Tuberous Sclerosis Complex (TSC), a key negative regulator of mTORC1 (Dibble and Cantley, 2015). TSC is a heterotrimeric complex comprising TSC1, TSC2 and TBC1D7 (Dibble et al., 2012), which acts together as a GAP for Rheb (Garami et al., 2003; Inoki et al., 2003; Tee et al., 2003).

In *S. cerevisiae*, the Gtr1-Gtr2 complex associates with the EGO complex (Figure 6, middle), which is likely the functional orthologue of Ragulator (Powis et al., 2015; Zhang et al., 2012). As in mammalian cells, the Gtr1-Gtr2 complex binds to Kog1 (Raptor) and activates TORC1. However, amino acids do not alter TORC1 localisation, that is constitutively tethered to the vacuole, the equivalent of metazoan lysosome, by the EGO-Gtr1-Gtr2 complex (Binda et al., 2009; Kira et al., 2014, 2016). Interestingly, Hatakeyama et al., 2019 have recently described that the EGO complex spatially controls distinct pools of the *S.cerevisiae* TORC1: vacuolar TORC1 promotes protein synthesis through the activation of Sch9, the orthologue of p70S6 kinase (S6K1), whereas endosomal TORC1 inhibits autophagy. The GATOR1-GATOR2 axis is also conserved in budding yeast as the SEACIT and SEACAT complexes are GATOR1 and GATOR2 orthologues, respectively (Panchaud et al., 2013). By contrast, there are no orthologues of CASTOR1 or Sestrin2, suggesting an alternative mechanism in yeast.

As in mammalian cells, the TSC-Rheb (Tsc1/Tsc2-Rhb1) axis controls TORC1 activity in *S. pombe* (Mach et al., 2000; Matsumoto et al., 2002; Matsuo et al., 2007; Van Slegtenhorst et al., 2004) (Figure 6, right). The Rag GTPases (Gtr1 and Gtr2) are also positive regulators of TORC1 (Laor et al., 2014; Ma et al., 2013; Valbuena and Moreno, 2012). Moreover, both Ragulator, comprised by Lam1, Lam2, Lam3 and Lam4, and GATOR1, formed by Iml1, Npr2 and Npr3, complexes regulate Gtr1-Gtr2 activity (Ma et al., 2013, 2016). The mechanism by which these proteins act on Gtr1-Gtr2 GTPases remains elusive though. Intriguingly, in *S. pombe* the Ragulator-Gtr1-Gtr2 complex is not required for TORC1 activation, but for its downregulation (Chia et al., 2017).

Downstream of TORC1: effectors of TORC1

Many of the functions of the TOR complexes have been uncovered through the analysis of their main effectors: the AGC family of protein kinases, which include members such as protein kinase A and C (PKA and PKC), S6K1 or Akt (Pearce et al., 2010). S6K1 and eIF4E binding protein (4EBP) act downstream TORC1 to regulate protein synthesis (Saxton and Sabatini, 2017). TORC1 phosphorylates and activates S6K1, that promotes transcription (Holz et al., 2005) and translation (Ma et al., 2008). Interestingly, this mechanism is conserved since both yeasts contain S6K1 orthologues. However, unlike *S. pombe*, that has three S6K1 orthologues (Sck1, Sck2 and Psk1), there is only one S6K1 orthologue (Sch9) in *S. cerevisiae* (Powers, 2007). TORC1 also phosphorylates 4EBP, triggering its dissociation from eIF4E and allowing translation to occur (Saxton and Sabatini, 2017). Other TORC1 effectors are involved in the synthesis of lipids (Lipin1) and nucleotides (ATF4), glucose metabolism (HIF1α) or autophagy (ULK1, TFEB) (Saxton and Sabatini, 2017).

3.1.2. TORC2

In mammals, mTORC2 controls cell proliferation, survival and the actin cytoskeleton (Sarbassov et al., 2004; Jacinto et al., 2004; Manning and Toker, 2017; Sarbassov et al., 2005) mainly by phosphorylating some AGC kinases such as PKC and SGK1 (Serum/Glucocorticoid-regulated kinase 1) (García-Martínez and Alessi, 2008; Sarbassov et al., 2005). However, the most important mTORC2 effector is Akt (Sarbassov et al., 2005), that also promotes mTORC2 activity (Yang et al., 2015). Furthermore, Akt modulates mTORC1 through inhibition of Tsc2 (Dibble and Cantley, 2015) (Figure 6, left). Interestingly, mTORC2 is also regulated by mTORC1, since mTORC1 signalling downregulates the insulin/PI3K (Phosphoinositide 3-kinase) pathway (Hsu et al., 2011; Yu et al., 2011), the main upstream regulator of mTORC2 (Liu et al., 2015).

In budding yeast, TORC2 regulates endocytosis, sphingolipid biosynthesis, homeostasis of the plasma membrane, cell wall synthesis (reviewed in Roelants et al., 2017) and the actin cytoskeleton (Schmidt et al., 1996). The *S. cerevisiae* TORC2 has three major effectors: Ypk1 (the orthologue of SGK1), Ypk2 and Pkc1 (Roelants et al., 2017).

In *S. pombe*, TORC2 acts through the AGC Gad8 kinase (Matsuo et al., 2003), the orthologue of mammalian Akt. TORC2 signalling is involved in the regulation of the actin cytoskeleton, cytokinesis or the response to several stresses and DNA damage (Ikai et al., 2011; Ikeda et al., 2008; Kawai et al., 2001; Weisman and Choder, 2001). Furthermore, the TORC2-Gad8 pathway is required for the G2/M transition (Ikai et al., 2011; Petersen and Nurse, 2007). Recently, it has been shown that the TORC2-Gad8 axis regulates the transcription of the MluI cell Cycle Box (MCB) Binding Factor (MBF) dependent genes under replicative stress (Cohen et al., 2016), as well as gene silencing (Laribee and Weisman, 2020) and telomere length maintenance (Kupiec and Weisman, 2012). TORC2 is also required for the sexual differentiation response (Matsuo et al., 2003), as deletion of both *tor1*$^{+}$ and *gad8*$^{+}$ causes sterility (Weisman and Choder, 2001). Interestingly, in *S. pombe*, TORC1 inactivation triggers the mating response (Alvarez and Moreno, 2006; Uritani et al., 2006). Recently, it has been described that TORC1 regulates TORC2 signalling to inhibit the sexual differentiation response (Martín and López-Áviles, 2018). Specifically, this TORC1 regulation is mediated by PP2A/B55 (PP2A/Pab1) phosphatase (Martín et al., 2017) and the transcriptional coactivation complex SAGA (Spt-Ada-Gcn5 acetyltransferase) (Laboucarié et al., 2017).

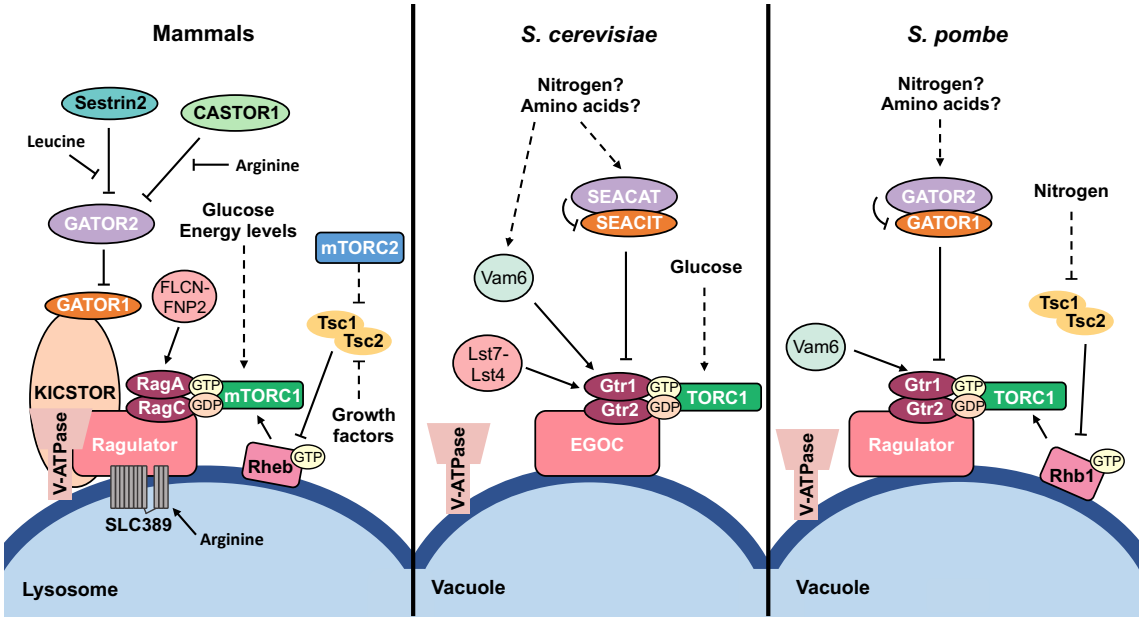

Figure 6. Regulation of TORC1 in mammals and yeasts. The mTORC1/TORC1 complex locates on the vacuole/lysosome membrane through Rag GTPases (RagA-B and RagC-D in mammals, and Gtr1 and Gtr2 in fission and budding yeasts). These GTPases are tethered to the vacuole/lysosome surface by the EGO/Ragulator complex. mTORC1/TORC1 is also subjected to the regulation of the TSC-Rheb (Tsc1-Tsc2-Rheb/Rhb1) axis, that responds to mTORC2 activity and growth factors in mammals, and nitrogen in *S. pombe*. Moreover, mTORC1/TORC1 activity is controlled by the GATOR1 and GATOR2, SEACAT-SEACIT in S. cerevisiae, complexes, which act on Rag GTPases. Vam6, conserved in both yeasts, is a Gtr2 GEF, whereas Lst4-Lst7/FLCN-FNIP2 is a RagC/Gtr2 GAP in mammals and *S. cerevisiae*, respectively. In mammals, leucine and arginine sensors, Sestrin2 and CASTOR1, downregulate mTORC1 activity through GATOR2 inhibition.

4. The Greatwall-Endosulfine-PP2A/B55 pathway in fission yeast

4.1. The Greatwall-Endosulfine molecular switch connects cell growth to cell cycle

The rate of cell growth, or increase in cell mass, is normally coupled to the rate of cell division, or increase in cell number, to give rise to an organ or organism of a certain size. Cell growth is modulated by nutritional conditions (Fantes and Nurse, 1977). When nutrients are plentiful, the biosynthetic rate is high to promote growth and increase cell size. Conversely, when nutrients are scarce, cells restrain biosynthesis and reduce cell size. Cell growth is regulated by the TORC1 signalling pathway (reviewed in Loewith and Hall, 2011), while cell cycle is driven by the activity of CDK/Cyclin complexes (Nurse, 1990). Protein phosphatases are also important for cell-cycle progression though (Cundell et al., 2013, 2016; Domingo-Sananes et al., 2011; Grallert et al., 2015; Mochida and Hunt, 2012). Notably, the PP2A/B55 phosphatase complex plays a central role in cell-cycle control since it reverts CDK/Cyclin phosphorylation (Mochida et al., 2009). In both budding and fission yeasts, the Greatwall-Endosulfine module connects cell growth to cell cycle by regulating the activity of the PP2A/B55 phosphatase. In *S. cerevisiae*, PKA and TORC1 activities downregulate the Greatwall-Endosulfine switch (Pedruzzi et al., 2003), whereas, in *S. pombe*, only TORC1 negatively regulates the Greatwall-Endosulfine module (Chica et al., 2016; Pérez-Hidalgo and Moreno, 2016, 2017).

4.1.1. Regulation of the G2/M transition by the TORC1-Greatwall-Endosulfine-PP2A/B55 pathway

In *S. pombe*, PP2A/B55 activity delays cell division. As in metazoans, mitotic entry is the result of a controlled balance between Cdk1/CyclinB protein kinase and PP2A/B55 protein

phosphatase activities (Glover, 2012; Lorca and Castro, 2013). In fission yeast, TORC1 modulates entry into mitosis and cell size at division by downregulating Greatwall-Endosulfine activity (Chica et al., 2016; Pérez-Hidalgo and Moreno, 2016, 2017). In this yeast, there are two Greatwall kinases, encoded by the *cek1+* and the *ppk18+* genes, and a single Endosulfine, encoded by the *igo1+* gene (Chica et al., 2016). On the other hand, PP2A/B55 is a heterotrimeric complex encoded by *paa1+*, which constitutes the scaffold subunit, *ppa1+* or *ppa2+*, that are the catalytic subunits, and *pab1+*, which is the regulatory subunit. In nitrogen-rich media, TORC1 activates the Sck2 S6 kinase which inhibits Greatwall. This inhibition of Greatwall leads to full activation of PP2A/B55, which opposes Cdk1/CyclinB activity (Figure 7). As a result, cells delay entry into mitosis and divide with a larger cell size. Conversely, in nitrogen-poor media, TORC1 activity drops, relieving Greatwall inhibition by Sck2. Active Greatwall phosphorylates Endosulfine, which inhibits PP2A/B55 (Figure 7). Low levels of PP2A/B55 activity enable cells to divide with reduced Cdk1/CyclinB activity levels, and therefore, with a smaller size.

In summary, the Greatwall-Endosulfine module responds to nutritional cues and couples cell growth (TORC1) to cell division (CDK/Cyclin complexes) through the regulation of PP2A/B55 phosphatase complex. This connection unravels why *S. pombe* cells divide with larger size in nitrogen-rich media, and why cell-cycle distribution varies if cells are cultured in nitrogen-poor media. When nutrients are scarce, cells divide with a smaller size due to reduced levels of PP2A/B55. As a consequence, G2 is short and G1 is extended in order to reach the cell size required for S phase.

4.2. The Greatwall-Endosulfine-PP2A/B55 pathway connects TORC1 to TORC2, providing a switch from cell proliferation to cell differentiation

In fission yeast, TORC1 and TORC2 have opposite functions. TORC1 becomes activated by nitrogen and promotes cell growth, whereas TORC2, which is activated by nitrogen starvation and several other stress conditions, promotes cell differentiation. Cells deleted for *tor1+* (TORC2) or its effector *gad8+* are unable to arrest in G1, causing sterility (Kawai et al., 2001; Weisman and Choder, 2001). Remarkably, a recent study has shown that the shift from cell proliferation to cell differentiation in response to nitrogen deprivation is controlled by the PP2A/B55 phosphatase complex (Martín et al., 2017). When nutrients are abundant, TORC1 activity is high, promoting the activation of PP2A/B55. High levels of PP2A/B55 phosphatase counteracts TORC2 activation of Gad8 by dephosphorylating Gad8 at serine 546 (Martín and López-Áviles, 2018; Martín et al., 2017) (Figure 7). Conversely, upon TORC1 inactivation, the Greatwall-Endosulfine module is active and inhibits PP2A/B55, leading to active Ser546 phosphorylated Gad8 and the initiation of the cell differentiation programme (Figure 7).

In conclusion, TORC1 and PP2A/B55 play a negative role in the sexual differentiation response, while TORC2-Gad8 and Greatwall-Endosulfine pathways have a positive one. According to this, deletion of *ppk18+* and *cek1+*, or *igo1+*, reduces mating efficiency (Chica et al., 2016; Laboucarié et al., 2017). Conversely, cells deleted for the B55 regulatory subunit of PP2A, *pab1+*, shows hyperfertility due to enhanced Gad8 activity (Martín et al., 2017). This crosstalk between TORC1 and TORC2 through the Greatwall-Endosulfine-PP2A/B55 pathway and phosphorylation of Gad8 may shed light on their antagonistic roles regarding the sexual differentiation response in fission yeast. Moreover, in *S. cerevisiae*, TORC1 and PKA activities downregulate cell differentiation, which also requires Greatwall-Endosulfine-PP2A/B55 activity (Sarkar et al., 2014). Interestingly, in metazoans, where no connection between TORC1 and the Greatwall-Endosulfine module has been described, overexpression of Greatwall increases phosphorylation and activation of the Gad8 orthologue, Akt, by degrading a protein phosphatase (Vera et al., 2015).

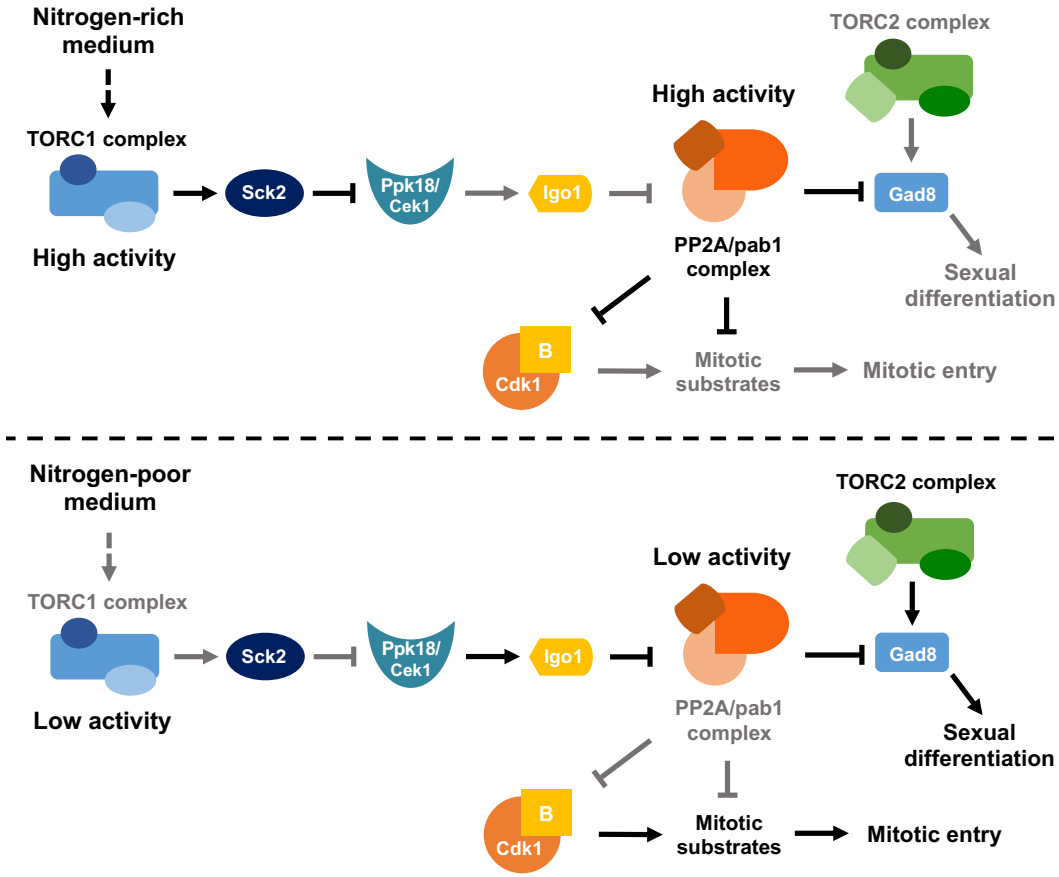

Figure 7. In *S. pombe*, nitrogen regulates cell size and cell differentiation through the TORC1-Greatwall-Endosulfine-PP2A/B55 pathway. In nitrogen-rich media, TORC1 activity is high promoting Ppk18 and Cek1 inhibition by the S6 kinase orthologue, Sck2. As a result, PP2A/B55 is active and reverts Cdk1/CyclinB phosphorylation, delaying entry into mitosis and promoting cell division with a large size. High activity of PP2A/B55 also inhibits Gad8 activation and therefore, the sexual differentiation response. In low nitrogen conditions, TORC1-Sck2 activity drops, releasing Ppk18 and Cek1 inhibition, that become activated and phosphorylate Igo1. As a consequence, PP2A/B55 is inhibited, enabling cells to enter mitosis with low levels of Cdk1/CyclinB activity and with a small size. Moreover, the sexual differentiation response is induced due to Gad8 activation. Modified from García-Blanco et al., 2019.

5. Ageing

Ageing can be defined as the time-dependent functional decay that affects the majority of living organisms (López-Otín et al., 2013). It is a complex process during which molecular, cellular and organ damage accumulates, resulting in functional loss, increased susceptibility to disease and, eventually, death (Fontana et al., 2010). There are nine common denominators that participate in the process of ageing and determine the ageing phenotype (López-Otín et al., 2013). Genomic instability and epigenetic perturbations accumulate throughout life, constituting two hallmarks of ageing (Moskalev et al., 2013; Oberdoerffer and Sinclair, 2007; Tsurumi and Li, 2012). Deficient DNA damage repair and alterations in DNA methylation and histone modifications can be found in ageing-related diseases, favouring the ageing process (Gregg et al., 2012; Li et al., 2009; Osorio et al., 2010; Shumaker et al., 2006). Moreover, there are certain regions of chromosomes, such as telomeres, that are more vulnerable to age-related decline (Blackburn et al., 2006). Notably, telomere attrition accompanies the ageing process, constituting another of its hallmarks (López-Otín et al., 2013). Loss of protein homeostasis and mitochondrial dysfunction are also linked to ageing and ageing-related diseases (Green et al., 2011; Powers et al., 2009), as well as cellular senescence and stem cell exhaustion (López-Otín et al., 2013).

Furthermore, intercellular communication seems to be important since ageing involves alterations in cell to cell communications (Laplante and Sabatini, 2012; Russell and Kahn, 2007; Zhang et al., 2013). However, deregulation of nutrient-signalling pathways is perhaps the most studied ageing feature. Many of the mutations that alter nutrient-sensing pathways, such as the **Igf1** (Insulin-like growth factor 1)/insulin and TOR pathways, have been linked to longevity in different organisms (Fontana et al., 2010). Interestingly, inactivation of TORC1 or its inhibition by rapamycin prolongs life span in a variety of organisms, such as yeast, fish, worms or rodents (Blagosklonny and Hall, 2009; Fontana et al., 2010). Consistent with a role of deregulated nutrient-signalling pathways in ageing, dietary restriction, a reduction in food intake without malnutrition, promotes longevity in diverse eukaryotes species, including monkeys (Blagosklonny and Hall, 2009; Colman et al., 2009; Fontana et al., 2010; Mattison et al., 2012). All these results suggest that there might be an evolutionary conserved role for nutrient-signalling pathways in ageing.

5.1. Yeast ageing

In the last decade, we have witnessed many breakthroughs in the molecular mechanisms of ageing. Much of this progress has been carried out in invertebrate eukaryotic organisms. In particular, studies in budding yeast have identified many pro-ageing and anti-ageing factors (TOR, PKA, AMPK and SIR2) that are functionally conserved in higher eukaryotes, including mammals (Burkewitz et al., 2014; Enns and Ladiges, 2010; Johnson et al., 2013; Poulose and Raju, 2015). The first study of ageing in yeast was published 60 years ago and showed that yeast cells have a limited replicative capacity (Mortimer and Johnston, 1959). This model of ageing is termed replicative lifespan (RLS) and refers to the number of daughter cells produced by a mother cell before senescence. Recent studies have introduced a new model of ageing known as chronological ageing (Fabrizio and Longo, 2003). Chronological lifespan (CLS) is defined as the length of time that a population of yeast cells can survive in a no division state, also known as quiescence or G_0 phase. These two types of yeast ageing (Figure 8) allow to compare the ageing process in both proliferating and non-proliferating cells (Kaeberlein, 2006).

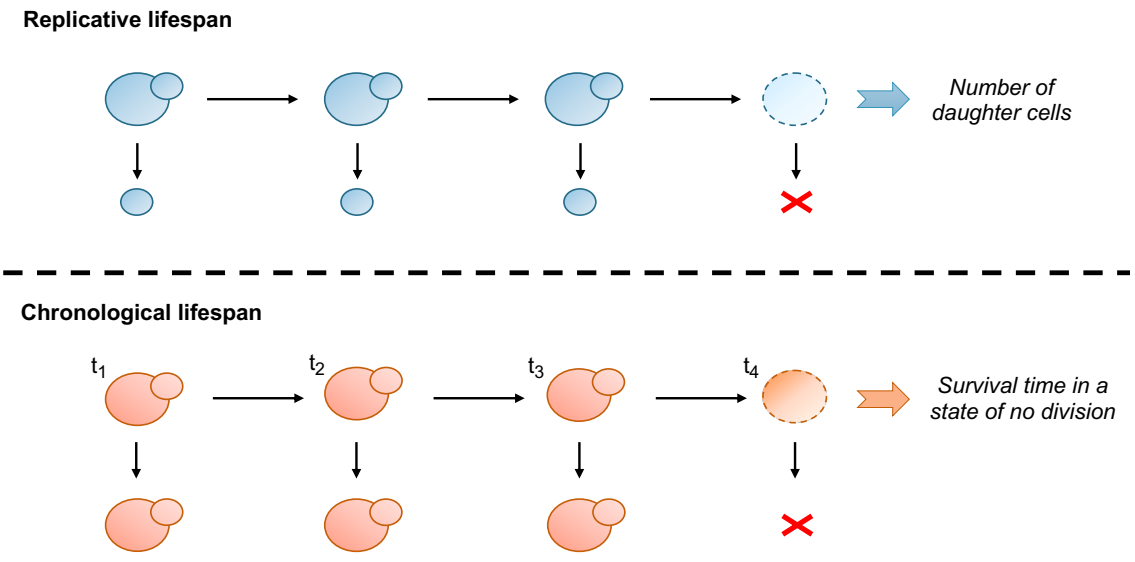

Figure 8. Models of ageing in yeasts. Replicative lifespan, or RLS (**top**), describes the number of daughter cells that a mother cell can produce, whereas chronological lifespan, or CLS (**bottom**), measures the length of time a cell in a no division state can remain viable. Replicative viability is calculated as the mean of progenies produced from mothers of a yeast strain before senescence. By contrast, chronological viability is calculated by the portion of a cell population able to resume proliferation after a period of quiescence. Modified from He and Kennedy, 2015.

5.1.1. Quiescence in *Schizosaccharomyces pombe*

The G_0 phase, or cellular quiescence, describes the cellular state in which a cell stops proliferating but retains the ability to re-enter the replicative cell cycle. Quiescence is induced by removal of growth and proliferation cues, and its establishment involves physiological and molecular changes. In multicellular organisms, most cells are maintained in this state of no division, such as skeletal muscle cells, neurons or adult stem cells (Yao, 2014). Like in mammalian cultured cells, where G_0 entry is induced by serum depletion (Zetterberg and Larsson, 1985), fission yeast cells enter G_0 in response to nitrogen starvation (Su et al., 1996). Unlike *S. cerevisiae*, where ageing can be monitored as both RLS and CLS, in fission yeast, RLS analyses are complicated since mother and daughter cells are indistinguishable. Hence, *S. pombe* lifespan is assayed as CLS (Chen and Runge, 2009; Su et al., 1996).

The establishment of *S. pombe* G_0 takes about 24 hours and is associated with morphological changes, including loss of cell polarity, reduction in cell size and nuclear volume, and chromatin flattening (Su et al., 1996). Quiescent cells remain viable for months, resist different stresses, and can resume proliferation upon nitrogen replenishment (Mochida and Yanagida, 2006; Su et al., 1996). Moreover, vacuoles enlarge during quiescence, reflecting an increase in catabolic activity (Su et al., 1996). Maintaining this quiescence state requires glucose (Su et al., 1996). In fact, transcripts that encode glycolysis-related proteins are the more abundant among G_0 transcripts (Shimanuki et al., 2007), illustrating that quiescence cells are metabolically active (Marguerat et al., 2012). Furthermore, free amino acids decrease rapidly during quiescence (Sajiki et al., 2013). Hence, autophagy is crucial for quiescence maintenance since it contributes to recycle amino acids (Kohda et al., 2007; Sideri et al., 2015). In addition to autophagy, the proteasome is required for proper mitochondrial function during quiescence (Takeda and Yanagida, 2010; Takeda et al., 2010). Finally, G_0 cells are highly efficient in DNA damage repair. Unlike vegetative cells, where homologous recombination is the preferred mechanism to repair DNA lesions, quiescent cells use non-homologous end joining (NHEJ) (Mochida and Yanagida, 2006).

Remarkably, dietary restriction and downregulation of TORC1 activity extend lifespan in different organisms (Blagosklonny and Hall, 2009; Fontana et al., 2010). In budding yeast, Rim15 and Igo1/2 (Greatwall and Endosulfine orthologues, respectively) are required for G_0 entry, survival in stationary phase and CLS extension (Talarek et al., 2010; Wei et al., 2008). During G_0, Rim15 also limits ROS levels and ensures that cells accumulate carbohydrates needed for quiescence maintenance (Zhang and Cao, 2017). In both budding and fission yeasts, deletion of S6 kinase orthologue, Sck2 in *S. pombe* and Sch9 in *S. cerevisiae*, which inhibits Greatwall, promotes CLS extension (Chen and Runge, 2009; Fabrizio et al., 2001). Moreover, mutants lacking *ppk18*$^{+}$, encoding the Greatwall orthologue in fission yeast, show reduced CLS (Chen et al., 2013a). Interestingly, a recent screening reported that *igo1*$^{+}$, the Endosulfine orthologue in fission yeast, is one of the 85 essential genes required for quiescence (Sajiki et al., 2018).

Materials and Methods

1. Microorganisms

1.1. *Schizosaccharomyces pombe* strains

Table 1 lists the fission yeast strains used in this work.

Table 1. *Schizosaccharomyces pombe* strains.

Strain	Genotype	Source
S2049	*h^{90} 968*	P. Nurse
S2055	*h$^-$ tor1::KanMX6*	S. Moreno
S2199	*h$^-$ kanMX6:P3nmt1:tor2$^+$*	S. Moreno
S2309	*h$^+$ aur-mcherry:atb2$^+$ hht2:GFP:ura4$^+$ ura4-D18*	S. Moreno
S2313	*h^{90} igo1::kanMX6*	S. Moreno
S2337	*h$^+$ ppa2::natMX6*	S. Moreno
S2338	*h$^+$ igo1::kanMX6 ppa2::natMX6*	S. Moreno
S2389	*h$^-$ sck2::kanMX6*	S. Moreno
S2341	*h$^-$ ppk18::kanMX6*	S. Moreno
S2365	*h$^+$ aur-mcherry:atb2 hht2:GFP:ura4$^+$ ura4-D18 igo1::kanMX6*	S. Moreno
S2392	*h$^-$ kanMX6:P41nmt1:GFP:ppk18$^+$*	S. Moreno
S2339	*h$^-$ igo1::ura4$^+$*	S. Moreno
S2431	*h$^+$ kanMX6:P41nmt1:GST:pab1$^+$*	S. Moreno
S2432	*h$^+$ igo1::kanMX6 kanMX6:P41nmt1:GST:pab1$^+$*	S. Moreno
S2433	*h$^+$ 975*	S. Moreno
S2457	*h$^-$ kanMX6:P3nmt1:sck2$^+$*	S. Moreno
S2666	*h$^-$ 972*	S. Moreno
S2727	*h$^-$ igo1::kanMX6*	S. Moreno
S2800	*h$^-$ rum1::kanMX6 ste9::ura4$^+$ ura4-D18*	S. Moreno
S2874	*h$^-$ igo1:GFP:kanMX6*	This work
S2875	*h^{90} cek1::natMX6 ppk18::kanMX6 ppk31::hphMX6*	This work
S2876	*h$^-$ ppk31::hphMX6*	This work
S2877	*h^{90} ppk31::hphMX6*	This work
S2878	*h$^-$ cek1::natMX6*	This work
S2879	*h^{90} cek1::natMX6*	This work
S2880	*h^{90} ppk18::kanMX6 ppk31::hphMX6*	This work
S2881	*h$^-$ ppk18::kanMX6 ppk31::hphMX6*	This work
S2882	*h^{90} cek1::natMX6 ppk18::kanMX6*	This work
S2883	*h$^-$ cek1::natMX6 ppk18::kanMX6*	This work
S2884	*h$^-$ cek1::natMX6 ppk31::hphMX6*	This work
S2885	*h$^-$ ppk18::kanMX6 ppk31::hphMX6 cek1::natMX6*	This work
S2886	*h^{90} ppk31::hphMX6 cek1::natMX6*	This work
S2887	*h$^-$ gad8::hphMX6 igo1::kanMX6*	This work
S2888	*h$^-$ gad8::hphMX6*	This work

S2889	*h90 ppa2::natMX6*	This work
S2890	*h90 ppa2::natMX6 igo1::kanMX6*	This work
S2891	*h+ ppa2::natMX6 gad8::hphMX6*	This work
S2892	*h- igo1:polylinker:HBH:kanMX6*	This work
S2893	*h- mst2::hphMX6*	This work
S2894	*h- pab1:3HA:kanMX6*	This work
S2895	*h- kanMX6:P41nmt1:GFP:pab1+*	This work
S2896	*h+ mst2:13myc:kanMX6*	This work
S2897	*h- igo1::hphMX6 mst2::hphMX6*	This work
S2898	*h- igo1::hphMX6 mst2::hphMX6*	This work
S2899	*h+ igo1:igo1-4A*	This work
S2900	*h- mst2:13myc:kanMX6 kanMX6:P41nmt1:GFP:pab1+*	This work
S2901	*h- mst2:13myc:kanMX6 pab1:3HA:kanMX6*	This work
A17	*h90 kanMX6:P41nmt1:GFP:ppk18+*	A. Vázquez-Bolado
SR7	*h- tsc2::kanMX4*	S. Rubiales
L294	*h- ppk18:GFP:kanMX6*	L. Pérez-Hidalgo
L397	*h- atg3::kanMX6*	L. Pérez-Hidalgo

1.2. *Escherichia coli* strains

E. coli DH5α cells (Table 2) were used to produce *igo1+* and *igo1+*-mutagenized recombinant DNA in *pBluescript SK+* vector, whereas 6xHis-Igo1 protein was expressed and purified from Rosetta™ or BL21 cells (Table 2). Competent cells were prepared according to the protocol described by Inoue et al., 1990.

Table 2. *Escherichia coli* strains.

Strain	Genotype	Source
BL21 (DE3)	F– *ompT gal dcm lon hsdS$_B$*($r_B^-m_B^-$) λ(DE3 [*lacI lacUV5-T7p07 ind1 sam7 nin5*]) [*malB+*]$_{K-12}$(λ^S)	IBFG
DH5α	F– Φ80lacZΔM15Δ (lacZYA-argF) U169 recA1 endA1 hsdR17 (rK–, mK+) phoA supE44λ– thi-1 gyrA96 relA1	IBFG
Rosetta™	F– *ompT hsdS$_B$* (r_B^- m_B^-) *gal dcm* (DE3) pRARE2 (Cam^R)	Dr. K. Gould

2. Media and growth conditions

2.1. *Schizosaccharomyces pombe* cultures

Fission yeast cells were grown as described in Moreno et al., 1991. Cells were typically grown in supplemented yeast extract (YES) and Edinburgh minimal medium (MM). YES contains 0.5% yeast extract, 3% glucose and 250 µg/ml histidine, leucine, uracil, adenine and lysine. Minimal medium contains 14.7µM hydrogenated potassium phthalate, 15.5 µM sodium bisphosphate, 2% glucose, salts, vitamins and minerals. Two nitrogen sources were employed to supplement minimal media: 93.5 mM ammonium chloride (MM) and 20 mM phenylalanine (MMF). For nitrogen-starvation experiments, cells were grown in MM without nitrogen (MM-N). When working with *nmt1* construction, MM and MM-N were supplemented with 5 µg/ml of thiamine (Sigma) to repress expression from the *nmt1* promoter (Maundrell, 1990). Sporulation was

performed on Malt extract agar (MEA), whereas either MEA or MM-N were used for mating efficiency experiments. For growth in solid media, 2% agar was added to the above media.

To select antibiotic-resistant strains, 100 µg/ml geneticin (G-418, Duchefa Biochemie), 50 µg/ml hygromycin B (Roche) or 75 µg/ml nourseothricin (ClonNat, Werner BioAgents) were added to YES-agar medium.

To start each experiment, -80 ºC glycerol stock strains were streaked in YES-plates at 25-32ºC for 2-3 days. Pre-cultures were grown overnight in YES and then shifted to MM. To transfer cells from one medium to another, they were washed once or twice with the destination medium. All experiments were performed with prototrophic strains to avoid adding amino acids that could be used as a nitrogen source. Cells were grown either in water baths at 110 rpm or in air incubators at 200 rpm at 25ºC. Occasionally, the temperature used to grow fission yeast cells was 32ºC.

2.2. *Escherichia coli* cultures

Escherichia coli cells were cultured using protocols described by Sambrook et al., 1989. Cells were grown in Luria-Bertani medium (LB) at 37 ºC. To select antibiotic-resistant clones, 50-100 µg/ml ampicillin (Roche) was added to the LB medium.

3. Molecular biology techniques

3.1. Analysis of nucleic acids

3.1.1. Extraction of *S. pombe* chromosomal DNA

To extract *S. pombe* genomic DNA, 10^8 cells were harvested at 3000 rpm for 5 minutes and resuspended in 1 ml of a solution containing 50 mM citrate-phosphate pH 5.6, 40 mM EDTA pH 8.0, 1.2 mM sorbitol and 2.5 mg of Zymolyase 20T (Seikagaku Corporation), a yeast cell wall degrading enzyme. Next, cells were incubated for 30 minutes at 37 ºC, spun down and resuspended in 550 µl of Tris-EDTA buffer (TE) containing 1% SDS and incubated for one hour at 65 ºC. For protein precipitation, 175 µl of 5 M potassium acetate was added. The mix was incubated for five minutes on ice and centrifuged at 5000 rpm for 15 minutes at 4ºC to retain the supernatant.

Nucleic acids were precipitated by adding 500 µl of cold isopropanol to supernatants and incubating them for at least 10 minutes at -20 ºC. Subsequently, pellets were washed with 500 µl of 70% (v/v) cold ethanol. To eliminate RNA, pellets were resuspended in 350 µl of TE containing 50 µg/ml RNase (Roche) and incubated for 10 minutes at 65 ºC. Two phenol-chloroform extractions were used for DNA purification. In each extraction, 350 µl of 1:1 phenol-chloroform were added to the samples. After that, DNA was precipitated by adding 1:10 volumes of 3 M sodium acetate and 2.5 volumes of ethanol and incubating the mixture at -20 ºC for several hours. Finally, samples were centrifuged at 10000 rpm for 10 minutes at 4ºC and pellets were washed with 1 ml of 70% cold ethanol, dried and resuspended in 50 µl of TE.

3.1.2. Extraction of *E. coli* plasmid DNA

Extractions of *E. coli* DNA plasmid for transformations, sequencing or cloning were carried out using NZYMiniprep columns (Nzytech) and following manufacturer's instructions.

For routine DNA plasmid preparations, the boiling miniprep protocol described by Holmes and Quigley, 1981 and Sambrook et al., 1989 was used.

3.1.3. DNA digestion using restriction enzymes

DNA digestion was carried out using restriction endonucleases from Thermo Scientific and New England Biolabs. Buffer solutions, temperature and time used in each reaction were the ones recommended by manufacturers.

3.1.4. Polymerase chain reaction (PCR)

DNA fragment amplification by PCR was carried out in a T300 thermal cycler from Biometra. Reaction conditions depended on the size of the DNA fragment to be amplified, manufacturer's instructions for DNA polymerase and oligonucleotide primers used in each case. The reaction volume was 50 µl or 100 µl and contained the template DNA, 250 µM of each dNTP, 1 µM of each primer, 1.5 mM $MgCl_2$, 0.25 U of DNA polymerase and the reaction buffer supplied with the enzyme. The amount of template DNA depended on whether it was genomic, plasmid or *S. pombe* cell mass. For gene deletion and checking PCRs, Biotaq™ DNA polymerase (Bioline) was used. Conversely, the low error rate-High Fidelity DNA polymerase (Roche) was employed for gene tagging and mutagenesis.

The oligonucleotide primers used in this work were supplied by Biomers or Sigma and are listed in Table 3.

Table 3. Oligonucleotides.

Gene deletion and Gene tagging		
Name	**Sequence**	**Use**
Cek1-D1 (N1)	5'- AGCATACTTACTGCTCATACTTCTAATGATCCTATCCCTCTAT TGAATTTACTGTATGCTGGAGACTCCGTCAGTTGTATATCGT ACGCTGCAGGTCGAC -3'	*cek1*⁺ deletion
Cek1-D2 (N2)	5'- AATGTGCATGGGAAGTTATAAAATGAAAGGAAAGAAACA GTATATGAAGCTGATCTGGCATTTAGTATGTAAGATTCAAT TATCGATGAATTCGAGCTCG -3'	*cek1*⁺ deletion
Gad8-D1 (N10)	5'- TTAAAAGAAAAGATAGAGGGAAAGCGAGCTTTTAAAAA TCAGTTCATTTTTTTTTTCTACTCCAAACAGACGTTACCG AAATCGTACGCTGCAGGTCGAC -3'	*gad8*⁺ deletion
Gad8-D2 (N11)	5'- ATGTAAAAGAGGCAAGAAAAGCGGCATGTATGAGTA AAAATGAGAAAACTTTCAAAATAAACAAAGAAGTGTCAAA TTCTATCGATGAATTCGAGCTCG -3'	*gad8*⁺ deletion
Igo1-3HA-F2 (NC)	5'- GACCCTCAGAGTCCTCGCCTAGTGGTGCCAGTAGCAG AAGGGAATCTGTCACGCGACACGACTTGGAAAGCAAT GAAAATCGGATCCCCGGGTTAATTAA -3'	GFP and HBH tagging of *igo1*⁺
Igo1-3HA-R1 (NC)	5'- ACGACAAGCAATACCAAATTTTAAGAGCCAAGCCAAATTAA ACCTC CAACCTTGTCGCAAAAATAGCAACGTGTATGACCG CACTGAGCAGCGTAATCTG -3'	GFP tagging of *igo1*⁺
Mst2-D1 (N14)	5'- TTGACCAAAGGATTAAATGGGGCCATTAGGAAAACTAT GAACGATCTGTAAATATAAACAATCTTTTTTTTTTATGTA TAATCGTACGCTGCAGGTCGAC -3'	*mst2*⁺ deletion
Mst2-D2 (N15)	5'- TATAGAGCAACAACCAAGCCGTAGATGATACAAATGCTT CACGACAAATATCGAAAGATTAAAATACTTATTTATTTGAAT ATCGATGAATTCGAGCTCG -3'	*mst2*⁺ deletion

Mst2-F1-myc (N18)	5'- ACCTTTTACTTAAAGAAAATATACTTATTCCTCTACCTCAA AAGCGTCTATTAGATAACTCTCATCATCTGGATTCCGTTCG GATCCCCGGGTTAATTAA -3'	13Myc tagging of *mst2+*

PCR checking of mutant strains

Name	Sequence	Use
Cek1-5 (NV5)	5'- TTCCCGATTAATGTATTCAG -3'	Checking of *cek1+* deletion and tagging
Cek1-6 (NV6)	5'- TCCGTATAAAGTAAAACAAC -3'	Checking of *cek1+* deletion and tagging
Gad8-C1 (L106)	5'- GATTGTTCGTTCGTATTCGC -3'	Checking of *gad8+* deletion
Gad8-C2 (L107)	5'- TAGCCGTTACGTTCTTATGC -3'	Checking of *gad8+* deletion
Igo1-3HA-C1 (NC)	5'- TCACCGTGTTGTCAGTGCTG -3'	Checking of *igo1+* tagging and mutagenesis
Igo1-BamHI (LP-H)	5'- TTTTGGATCCTCAATTTTCATTGCTTTCCAAGTCG -3'	Checking of *igo1+* mutagenesis
Igo1-C1 (NC)	5'- AGATTAGCTCATTCAGCCGC -3'	Checking of *igo1+* tagging and mutagenesis
Igo1-C2 (NC)	5'- CAGAAGTGTTGTCCTCCATC -3'	Checking of *igo1+* tagging
Igo1-NdeI (LP-H)	5'- TTTTCATATGGTAAGAACGCGCAAATGG -3'	Checking of *igo1+* mutagenesis
Kan-C1	5'-AGCTGCGCACGTCAAGACTG -3'	Checking of transformed strains
Kan-C2	5'- CAGATGCGAAGTTAAGTGCG -3'	Checking of gene deletion
Mst2-C1 (N14)	5'- TCGTTGAATCACCCAAGGTG -3'	*Checking of mst2+* tagging
Mst2-C2 (N15)	5'- CCTTGCTGAAGAAGAAATCG -3'	*Checking of mst2+* tagging
nmt1-Igo1-I2 (NC)	5'- GCTCTGAATTGCTAGAAGAC -3'	Checking of *igo1+* mutagenesis

Mutagenesis

Name	Sequence	Use
5' igo1-BamHI (NC)	5'- TTTTGGATCCGAGTATGCAAAGTCTTCGTC-3'	*igo1-4A* cloning in *pBluescript SK+*
3' igo1-EcoRI (NC)	5'- TTTTGAATTCACGAAGAAAAGGAATGCGCG -3'	*igo1-4A* cloning in *pBluescript SK+*
Igo1-NdeI (LP-H)	5'- TTTTCATATGGTAAGAACGCGCAAATGG -3'	*igo1-4A* cloning in *pET·15b*
Igo1-BamHI (LP-H)	5'- TTTTGGATCCTCAATTTTCATTGCTTTCCAAGTCG -3'	*igo1-4A* cloning in *pET·15b*

3.1.5. DNA electrophoresis

Size-dependent separation of DNA molecules was carried out by agarose gel electrophoresis. Depending on the size of the DNA fragments to be separated, the concentration of gels varied between 0.8 and 2 % of agarose (Seakem® LE). The gel and the electrophoresis buffer used in this work contained 40 mM Tris-acetate pH 8.0 and 1 mM EDTA (TAE). 1:20000 volumes of Midori Green (Nippon Genetics) were added to gels so that DNA molecules could be visualized with an ultraviolet (UV) transilluminator. Electrophoresis was run at constant voltage (80 or 90 V). The 1 kb plus DNA ladder (Invitrogen) DNA marker was used for the molecular weight estimation of DNA fragments. Electrophoresis tanks were from Apelex and power supplies from BioRad.

3.1.6. Purification, quantification and sequencing of DNA fragments

NZYGelpure kits (Nzytec) were used for DNA purification of PCR products. DNA concentration was estimated by measuring the absorbance at 260 nm in a NanoDrop 1000 spectrophotometer (Thermo Scientific), considering a ratio of 260/280 absorbance of 1.8 as an estimate of the DNA purity degree. Sequencing of DNA plasmid and PCR products were carried out by Eurofins Genomics.

3.1.7. DNA plasmids

Table 4 lists the DNA plasmids used in this work and specifies their source and application.

Table 4. DNA plasmids.

Name	Description	Use	Source
p1064	pBluescriptKS+	*igo1+* cloning	S. Moreno
pN1	pBluescriptKS+-*igo1-4A-BE*	igo1-4A mutant construction	This work
p1156	pFA6a-GFP-KanMx6	*igo1+* tagging with GFP	S. Moreno
p1128	pFA6a-13myc-KanMx6	*mst2+* tagging with 13Myc	S. Moreno
p1204	pET·15b	*igo1+* cloning	S. Moreno
p1228	pET·15b-*igo1^{cDNA}*	6His-Igo1 purification from *E. coli*	S. Moreno
pN2	pET·15b-*igo1-4A-NE*	6His-Igo1-4A purification from *E. coli*	This work
p1216	pFA6a-natMX6	*cek1+* deletion	S. Moreno

p1240	pFA6a-hphMX6	*gad8+*, *mst2+ and ppk31+* deletion	S. Moreno

3.2. Transformation techniques

3.2.1. *S. pombe* transformation

S. pombe transformation was carried out following a modification of the Lithium acetate (LiAc) method described by Bähler et al., 1998. Deletion mutants, the *igo1-4A* strain and cells carrying gene-tagged constructions were obtained using this technique.

$2x10^8$ cells were spun down at 3000 rpm for 5 minutes, washed with an equal volume of distilled water and resuspended in a solution of 100 mM LiAc, 10 mM Tris-HCl pH 7.5, 1 mM EDTA and 1 M sorbitol. After a 30-minute incubation at room-temperature, cells were harvested and resuspended in 100 µl of the same solution. Subsequently, 4 µl of denatured salmon sperm DNA and 10-20 ng of transforming DNA were added, and the mixture was kept at room temperature for 10 minutes. After that, 260 µl of a solution containing 40% PEG, 100 mM LiAc, 10 mM Tris-HCl pH 7.5 and 1 mM EDTA was added, and samples were incubated for one hour at room temperature. Next, 43 µl DMSO was added, and a 5-minute heat shock (42 ºC) was applied. Finally, cells were harvested, washed in 1 ml of distilled water, resuspended in 500 µl of distilled water and plate out onto two YES-plates. After 18-20 hours, cells were transferred to selective medium (YES with G418, ClonNat or Hygromycin B, or MM supplemented with FOA) by replica plating and incubated until colonies were formed.

3.2.2. *E. coli* transformation

E. coli cells were transformed using the protocol described by Kushner, 1988. *E. coli* competent cells were thawed on ice, mixed with 1-10 ng of DNA and incubated for 20 minutes on ice. Subsequently, a 90-second heat shock (42 ºC) was applied, and cells were then transferred to ice for 1-2 minutes. Four volumes of LB were added, and cells were grown for one hour at 37 ºC. Finally, 100 µl of cells were plated out onto LB-plates supplemented with ampicillin.

4. Construction of *S. pombe* strains

4.1. Gene deletion

The following approach was used to construct *cek1+*, *ppk31+*, *gad8+* and *mst2+* deletion mutants. Briefly, at least three 100 µl PCRs were performed to amplify antibiotic resistance cassettes using pFA6a-kanMX6 as template DNA for kanamycin, pFA6a-natMX6 for nourseothricin or pFA6a-hphMX6 for hygromycin B (Bähler et al., 1998; Hentges et al., 2005; Sato et al., 2005) (Table 4). Primers used (geneX-D1 was the forward primer, whereas geneX-D2 was the reverse (Table 3), were 100 base pair long. The first 80 nucleotides of the primers corresponded to the upstream sequence of the start codon of the gene of interest for geneX-D1 primers and the downstream sequence of the stop codon of the same gene for geneX-D2 primers. These 80 bp were sufficient to replace the target gene with the resistance marker by homologous recombination. The remaining 20 nucleotides, which matched the flanking regions of the antibiotic-resistance cassettes: the upstream sequence for forward primers and the downstream region for reverse primers, allowed the amplification of the cassette. PCR products were precipitated at -20 ºC using 3 M sodium acetate and 100% ethanol, resuspended in 10 µl of TE and used to transform *S. pombe* cells.

To check if the transformed clones carried the target-gene replacement, deletion ends were amplified by PCR using geneX-C1 and geneX-C2 primers (Table 3) along with kan-C1 and kan-C2 primers. GeneX-C1 and geneX-C2 oligonucleotides corresponded to the region of 200-300 bp upstream of the start codon and the sequence of 200-300 bp downstream of the stop

codon, respectively. Conversely, kan-C1 matched the promoter region of the resistance marker and kan-C2 the terminator sequence.

4.2. Tagging of proteins at the carboxy-terminus

At least three 100 µl PCRs were performed to amplify the epitope of interest along with the antibiotic-resistance marker using the proper plasmid as DNA template (Table 4) and geneX-tagX-F1 and geneX-D2 primers. The 80 5'-end base pairs of geneX-tagX-F1 matched the upstream sequence of the stop codon of the target gene. As a result of the homologous recombination during *S. pombe* transformation, the stop codon was deleted, allowing tag fusion to the carboxy-terminus of the selected gene.

The transformed clones were checked by PCR and sequencing to confirm that the tag had been correctly integrated, and that the PCR reactions had not introduced undesired mutations. A primer that corresponded to an internal sequence of the target gene, geneX-tagX-I1, and primers that matched the tag were used for this purpose (Table 3).

This method was used to obtain *igo1:GFP, igo1:polylinker:HBH and mst2:13myc* strains. The functionality of tagged-proteins was assayed by comparing the phenotype of the tagged-strains with the wild-type and the deletion of *igo1*$^+$ or *mst2*$^+$.

4.3. Genetic crosses

To generate double and triple mutants, parental strains were crossed on MEA plates and incubated for 2-4 days at 25ºC. Mating was checked by observing the formation of zygotic asci on a brightfield microscope. In most cases, spores were isolated on YES plates using a micromanipulator (Singer Instruments). Firstly, asci were selected and placed onto YES plates. Asci cell walls were allowed to breakdown for 2-4 hours at 32ºC. Finally, each ascus was micromanipulated to give a line of 4 isolated spores.

Random spore analysis was performed after treating asci with ß-glucuronidase (Sigma) to digest asci walls. In these cases, a small amount of the cross was resuspended in 500 µl of distilled water containing 10 µl of 1:10 volumes of ß-glucuronidase and incubated overnight at 25ºC. Spores were then plated out on YES.

In both cases, spores were allowed to germinate and form colonies. Clones of interest were selected by replica plating to selective medium, PCR and microscopy.

5. Site-directed mutagenesis of *igo1*$^+$

5.1. Construction of the *igo1-4A* fission yeast mutant

The *igo1-4A-BE* DNA construction contained 1132 pb and was synthetically produced by Integrated DNA Technology (IDT). This DNA fragment contained *BamHI* and *EcoRI* restriction sites at the 5' and 3' ends, respectively, followed by sequences of the *igo1*$^+$ promoter, the *igo1-4A* sequence and the *igo1*$^+$ terminator regions. The *igo1-4A* sequence contained the *igo1*$^+$ ORF with the serines 31, 89, 102 and 118 codons replaced by alanine codons (Figure II.6, Results). This synthetic DNA was amplified using 5'-igo1-BamHI and 3'-igo1-EcoRI primers (Table 3), and the PCR product was subsequently purified and cloned into *pBluescriptKS*$^+$ to obtain *pBluescriptKS*$^+$*-igo1-4A-BE* (Table 4). For this purpose, the vector and the insert were digested with *BamHI* and *EcoRI* restriction enzymes overnight at 37 ºC. The vector digestion was then treated with alkaline phosphatase (CIAP, 20U/µl, Roche) to avoid plasmid religation. Digested molecules were purified and ligated using T4 DNA ligase (1U/µl, Thermo Scientific). Ligation reactions were incubated overnight at 16 ºC, and half of the reactions were used to transform *E. coli* competent cells. Plasmid DNA was isolated from transformants clones and digested with *BamHI* and *EcoRI* to confirm that it contained the *igo1-4A-BE* construction. These digestions were

purified and sequenced to check that the *igo1-4A-BE* construction did not contain additional mutations (Table 3).

The *igo1-4A-BE* construction was amplified with 5'-igo1-BamHI and 3'-igo1-EcoRI primers (Table 3), ethanol precipitated and used to transform *igo1::ura4+* fission yeast strain (Table 1). Transformed cells were recovered in MM plates supplemented with uracil. After one day of incubation at 25ºC, cells were replica plated to MM containing 0.1% FOA (Apollo Scientific) to select *S. pombe* transformants carrying the *igo1-4A* mutant allele. Positive clones were confirmed by PCR analysis followed by direct DNA sequencing of the PCR products (Table 3) and stored at -80ºC (Table 1).

5.2. Construction of *6His:igo1* and *6His:igo1-4A* mutants

6His-tagged Igo1 and 6His-tagged Igo1-4A proteins were used as substrates in Cdk1/CyclinB protein kinase assays. To generate the *6His:igo1-4A* construction, the *igo1-4A-NB* construction was synthetically generated by IDT. This 537 pb DNA molecule contained the mutagenised *igo1+* cDNA flanked by the *NdeI* and *BamHI* restriction sites. The mutagenised *igo1+* cDNA corresponded to the above-described *igo1-4A* sequence (Figure II.6, Results). This synthetic DNA fragment was amplified using igo1-NdeI and igo1-BamHI primers (Table 3) and subsequently purified. To clone the *igo1-4A-NB* construction into *pET·15b* (Table 4), the plasmid and the insert were digested with *NdeI* and *BamHI* restriction enzymes overnight at 37ºC, purified and ligated using T4 DNA ligase overnight at 16 ºC. The vector digestion was treated with alkaline phosphatase before ligation. Half of the ligation reaction was employed to transform *E. coli* competent cells. *pET·15b-igo1-4A-NB* was extracted from transformants clones, digested with *NdeI* and *BamHI* and sequenced to check the *igo1-4A-NB* construction. *pET·15b-igo1-4A-NB* was then purified from positive clones and used to transform *E. coli BL21* or *Rosetta™* competent cells (Table 2). Transformants carrying *pET·15b-igo1-4A-NB* were identified, further confirmed by PCR analysis followed by DNA sequencing (Table 3) and stored at -80ºC.

To obtain the *6His:igo1* construction, the *igo1+* cDNA flanked by the *NdeI* and *BamHI* restriction sites was previously cloned into *pET·15b* to generate pET·15b-*igo1cDNA* (Table 4). The vector and insert were digested, purified and ligated as mentioned above. Half of the ligation reaction was employed to transform *E. coli* competent cells. pET·15b-*igo1cDNA* was extracted from positive clones and employed to transform *E. coli BL21* competent cells (Table 2). Transformants carrying pET·15b-*igo1cDNA* were then confirmed by PCR analysis followed by DNA sequencing (Table 3) and stored at -80ºC.

The *pET·15b* vector carries an N-terminally His·Tag® sequence. By cloning *igo1+* and *igo1-4A* cDNAs into this plasmid, we were able to produce and purify 6His-tagged Igo1 and 6His-tagged Igo1-4A proteins.

6. Cell survival and cell viability assays

6.1. Cell survival measurement by methylene blue staining

Methylene blue (Sigma) was used to estimate the percentage of cell death under nitrogen starvation. For this purpose, cells grown in MM for one day were transferred to MM-N and kept under nitrogen starvation for 14-20 days. For each sample, 10^7 cells were harvested on the days indicated, washed with 200 µl of PBS and resuspended in 5 µl of a solution containing 2 µl of PBS and 3 µl of 0.4% methylene blue. Subsequently, 2.5 µl of cells were spread on a slide and observed under a microscope. Cell survival was expressed as the percentage of unstained cells. A total of 300 cells were counted.

6.2. Chronological lifespan assays

When *S. pombe* cells are deprived of nitrogen, they divide twice without growth and arrest in G1. If they meet a partner of the opposite mating type or switch mating type, they initiate sexual differentiation; otherwise, they enter quiescence. When nitrogen is replenished, quiescent cells are able to return to the vegetative cycle and divide. In this study, viability loss was monitored by measuring the chronological lifespan (CLS) of *S. pombe* cells after nitrogen starvation conditions. CLS can be defined as the time a yeast cell can survive in the non-dividing G_0 state also known as quiescence (Bähler et al., 1998; Hentges et al., 2005; Sato et al., 2005). In these assays, quiescent cells are plated out on nitrogen-rich medium, showing the mitotic competence or cell ability to restart the cell cycle.

6.2.1. Spot tests

Spot assays were used to qualitatively analyse the CLS of several fission yeast strains. For this purpose, cells were grown in MM for one day, shifted to MM-N and kept under nitrogen starvation for ten days. To monitor cell viability over time, cell samples were collected on the days indicated. 10^7 cells were harvested, resuspended in 120 µl of MM-N and serially diluted in MM-N using six ten-fold dilutions and a multichannel micropipette (Finnpipette, Thermo scientific). Finally, 4 µl of each dilution were plated out on YES, incubated for three days at 25ºC and scanned. When comparing different mutants, all drop assays were performed simultaneously.

6.2.2. Cell viability curves

To quantify the cell viability of *S. pombe* mutants, CLS assays were performed as described by Fabrizio et al., 2001. Briefly, cells grown in MM for one day were transferred to MM-N and incubated under nitrogen starvation for 20-22 days. To analyse cell viability over time, cell samples were collected on the days indicated and diluted in H_2O to plate 300 cells on three YES plates. After 3-6 days at 32ºC, the number of colonies formed were counted. To avoid cell aggregation, samples were softly sonicated for one minute in a Bioruptor® plus sonication device (Diagenode). Cell viability was expressed as the percentage of colonies formed against 300, the total number of cells plated in YES. For statistical analysis, each CLS assay was repeated three times. When comparing different mutants, all CLS assays were performed at the same time.

7. Mating efficiency assays

When nitrogen is scarce, fission yeast cells initiate sexual differentiation to form spores. To study the role of certain genes in this process, mating assays were performed on nitrogen-poor medium (MEA) or in nitrogen-free medium using a homothallic strain (h^{90}).

7.1. Mating analysis by iodine staining

Drop assays were employed to qualitatively analyse the sporulation rate of several fission yeast mutants. For this purpose, $5x10^6$ cells grown in MM were harvested and resuspended in 120 µl of distilled water. Cells suspensions were then serially diluted in water to generate 1:1, 1:4, 1:10, 1:20 and 1:50 dilutions. 4 µl of each dilution were plated out on MEA and incubated for 3-5 days at 25ºC to allow conjugation and sporulation to occur. Finally, formed colonies were exposed to iodine vapours for 20 minutes and scanned. Iodine vapours stain spore walls due to the presence of starch. Therefore, the spots containing more spores are stained darker, allowing to compare the sporulation phenotypes of different mutants. When comparing different mutants, all drop assays were performed simultaneously.

7.2. Mating efficiency assay

For quantitative mating assays, cells were grown in MM for one day, shifted to MM-N and kept under nitrogen starvation for 8-24 hours. Next, 10^7 cells were harvested, washed with

distilled water and fixed in 1 ml of 70% cold ethanol. 300 µl of each sample were rehydrated with PBS, centrifuged and resuspended in 10 µl of PBS. Lastly, 2.5 µl of cell suspension were spread on a slide and observed on a Nikon Eclipse 90i microscope. Mating efficiency was expressed as the proportion (%) of differentiated cells. It was calculated by dividing the number of zygotes and asci (one zygote/asci was counted as two differentiated cells) by the total number of cells. In all experiments, a total of 300 cells were counted. For statistical analysis, each mating assay was repeated twice. When comparing different mutants, all experiments were carried out at the same time.

8. Microscopy techniques

8.1. Bright-field microscopy

An Olympus BX60 microscope with 20x, 10x and 4x LMPlanFI objectives was routinely used to observe cells in liquid or solid media. An Olympus C-5050 digital camera coupled to the microscope was used to obtain images.

8.2. Differential interference contrast (DIC) and fluorescence microscopy

A Nikon Eclipse 90i microscope equipped with a halogen lighting system and an ORCA ER (Hamamatsu) camera was used for nuclear morphology, mating efficiency and cell size measurement assays. Cells were visualised with a 60x or 100x Plan Apo-Chromat VC oil objective, and images were captured with MetaMorph® software (Molecular Devices). Methylene blue staining was analysed in a Leica DM RXA microscope equipped with an ORCA ER (Hamamatsu) camera. Cells were observed with a 63x Plan Apo-Chromat VC oil objective, and images were acquired with Cw4000 Cytofish software (Leica Microsystems).

8.3. Cell size measurements

The cell size of wild-type and igo1-4A cells was measured in cells stained with blankophor (Bayer). For this purpose, cells were grown in MM and MMF to mid-log phase. Subsequently, a 200 µl cell sample was taken, washed in PBS, resuspended in 2 µl of PBS and 3 µl of 50 µg/ml blankophor and observed under a Nikon Eclipse 90i microscope. After image acquisition, cell size was determined in ImageJ by measuring the cell length of 100 septated cells, since cells undergoing mitosis and cytokinesis do not vary in cell size. Average cell length and standard deviations were determined in 100 cells. Cell size measurements were repeated three times for statistical analysis.

8.4. Nuclear morphology assay

8.4.1. DAPI staining

Cells grown in MM for one day were shifted to MM-N and kept under nitrogen starvation for 12 days. For monitoring changes in nuclear morphology over time, samples were collected at different days of the incubation in MM-N. For each sample, 10^7 cells were centrifugated, washed with 1 ml of distilled water and fixed in 1 ml of 70% cold ethanol. 300 µl of each sample were then rehydrated with PBS, centrifuged and resuspended in 6 µl of a solution containing 5 µl of PBS and 1 µl of 0.1 mg/ml DAPI (Sigma). Finally, 2.5 µl of cell suspension were spread on a slide and observed under a microscope.

For analysis, nuclei were categorised into four groups depending on their morphology. Changes in nuclear morphology were expressed as the percentage of each nuclear group and calculated by dividing the number of nuclei of each group by 300 (total of counted nuclei). For statistical analysis, each assay was repeated twice. Moreover, when comparing different mutants, all experiments were carried out simultaneously.

8.4.2. Nuclei observation using the *aur-mcherry:atb2+ hht2:GFP* genetic background

For *in vivo* observation of *S. pombe* nuclei, an *aur-mcherry:atb2+ hht2:GFP* genetic background was used. Cells were grown in MM for one day, transferred to MM-N and kept under nitrogen starvation for 12 days. Samples were collected at different time points after the shift to monitor nuclear changes over time. For each sample, $5x10^5$ cells were centrifuged, spread on a slide and observed under a microscope.

For analysis, nuclei were classified as in DAPI staining, and changes in nuclear morphology were also expressed as the percentage of each nuclear group. When comparing different mutants, all experiments were performed at the same time.

9. Fluorescence-activated cell sorting (FACS)

Cell-cycle distribution of several *S. pombe* mutants was analysed by flow cytometry. Experiments were carried out following a protocol described by Sazer and Sherwood, 1990 and an adapted method from Knutsen et al., 2011.

10^7 cells were centrifuged and fixed using 1 ml of 70% cold ethanol. 300 µl of each sample were washed twice with a solution of 50 mM of sodium citrate, resuspended in 500 µl of RNAse solution (50 mM of sodium citrate containing 100 µg/ml RNase) and incubated overnight at 37 ºC. Subsequently, cells were centrifuged again and resuspended in 500 µl of propidium iodide solution (50 mM of sodium citrate and 4 µg/µl of propidium iodide). Cell suspensions were sonicated for 20 seconds with a Labsonic M sonicator (Sartorius) at 40% amplitude. Finally, samples were examined in a FACSCalibur BD cytometer using the BD Cell Quest ProTM 6.0.3 (Biosciences) data acquisition and analysis software. A total of 10^5 events were analysed. FL2-A and FL2-W were employed to measure DNA content and FSC for cell size.

10. Protein analysis

10.1. Western Blot detection

10.1.1. Protein extraction under denaturing conditions

Protein extraction was carried out using trichloroacetic acid (TCA) and following a modified version of the protocol described by Foiani et al., 1994.

$2x10^8$ cell samples were harvested and washed with 1 ml of 20% cold TCA. They were then resuspended in 50 µl of 20% TCA and frozen at -20 ºC. For protein extraction, 500 µl of glass beads (4mm, Sartorius) were added to previously thawed samples, and cells were lysed in a Fast-prep (Bio-101) using three 15-second cycles of 5.5 speed. Subsequently, 400 µl of 5% TCA was added to lysates. They were vortexed and transferred to a clean tube by drilling a hole at the bottom of the tube and centrifuging into another tube for 10 seconds at 7000 rpm. Next, samples were spun down for 10 minutes at 3000 rpm. Supernatants were mixed with 200 µl of a SDS-Tris base solution containing 60 µl of 10% SDS and 40 µl of 1M Tris-base and boiled for 5 minutes. Finally, samples were centrifuged for 2 minutes at 13200 rpm and supernatants were frozen at -20 ºC.

10.1.2. Determination of protein concentration

1 µl of each protein extract was separated before freezing to determine the protein concentration using the Pierce™ BCA Protein Assay kit (Thermo Scientific). A standard curve was prepared utilising known concentrations of bovine serum albumin (BSA). A colorimetric reaction determined the concentration of protein extracts. Absorbance was measured at 537 nm in a Multiskan SkyHigh Microplate spectrophotometer (Thermo Scientific).

10.1.3. SDS-PAGE protein electrophoresis

Protein separation was carried out in SDS-polyacrylamide gels (King and Laemmli, 1971). Protogel® 30% solution (37.5 volumes of acrylamide to 1 volume of bisacrylamide, National Diagnostics) was used to prepare gels. Gel percentage varied from 10% to 15% depending on the size of the proteins to be analyse. When analysing samples for mass spectrometry, 4-12% polyacrylamide gels (NuPAGE Bis-Tris Gels, Thermo Scientific) were employed. Firstly, protein extracts were boiled for 5 minutes and centrifuged for 2 minutes at 13200 rpm. The loading buffer used was 2x SB (80 mM Tris-HCl pH 6.8, 5 mM DTT, 2% SDS, 7.5% glycerol, 5 mM EDTA and 0.002% bromophenol blue). The amount of protein and final volume depended on the protein to be studied. Electrophoresis were run in running buffer (25 mM Tris, 192 mM glycine and 0.1% SDS). Protein stacking was performed with constant voltage (100 V), whereas 20 mA were used for protein separation. The PageRuler™ Prestained Protein Ladder (Thermo Scientific) was employed to determine the molecular weight of the proteins. Mini-Protean II (BioRad) or XCell SureLock Mini-Cell (Life Technologies) tanks were used for electrophoresis.

10.1.4. Western blotting on PVDF membranes

After gel electrophoresis, proteins were transferred to Polyvinylidene fluoride (PVDF) membranes using transfer buffer (10 mM CAPS pH 11 and 10% ethanol). Transfers were performed with constant current (300 mA) for two hours. Transfer tanks were placed on ice to dissipate the heat produced. Membranes were stained with Ponceau (BioRad) for 10 minutes to assess the quality of each transfer. Subsequently, membranes were incubated in blocking solution (20mM Tris-base-NaCl pH 7.5, 150mM NaCl, 5% non-fat powdered milk (Nestle) and 0.05% Tween20) for at least one hour. They were then probed with the appropriate primary antibody diluted in blocking solution (Table 5). For protein detection, blots were exposed to anti-mouse IgG-horseradish conjugated antibody (Amersham) for 45 minutes at room temperature. Three wash steps with TBST buffer (20mM Tris-base-NaCl pH 7.5, 150mM NaCl and 0.05% Tween20) were carried out between incubations to remove excess unbound material and minimise non-specific signal on membranes. Armersham detection kits (ECL™ Western Blotting Detection reagents, GE Healthcare) and Agfa development films were employed for chemiluminescent detection. For protein loading control, membranes were incubated with anti-tubulin TAT1 antibody (Table 5).

When protein samples were analysed for mass spectrometry, transfers were carried out in iBlot 2 Dry Blotting System (ThermoFisher) at 20 V for 6-9 minutes. Membranes were then blocked with a 1:1 blocking solution of PBS-0.1% Tween20 and Odyssey® blocking solution for one hour at room temperature. Subsequently, blots were incubated for 45 minutes with IRDye® 680RD Streptavidin diluted in blocking buffer (Table 6). Finally, protein fluorescence was detected using an Odyssey® CLx imaging system.

10.2. Antibodies

Table 5 and Table 6 list the antibodies and fluorescent dyes used in this work. Source and other details are also included in the table.

Table 5. Antibodies used.

Name	Organism	Type	Conditions	Source
anti-Igo1 (C-terminus)	Rabbit	Polyclonal	WB 1:200 o/n² 4ºC	S. Moreno
anti-P-S64-Igo1	Rabbit	Polyclonal	WB 1:100 o/n² 4ºC	S. Moreno

C2 anti-Cdc2 serum	Rabbit	Polyclonal	IP 5µg 1 h 4ºC	S. Moreno
SP4 anti-Cdc13 serum	Rabbit	Polyclonal	IP 5µg 1 h 4ºC	S. Moreno
anti-GFP (JL-8)	Mouse	Monoclonal	WB 1:3000 o/n[2] 4°C	Clontech
anti-c-Myc (clon9E10)	Mouse	Monoclonal	WB 1:3000 o/n[2] 4°C IP 2.5 µg 1h 4ºC	Sigma
anti-HA (12CA5)	Mouse	Monoclonal	WB 1:5000 o/n[2] 4°C IP 2.5 µg 1h 4ºC	Roche
anti-tubulin TAT1	Mouse	Monoclonal	WB 1:3000 2 h RT[1]	K. Gull
anti-IgG-mouse	Sheep	Polyclonal	WB 1:2500 45' RT[1]	Amersham
anti-IgG-rabbit	Donkey	Polyclonal	WB 1:2500 45' RT[1]	Amersham

Table 6. Infrared fluorescent dyes used.

Name	$Absorption_{max}$	$Emission_{max}$	Conditions	Source
IRDye® 680RD Streptavidin	676 nm	694 nm	WB 1:5000 45' RT[1]	LI-COR

[1]RT (room-temperature), [2]o/n (overnight)

10.3. Protein immunoprecipitation

10.3.1. HBH purification

Cells were grown in 4 l of MM to mid-log phase. Subsequently, 2 l of the culture were transferred to MM-N. After 30 minutes incubation in nitrogen starvation, MM and MM-N grown cells were harvested by centrifugation and frozen at -80 ºC.

HBH-tagged Igo1 was purified using a modified version of a two-step tandem affinity purification protocol under denaturing conditions (Tagwerker et al., 2006). Briefly, cell pellets were lysed by bead disruption in 100 ml of buffer 1 (8 M urea, 0.5% NP-40, 300 mM NaCl, 50 mM NaH_2PO_4, 50 mM Na_2HPO_4 and 20 mM imidazole) using a bead beater (Biospec Products Inc.) and cleared by centrifugation (10 minutes at 3000 rpm, 4 ºC). Supernatants were mixed with 4 ml of 50% slurry Ni-NTA resin equilibrated in buffer 1 and incubated for 4 hours on a nutator. Samples were then spun down for 3 minutes at 2000 rpm and washed twice with 40 ml of buffer 1, twice with 40 ml of wash buffer 2 (8 M urea, 0.5% NP-40, 300 mM NaCl and 50 mM NaH_2PO_4) and once with 40 ml of wash buffer 3 (8 M urea, 0.5% NP-40, 300 mM NaCl, 50 mM NaH_2PO_4 and 20 mM imidazole). Next, samples were eluted twice with 20 ml of buffer 4 (8 M urea, 0.5% NP-40, 300 mM NaCl, 50 mM NaH_2PO_4, 2% SDS, 100 mM Tris and 10mM EDTA). After adjusting the pH to 8, samples were mixed with 800 µl of 50% slurry Streptavidin Ultralink Immobilised beads (Pierce, Rockford, IL) equilibrated with buffer 7 (8 M urea, 200 mM NaCl, and 100 mM Tris) and nutated overnight at room temperature. Samples were centrifuged, and pellets were washed twice with 5 ml of wash buffer 5 (8 M urea, 200 mM NaCl, 0.2% SDS and 100 mM Tris), once with 5 ml of wash buffer 6 (8 M urea, 200 mM NaCl, 2% SDS and 100 mM Tris) and twice with 5 ml of wash buffer 7 (8 M urea, 200 mM NaCl and 100 mM Tris). Purified Igo1:HBH protein was digested off beads for mass spectrometry analysis. A small bead sample was analysed by immunoblotting to check that the Igo1:HBH protein was properly purified.

Before carrying out the large-scale purification for mass spectrometry analysis, Igo1-HBH fusion protein was immunoprecipitated from 30 ml YES cultures and analysed by western blotting using IRDye® 680RD Streptavidin (Table 6).

10.3.2. GFP-TRAP purification

GFP-tagged proteins were purified from *S. pombe* cultures of 8 l of *S. pombe* cells. Firstly, cells were grown in 16 l of MM. After one day of incubation, half of the culture was shifted to MM-N and kept under nitrogen starvation for 30 or 60 minutes. Subsequently, cells were harvested by centrifugation and frozen at -80 ºC.

Cells were lysed using glass beads and a bead beater in 100 ml of NP-40 buffer (6mM Na_2HPO_4, 4 mM NaH_2PO_4, 1% NP-40, 150 mM NaCl, 2 mM EDTA, 50 mM NaF and 0.1 mM Na_3VO_4) supplemented with Complete EDTA-free Protease inhibitor cocktail (Roche), 1.3 mM benzamidine (Sigma) and 1 mM PMSF (Sigma). Lysates were cleared by centrifugation, and supernatants were mixed with 60 µl of 50 % slurry GFP-TRAP magnetic agarose beads (GFP-Trap® magnetic agarose, ChromoTek) equilibrated with NP-40 buffer. After 90 minutes of incubation at 4ºC, beads were magnetically separated from lysates and washed twice with 5 ml of NP-40 buffer. Samples were washed with 5 ml of low-NP-40 buffer (0.02% NP-40) to reduce total detergent in purified proteins and subsequently resuspended in 1 ml of low-NP-40 buffer. Proteins were eluted twice with 150 µl of elution buffer (200 mM glycine-HCl pH 2.5) and precipitated for 30 minutes on ice using 100 µl of 100% TCA. Samples were then spun down for 30 minutes at 13000 rpm and 4 ºC, washed with 1 ml of cold acetone containing 0.05 N HCl and 1 ml of cold acetone. Finally, pellets were dried at room temperature and stored at 4ºC for mass spectrometry analysis. A small amount of each sample was used to confirmed proper purification of GFP-tagged proteins. For that purpose, the Plus One Silver Staining protein kit (GE Healthcare) was employed following manufacturer instructions.

Before carrying out the large-scale purifications for mass spectrometry analyses, GFP-fusion proteins were immunoprecipitated from 30 ml YES cultures and analysed by western blotting using anti-GFP antibody (Table 5).

10.3.3. Recombinant protein purification

Plasmids encoding 6His-fused Igo1 and 6His-fused Igo1-4A protein were transformed into *E. coli* competent cells (BL21 or Rosetta™) by standard heat shock protocol. Transformants were selected on LB plates containing 50-100 µg/ml of ampicillin. 350 ml of cells were grown until they reached OD_{600} of 06-0.8 in LB with ampicillin, and protein expression was induced with 0.4 mM IPTG overnight at 16 ºC. Subsequently, cells were harvested and frozen at -80ºC. Bacterial pellets were thawed on ice and resuspended in 20 ml of lysis buffer (50 mM Tris-HCl pH 7.9, 5 mM imidazole, 500 mM NaCl and 0.1% Triton X-100) with 6 µl/ml of lysozyme (Roche). After 20 minutes of incubation on ice, samples were lysed by sonication (4 cycles at 70% amplitude, 30 seconds on, 30 seconds off, on ice) with a Labsonic M sonicator (Sartorius) and centrifuged at 12000 rpm for 20 minutes at 4ºC. Supernatants were mixed with 1 ml of 50% slurry His-resin (Roche) equilibrated in lysis buffer and incubated at 4ºC for 2 hours on a nutator. Samples were spun down for 5 minutes at 4ºC and washed three times with lysis buffer. Subsequently, proteins were eluted with 1.5 ml of elution buffer (50 mM Tris-HCl pH 7.9, 500 mM imidazole, 500 mM NaCl and 5 mM 2-BME) for 15 minutes at 4ºC. Finally, supernatants were dialysed against a solution of 20 mM Tris-HCl pH 7.5, 150mM NaCl, 1mM DTT and 10% glycerol.

10.3.4. Co-immunoprecipitation

$3x10^8$ cells expressing the indicated fusion proteins were harvested by centrifugation. Pellets were washed once with 10 ml of cold stop buffer (0.9% NaCl, 50mM NaF, 1mM NaN_3 and 10 mM EDTA), spun down and subsequently frozen at -80ºC. Cells were lysed using a Fast-Prep

(3 cycles at 5.5 speed, 15 s on, 15 s off) in HB buffer (25 mM MOPS pH 7.2, 60 mM ß-glycerophosphate, 0.1 mM Na-Vanadate, 15 mM $MgCl_2$, 1 mM DTT, 1% TritonX-100, 15 mM p-NPP and 5 mM EGTA) supplemented with Complete EDTA-free Protease inhibitor cocktail (Roche), 1 mM PMSF and 1.3 mM benzamidine. Lysates were cleared by centrifugation, and Pab1:3HA and Mst2:13Myc proteins were immunoprecipitated with Dynabeads Protein G (Thermo Scientific) equilibrated in HB buffer and bound to 2.5 µg of anti-HA and anti-Myc antibodies (Table 5), respectively. After one hour of incubation on a rotating wheel at 4ºC, beads were washed three times with 500 µl HB buffer, and proteins were then eluted twice in 30 µl of elution buffer (200 mM glycine-HCl pH 2.5). Co-immunoprecipitated Pab1:HA or Mst2:13Myc was determined by immunoblot analysis using anti-HA and anti-Myc antibodies (Table 5), respectively.

GFP-TRAP purification was also used for co-immunoprecipitation experiments. Briefly, 40 ml of cells overexpressing *GFP:pab1* construction (*P41nmt1:GFP:pab1+*) were harvested and subsequently frozen at -80ºC. Lysates were prepared as mentioned above, and GFP-tagged Pab1 was purified using 40 µl of 50% slurry GFP-TRAP magnetic agarose beads equilibrated in HB buffer. After 90 minutes of incubation at 4ºC, beads were washed three times with 1 ml of HB buffer and proteins were then eluted twice in 30 µl of elution buffer. Co-immunoprecipitated Mst2:13Myc was analysed by immunoblotting using anti-Myc antibody.

10.4. Mass spectrometry

To map the phosphorylation sites on Igo1 and to identify binding partners of Igo1 and Pab1 proteins, 2D LC-MS/MS was used. Samples were outsourced to Dr. K. Gould's group at Vanderbilt University, where proteins were digested using trypsin, elastase and quimiotrypsin (Promega, Madison, WI). Mass spectrometry (MS) was carried out according to McDonald et al., 2002 and following modifications described by Roberts-Galbraith et al., 2009. Peptides were loaded onto columns using a pressure cell and separated by three-phase multidimensional protein identification technology on a linear trap quadrupole instrument (Thermo Electron). For analysis, peptides eluted directly into an LCQ ion trap tandem mass spectrometer (Thermo-Finnigan).

11. Cdk1 protein kinase assay

The Cdk1/CyclinB complex was immunoprecipitated from metaphase arrested *nda3-KM311 S. pombe* cells. These cells were grown at 32ºC in YES and then transferred for 6 hours at 20ºC. $3x10^8$ cells were harvested, washed once with 10 ml of ice-cold stop buffer (150 mM NaCl, 50 mM NaF, 10 mM EDTA, 1 mM NaN_3 pH 8) and lysed using a Fast-Prep (3 cycles at 5.5 speed, 15 s on, 15 s off) in 40 µl of HB buffer supplemented with Complete EDTA-free Protease inhibitor cocktail (Roche),1 mM PMSF and 1.3 mM benzamidine. Lysates were resuspended in 400 µl of HB supplemented with protease inhibitors, cleared by centrifugation at 13.200 rpm at 4ºC, and supernatants were incubated with 5 µl of C2 anti-Cdc2 or SP4 anti-Cdc13 serums on ice for one hour (Table 5). Samples were then mixed with 60 µl of 50% slurry A/G agarose (Santa Cruz) equilibrated in HB buffer and incubated for 50 minutes on a rotating wheel at 4ºC. Beads were washed five times with 800 µl of HB buffer and twice with 800 µl of kinase buffer (20 mM HEPES pH 7.6, 10 mM $MgCl_2$, 3 mM BME). We also used Cdk1 kinase-active and kinase-inactive versions previously expressed and purified from insect cells (Dr. K. Gould's group).

Kinase assays were performed by incubating the Cdk1 kinase (300 ng or 1/3 of the IP) with 30 µl of kinase buffer supplemented with 50 µM ATP, 5 µCi of γ-^{32}P-ATP and 2 µg of purified 6His-Igo1 or 6His-Igo1-4A at 30ºC for 30 minutes. Reactions were stopped by adding 5x SB and boiling for 5 minutes. Samples were run on 13% or 4-12% polyacrylamide gels. Gels were then dried and exposed to X-ray films at room temperature or -80 ºC. Purified recombinant Imp2 protein (Dr. K. Gould's group) or Histone H1 (Calbiochem®) were used as positive controls.

12. Computing analysis

12.1. Sequence analysis

DNA and protein sequences were obtained from Pombase (https://www.pombase.org/) and UniProt (http://www.uniprot.org/) databases and analysed with Seqman (DNAstar Inc.) and SnapGene Viewer (SnapGene®) software. To align protein sequences, Clustal W2 (http://www.ebi.ac.uk/Tools/msa/clustalw2/) software was used.

12.2. Statistical analysis

Prism 6 (GraphPad Softwware, Inc.) software was employed for all statistical analyses. Comparison between strains was accomplished using one-way or two-way ANOVA.

12.3. Mass spectrometry analysis

Mass spectrometry analysis was performed as previously described by Chen et al., 2013b. Briefly, spectral data were searched using the SEQUEST algorithm (TurboSequest v.27 rev12) against the fission yeast protein database (https://www.pombase.org/). Peptide identifications were filtered and assembled in Scaffold (Proteome Software, version 4.8.4). Phosphorylation sites were identified using Scaffold PTM (version 3.1.0). Results were exported to Excel for further filtering: contaminant proteins (e.g., keratin) and nonspecific proteins (identified in GFP preparations from a strain lacking the GFP tag) were removed.

12.4. Writing, figures and graphs

All graphs included in this work were made on Prism 6 (GraphPad Software, Inc.). Microscopy images were processed with ImageJ (http://rsbweb.nih.gov/ij/) and edited using Photoshop CS5 (Adobe). HP Scanjet G4050 was used for image scanning. Bibliographic references were obtained from Pubmed-NCBI database (http://www.ncbi.nlm.nih.gov/pubmed) and organised with Mendeley software (Elsevier). Microsoft Word 2016 (Microsoft Corporation) was used for word processing, while figures were laid out in Illustrator CS5 (Adobe) or PowerPoint 2016 (Microsoft Corporation).

Objectives

The main objective of this thesis is to study the molecular mechanisms involved in the regulation of the Greatwall-Endosulfine-PP2A/B55 pathway in fission yeast. In particular:

I. To examine its implication in the regulation of the G1 arrest that occurs under nitrogen-starvation conditions.

II. To dissect its involvement on the sexual differentiation response.

III. To analyse the role of this pathway in ageing.

IV. To characterise the phosphorylation changes that regulate Endosulfine activity.

V. To identify potential new targets of Endosulfine and B55 proteins.

Results

Chapter I: Roles of the fission yeast Greatwall-Endosulfine-PP2A/B55 pathway in G1 arrest, cell differentiation and ageing

1. The Greatwall-Endosulfine-PP2A/B55 pathway is required for G1 arrest under nitrogen starvation

1.1. The Greatwall-Endosulfine molecular switch promotes G1 arrest under nitrogen deprivation

When *S. pombe* cells are deprived of nitrogen, they undergo two rounds of cell division, reducing cell size and eventually arresting in G1 (Figure 2, Introduction). If they meet a partner of the opposite mating type or switch mating type (homothallic h^{90}), they initiate the sexual differentiation response (Nurse and Bissett, 1981); otherwise, if they are heterothallic, they enter a differentiated G_0-like state, called quiescence (Su et al., 1996). Our group has recently shown that the Greatwall-Endosulfine module promotes entry into mitosis upon nutritional shift-down (Chica et al., 2016). In nitrogen-rich media, TORC1 activity is high, promoting the inhibition of Greatwall-Endosulfine activity. Consequently, PP2A/B55 is active and counteracts Cdk1/CyclinB activity, delaying mitosis. On the contrary, when cells are transferred to nitrogen-poor media, TORC1 activity drops leading to Greatwall activation, Endosulfine phosphorylation and PP2A/B55 inhibition, accelerating entry into mitosis.

Since the Greatwall-Endosulfine module takes part in regulating the G2/M transition when nitrogen is limiting, we wondered if it might also play a role in the cellular response to nitrogen starvation. To address this hypothesis, we shifted cells from minimal medium (MM) to minimal medium without nitrogen (MM-N) and analysed the cell-cycle distribution by flow cytometry. Unlike wild-type cells, that divided and arrested in G1, cells lacking Endosulfine (*igo1Δ*) were unable to arrest in G1, even after 24 hours in MM-N (Figure I.1), suggesting that Igo1 is crucial for G1 arrest under nitrogen starvation. When we deleted *cek1⁺*, *ppk18⁺* or *ppk31⁺* genes, which are the fission yeast kinases with the highest homology degree to metazoan Greatwall, various phenotypes were obtained. Whereas *cek1⁺* or *ppk31⁺* deletion mutants (*cek1Δ* or *ppk31Δ*) behaved similarly to the wild-type, cells lacking *ppk18⁺* (*ppk18Δ)* showed a delayed nitrogen-starvation response, as the 1C-G1 population did not appear until 8 hours in MM-N (Figure I.1). Only when we combined *cek1⁺* and *ppk18⁺* deletions (*cek1Δ ppk18Δ)*, the phenotype was similar to that of the *igo1Δ* mutant, hinting that Ppk18 promotes G1 arrest under nitrogen deprivation and that Cek1 could be significant in its absence. Furthermore, the triple deletion mutant (*cek1Δ ppk18Δ ppk31Δ*) displayed a similar phenotype to that of *cek1Δ ppk18Δ* cells, indicating that deletion of *ppk31⁺* has no additive effect.

We have also reported that moderate overexpression of *ppk18⁺* promoted entry into mitosis, generating small cells with a 1C DNA content in MM (Chica et al., 2016). Consistent with those observations, cells expressing *ppk18⁺* from the *nmt41* promoter (*P41nmt1:GFP:ppk18⁺*) showed a 1C-G1 population even in nitrogen-rich medium (Figure I.2), and they also arrested more readily in G1 (Figure I.2) under nitrogen starvation.

These results are consistent with the idea that the Greatwall-Endosulfine module is required to promote mitotic entry and G1 arrest under nitrogen starvation.

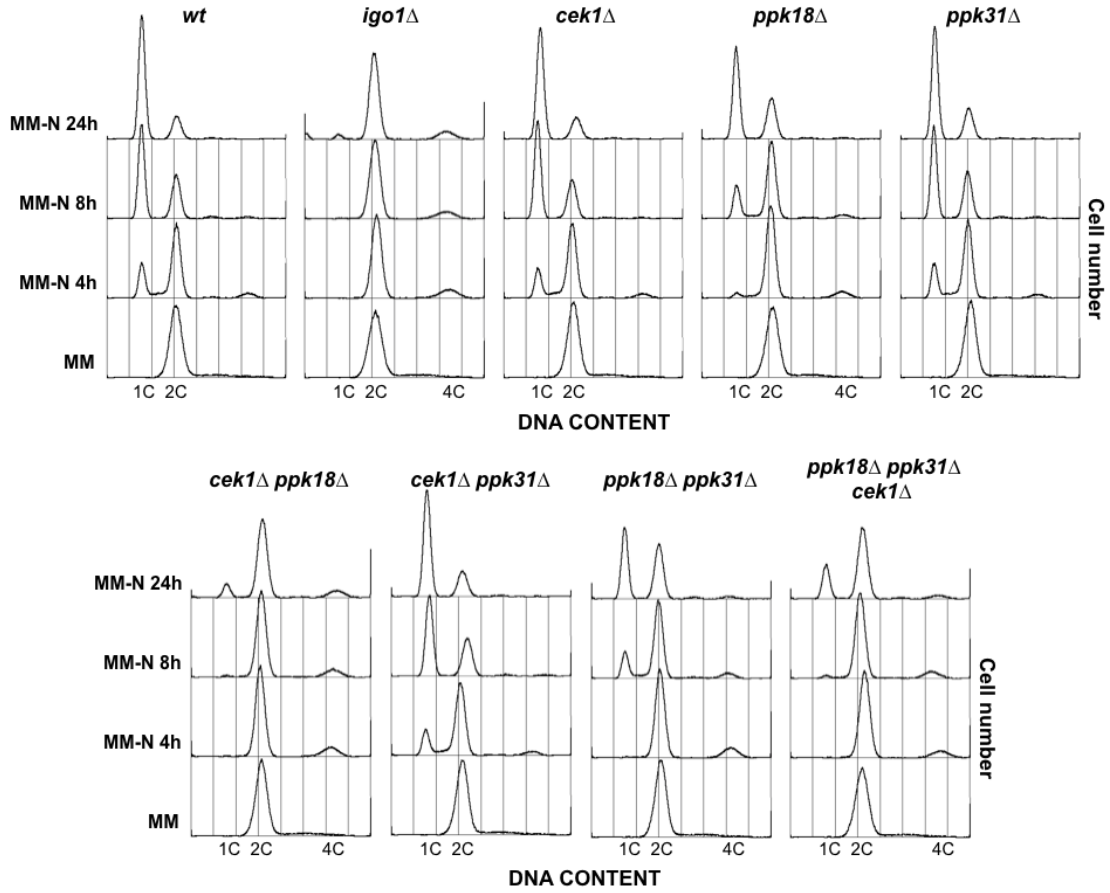

Figure I.1. The Greatwall-Endosulfine module is required for G1 arrest under nitrogen starvation. FACS (DNA content, 1C and 2C) profile of ethanol-fixed cells stained with propidium iodide. Cells were grown in nitrogen-rich medium (MM) for one day at 25ºC and then transferred to minimal medium without nitrogen (MM-N) at the same temperature. Samples were collected at the indicated time points after the shift.

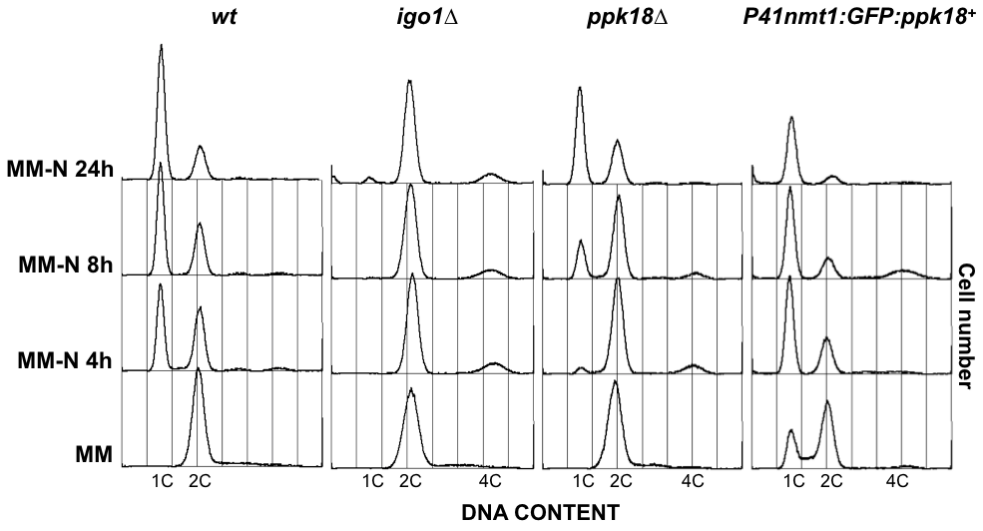

Figure I.2. Moderate overexpression of *ppk18+* promotes mitotic entry and G1 arrest under nitrogen starvation. Wild-type, *igo1Δ* and *ppk18Δ* strains, and mutant cells containing one copy of the nmt1 promoter (version 41) integrated upstream from *ppk18+* open reading frame were grown in MM for one day at 25ºC, and then shifted to MM-N at the same temperature. FACS profile (DNA content, 1C and 2C) of ethanol-fixed cells stained with propidium iodide. Samples were collected at the indicated time points after the shift.

1.2. PP2A/B55 inhibition by the Greatwall-Endosulfine molecular switch is crucial for G1 arrest under nitrogen starvation

In *S. pombe*, two genes, *ppa1⁺* and *ppa2⁺*, encode the catalytic subunit of PP2A phosphatase, and one gene, *pab1⁺*, the B55 regulatory subunit (Kinoshita et al., 1996, 1990). When we analysed the cell-cycle distribution of cells lacking *ppa2⁺* or those with reduced levels of *pab1⁺*, we observed that these mutants were able to arrest more readily in G1 (Aono et al., 2019) (Figure I.3), suggesting a negative role of PP2A/B55 in the nitrogen-starvation response. Furthermore, deleting the *ppa2⁺* gene or reducing the expression of *pab1⁺* completely rescued the G1 arrest defect of the *igo1Δ* mutant.

All these data suggest that the fission yeast Greatwall-Endosulfine module promotes G1 arrest under nitrogen starvation by inhibiting the PP2A/B55 phosphatase complex.

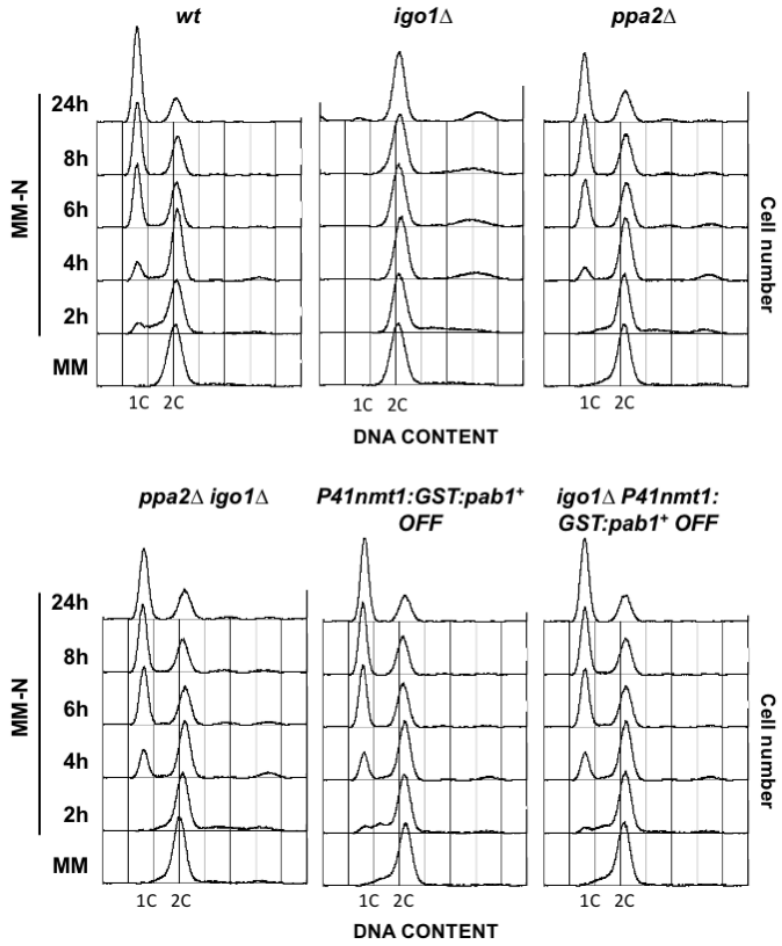

Figure I.3. Lowering the expression of *pab1⁺* or deleting *ppa2⁺* rescued the G1 arrest defect of *igo1Δ* mutant under nitrogen starvation. FACS profile (DNA content, 1C and 2C) of ethanol-fixed cells stained with propidium iodide. Cells containing a copy of the P41nmt1 promoter integrated upstream from *pab1⁺* ORF in *igo1⁺*, and *igo1Δ* genetic backgrounds, and wild-type, *igo1Δ*, *ppa2Δ* and *igo1Δ ppa2Δ* strains were grown in MM for one day and then shifted to MM-N. Thiamine was added to the media to repress *pab1⁺* expression. Samples were collected at the indicated time points after the shift.

2. The Greatwall-Endosulfine-PP2A/B55 pathway is required for cell differentiation

In *S. pombe*, the transition from cell proliferation to cell differentiation is tightly controlled by nitrogen. In the presence of nitrogen, fission yeast cells grow and divide. Nevertheless, when

nitrogen concentration drops below a certain level, the differentiation programme is triggered, and cells undergo mating, meiosis and sporulation (Yamamoto, 1996). Moreover, G1 arrest is essential for the differentiation process, since only G1 cells can differentiate and therefore, mate and form spores to survive when nutrients are scarce. In fission yeast, both TORC1 and TORC2 complexes regulate cell differentiation. While inactivation of TORC1 triggers the mating response (Alvarez and Moreno, 2006; Uritani et al., 2006), deletion of *tor1⁺* (TORC2) or its target *gad8⁺* causes sterility (Weisman & Choder, 2001). Interestingly, recent research has shown that the transition from cell growth to cell differentiation in response to nitrogen starvation is regulated by PP2A/B55 complex (Laboucarié et al., 2017) through the dephosphorylation of Gad8 (Martín and López-Áviles, 2018; Martín et al., 2017).

Giving all this evidence, we wondered if the Greatwall-Endosulfine molecular switch might also be necessary for the differentiation response.

2.1. Greatwall and Endosulfine promote the cell differentiation response upon nutritional shift-down

To address the hypothesis mentioned above, we first studied the mating efficiency of Greatwall and Endosulfine mutants upon nutritional shift-down. Haploid homothallic cells (*h⁹⁰*) were grown in MM for one day and then transferred to nitrogen-poor medium (malt extract agar, MEA), which allowed conjugation and sporulation to occur. We observed that cells lacking *igo1⁺* showed a reduction in the frequency of mating and sporulation of approximately 50% compared to wild type cells (Chica et al., 2016) (Figure I.4 B). This phenotype is consistent with the G1 arrest defects observed in the *igo1Δ* mutant and suggests that Endosulfine might play a key role in regulating the differentiation response in fission yeast. The sporulation efficiency was also analysed using iodine vapours, which stain spore walls allowing rapid identification of mutants with mating defects. Unlike *cek1⁺* or *ppk31⁺* deletion mutants, that exhibited hyperfertile phenotypes, cells lacking *igo1⁺* displayed a severe reduction in the iodine staining, and cells deleted for *ppk18⁺* showed little staining (Figures I.5 B and I.5C), which indicated that these mutants were unable to sporulate. Only combining *cek1⁺* and *ppk18⁺* deletions the phenotype was similar to that of the *igo1Δ* mutant (Figure I.5 C). Furthermore, moderate overexpression of *ppk18⁺* became more stained than wild-type cells (Figure I.5 D). Taken together, this data suggested a positive role of Ppk18 and Igo1 in the differentiation response when nitrogen is limited, and that Cek1 could play a partially redundant function with Ppk18.

These results hint that the fission yeast Greatwall-Endosulfine module is required for the cell differentiation response upon nitrogen shift-down.

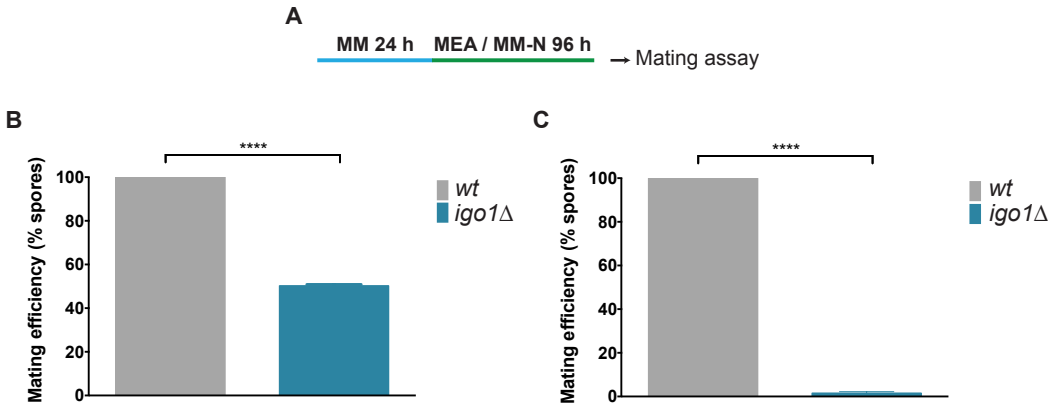

Figure I.4. Endosulfine is required for the sexual differentiation response in nitrogen-poor media and under nitrogen starvation. Mating efficiency assays. Wild-type and *igo1Δ* cells were grown in MM and then shifted to nitrogen-poor medium (MEA) or nitrogen starvation (MM-N). Cultures were diluted to plate

appoximately 500 spores on nitrogen-rich medium (YES) and incubated until colonies were formed. Mating efficiency was expressed as the number of grown colonies against 500. **A.** Procedure employed in the mating efficiency assays. **B.** Mating efficiency assay in MEA. **C.** Mating efficiency assay in MM-N.

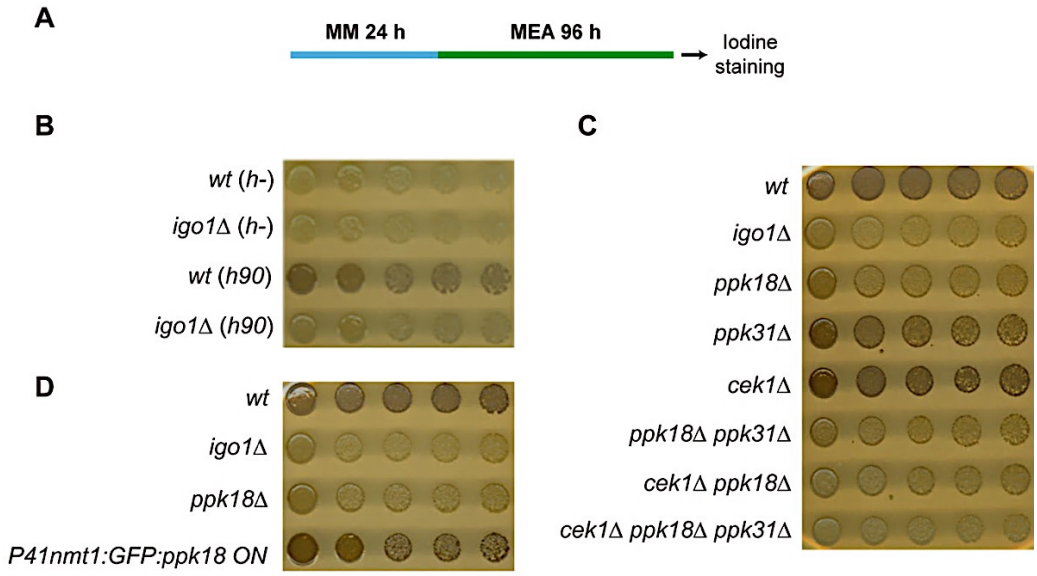

Figure I.5. The Greatwall-Endosulfine module promotes the sexual differentiation response upon nutritional shift-down. Sporulation assay using Iodine vapours. Cells were grown in MM, serially diluted (1:1, 1:4, 1:10, 1:20 and 1:50) and plated out on MEA. Plates were incubated for 3-5 days and then exposed to iodine vapours for 20 minutes. **A.** Procedure employed in the sporulation assays. **B.** Sporulation assay of heterothallic and homothallic wild-type and *igo1Δ* cells. **C.** Sporulation assay of homothallic wild-type and Greatwall and Endosulfine deletion mutants. **D.** Sporulation assay of homothallic wild-type, *igo1Δ* and *ppk18Δ* strains, and cells moderately overexpressing *ppk18+* from the nmt41 promoter.

2.2. The Greatwall-Endosulfine-PP2A/B55 pathway is required for the cell differentiation response under nitrogen starvation

When nitrogen is limiting, fission yeast cells divide twice and arrest in G1. Subsequently, if they meet a partner of the opposite mating type, they initiate the sexual differentiation response to form spores that can survive in a poor nutritional environment. This differentiation process is accelerated under nitrogen starvation, and zygotes and even some asci can be observed after 8 hours in MM-N.

Due to this enhanced response, we also studied the mating efficiency of Greatwall and Endosulfine mutants under nitrogen starvation. For this purpose, cells were grown in MM for one day and shifted to MM-N. After that, they were kept under nitrogen starvation for 8, 24 or 96 hours, and we analysed the formation of asci. Compare to wild-type, sporulation was almost abolished in cells lacking *igo1+* (Figure I.4 C). When mating efficiency was expressed as the proportion of differentiated cells, we observed that it was significantly reduced in the *igo1Δ* mutant (Figure I.6). Furthermore, deletion of *ppk18+* exhibited low mating efficiency, whereas the *cek1Δ* and *ppk31Δ* single mutants behaved like the wild-type (Figure I.6). These results suggest that Ppk18 and Igo1 proteins are essential for the sexual differentiation response under nitrogen deprivation. Deletion of *cek1+* and *ppk18+* displayed a similar phenotype to that of the *igo1Δ* mutant (Figure I.6), suggesting a partial redundancy between Ppk18 and Cek1. On the contrary, high levels of Ppk18, deletion of *ppa2+* (Figures I.7B and I.7C) or *pab1+* (Laboucarié et al., 2017; Martín et al., 2017) showed higher mating efficiency than wild-type cells, which is consistent with a negative role of PP2A/B55 in the regulation of the differentiation response. Moreover, deletion of *ppa2+* completely rescued the sterility phenotype of the *igo1Δ* mutant (Figure I.7).

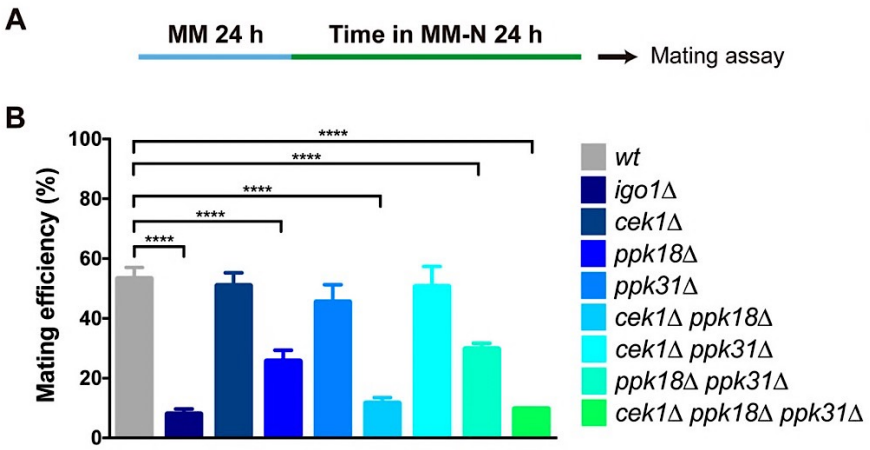

Figure I.6. The Greatwall-Endosulfine module promotes the sexual differentiation response under nitrogen starvation. Mating efficiency assays. Cells were grown in MM, shifted to MM-N and kept under nitrogen starvation for one day. Mating efficiency was expressed as the proportion (%) of differentiated cells (zygotes and asci were counted as two differentiated cells). **A.** Procedure employed in the mating efficiency assays. **B.** Average mating efficiency plus standard deviation of wild-type cells and Greatwall-Endosulfine deletion mutants. For statistical analysis, the assay was repeated twice. Only p-values of wt vs. mutant are shown (****$p < 0.0001$).

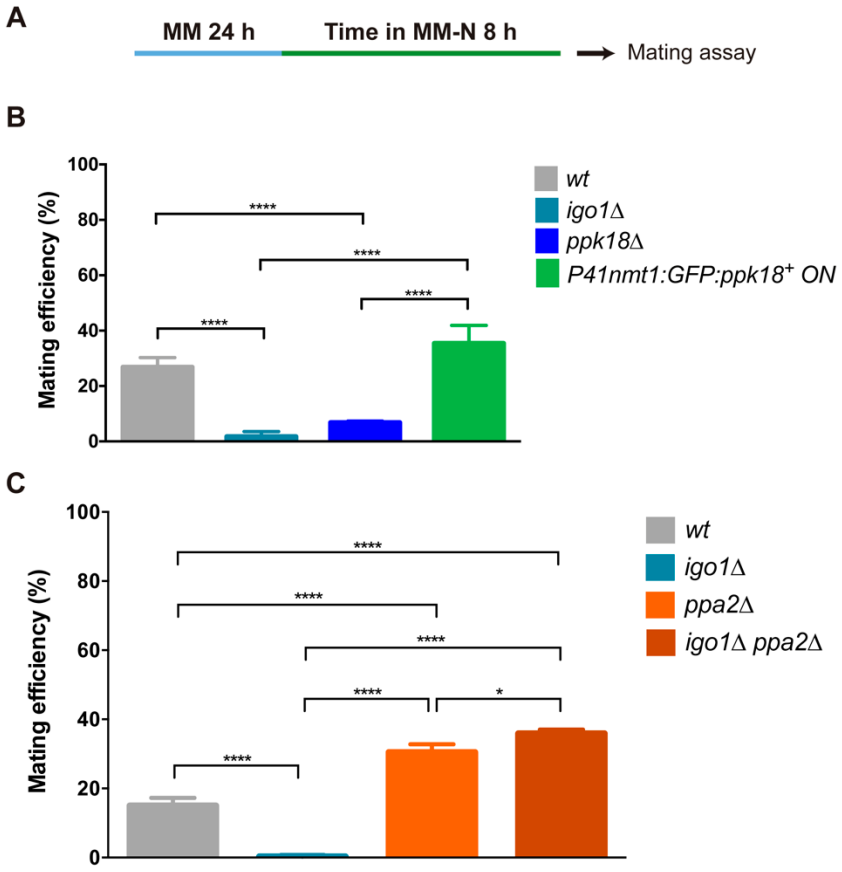

Figure I.7. The Greatwall-Endosulfine-PP2A/B55 pathway promotes the sexual differentiation response under nitrogen starvation. Mating efficiency assays. Cells were grown in MM, shifted to MM-N and kept under nitrogen starvation for only 8 hours due to the hyperfertility of the mutants analysed. Mating efficiency was expressed as the proportion (%) of differentiated cells. **A.** Procedure employed in the mating efficiency assays. **B and C.** Average mating efficiency plus standard deviation of wild-type cells, *ppk18Δ*, *igo1Δ*, *ppa2Δ* and *ppa2Δ igo1Δ* deletion mutants, and cells containing a copy of the P41nmt1 promoter

integrated upstream from the *ppk18⁺* ORF. For statistical analysis, the assay was repeated twice. (*p < 0.05, ****p < 0.0001).

Remarkably, transcriptional analysis performed in our laboratory has shown that the expression of genes involved in the sexual differentiation response was reduced in mutant cells lacking Endosulfine (*igo1Δ*) or Greatwall (*cek1Δ ppk18Δ*) after a 4-hour incubation in MM-N. On the contrary, the *pab1Δ* mutant exhibited upregulation of genes implicated in conjugation or meiosis (Laboucarié et al., 2017; Martín et al., 2017).

All this data suggests that the fission yeast Greatwall-Endosulfine module promotes the sexual differentiation response through the inhibition of the PP2A/B55 phosphatase complex.

3. The Greatwall-Endosulfine-PP2A/B55 pathway promotes longevity under nitrogen starvation

Ageing is a complex process characterised by a progressive accumulation of molecular, cellular and organ damage, which leads to increased susceptibility to disease and, ultimately, death. Yeast lifespan can be monitored as both RLS, which describes the number of progenies produced by a mother cell before senescence (Mortimer and Johnston, 1959), and CLS, defined as the period of time non-dividing cells remain viable (Fabrizio and Longo, 2003) (Figure 8, Introduction). This no division state is also known as quiescence or G_0 phase, and in fission yeast, it is induced in response to nitrogen starvation (Su et al., 1996).

Notably, many of the mutations that impact lifespan are related to nutrient-signalling pathways. Dietary restriction and downregulation of TORC1 activity increase longevity in many organisms, such as yeast, flies or rodents (Blagosklonny and Hall, 2009; Fontana et al., 2010). In budding yeast, the Greatwall-Endosulfine module regulates survival in quiescence and ageing (Talarek et al., 2010; Wei et al., 2008). Moreover, deletion of the S6 kinase orthologue, Sck2 in *S. pombe* and Sch9 in *S. cerevisiae*, that inhibits Greatwall, extends CLS (Chen and Runge, 2009; Fabrizio et al., 2001). Conversely, cells deleted for *ppk18⁺*, the Greatwall orthologue in fission yeast, show reduced CLS (Chen et al., 2013a), and *igo1⁺* has been reported as an essential quiescence gene (Sajiki et al., 2018).

In this section, we deepened in the study of the possible role of the Greatwall-Endosulfine-PP2A/B55 pathway in the regulation of ageing in fission yeast.

3.1. The Greatwall-Endosulfine-PP2A/B55 pathway is required for cell survival under nitrogen starvation

To study if the Greatwall-Endosulfine-PP2A/B55 pathway could be involved in ageing, we analysed the cell survival of quiescent cells using methylene blue. This dye penetrates every cell. However, whereas living cells enzymatically reduce it to a colourless product and become unstained, dead cells are blue stained (Painting and Kirsop, 1990; Bapat et al., 2006). Nitrogen starvation was used to induce G_0 entry and quiescence maintenance.

Quiescent wild-type fission yeast cells were hardly stained with methylene blue, indicating that they remained viable for an extended period of time in the absence of nitrogen. By contrast, cells lacking *igo1⁺* began to die after 5-8 days in MM-N. By day 15 in MM-N, almost all cells were dead (Figure I.8), suggesting that Endosulfine is crucial for cell survival under nitrogen starvation. We also analysed the viability of cells with reduced expression of *pab1⁺*, observing that they showed a wild-type phenotype (Figure I.8), which is consistent with a negative role of PP2A/B55 in cell survival. Furthermore, lowering the expression of *pab1⁺* rescued *igo1Δ* mutant lethality (Figure I.8), indicating that the phenotype of *igo1Δ* cells might be caused by insufficient inhibition of PP2A/B55 activity. Moreover, flow cytometry analysis revealed a sub-G1 population, which

corresponded to dead cells, in the *igo1Δ* mutant observed. This sub-G1 population was not observed neither in the wild-type nor in cells with reduced expression of the *pab1⁺* gene (Figure I.9, arrows). Interestingly, the sub-G1 cell population in the *igo1Δ* mutant was significantly reduced by down-regulation of *pab1⁺* expression (Figure I.9, arrow).

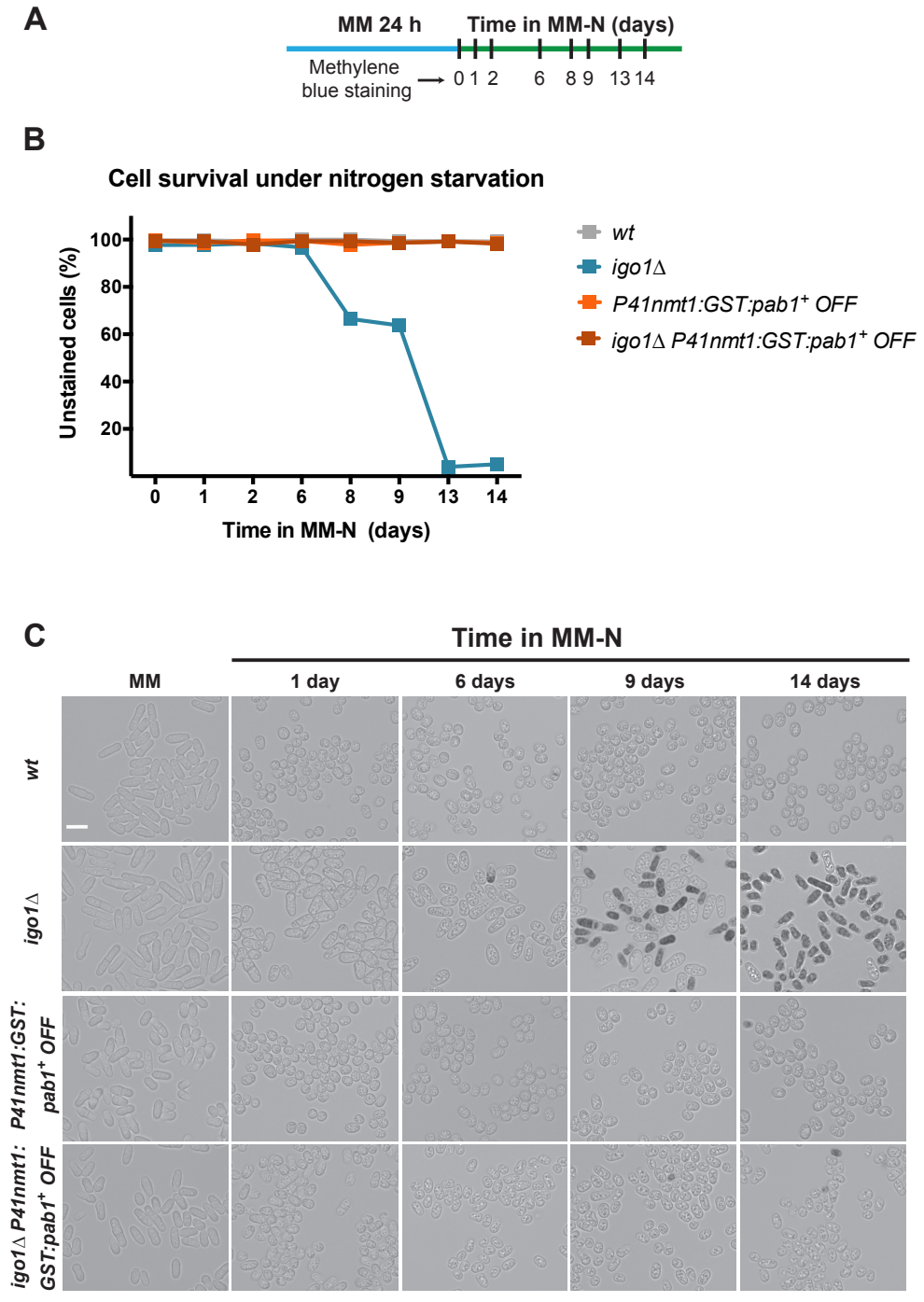

Figure I.8. Reducing the expression of the PP2A/B55 regulatory subunit (*pab1⁺*) rescues igo1Δ lethality in MM-N. Cell survival was estimated using methylene blue: dead cells were blue stained, while viable cells became unstained. **A.** Procedure employed in the cell survival measurements. Cells containing a copy of the P41nmt1 promoter integrated upstream from the *pab1⁺* ORF in *igo1+* and *igo1Δ* genetic backgrounds, and wild-type and *igo1Δ* strains were grown in MM, shifted to MM-N and kept in MM-N for 14 days. Cell samples were collected and stained with methylene blue at the indicated times. Thiamine was added to the media to repress pab1+ expression. **B.** Percentage of cell survival in MM-N. **C.** Images of wild-

type, *igo1Δ*, *P41nmt1:GST:pab1⁺* and *igo1Δ P41nmt1:GST:pab1⁺* cells stained with methylene blue. Scale bar, 10 μm.

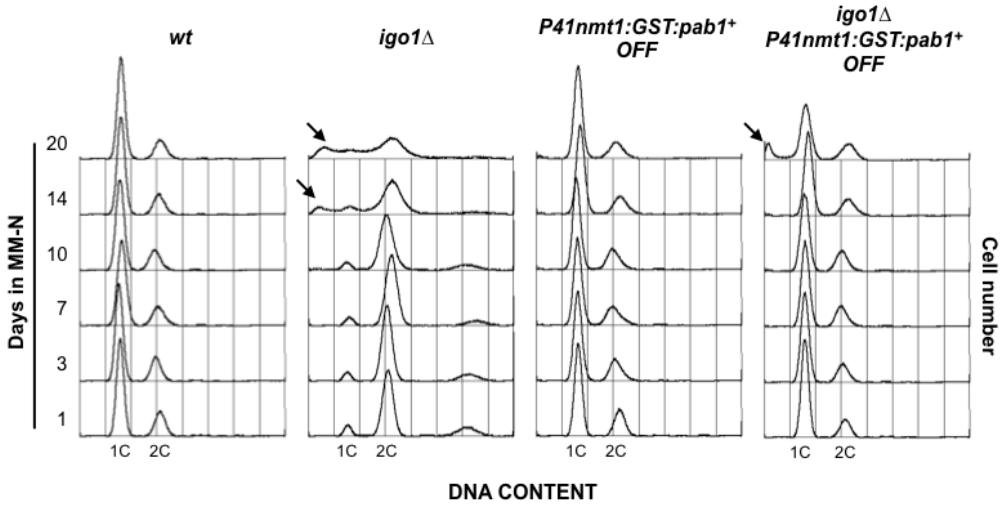

Figure I.9. Lowering the expression of *pab1⁺* partially suppresses the sub-G1 population caused by deletion of *igo1⁺*. FACS profile (DNA content, 1C and 2C) of ethanol-fixed cells stained with propidium iodide. Cells containing a copy of the P41nmt1 promoter integrated upstream from *pab1⁺* ORF in *igo1⁺* and *igo1Δ* genetic backgrounds, and wild-type and *igo1Δ* strains were grown in MM for one day at 25ºC and then shifted to MM-N at 25ºC and kept under nitrogen starvation for 20 days. Thiamine was added to the media to repress *pab1⁺* expression. Samples were collected at the indicated time points.

All this data suggests that inhibition of PP2A/B55 by Endosulfine is essential for cell survival under nitrogen starvation in fission yeast.

3.2. The Greatwall-Endosulfine-PP2A/B55 pathway is essential for G_0 entry and quiescence maintenance in nitrogen-starved cells

The establishment of quiescence takes about 24 hours and is associated with a reduction of cell size, loss of cell polarity and chromatin condensation (Su et al., 1996). During this dormant state, cells remain metabolically active and viable for months. Giving the lethality caused by *igo1⁺* deletion in the absence of nitrogen, we decided to continue studying the involvement of the Greatwall-Endosulfine-PP2A/B55 pathway in G_0 entry and quiescence maintenance. To induce quiescence, cells grown in MM were transferred to MM-N and kept under nitrogen starvation for 10-22 days. Cell samples were collected at different time points and plated on rich medium, and ageing was monitored as CLS. Unlike methylene blue experiments, which measures cell survival in MM-N, CLS assays reflects mitotic competence or cell ability to restart the cell cycle and generate new colonies.

In drop assays, wild-type cells remained viable throughout the experiment, whereas cells lacking *igo1⁺* or *ppk18⁺* showed reduced CLS after 7 and 10 days in MM-N, respectively (Figure I.10). However, deletion of *cek1⁺* and *ppk31⁺*, the other Greatwall orthologues, displayed a wild-type phenotype. Only combining deletion of *ppk18⁺* with *cek1⁺* and *ppk31⁺* (*ppk18Δ cek1Δ*, *ppk18Δ cek1Δ* and *ppk18Δ cek1Δ ppk31Δ*), the CLS was shortened, and cells exhibited a similar phenotype to that of the *igo1Δ* mutant (Figure I.10), suggesting that the Greatwall-Endosulfine module is required for survival under nitrogen starvation. Subsequently, we wondered if these mutants' G1 arrest defect could be accountable for their viability loss. To address this hypothesis, we carried out CLS analysis of *rum1Δ ste9Δ* mutant, which is also unable to arrest in G1 in MM-N (Kominami et al., 1998; Moreno and Nurse, 1994; Rubio et al., 2018; Stern and Nurse, 1998). We observed that cells lacking *rum1⁺* and *ste9⁺* exhibited more viability than Greatwall or Endosulfine deletion mutants (Figure I.10), suggesting that the G1 arrest defect might not be the

cause of the CLS reduction in this double mutant. We also analysed the viability of cells lacking *atg13⁺*, indispensable for autophagy, as autophagic flux is decreased in Greatwall and Endosulfine deletion mutants (Vázquez-Bolado et al., unpublished data). The *atg13Δ* mutant remained viable after ten days in MM-N (Figure I.10) as previously described by Kohda et al., 2007, suggesting that the autophagic defect of Greatwall and Endosulfine deletion mutants may not be accountable for their loss of viability. Then, we carried out a CLS analysis of mutants lacking upstream elements of the Greatwall-Endosulfine module, including Tsc2, a negative regulator of TORC1, and Sck2, the fission yeast orthologue of the S6 kinase; or overexpressing Tor2, the catalytic subunit of TORC1, and Sck2. We have previously reported that the Greatwall-Endosufilne molecular switch is negatively regulated by the TORC1 pathway (Chica et al., 2016). In nutrient-rich media, TORC1 activity is high due to Tsc2 inhibition, leading to Greatwall phosphorylation and inhibition by Sck2, a conserved downstream target of TORC1 complex (Chica et al., 2016). Like cells lacking Endosulfine (*igo1Δ*) or Greatwall (*ppk18Δ cek1Δ* and *ppk18Δ cek1Δ ppk31Δ*), high levels of *sck2⁺* (*P3nmt1:skc2⁺*) exhibited a short CLS (Figure I.11), supporting the notion that the Greawall-Endosulfine module promotes longevity. Surprisingly, TORC1 hyperactivation, by deleting *tsc2⁺* or overexpressing of *tor2⁺* (*P3nmt1:tor2⁺*), behaved like wild-type cells (Figure I.11). Cells lacking *sck2⁺* (*sck2Δ*) or overexpressing Greatwall (*nmt41:GFP:ppk18⁺*) also displayed a wild-type phenotype (Figure I.11). Finally, we studied the phenotype of mutants with reduced PP2A/B55 activity by deleting *ppa2⁺* (*ppa2Δ*) or repressing *pab1⁺* (*P41nmt1:GST:pab1⁺*), observing that they behaved like wild-type cells (Figure I.11), which is consistent with a negative role of PP2A/B55 in longevity.

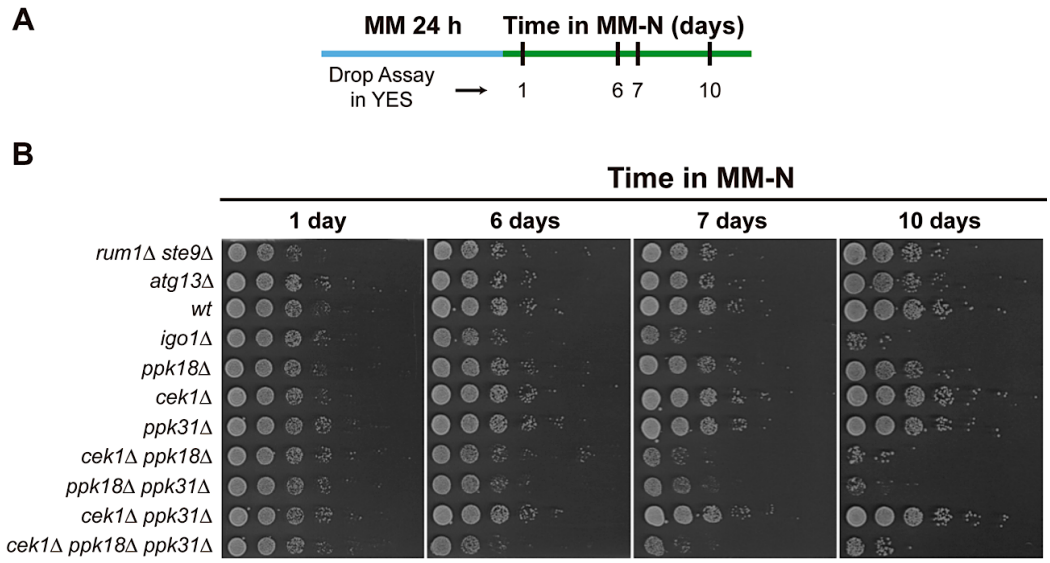

Figure I.10. Deletion of the Greatwall-Endosulfine molecular switch shortens the lifespan of fission yeast cells under nitrogen starvation. Qualitative analysis of chronological lifespan (CLS). **A.** Procedure employed in the CLS measurements. Cells were grown in MM, shifted to MM-N and kept under nitrogen starvation for ten days. Aliquots of the cultures were taken at the indicated time points after the shift, spotted on YES in sequential ten-fold dilutions and incubated for 3-5 days. **B.** Drop assays showing the CLS analysis of wild-type and Greatwall and Endosulfine deletion mutants.

Drop assays were used to analyse qualitatively the lifespan of several mutants. To carefully monitor the CLS, cell viability was determined by counting the number of colonies formed on YES-plates. Cells were harvested at different days of incubation in MM-N. Using this method, we performed CLS measurements of wild-type, *igo1Δ* and *cek1Δ ppk18Δ* mutants. Mutant cells started to lose viability after 24 hours in MM-N. Viability continued to decrease for the following seven days, when it was entirely lost (Figure I.12). As quiescence establishment takes about 24

hours, this data suggests that the Greatwall-Endosulfine module is required for both G_0 entry and quiescence maintenance. Next, we examined if PP2A/B55 activity was involved in the loss of viability of the *igo1Δ* cells. Like in the drop assays, repression of *pab1⁺* (*P41nmt1:GST:pab1⁺* in the presence of thiamine) partially rescued the G_0 defect caused by the deletion of *igo1⁺*, although this double mutant completely lost viability after 20 days in MM-N (Figure I.13). This result suggests that the defects of *igo1Δ* cells in both G_0 entry and quiescence maintenance under nitrogen starvation might be produced by a deficient inhibition of PP2A/B55 activity.

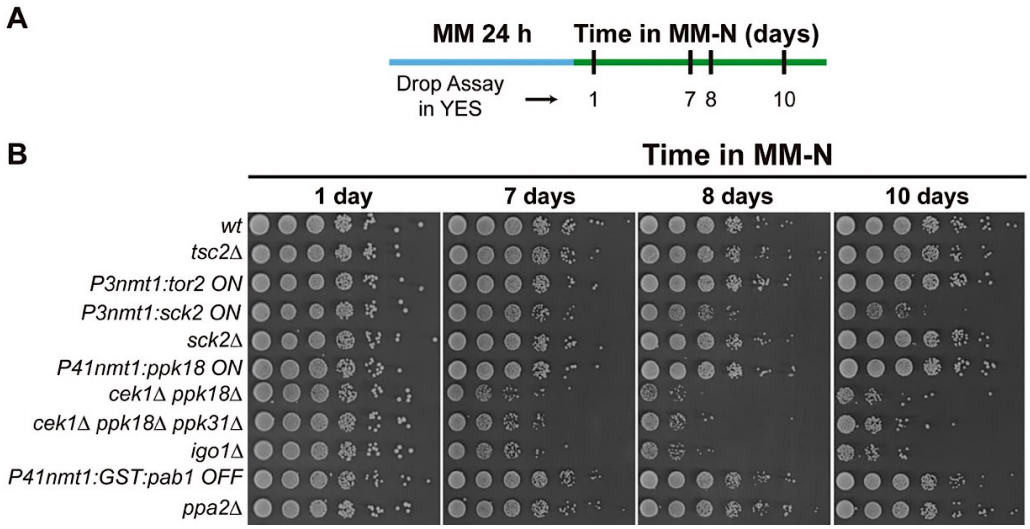

Figure I.11. The Greatwall-Endosulfine-PP2A/B55 promotes longevity under nitrogen deprivation. Qualitative analysis of CLS. **A.** Procedure employed in the CLS measurements. Cells were grown in MM, transferred to MM-N and incubated for ten days under nitrogen starvation. Thiamine was added to the media to repress *pab1⁺* expression. Aliquots of the cultures were taken at the indicated time points after the shift, spotted on YES in sequential ten-fold dilutions and incubated for 3-5 days. **B.** Drop assays showing the CLS analysis of wild-type and TORC1-Greatwall-Endosulfine-PP2A/B55 pathway mutants.

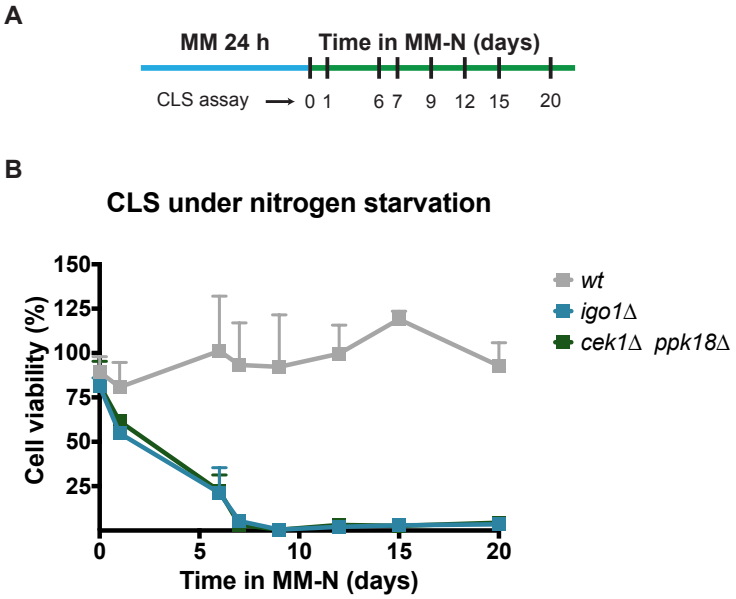

Figure I.12. The Greatwall-Endosulfine module is crucial for G_0 entry and to sustain long-term viability under nitrogen deprivation. Chronological lifespan (CLS) curve showing the percentage of cell viability. **A.** Procedure employed in the CLS measurements. Cells were grown in MM, transferred to MM-N and incubated for 20 days under nitrogen starvation. Aliquots of the cultures were taken at the indicated time

points after the shift, diluted to plate 300 cells on three YES plates and incubated for 3-5 days. **B.** Average cell viability plus standard deviation of wild-type cells and Greatwall-Endosulfine deletion mutants. For statistical analysis, the assay was repeated three times.

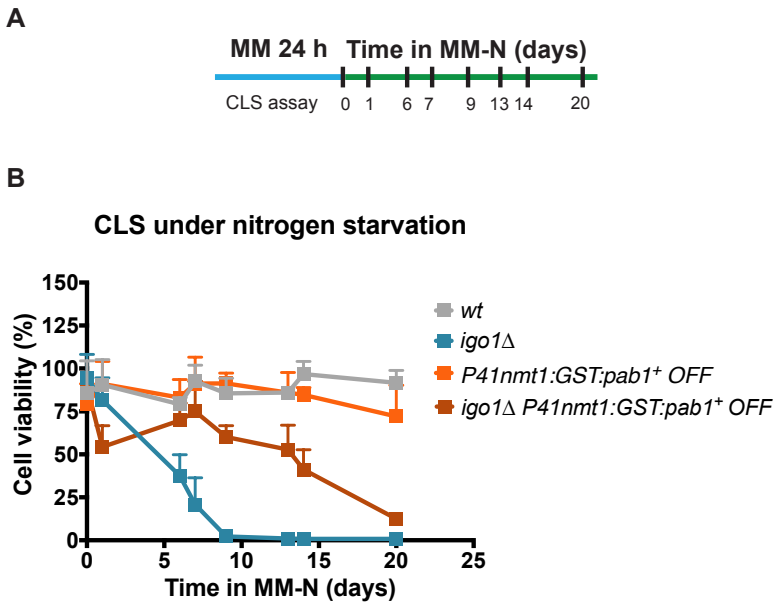

Figure I.13. Lowering expression of *pab1⁺* partially suppresses the loss of viability of the *igo1Δ* mutant under nitrogen starvation. CLS curve showing quantification of cell viability. **A.** Procedure employed in the CLS measurements. Cells were grown in MM, shifted to MM-N and kept in MM-N for 20 days. Thiamine was added to the media to repress *pab1⁺* expression. Aliquots of the cultures were taken at the indicated time points after the shift, diluted to plate 300 cells on three YES plates and incubated for 3-5 days. **B.** Average cell viability plus standard deviation of wild-type, *igo1Δ* mutant and cells containing a copy of the P41nmt1 promoter integrated upstream from *pab1⁺* ORF. The assay was repeated three times for statistical analysis.

3.3. Endosulfine activity is necessary for proper chromatin dynamics of quiescent cells under nitrogen starvation

During proliferation, interphase nuclei display a spherical morphology (Toda et al., 1981) (Figures I.14C and I.15C). By contrast, the establishment of quiescence is accompanied by several cellular changes, such as loss of cell polarity or cell size reduction. Interestingly, the shrinkage of nuclear chromatin is also a feature of G_0 cells (Su et al., 1996). When fission yeast cells are kept under nitrogen starvation for long periods, chromatin is dramatically altered, becoming flat and close to the cell periphery (Su et al., 1996).

We have shown that the pre-quiescence response to nitrogen starvation is altered in Greatwall-Endosulfine mutants (Figure I.16). Wild-type cells divided twice and arrested in G1, reducing cell size and becoming almost spherical. Nonetheless, cells lacking *igo1⁺* were unable to arrest in G1 and did not reduce their size, remaining elongated instead of rounded (Figure I.16), as previously reported by Chica et al., 2016 and Aono et al., 2019. Given that *igo1Δ* cells did not show a spherical cell shape, we decided to examine the nuclear morphology. DAPI images showed that approximately 50% of the nuclei of *igo1Δ* cells became stretched after five days in MM-N (Figure I.14). Moreover, deformed nuclei, observed as several pieces or abnormal shapes, increased over time (Figure I.14). After 12 days under nitrogen starvation, around 20% of the *igo1Δ* mutant nuclei were degraded (Figure I.14). Since cells have to be fixed with ethanol for DAPI staining, we decided to analyse the changes in nuclear morphology *in vivo* using the *mcherry-atb2⁺ hht2-GFP* genetic background, that allowed observation of Atb2 (tubulin α2) and Hht2 (histone H3) proteins. After five days in MM-N, normal nuclei began to decrease in *igo1Δ*

mutant. By contrast, most wild-type nuclei were spherical (Figure I.15). In *igo1Δ* mutant, stretched nuclei increased over time, while rounded nuclei continued to decrease until day 12 in MM-N, when almost 80% of cells showed colocalisation of Hht2 and Atb2 (Figure I.15), indicating nuclear degradation. Both DAPI staining and *in vivo* microscopy showed that flattening of chromatin in the *igo1Δ* mutant started early in the G_0 phase and that nuclear integrity was also compromised in this genetic background.

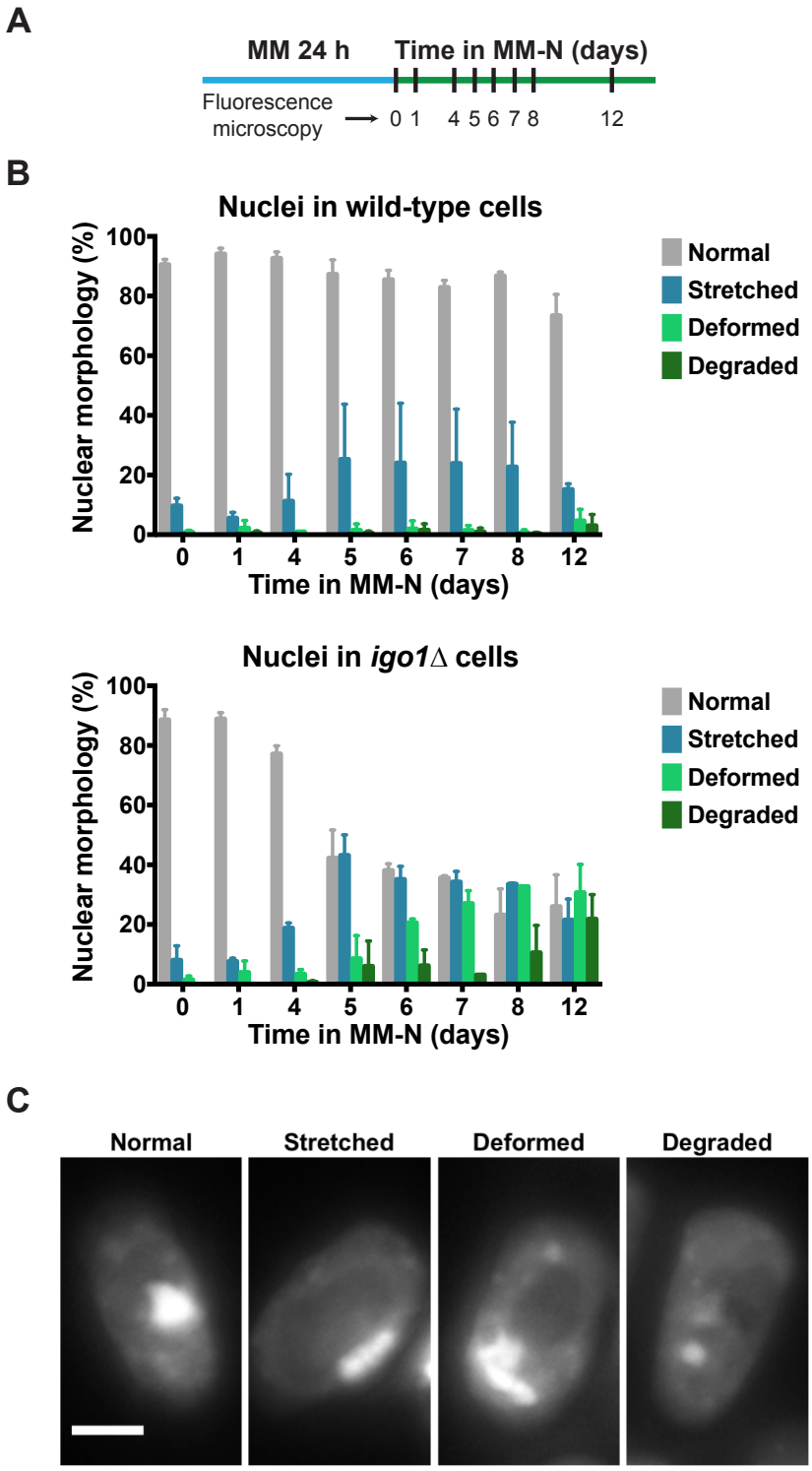

Figure I.14. Deletion of *igo1*$^+$ showed altered chromatin dynamics and caused nuclear defects during the G_0 phase induced by nitrogen starvation. **A**. Procedure employed in the nuclear morphology studies. Cells were grown in MM, shifted to MM-N and kept under nitrogen starvation for 12 days. Samples

were collected, fixed with ethanol and stained at the indicated time points after the shift. **B**. Average percentages plus standard deviation of DAPI-stained nuclear shapes found in wild-type and *igo1Δ* cells. Three hundred cells for each strain were counted. **C**. Images of *igo1Δ* cells stained with DAPI. Scale bar, 10 *μ*m. For statistical analysis, the assay was repeated twice.

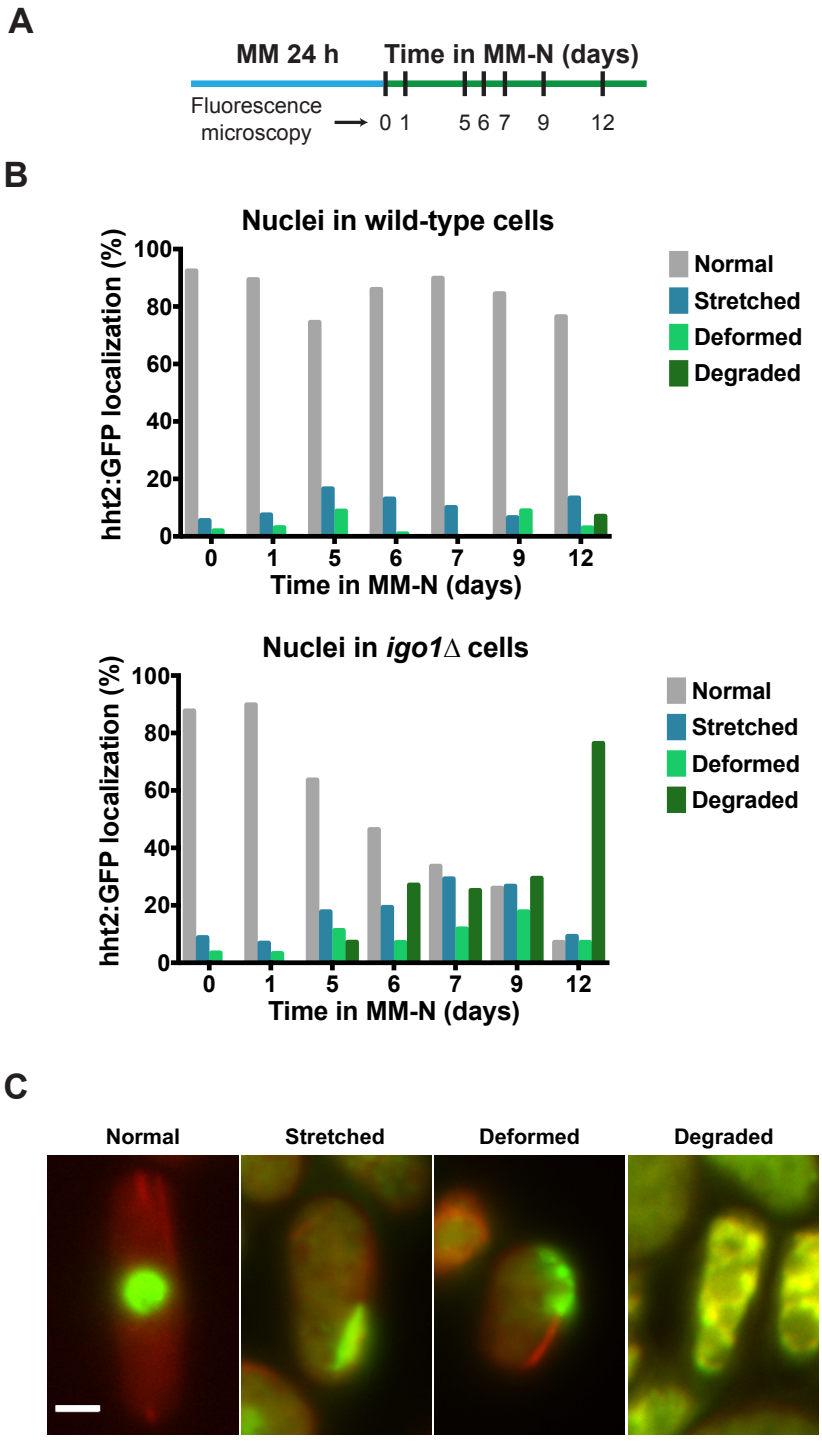

Figure I.15. Deletion of *igo1*⁺ showed altered chromatin dynamics and caused nuclear defects during the G_0 phase induced by nitrogen starvation. **A**. Procedure employed in the nuclear morphology studies. Cells were grown in MM, shifted to MM-N and kept under nitrogen starvation for 12 days. Samples were collected and observed under a fluorescence microscope at the indicated time points after the shift. **B**. Average percentages of *hht2:GFP* nuclear shapes found in wild-type and *igo1Δ* cells. Three hundred cells for each strain were counted. **C**. Fluorescence microscopy images of *igo1Δ* cells. Scale bar, 10 *μ*m.

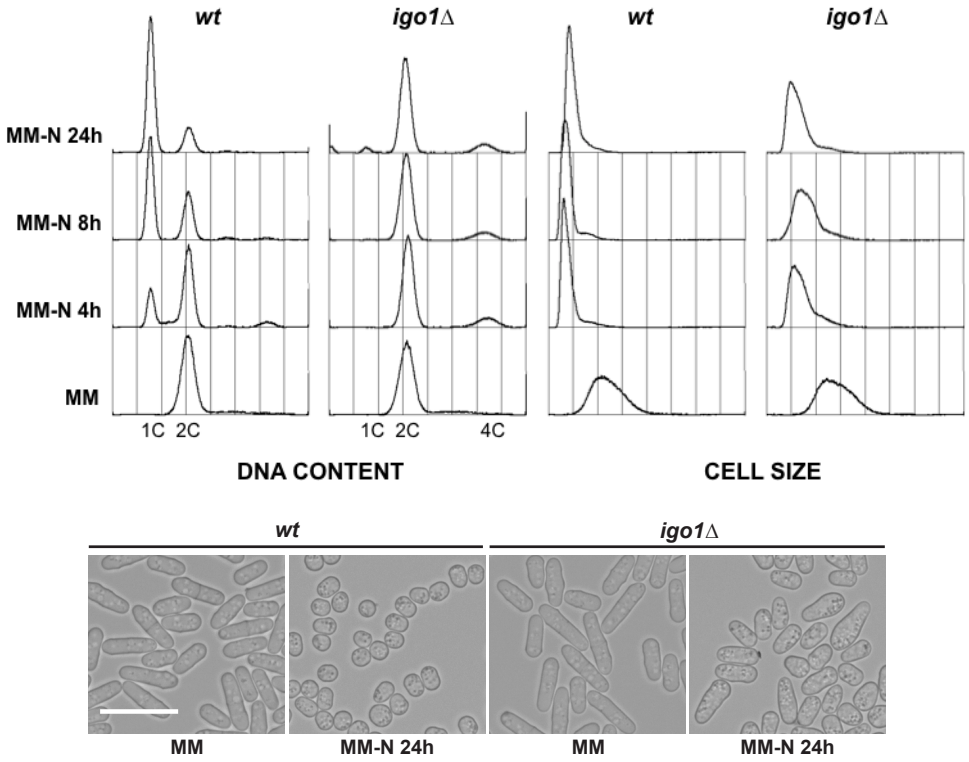

Figure I.16. Endosulfine is required for G1 arrest and cell size reduction under nitrogen starvation. Cells were grown in MM for one day at 25ºC and then transferred to MM-N. Samples were collected at the indicated time points after the shift. (**Top**) FACS profile of ethanol-fixed wild-type and *igo1Δ* cells. DNA content (1C and 2C) after propidium iodide staining (left) and forward scatter (FSC), which correlates with cell size (right), are shown. (**Bottom**) Images of wild-type and *igo1Δ* cells. Scale bar, 10 μm.

These results suggest that deletion of Endosulfine impairs nuclear integrity during the G_0 phase induced by nitrogen deprivation in fission yeast. Moreover, these nuclear defects could account for the loss of viability observed in *igo1Δ* mutant.

3.4. TORC2 signalling might not be needed for the G_0 phase induced by nitrogen starvation

The highly conserved TOR kinase assembles into two multiprotein complexes, TORC1 and TORC2. In contrast to mammals, where a single mTOR kinase is the catalytic subunit of both complexes, yeast cells contain two Tor kinases, Tor1 and Tor2. In *S. pombe*, Tor2 is part of TORC1 complex, which promotes cell growth, whereas TORC2 complex carries the catalytic subunit Tor1 (reviewed in Kanoh and Yanagida, 2010) and is required for cell survival under different stress conditions (Eltschinger and Loewith, 2016; Weisman, 2016).

It has been recently reported that the transition from cell growth to cell differentiation in response to nitrogen starvation is regulated by PP2A/B55 (Laboucarié et al., 2017) through the phosphorylation of the main TORC2 effector, Gad8 (Martín and López-Áviles, 2018; Martín et al., 2017). In nitrogen-poor media, low levels of TORC1 activity results in activation of the Greatwall-Endosulfine module and inhibition of PP2A/B55, which leads to the accumulation of active Ser546 phosphorylated Gad8 and induction of the differentiation response (Martín and López-Áviles, 2018; Martín et al., 2017). We wondered if this connection between TORC1 and TORC2 through the Greatwall-Endosulfine-PP2A/B55 pathway might also be important for the G_0 induced by nitrogen-starvation. To address this question, we studied the phenotype of *gad8⁺* deletion mutant under nitrogen deprivation. Flow cytometry analysis revealed that *gad8Δ* cells, like *igo1Δ* cells, were unable to reduce size nor arrest in G1, even after 24 hours in MM-N (Weisman and Choder,

2001; Weisman et al., 2007) (Figure I.17), suggesting that TORC2 signalling is required for the pre-quiescence response to nitrogen starvation. Next, we examined the survival of *tor1Δ* and *gad8Δ* mutants under prolonged nitrogen starvation. If the Greatwall-Endosulfine-PP2A/B55 pathway regulates Gad8 activity, cells deleted for *gad8⁺* should behave similarly to the *igo1Δ* mutant. Surprisingly, *tor1Δ* and *gad8Δ* cells were hardly stained with methylene blue (Figure I.18), indicating that, unlike the *igo1Δ* mutant, they remained viable for at least 15 days in the absence of nitrogen. Moreover, we studied the mitotic competence, which defines the cell ability to exit from G_0 and re-enter cell-cycle, of quiescent TORC2 mutants. For this purpose, we compared the CLS of *gad8Δ* and *igo1Δ* mutants. We observed a slight shortening of the CLS in the *gad8Δ* mutant (Figure I.19). Specifically, *gad8Δ* cells showed approximately 70% of viability, while cells deleted for *igo1⁺*, as previously indicated, completely lost viability after nine days in MM-N (Figure I.20). These results suggest that Gad8 activity is not crucial for G_0 entry and quiescence maintenance under prolonged nitrogen deprivation.

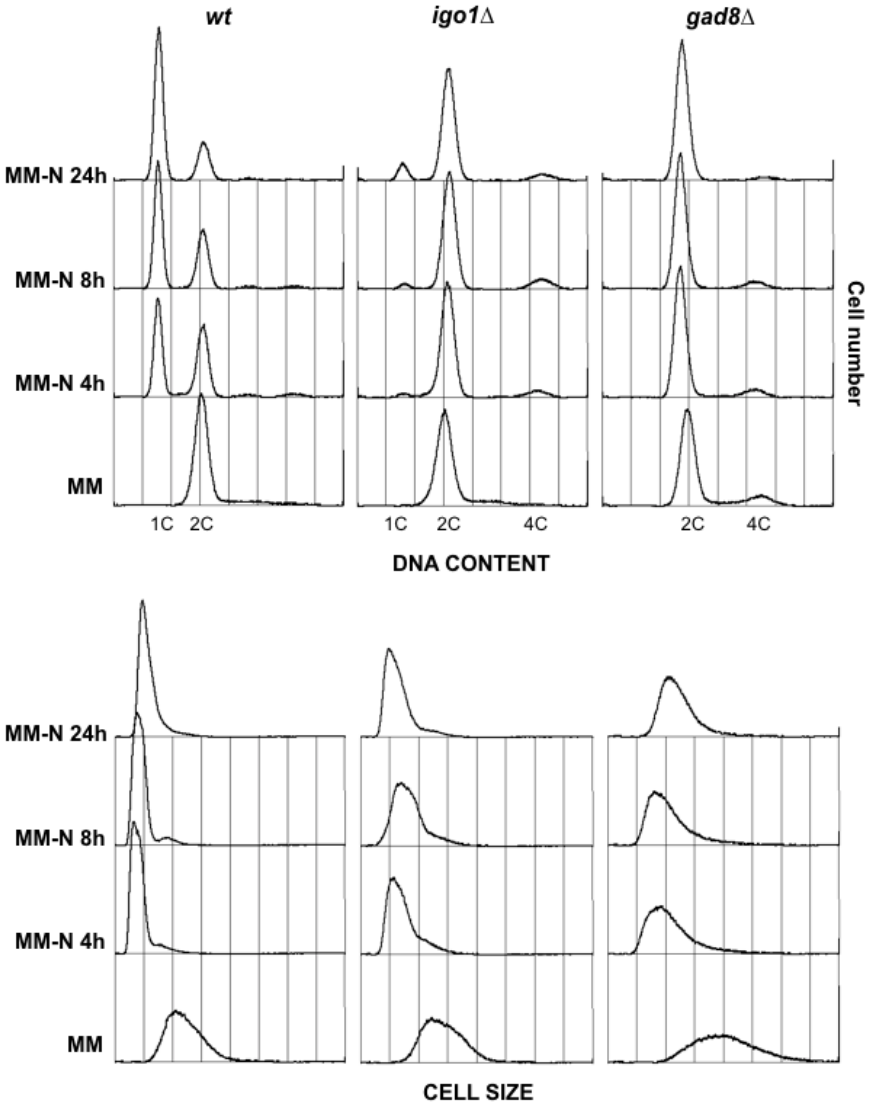

Figure I.17. Gad8 activity is required for the pre-quiescence response to nitrogen starvation. FACS profile of ethanol-fixed wild-type, *igo1Δ* and *gad8Δ* cells. DNA content (1C and 2C) after propidium iodide staining (**top**) and forward scatter (FSC, **bottom**), which correlates with cell size. Cells were grown in MM for one day at 25ºC and then shifted to MM-N at the same temperature. Samples were collected at the indicated time points after the shift.

Briefly, this data indicates that the Greatwall-Endosulfine-PP2A/B55 pathway is not acting through the TORC2-Gad8 molecular axis to regulate cell survival in quiescent cells.

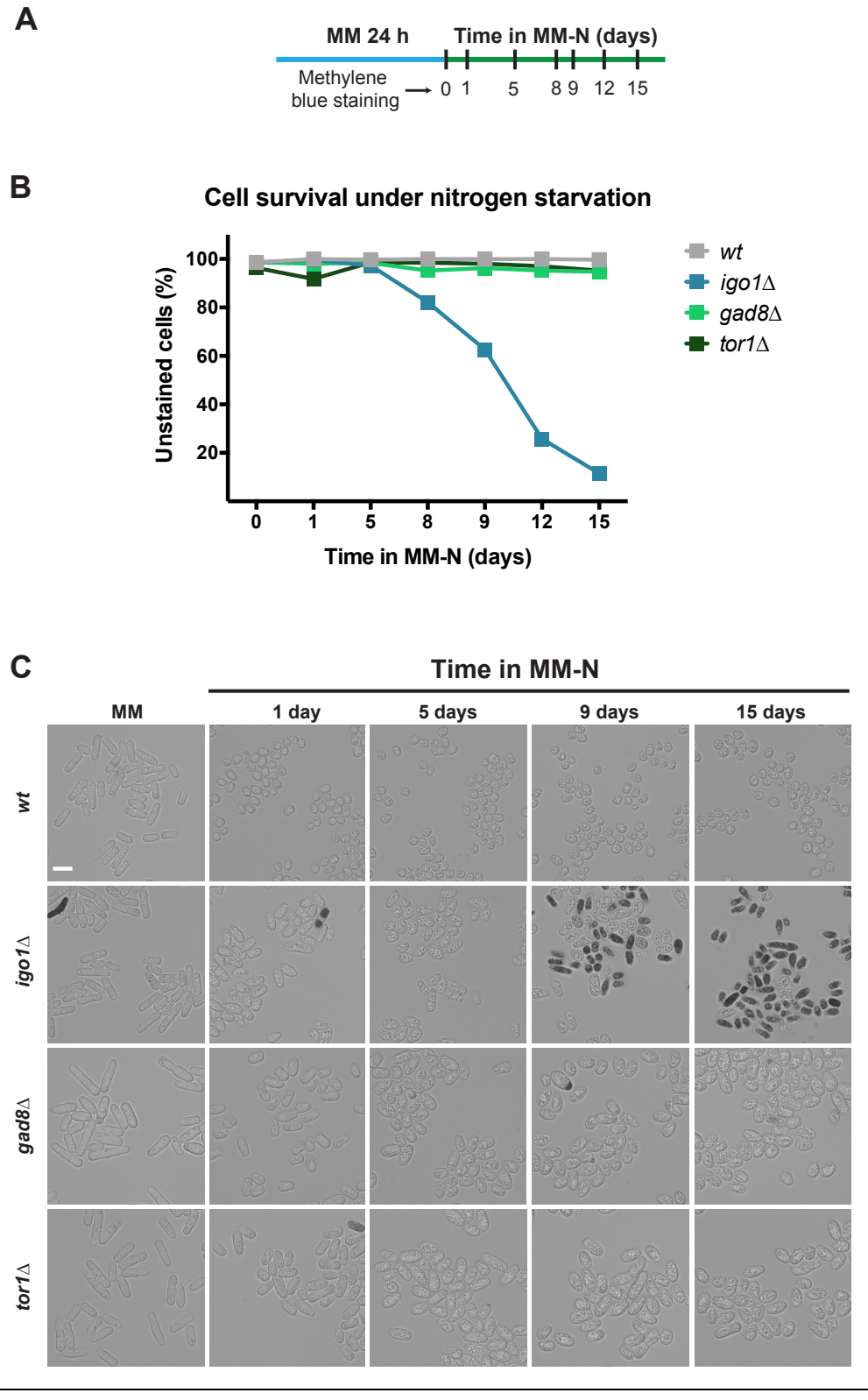

Figure I.18. TORC2 signalling is dispensable for cell survival in the absence of nitrogen. Cell survival was estimated using methylene blue: dead cells were blue stained, while viable cells were not stained. **A.** Procedure employed in the cell survival measurements. Cells were grown in MM, shifted to MM-N and kept under nitrogen starvation for 15 days. Samples were collected and stained at the indicated time

points after the shift. **B.** Proportion (%) of survival of wild-type, *igo1Δ*, *gad8Δ* and *tor1Δ* cells in MM-N. **C.** Images of wild-type, *igo1Δ*, *gad8Δ* and *tor1Δ* cells stained with methylene blue. Scale bar, 10 μm.

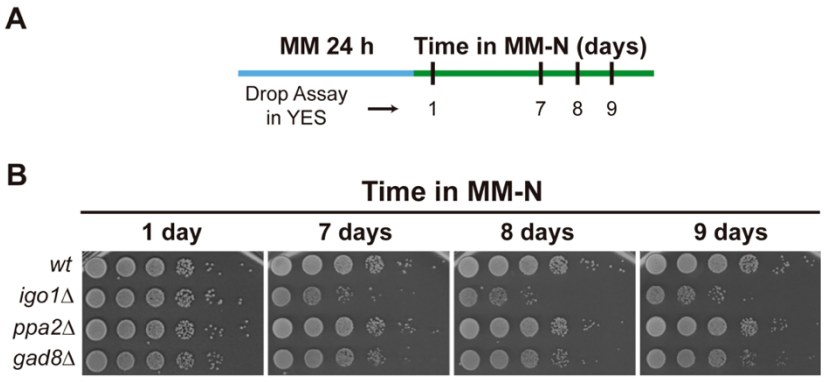

Figure I.19. Deletion of *gad8⁺* caused a slight decrease in cell viability under nitrogen starvation. Qualitative analysis of chronological lifespan (CLS). **A.** Procedure employed in the CLS measurements. Cells were grown in MM, transferred to MM-N and incubated for nine days under nitrogen starvation. Aliquots of the cultures were taken at the indicated time points after the shift, spotted on YES in sequential ten-fold dilutions and incubated for 3-5 days. **B.** Drop assays showing the CLS analysis of wild-type, *igo1Δ*, *ppa2Δ* and *gad8Δ* cells.

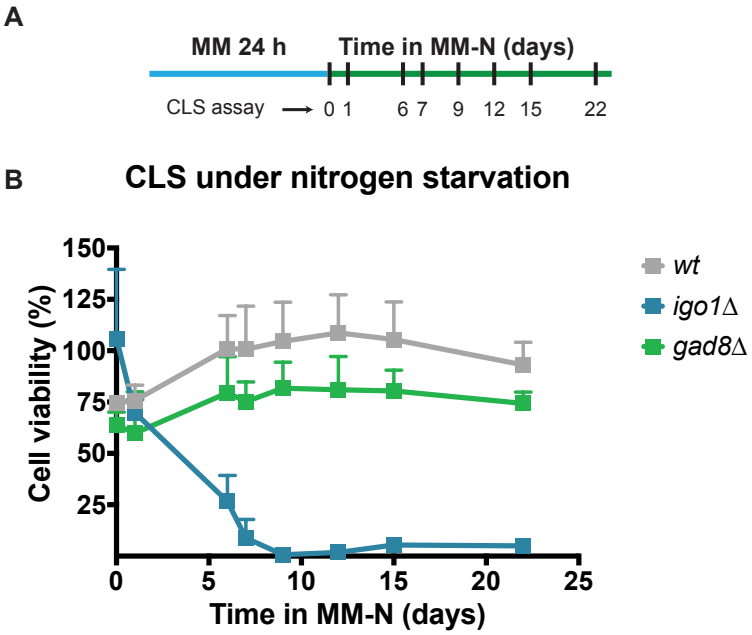

Figure I.20. *gad8Δ* cells remain highly viable during the G_0 induced by nitrogen starvation. CLS curve showing quantification of cell viability. **A.** Procedure employed in the CLS measurements. Cells were grown in MM, shifted to MM-N and kept under nitrogen starvation for 22 days. Samples of the cultures were taken at the indicated time points after the shift, diluted to plate 300 cells on three YES plates and incubated for 3-5 days. **B.** Average cell viability plus standard deviation of wild-type, *igo1Δ* and *gad8Δ* cells. For statistical analysis, the assay was repeated three times.

Chapter II: Role of the Greatwall-Endosulfine module in cell-cycle regulation

Cell-cycle progression is driven by the periodic activation and inactivation of CDK/Cyclin complexes. Changes in CDK/Cyclin activity depend on the phosphorylation status of the CDK and on cyclin levels (Nurse, 1990). Interestingly, numerous recent studies have highlighted the role of protein phosphatases in cell-cycle control (Cundell et al., 2013, 2016; Domingo-Sananes et al., 2011; Grallert et al., 2015). In particular, mitotic entry is the result of the balance between Cdk1/CyclinB protein kinase and PP2A/B55 protein phosphatase activities (Glover, 2012; Lorca and Castro, 2013). In G2, PP2A/B55 dephosphorylates Cdk1/CyclinB substrates, opposing Cdk1/CyclinB activity and delaying entry into mitosis until Cdk1/CyclinB activity levels increase above a certain threshold (Mochida et al., 2009). The conserved Greatwall-Endosulfine module behaves as a molecular switch that inactivates PP2A/B55 at the onset of mitosis (Glover, 2012; Lorca and Castro, 2013). Greatwall, also known as Mastl in mammals, Rim15 in budding yeast, and Ppk18 and Cek1 in fission yeast, triggers the phosphorylation of Endosulfine, two small proteins in animal cells (ENSA and ARPP-19) and in budding yeast (Igo1 and Igo2) and a single protein in fission yeast (Igo1), that when phosphorylated by Greatwall becomes a potent and specific inhibitor of PP2A/B55 (Gharbi-Ayachi et al., 2010; Mochida et al., 2010).

In metazoans, Greatwall kinase activity is regulated throughout the cell cycle. Its activity is low in interphase, peaks at mitotic entry, and decreases at the metaphase-anaphase transition (Hara et al., 2012; Voets and Wolthuis, 2010; Yu et al., 2006). At G2/M transition, Cdk1/CyclinB phosphorylates and activates Greatwall, triggering Endosulfine phosphorylation and PP2A/B55 inhibition. Conversely, cell-cycle regulation of Greatwall has not been described in yeast, where the Greatwall-Endosulfine switch is subjected to nutritional control. In Saccharomyces cerevisiae, TORC1 and PKA activities inhibit the Greatwall-Endosulfine switch (Reinders et al., 1998; Pedruzzi et al., 2003), whereas only TORC1 has been reported to downregulate Greatwall-Endosulfine activity in fission yeast (Chica et al., 2016).

According to our theoretical model, the Greatwall-Endosulfine module is a hub for cell cycle and nutritional signals that switches on or off the PP2A/B55 phosphatase activity (Figure II.1). TORC1 senses nitrogen and amino acids availability, becoming active when these nutrients are abundant, and inactive if they are scarce. We have recently shown that the TORC1 complex, through Sck2, the orthologue of S6K in S. pombe, negatively modulates Greatwall-Endosulfine activity (Chica et al., 2016). In addition to nitrogen, PKA activity, which responds to glucose levels, might control the Greatwall-Endosulfine module, since both Ppk18 and Igo1, the fission yeast orthologues of Greatwall and Endosulfine, contain four and three (R/K)2-X-S/T or R/K-X-X-S/T sequences, respectively, that could be phosphorylated by PKA (Figure II.2). We have preliminary data indicating that the Greatwall-Endosulfine pathway may also be a target of Cdk1/CyclinB in fission yeast. For instance, in metaphase-arrested cells, where Cdk1/CyclinB levels were high, Ppk18 and Igo1 proteins underwent a mobility shift (Figure II.3) (Pérez-Hidalgo et al., unpublished data), suggesting that both proteins might become phosphorylated by Cdk1/CyclinB. Interestingly, both proteins contain multiple S/T-P sequences that fit the consensus for Cdk1 phosphorylation sites. Ppk18 contains 24 of these sites, whereas Igo1 contains four (Figure II.2). Moreover, we have mutated seven putative Cdk1-phosphorylation sites in Ppk18 and found that the mutant ppk18-7A shows reduced Igo1 phosphorylation (Pérez-Hidalgo et al., unpublished data), consistent with a reduction in Ppk18 activity. This preliminary data suggests that the Ppk18-Igo1 module could be phosphorylated and activated by Cdk1/CyclinB complex and therefore, its activity might be cell-cycle regulated.

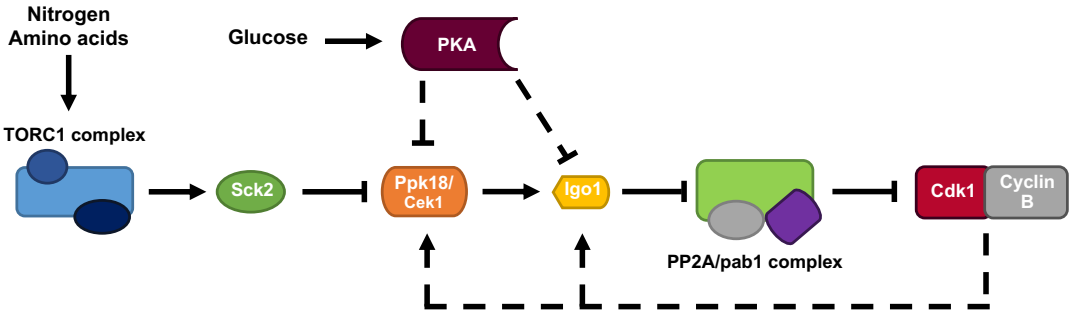

Figure II.1. The Greatwall-Endosulfine module is a hub for cell cycle and nutritional cues that switches on or off the PP2A/B55 phosphatase activity. Greatwall and Ensodulfine proteins are downregulated by TORC1 and PKA activities but activated by Cdk1/CyclinB, which results in a positive feedback loop on Cdk1/CyclinB activity. Dotted lines show hypothetical interactions. TORC1, Tor complex 1. Sck2, S6 kinase. Ppk18 and Cek1, Greatwall. Igo1, Endosulfine. PP2A-Pab1, PP2A/B55.

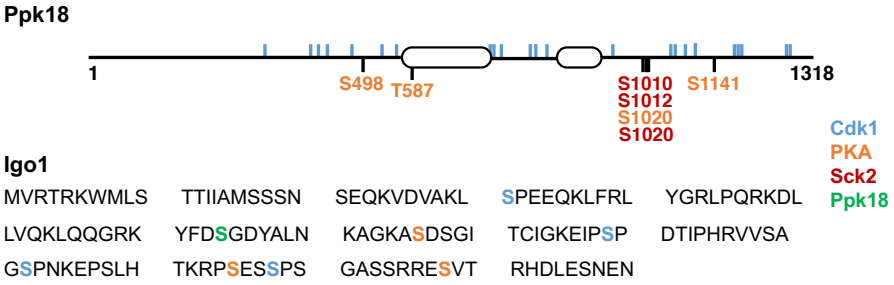

Figure II.2. Ppk18 and Igo1 proteins contain multiple putative phosphorylation sites for several kinases. Ppk18 is a 147 kDa protein with 24 sites that fit the consensus for Cdk1 phosphorylation (S/T-P), four potential sites for PKA phosphorylation ($(R/K)_2$-X-S/T or R/K-X-X-S/T) and three for Sck2 kinase (R-X-R-X-X-S/T). Igo1 is a 15 kDa protein that is phosphorylated on serine 64 by Ppk18 and contains four putative sites for Cdk1 phosphorylation and three for PKA activity.

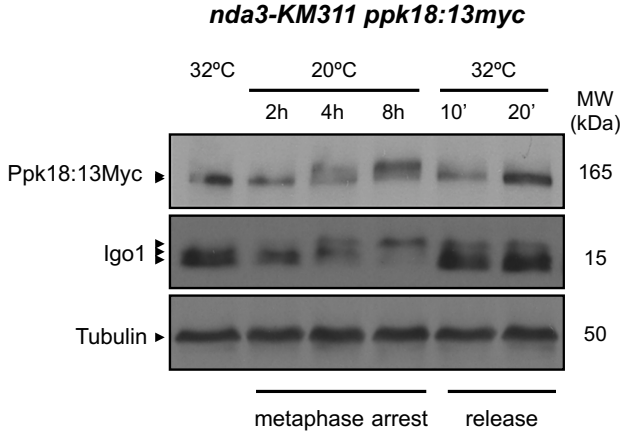

Figure II.3. Electrophoretic mobility changes (presumably by phosphorylation) of Ppk18 and Igo1 in cells arrested in metaphase using the *nda3-KM311* cold-sensitive mutant (Hiraoka et al., 1984). Ppk18 and Igo1 underwent a mobility shift in *nda3-KM311* mutant cells arrested in metaphase at the restrictive temperature of 20ºC. Upon release to the permissive temperature (32ºC), Ppk18 and Igo1 electrophoretic mobility rapidly increased within 10 minutes (probably by dephosphorylation), as cells progressed to anaphase.

In this chapter, we have studied the regulation of the Greatwall-Endosulfine molecular switch by phosphorylation. We hypothesised that the environmental cues, through TORC1 (nitrogen and amino acids) and PKA (glucose) signalling pathways, negatively regulate Greatwall-

Endosulfine activity, whereas Cdk1/CyclinB complex phosphorylates and activates both Greatwall and Endosulfine (Figure II.1).

1. Regulation of the Greatwall-Endosulfine molecular switch by protein phosphorylation

1.1. Endosulfine regulation by phosphorylation

1.1.1. Identification of phosphorylation sites in Endosulfine by mass spectrometry

Our theoretical model states that the Greatwall-Endosulfine module is subjected to both cell-cycle and environmental dependent regulation. We believe that the Greatwall-Endosulfine switch could be positively regulated by Cdk1/CyclinB and down-regulated by TORC1 and PKA (Figure II.1). This regulation is probably exerted by phosphorylation, giving that PKA, TORC1 and Cdk1/CyclinB have protein kinase activity. To address this question, we decided to analyse the phosphorylation changes in Greatwall and Endosulfine using two-dimensional liquid chromatography-tandem mass spectrometry (2D LC-MS/MS) (Figure II.4).

Briefly, 4x10^9 cells expressing HBH-tagged Igo1 protein were grown in MM for one day. Subsequently, half of the culture was transferred to MM-N and grown in this nutritional environment for 30 minutes. Igo1:HBH protein was purified from both media using a two-step affinity purification performed under denaturing conditions as described by Tagwerker et al., 2006. Isolated Igo1:HBH was digested with trypsin, quimiotrypsin and elastase to produce small peptides that were, then, separated by 2D LC and analysed by MS/MS. Finally, the spectral data was subjected to computer algorithms that mapped phosphosites on Igo1:HBH protein.

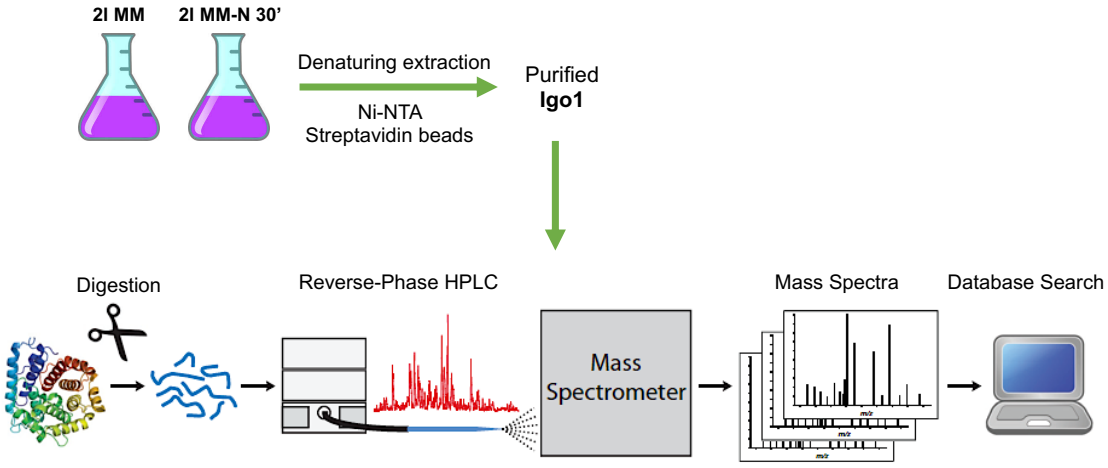

Figure II.4. Experimental procedure employed to map phosphorylation sites on Igo1 using 2D LC-MS/MS. Endogenously expressed HBH-tagged Igo1 protein (*igo1:HBH* mutant) was isolated on Streptavidin Ultralink Immobilised beads from lysates derived from MM and MM-N media. Next, protein samples were digested with trypsin, quimiotrypsin and elastase producing peptides separated by reverse-phase high-performance liquid chromatography and analysed in a mass spectrometer as they eluted from the column. Peptide matching was done algorithmically using spectral data and sequence database information.

We identified several serines and threonines residues phosphorylated in both MM and MM-N (Tables II.S1 and II.S2). Three putative sites, S31, S89 and S102, for Cdk1 phosphorylation and two serines, S76 and S115, that fit the consensus for PKA phosphorylation were mapped as phosphoresidues (Figure II.5), suggesting that these protein kinases might modulate Endosulfine activity in fission yeast (Figure II.1). Furthermore, we identified several phosphosites that could be phosphorylated by other kinases, including Casein kinase I and II (CKI and CKII), protein kinase C (PKC) or Glycogen synthase kinase 3 (GSK3) (Figure II.5), which

could be involved in other regulatory pathways. Phosphorylated serine 64 was also mapped, serving as a positive control for our experiment, as we have previously reported that Ppk18 phosphorylates this residue (Chica et al., 2016).

Igo1

MVRTRKWMLS TTIIAMS**SS**N SEQKVDVAKL **S**PEEQKLFRL YGRLPQRKDL LVQKLQQGRK

YFD**S**GDYALN KAGKA**S**DSGI **T**CIGKEIP**S**P D**T**IPHRVV**S**A G**S**PNKEP**S**LH **T**KRP**S**ESSPS

GASSRRESVT RHDLESNEN

Cdk1 → S31 S89 S102 PKA → S76 S115 Ppk18 → S64 **CKI/CKII/PKC/GSK3**

Figure II.5. Phosphorylation sites in Igo1 protein identified by 2D LC-MS/MS. Serines 31, 89 and 102, putative sites for Cdk1 phosphorylation, serine 64, phosphorylated by Ppk18, and serines 76 and 115, potential sites for PKA activity were mapped. Other phosphoresidues that fit the consensus for other kinases (**CKI**, **CKII**, **PKC** and **GSK3**) were also identified.

We were able to map several phosphorylation sites in MM and MM-N using 2D-LC MS/MS. We did not use a quantitative method in our mass spectrometry analysis, such as labelling peptide samples with stable-isotopes (reviewed in Dephoure et al., 2013). Thus, we could not rule out differences between both media. Nonetheless, our analysis did allow us to determine the Igo1 residues that were phosphorylated *in vivo*. Supplemental Tables 1 and 2 (Tables II.S1 and II.S2) list phosphosites mapped in MM and MM-N, respectively.

The mass spectrometry analysis of Endosulfine showed that this protein is phosphorylated *in vivo* in fission yeast. Interestingly, we have identified several putative Cdk1 and PKA phosphorylation sites, supporting our hypothesis that the Greatwall-Endosulfine module is regulated by cell-cycle and environmental signals.

1.1.2. Endosulfine is phosphorylated *in vitro* by Cdk1

The mass spectrometry analysis of Igo1:HBH protein mapped several potential sites for Cdk1 phosphorylation sites. To test whether Endosulfine is a direct target of Cdk1, we performed Cdk1 *in vitro* protein kinase assays using purified recombinant Igo1 and Igo1-4A as substrates. In *igo1-4A* cells, serines 31, 89, 102 and 118 were mutated to alanine (Figure II.6), producing a non-phosphorylatable version of Igo1 protein for all putative Cdk1 phosphorylation sites. Although phosphorylation of serine 118 was not detected in our *in vivo* analysis, we also replaced it with alanine. Cdk1 kinase, in an active or inactive version, were previously expressed in baculovirus and purified from insect cells (Dr. K. Gould's group) or immunoprecipitated from *S. pombe* extracts. Purified recombinant Imp2 protein (Dr. K. Gould's group) or Histone H1 were also used as positive protein kinase control substrates.

Igo1

MVRTRKWMLS TTIIAMSSSN SEQKVDVAKL **S**PEEQKLFRL YGRLPQRKDL LVQKLQQGRK

YFDSGDYALN KAGKASDSGI TCIGKEIP**S**P DTIPHRVVSA G**S**PNKEPSLH TKRPSES**S**PS

GASSRRESVT RHDLESNEN

Igo1-4A

MVRTRKWMLS TTIIAMSSSN SEQKVDVAKL **A**PEEQKLFRL YGRLPQRKDL LVQKLQQGRK

YFDSGDYALN KAGKASDSGI TCIGKEIP**A**P DTIPHRVVSA G**A**PNKEPSLH TKRPSES**A**PS

GASSRRESVT RHDLESNEN

Figure II.6. *S. pombe* Igo1 (top) and Igo1-4A (bottom) protein sequences. Serines 31, 89, 102 and 118 (blue) were substituted for alanines (red) in the *igo1-4A* mutant.

Figures II.7 and II.8 show that Cdk1/CyclinB was able to phosphorylate Imp2 and Histone H1 positive controls, as well as wild-type Igo1 protein. Interestingly, using an anti-Cdc13 (CyclinB)

antibody to immunoprecipitate Cdk1 resulted in increased phosphorylation of Histone H1 and Igo1 (Figure II.8), probably because Cdk1/Cdc13 is more active than other Cdk1/Cyclin complexes. Nonetheless, we could not detect Cdk1 dependent phosphorylation of Igo1-4A protein (Figure II.8), indicating that the mutated residues in Igo1 protein are phosphorylated by Cdk1/CyclinB complex at the mutated serine residues.

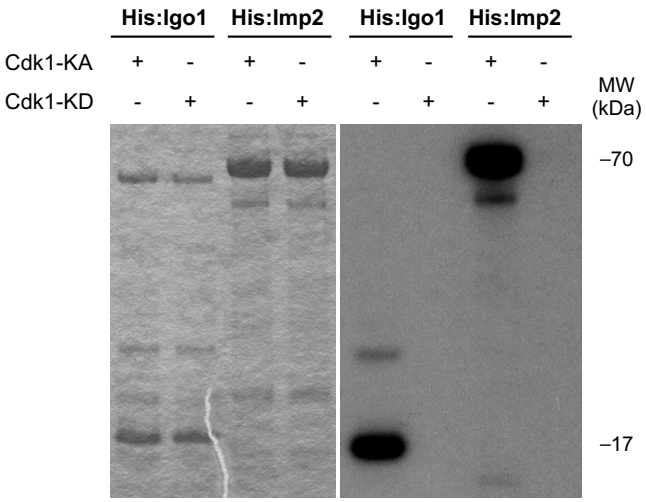

Figure II.7. Fission yeast Endosulfine (Igo1) is phosphorylated *in vitro* by Cdk1. Cdk1 kinase-active (Cdk1-KA) and kinase-inactive (Cdk1-KD) proteins were purified from insect cells. Protein kinase assays were carried out in the presence of γ-32P-ATP (**right**) and using purified recombinant Igo1 or Imp2 as substrates. Coomassie blue staining of the gel (**left**), γ-32P-labelled proteins (**right**).

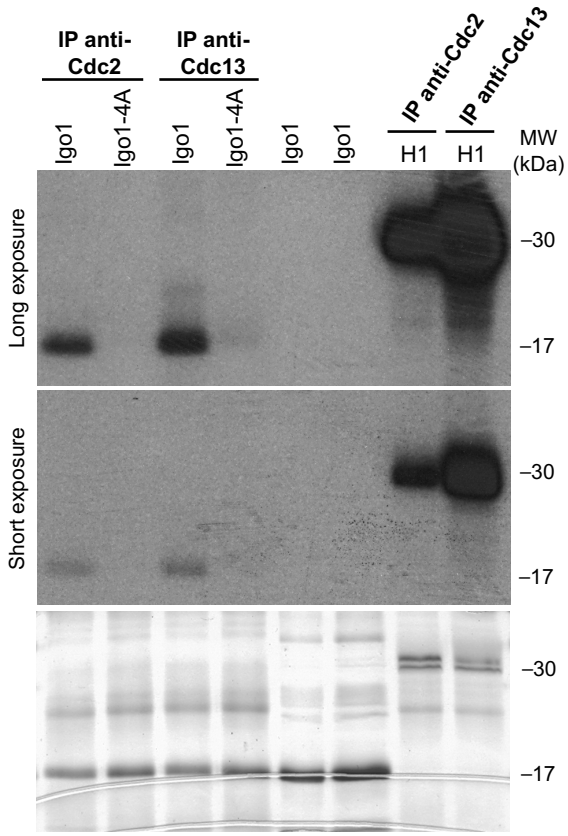

Figure II.8. Cdk1/CyclinB complex is unable to phosphorylate Igo1-4A protein. Cdk1 kinase activity was immunoprecipitated from metaphase-arrested cells (*nda3-KM311* mutant) using the C2 anti-Cdc2 or

the SP4 anti-Cdc13 sera. Protein kinase assays of Cdc2 (Cdk1) and Cdc13 (CyclinB) immunoprecipitates using purified recombinant Igo1 and Igo1-4A as substrates. γ-^{32}P-labelled proteins (**top**), coomassie blue staining of the gel (**bottom**).

The results described above indicate that serines 31, 89, 102 and 118 of Endosulfine could be phosphorylated by Cdk1/CyclinB activity in fission yeast, supporting our theoretical model (Figure II.1).

1.1.3. Cdk1/CyclinB complex positively regulates Endosulfine activity *in vivo*

The protein kinase assays previously described showed that Cdk1/CyclinB complex is capable of phosphorylating Igo1 *in vitro*. To further investigate the role of Igo1 phosphorylation by Cdk1/CyclinB *in vivo*, we generated an *igo1-4A* mutant by gene replacement (Figure II.6) According to our theoretical model, Cdk1/CyclinB complex promotes Greatwall-Endosulfine activity in fission yeast (Figure II.1). Hence, *igo1-4A* cells, that lack all the Cdk1 putative phosphorylation sites, would behave similarly to the *igo1Δ* mutant.

When nutrients are plentiful, fission yeast cells divide with a large size after a long G2 (Nurse, 1975). However, when wild-type cells are shifted to nitrogen-poor media, such as MMF, they shorten G2 and enter mitosis with a reduced size (Carlson et al., 1999; Fantes and Nurse, 1977; Petersen and Nurse, 2007) (Figure II.9). By contrast, cells lacking *igo1*$^{+}$ did not reduce cell size after being transferred to MMF (Chica et al., 2016) (Figure II.9). Moreover, *igo1Δ* mutant displayed a large cell size even in MM (Figure II.9). Promisingly, *igo1-4A* cells were also larger than the wild-type in MM (Figure II.9), suggesting that abrogating Igo1 phosphorylation by Cdk1/CyclinB complex decreased Igo1 function. Nevertheless, *igo1-4A* mutant behaved almost identical to wild-type cells when they were grown in MMF, becoming shorter in this medium (Figure II.9). These results suggest that Cdk1/CyclinB regulation of Igo1 is important in nitrogen-rich media (MM) and less relevant in nitrogen-poor media (MMF), where fission yeast Greatwall phosphorylates Igo1 at serine 64, promoting the inhibition of PP2A/B55 phosphatase complex and, therefore, cell size reduction (Chica et al., 2016).

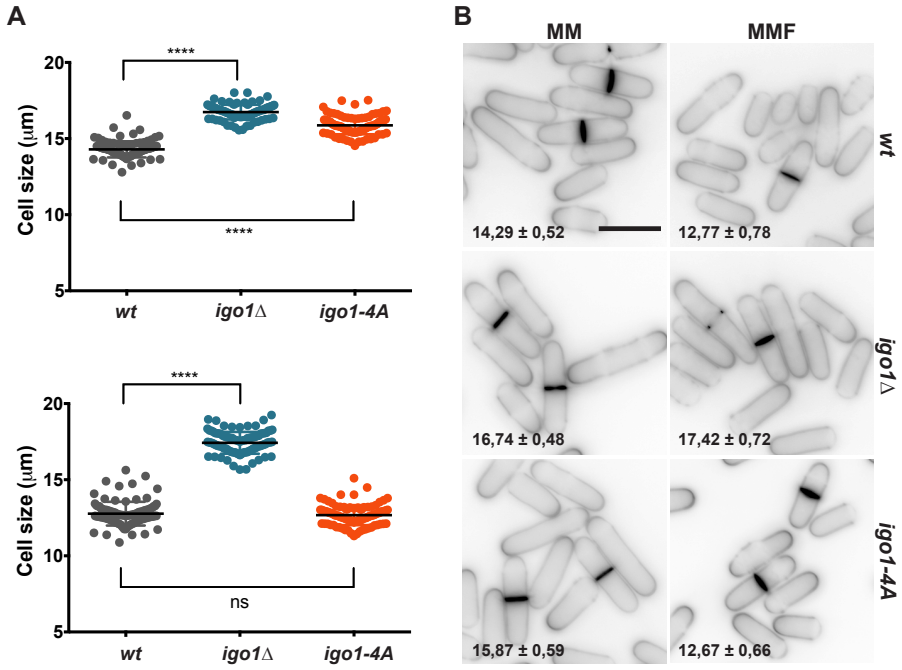

Figure II.9. Cdk1/CyclinB promotes Igo1 activation *in vivo*. Cell size measurements of wild-type, *igo1Δ* and *igo1-4A* cells in MM and MMF. For statistical analysis, the assay was repeated three times. **A**. Average cell length at division in MM (**top**) and MMF (**bottom**). Only p-values of wt vs. mutant are shown

(****p < 0.0001). **B**. Images of exponentially growing cells stained with blankophor. Cells growing in MM (**left**) and MMF (**right**) at 32ºC. Scale bar, 10 μm. The numbers in the images indicate the average length of 100 septated cells plus standard deviation.

Phosphorylation of Igo1 by Cdk1/cyclin B activates Endosulfine function *in vivo* in nitrogen-rich media and promotes entry into mitosis.

1.2. Greatwall regulation by phosphorylation

1.2.1. Identification of phosphorylation sites in Greatwall by mass spectrometry

Unfortunately, we were unable to successfully purify HBH-tagged Ppk18 from *S. pombe* cells. The reason for this could be either that the *in vivo* Ppk18 protein levels are very low or that the protein is very unstable. Therefore, we could not perform the mass spectrometry analysis of this protein. For the future, we will have to use alternative strategies to study protein phosphorylation regulation of the fission yeast Greatwall.

Chapter III: Identification of new targets of the Greatwall-Endosulfine-PP2A/B55 pathway in fission yeast

Our group has recently reported that the TORC1 signalling pathway modulates the G2/M transition and cell size at division (Chica et al., 2016). Upon nutritional shift-down, TORC1 activity drops, leading to Greatwall-Endosulfine activation and PP2A-B55 inhibition. Low levels of PP2A/B55 phosphatase activity enables cells to enter mitosis with reduced Cdk1/CyclinB activity, and hence, cells divide with a smaller size. Inhibition of PP2A/B55 by the Greatwall-Endosulfine molecular switch is also required for G1 extension and activation of TORC2 signalling (Martín and López-Áviles, 2018; Martín et al., 2017), which triggers the cell differentiation response (Laboucarié et al., 2017), and quiescence (Aono et al., 2019).

In this chapter, we have searched for proteins that interact *in vivo* with the Greatwall-Endosulfine-PP2A/B55 pathway using a proteomic approach. This analysis allowed us to identify new targets of this pathway in fission yeast, helping to better comprehend its physiological role.

1. Identification of proteins that interacts *in vivo* with the orthologues of Greatwall, Endosulfine and B55 in fission yeast

We have used affinity purification coupled to mass spectrometry to identify proteins that interact with the Greatwall-Endosulfine-PP2A/B55 pathway (reviewed in Dunham et al., 2012). This strategy allows detection of stable interactions and better reflects *in vivo* functional protein-protein interactions (Wodak et al., 2013). For this purpose, $8x10^9$ cells expressing GFP-tagged Igo1 and GFP-tagged Pab1 proteins (*igo1:GFP* and *P41nmt1:GFP:pab1⁺* mutants) were grown in MM. Half of the culture was shifted to MM-N after one day and kept under nitrogen starvation for 30-60 minutes (Figure III.1). GFP-tagged Igo1 and GFP-tagged Pab1 proteins were isolated on GFP-Trap® magnetic agarose beads from lysates derived from both media. Protein samples were then enzymatically digested, generating small peptides that were then separated by 2D LC and subsequently analysed by MS/MS (Figure III.1). Finally, the spectral data was subjected to computer algorithms that identified proteins associated with GFP-tagged Igo1 and GFP-tagged Pab1.

We did not obtain quantitative information since no quantitative method for mass spectrometry analysis was employed. Consequently, differences between MM and MM-N interactomes might not reflect the biological context, but they did help us identify new targets of the Greatwall-Endosulfine-PP2A/B55 pathway.

1.1. Identification of Endosulfine-interacting proteins

The mass spectrometry analysis identified 39 proteins that interacted with Igo1:GFP in MM and 88 in MM-N (Table III.S1 and III.S2). This data suggested that Igo1 interactome network became more complex under nitrogen starvation, where the Greatwall-Endosulfine module is active. Tables III.1 and III.2 list the 20 identified proteins that copurified with Igo1 and displayed the highest spectrum counts in MM and MM-N, respectively. The mass spectrometer detected around 400 peptides (spectrum counts) of Igo1 (Tables III.1 and III.2), which given the small size of the protein (15 kDa), served as a positive control for our experiment. The bigger the protein, the more peptides will be obtained and identified by mass spectrometry analysis.

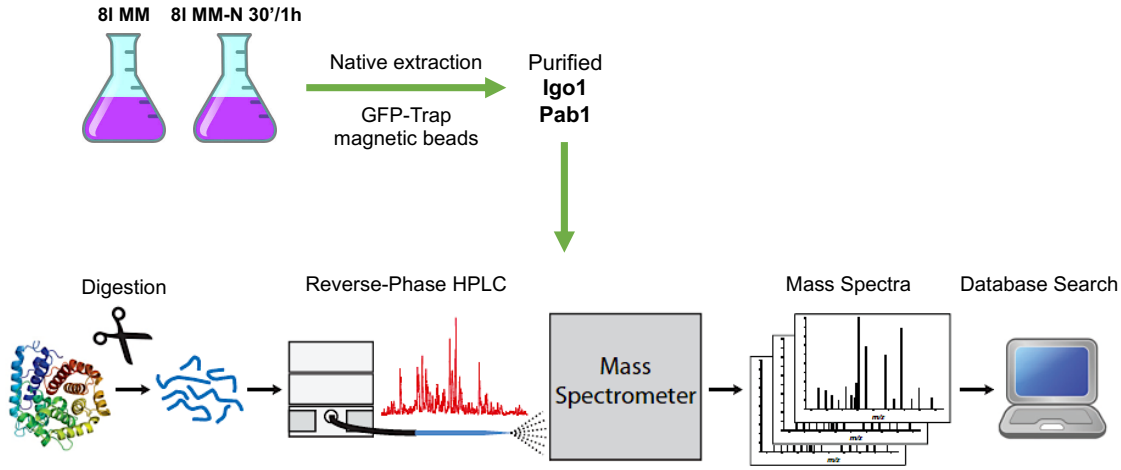

Figure III.1. Experimental procedure employed to identify proteins interacting with Igo1 and Pab1 using 2D LC-MS/MS. Endogenously expressed GFP-tagged Igo1 and GFP-tagged Pab1 proteins (*igo1:GFP* and *P41nmt1:GFP:pab1⁺* mutants) were isolated on GFP-Trap® magnetic agarose beads from lysates derived from MM and MM-N media. Next, protein samples were digested with proteases, producing peptides that were separated by reverse-phase high-performance liquid chromatography and analysed in a mass spectrometer as they eluted from the column. Peptide matching was done algorithmically using spectral data and sequence database information.

Table III.1. List of proteins identified from Igo1:GFP pull-down in MM that displayed the 20 highest spectrum counts.

Name	Description	Spectrum count
Igo1	**mRNA stability protein Igo1**	**443**
Rpl1201	60S ribosomal protein L12.1/L12A	61
Rps2801	40S ribosomal protein S28	25
Rpl3002	60S ribosomal protein L30	20
Tef101	translation elongation factor EF-1 alpha Ef1a-a	18
Rpl801	60S ribosomal protein L8	15
Rps1602	40S ribosomal protein S16	15
Rps1401	40S ribosomal protein S14	14
Rps1801	40S ribosomal protein S18	14
Ret3	coatomer zeta subunit	14
Rpl2301	60S ribosomal protein L23	11
Ret2	coatomer delta subunit Ret2	11
Rpl3401	60S ribosomal protein L34	10
Rps3001	40S ribosomal protein S30	9
Rps802	40S ribosomal protein S8 (predicted)	9
Mrt4	mRNA turnover and ribosome assembly protein Mrt4	9
Sec26	coatomer beta subunit	8
Rpl301	60S ribosomal protein L3	7

Sec21	coatomer gamma subunit Sec21	7
Rps2502	40S ribosomal protein S25	7

Table III.2. List of proteins identified from Igo1:GFP pull-down in MM-N that exhibited the 20 highest spectrum counts.

Name	Description	Spectrum count
Igo1	**mRNA stability protein Igo1**	**398**
Rpl1201	60S ribosomal protein L12.1/L12A	243
Tef102	translation elongation factor EF-1 alpha Ef1a-b	69
Rpl3601	60S ribosomal protein L36	60
Rps2801	40S ribosomal protein S28	53
Sec21	coatomer gamma subunit Sec21	53
Sec26	coatomer beta subunit	52
Pck1	protein kinase C (PKC)-like Pck1	42
Cop1	coatomer alpha subunit Cop1	35
Rps1602	40S ribosomal protein S16	31
Rpl2301	60S ribosomal protein L23	28
Ret2	coatomer delta subunit Ret2	27
Spapb2C8.01	cell surface glycoprotein, adhesion molecule	24
Rpl3401	60S ribosomal protein L34	23
Rps1401	40S ribosomal protein S14	23
Rpl3002	60S ribosomal protein L30	22
Rps1801	40S ribosomal protein S18	22
Rpl801	60S ribosomal protein L8	21
Rps23	40S ribosomal protein S23	20
Thi4	bifunctional thiamine-phosphate dipyrophosphorylase/hydroxyethylthiazole kinase	20

Enrichment analysis of proteins associated with GFP-tagged Igo1 revealed an over-representation of five GO biological processes (Figure III.2): 'Ribosome biogenesis', 'Translation', 'Retrograde vesicle-mediated transport, Golgi to ER', 'rRNA-containing ribonucleoprotein complex export from nucleus' and 'ribosome localization'. Careful analysis of Igo1 interactome also enabled us to spot other promising protein-protein interactions. Fission yeast PKC orthologue, Pkc1, was found among Igo1-interacting proteins (Table III.2, Tables III.S1 and III.S2). Intriguingly, it has been reported that PKC activity regulates binding of Endosulfine to PP2A/B55 in budding yeast (Thai et al., 2017). This result hints that PKC regulation of the Greatwall-Endosulfine-PP2A/B55 pathway may be conserved in *S. pombe*. Moreover, Ies6, a member of the Ino80 (inositol-requiring mutant 80) ATP-dependent chromatin-remodelling complex, and histone H2B Htb1 were identified in our mass spectrometry analysis (Tables III.S1 and III.S2), suggesting a possible role of Endosulfine in chromatin remodelling. Interestingly, transcriptional analysis of cells lacking *igo1*$^{+}$ showed drastic upregulation of *tf2* retrotransposons

and subtelomeric genes under nitrogen starvation (Vázquez-Bolado et al., unpublished data), which is a typical phenotype of mutants with silencing defects and thus, it supports the idea of a role of Greatwall-Endosulfine-PP2A/B55 activity in epigenetic control. Three transcription elongation factors, Tef101, Tef102 and Eft201(Tables III.1-III.S2) were also included in the interactome, suggesting a possible role of the pathway in transcription regulation.

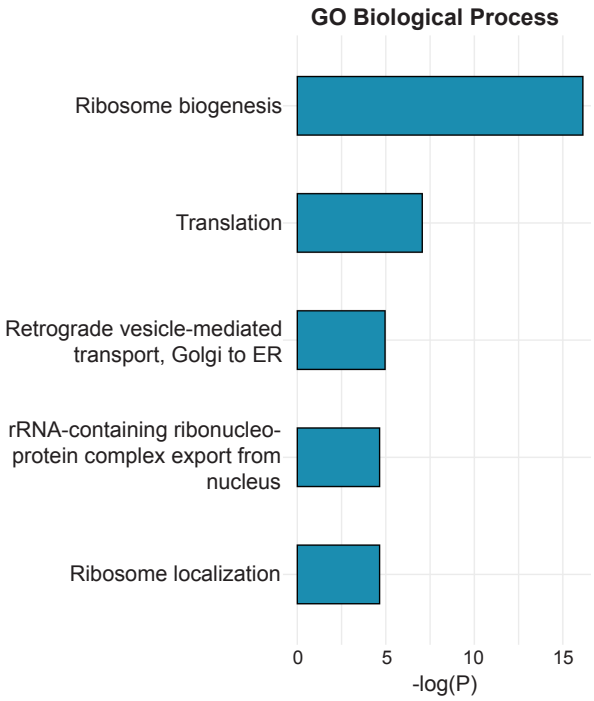

Figure III.2. Enrichment analysis of Pab1 interactome by GO Biological process. Igo1 was purified from cells containing *igo1:GFP* construction integrated at the *igo1⁺* locus. Statistical computing and graphics were performed with R software (© The R Foundation), $p < 0.01$.

The mass spectrometry analysis of Endosulfine-associated proteins revealed multiple protein-protein interactions. Some of them might reflect new targets of the Greatwall-Endosulfine-PP2A/B55 pathway in fission yeast.

1.2. Identification of B55-interacting proteins

The mass spectrometry analysis identified 176 proteins associated with GFP:Pab1 in MM and 630 in MM-N (Tables III.S3 and III.S4). These results suggested that the Pab1 interactome network also became more intricate under nitrogen starvation, where the Greatwall-Endosulfine module is active and inhibits PP2A/B55. However, Pab1-associated proteins were isolated from cells overexpressing GFP-tagged Pab1 cultured in MM for one day and MM-N for one hour. Hence, some interactions might be enhanced in this genetic background. Tables III.3 and III.4 list the 20 proteins that interacted with Pab1 and displayed the highest spectrum counts in MM and MM-N, respectively. Among them we identified Paa1, Ppa1 and Ppa2, that together with Pab1, conformed PP2A/B55 phosphatase complex (Table III.3 and III.4), serving as a positive control.

Table III.3. List of proteins identified from Pab1 pull-down in MM that exhibited the 20 highest spectrum counts.

Name	Description	Spectrum count
Pab1	**protein phosphatase regulatory subunit Pab1**	**441**
Paa1	protein phosphatase regulatory subunit Paa1	61

Ppa2	serine/threonine protein phosphatase Ppa2	39
Nup211	nucleoporin nup211	27
Cop1	coatomer alpha subunit Cop1 (predicted)	22
Yme1	mitochondrial inner membrane i-AAA protease complex subunit Yme1	22
Ppa1	minor serine/threonine protein phosphatase Ppa1	19
Nup40	nucleoporin Nup40	18
Sec21	coatomer gamma subunit Sec21	18
Cct6	chaperonin-containing T-complex zeta subunit Cct6	18
Sec26	coatomer beta subunit	17
Adn1	adhesion defective protein	15
Thi2	thiazole biosynthetic enzyme	13
Mdj1	mitochondrial DNAJ domain protein Mdj1	11
Elp1	elongator subunit Elp1	10
Mug72	oxidoreductase	10
Rad16	DNA repair endonuclease XPF	10
Sea4	SEA complex subunit, ubiquitin-protein ligase E3, Sea4	9
Rps802	40S ribosomal protein S8	9
Pho8	vacuolar membrane alkaline phosphatase	9

Table III.4. List of proteins identified from Pab1 pull-down in MM-N that displayed the 20 highest spectrum counts.

Name	Description	Spectrum count
Pab1	**protein phosphatase regulatory subunit Pab1**	**5547**
Paa1	protein phosphatase regulatory subunit Paa1	1427
Ppa2	serine/threonine protein phosphatase Ppa2	897
Tef101	translation elongation factor EF-1 alpha Ef1a-a	552
Cop1	coatomer alpha subunit Cop1	174
Ppa1	minor serine/threonine protein phosphatase Ppa1	146
Sec26	coatomer beta subunit	132
Yme1	mitochondrial inner membrane i-AAA protease complex subunit Yme1	122
Thi2	thiazole biosynthetic enzyme	112
Ppk19	serine/threonine protein kinase Ppk19	109
Nup211	nucleoporin nup211	106
Alm1	medial ring protein Alm1	96
Sec21	coatomer gamma subunit Sec21	96

Cct6	chaperonin-containing T-complex zeta subunit Cct6	93
Moc3	transcription factor Moc3	77
Spac1F7.09C	allantoicase (predicted)	72
Elp1	elongator subunit Elp1	72
Rad16	DNA repair endonuclease XPF	69
Sec18	secretory pathway protein Sec18	60
Mug72	oxidoreductase	58
Mst2	histone acetyltransferase Mst2	57

In this case, enrichment analysis of the Pab1 interactome revealed over-representation of nine GO biological processes including 'Cytoplasmatic transport', 'Protein localization', 'Regulation of mitotic nuclear division' or 'Regulation of intracellular signal transduction' (Figure III.3). Mass spectrometry analysis showed interesting protein-protein interactions. In particular, several subunits of chromatin-modifying complexes, including Mst2, SAGA and Clr6 complexes, were found among Pab1-interacting proteins (Table III.4, Tables III.S3 and III.S4), supporting the idea of a possible role of PP2A/B55 complex in epigenetic control. Intriguingly, cells lacking *igo1*$^{+}$, where PP2A/B55 is highly active, exhibited silencing defects under nitrogen starvation (Vázquez-Bolado et al., unpublished data). Since the assay was performed in cells overexpressing *pab1*$^{+}$, some Pab1 interacting proteins could cause the phenotypes observed in the *igo1Δ* mutant. Moreover, ten nucleoporins, constituents of the nuclear pore complex, were identified in our analysis (Tables III.3-III.S4). This data also suggested a possible function of the Greatwall-Endosulfine-PP2A/B55 pathway in chromatin remodelling, as nucleoporins are involved in the organisation and maintenance of heterochromatin (Iglesias et al., 2020). Atg6 and Atg14, which take part in autophagic processes, were also found in the Pab1 interactome (Tables III.S3 and III.S4). These interactions supported previous data from our laboratory that showed that the autophagic flux is reduced in Greatwall and Endosulfine mutants (Vázquez-Bolado et al., unpublished data). Finally, many subunits of the SEA (Seh1-associated) complex copurified with Pab1. In budding yeast, the SEA complex modulates TORC1 activity (reviewed in Dokudovskaya and Rout, 2015) and it is downregulated by PP2A (Sutter et al., 2013; Laxman et al., 2014), suggesting that this mechanism may be conserved in fission yeast.

The mass spectrometry analysis of B55-copurified proteins revealed numerous protein-protein interactions. Future experiments will be needed to stablish if they are new targets of the Greatwall-Endosulfine-PP2A/B55 pathway in fission yeast.

1.3. Identification of Greatwall-interacting proteins

We could not analyse the Ppk18 interactome, since we were unable to purify GFP-tagged Ppk18 protein. Hence, we will need to consider other strategies to identify targets of Greatwall in fission yeast.

2. The Mst2 complex might be a new target of the Greatwall-Endosulfine-PP2A/B55 pathway in fission yeast

We performed affinity purification of GFP:Pab1 and identified several proteins that are part of the Mst2 and SAGA histone acetyltransferase (HAT) complexes and the Clr3 and Clr6 histone deacetylate (HDAC) complexes (Table III.4, Tables III.S3 and III.S4), suggesting a role of PP2A/B55 in chromatin silencing during entry into quiescence. The Mst2 complex is similar in composition to mammalian HBO1/MOZ/MORF and *S. cerevisiae* NuA3 complexes (Wang et al.,

2012). It works together with Gcn5 to mediate H3K14 acetylation (Nugent et al., 2010; Wang et al., 2012), which is associated with active chromatin (Pokholok et al., 2005; Wang et al., 2008). Furthermore, Mst2 also acetylates Brl1 (Flury et al., 2017), a subunit of the histone H2B ubiquitin ligase complex (HULC). Ubiquitylation of H2B at lysine 119 also activates gene expression (Tanny et al., 2007; Zofall and Grewal, 2007). Mst2 complex consists of seven proteins: the lysine acetyltransferase Mst2, Pdp3, Nto1, Eaf6, Tfg3, Ptf1 and Ptf2 (Wang et al., 2012). Nto1 and Ptf2 are necessary for the integrity and assembly of the complex (Wang et al., 2012). Eaf6 is shared with the NuA4 acetyltransferase complex, and Tfg3 is present in Ino80, SWI/SNF, TFIID and TFIIF complexes. Interestingly, all the subunits of the Mst2 complex were affinity purified with GFP:Pab1 except for Pdp3 (Table III.4, Tables III.S3 and III.S4), a PWWP protein that interacts with H3K36me3. Pdp3 recruits the Mst2 complex to highly transcribed regions, where the histone H3-K36 methyltransferase Set2 interacts with the CTD domain of RNA polymerase Pol II (Flury et al., 2017). Cells lacking *pdp3⁺* showed silencing defects due to ectopic location of the Mst2 complex in heterochromatic regions (Flury et al., 2017).

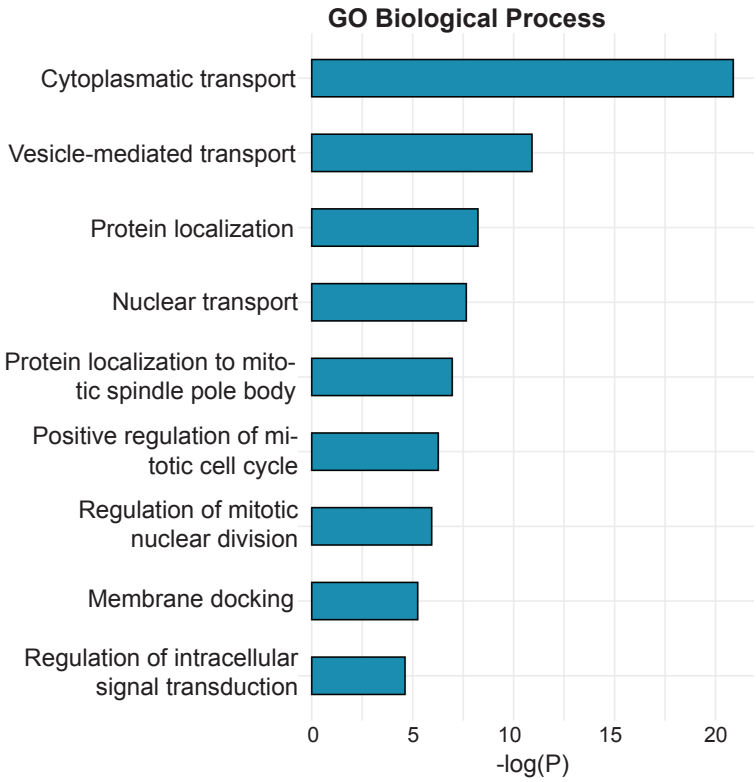

Figure III.3. Enrichment analysis of Pab1 interactome by GO Biological process. GFP:Pab1 was purified from cells containing a copy of the P41nmt1 promoter integrated upstream from *pab1⁺* ORF. Statistical computing and graphics were performed in R software (© The R Foundation), $p < 0.01$.

Given all this evidence, we decided to explore the possible connection between PP2A/B55 and Mst2 complexes. We believe that *igo1Δ* mutant cells, where PP2A/B55 is hyperactive in nitrogen-poor or nitrogen-free media, could be similar to *pdp3Δ* cells. In cells lacking *igo1⁺*, the Mst2 complex might lose its interaction with Pdp3, and might be ectopically located at subtelomeric regions where it could activate the expression of normally silenced genes (Figure III.4). Loss of Pdp3 interaction with the Mst2 complex may explain the silencing defects of the *igo1Δ* (Vázquez-Bolado et al., unpublished data).

2.1. Mst2 complex might interact with PP2A/B55 in fission yeast

The mass spectrometry analysis identified Mst2 with a high sequence coverage (52,60%) (Tables III.S3 and III.S4) and among proteins with the highest spectrum count (Table III.4),

supporting a possible interaction between Mst2 and PP2A/B55 complexes in fission yeast. To confirm that Pab1 interacts with Mst2 in vivo, reciprocal coimmunoprecipitation assays were carried out in protein extracts from Mst2:13Myc, GFP:Pab1 or Pab1:3HA that were immunoprecipitated with anti-Myc, anti-HA antibodies or GFP-nanobodies and then immunoblotted with anti-Myc, anti-HA or anti-GFP antibodies. Unfortunately, we were unable to successfully copurify these proteins even when Pab1 was overexpressed (Figure III.5), suggesting that Mst2 may be degraded during the immunoprecipitation. This would explain why the interactomic assay, where proteins samples are digested with proteases, identified Mst2 as a Pab1 interacting protein and coimmunoprecipitation experiments did not

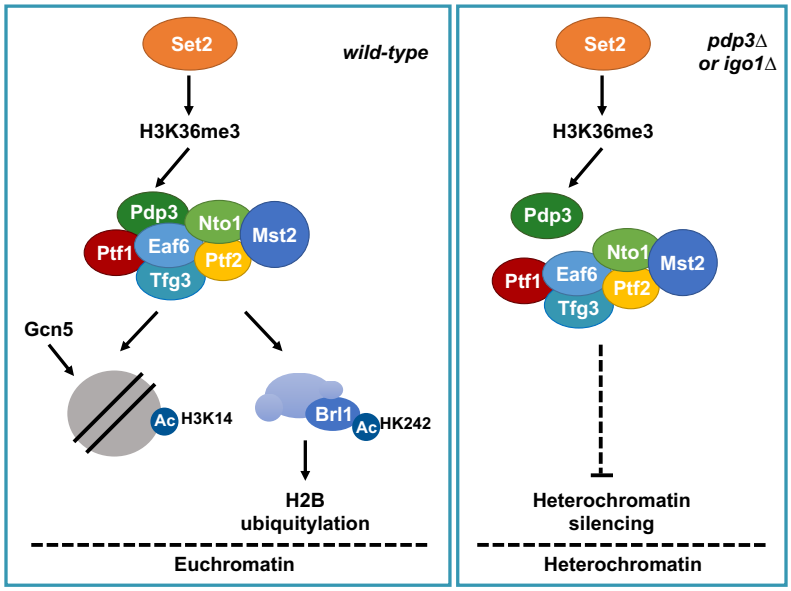

Figure III.4. Model for the Mst2 complex-dependent functional pathways in the presence or absence of Ppd3-mediated tethering to H3K36me3. In wild-type cells, Pdp3 recruits Mst2 complex to actively transcribed regions via H3K36me3 (**left**). *pdp3Δ* mutant shows silencing defects due to promiscuous access of Mst2 complex to heterochromatin. Our results suggest that the *igo1Δ* mutant could behave in a similar way to the *pdp3⁺* deletion. In cells lacking *igo1⁺*, the Mst2 complex might lose its interaction with Pdp3 and locate at heterochromatic regions due to high PP2A/B55 phosphatase activity (**right**). The Dotted line represents unknown targets of Mst2 complex in silenced regions.

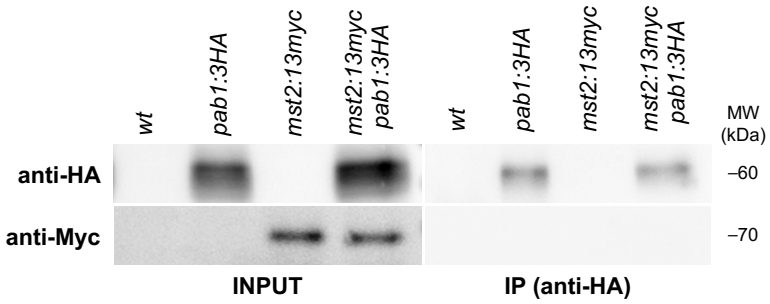

Figure III.5. Coimmunoprecipitation assay of Pab1 and Mst2 proteins. Wild-type, *pab1:3HA*, *mst2:13myc* and *mst2:13myc pab1:3HA* cells were grown in MM and shifted to MM-N. Protein samples were taken at one hour after the shift to MM-N. Pab1:3HA was immunoprecipitated using anti-HA antibody and Mst2:13Myc with anti-Myc antibody, and bound proteins were identified by immunoblotting with either anti-HA or anti-Myc antibodies. Only Pab1:3HA immunoprecipitation is shown.

Future experiments crosslinking the proteins before immunoprecipitation or using cryogenic mills will be required to confirm the *in vivo* interaction between PP2A-B55 and Mst2 complexes.

2.2. Role of Mst2 complex in quiescence

PP2A/B55 may play a crucial role in the regulation of Mst2 and Pdp3 interaction. In nitrogen-starved *igo1Δ* mutant cells, high levels of PP2A/B55 activity might weaken the binding of the Mst2 complex to Pdp3, causing ectopic localisation of Mst2 complex and silencing defects. To test this hypothesis, we studied the phenotype of the *igo1Δ mst2Δ* double mutant searching for genetic interactions between these genes. Since Igo1 is essential for the G_0 phase induced by nitrogen starvation, we decided to analyse quiescence dynamics in the *igo1Δ mst2Δ* mutant.

When fission yeast cells are shifted from MM to MM-N, they reduce their cell size and arrest in G1 before entering into quiescence. As indicated earlier, the *igo1Δ* mutant showed G1 arrest defects. When analysing cells lacking both *igo1⁺* and *mst2⁺*, we did not detect G1 arrested cells until one day in MM-N, when a small G1 cell population was observed (Figure III.6). According to this, *igo1Δ mst2Δ* cells were smaller than *igo1Δ* cells after 24 hours in MM-N. Both data indicated that deletion of *mst2⁺* slightly ameliorated the G1 arrest defect of the *igo1Δ* mutant, indicating that Mst2 might be partly responsible for the *igo1Δ* mutant phenotype under nitrogen starvation. Single *mst2Δ* mutant cells behaved essentially like wild-type cells. Almost all cells reduced cell size and arrested in G1 after one day without nitrogen (Figure III.6), suggesting that Mst2 is not required for the pre-quiescence response. This result is consistent with a no role of Mst2 in cell-cycle regulation.

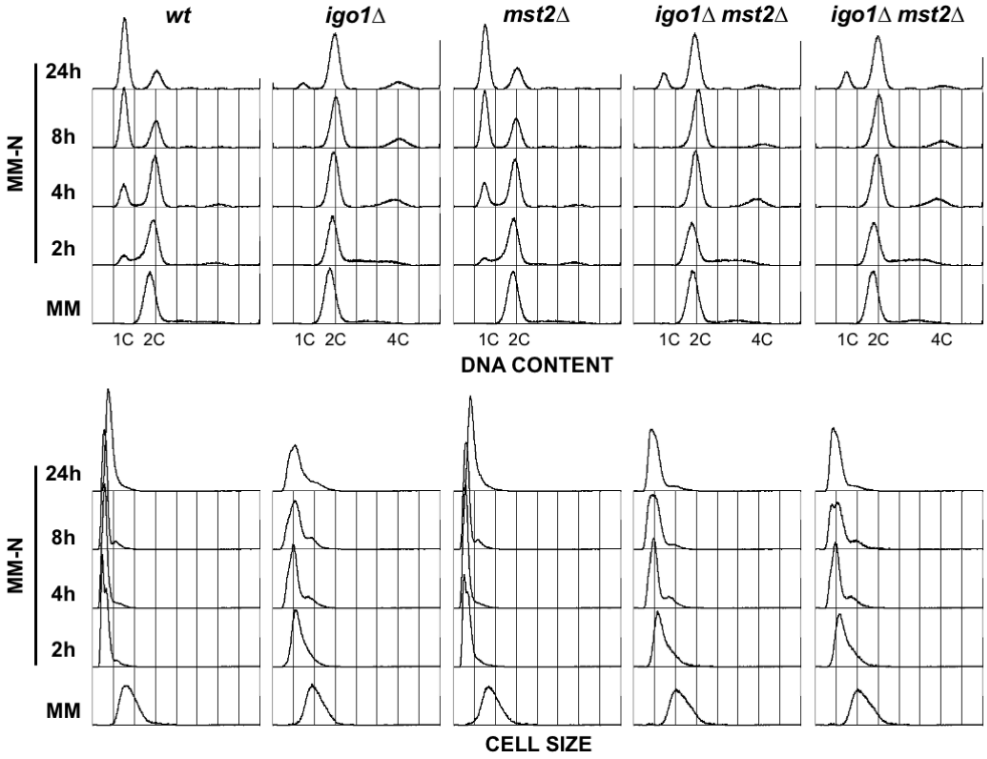

Figure III.6. Mst2 activity is dispensable for the pre-quiescence response to nitrogen deprivation. FACS profile of ethanol-fixed wild-type, *igo1Δ*, *mst2Δ and igo1Δ mst2Δ* (two independent clones) cells. DNA content (1C and 2C) after propidium iodide staining (**top**) and forward scatter (FSC, **bottom**), which correlates with cell size, are shown. Cells were grown in MM for one day at 25ºC and then shifted to MM-N. Samples were collected at the indicated time points after the shift.

In fission yeast, the establishment of the G_0 phase takes about 24 hours. Remarkably, quiescent cells remain viable for months under nitrogen starvation conditions (Mochida and Yanagida, 2006; Su et al., 1996). We have previously shown that *igo1⁺* is required to enter into and maintain this quiescent state (Figure I.13). *igo1Δ* cells began to die around 6-8 days in MM-N (Figures I.8 and III.7). By contrast, deleting *mst2⁺* gene did not affect cell survival under nitrogen

deprivation (Figure III.7). *mst2Δ* cells remained viable throughout the experiment, indicating that Mst2 activity is not required for cell survival during a 15-day incubation in MM-N. When we deleted both *igo1*$^{+}$ and *mst2*$^{+}$, cell viability increased. However, the *igo1Δ mst2Δ* cell culture, like the *igo1Δ* mutant, was practically dead after 15 days without nitrogen (Figure III.7), suggesting that Mst2 activity may only account for part of the *igo1Δ* mutant defects under nitrogen starvation.

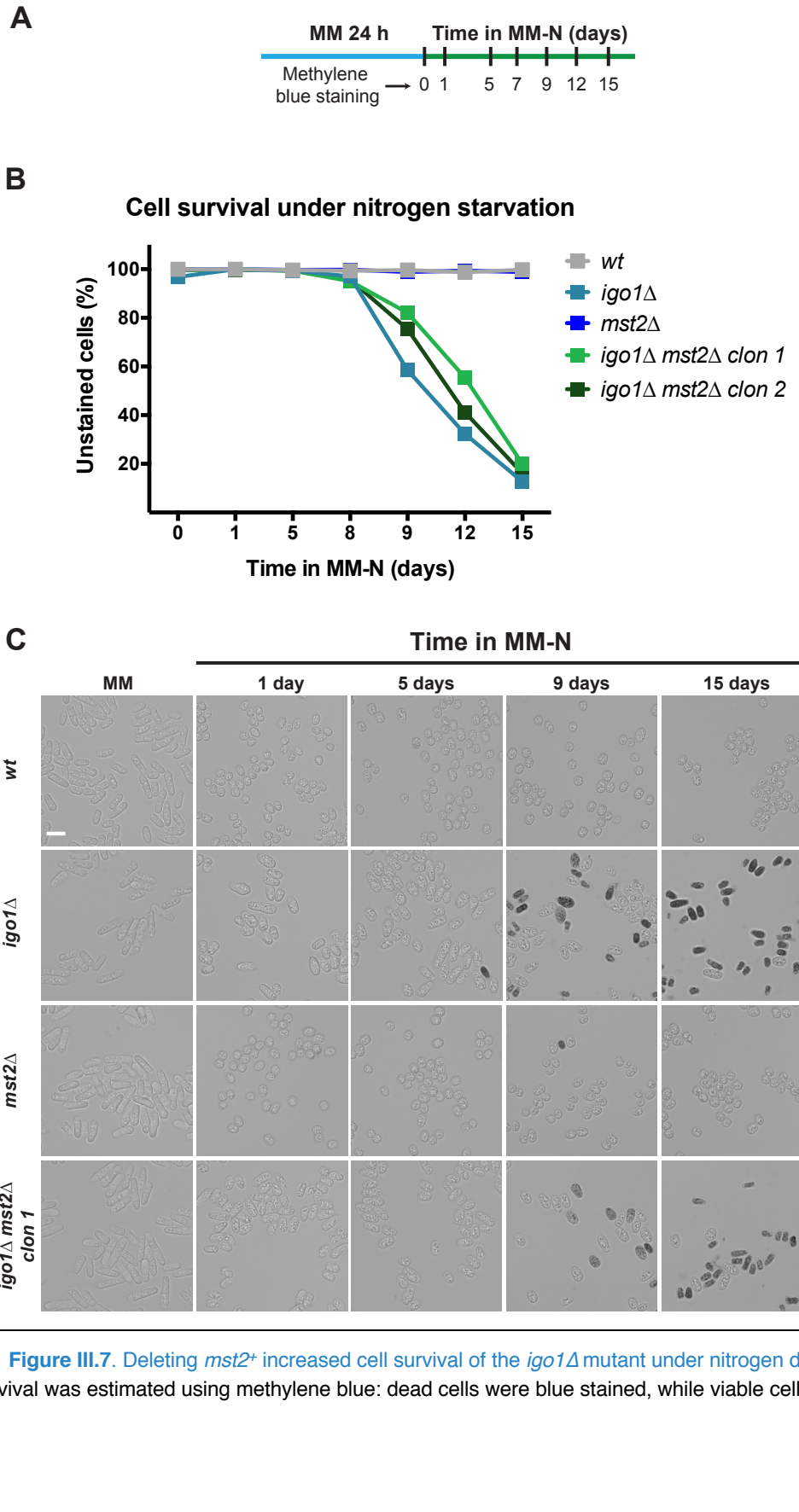

Figure III.7. Deleting *mst2*$^{+}$ increased cell survival of the *igo1Δ* mutant under nitrogen deprivation. Cell survival was estimated using methylene blue: dead cells were blue stained, while viable cells were not

stained. **A.** Procedure employed in the cell survival measurements. Cells were grown in MM, shifted to MM-N and kept under nitrogen starvation for 15 days. Samples were collected and stained at the indicated time points after the shift. **B.** Percentage of cell survival of wild-type, *igo1Δ*, *mst2Δ* and *igo1Δ mst2Δ* cells in MM-N. **C.** Images of wild-type, *igo1Δ*, *mst2Δ* and *igo1Δ mst2Δ* cells stained with methylene blue. Scale bar, 10 μm.

Hence, there is some genetic interaction between *igo1*$^{+}$ and *mst2*$^{+}$ genes since *mst2*$^{+}$ deletion partially rescues *igo1Δ* mutant defects under nitrogen starvation. High levels of PP2A/B55 activity in *igo1Δ* cells might alter Mst2 complex function, explaining why Mst2 activity might account for part of *igo1Δ* phenotype.

Discussion

1. The Greatwall-Endosulfine-PP2A/B55 pathway regulates the pre-quiescence response induced by nitrogen starvation

In multicellular organisms, most cells reside in a non-dividing G_0 state. This resting phase is commonly known as quiescence and describes a reversible cell-cycle arrest state. Although quiescent cells are often identified by low RNA content and lack of cell proliferation markers, they are capable of re-entering the cell cycle in response to extracellular or mitogenic signals (Fukada et al., 2007). Examples of quiescent cells include hematopoietic and neuronal stem cells (Codega et al., 2014; Morrison and Weissman, 1994), fibroblasts and memory T cells (Yao, 2014), or starved yeast cells (Dhawan and Laxman, 2015; De Virgilio, 2012). Despite the relevance of quiescence, little is known about how cells enter into, maintain and exit from the G_0 phase (Yanagida, 2009).

In fission yeast, G_0 entry is induced in response to nitrogen starvation (Su et al., 1996). *S. pombe* cells immediately cease growth and divide twice in the absence of nitrogen, resulting in G1 arrest and cell size reduction. These changes prepare cells for entry into quiescence and are also referred to as the pre-quiescence response. G_0 entry takes about one day, and once quiescence is established, cells are viable for months. Upon nitrogen replenishment, quiescent fission yeast cells will re-enter the cell cycle and resume proliferation (Mochida and Yanagida, 2006; Su et al., 1996).

Our group has recently reported that *S. pombe* cells couple TORC1 to the cell-cycle machinery by regulating the Greatwall-Endosulfine molecular switch, which inhibits PP2A/B55 phosphatase (Chica et al., 2016). In nitrogen-rich media, TORC1 is fully active, Greatwall and Endosulfine are inhibited, and therefore, they are unable to inactivate PP2A/B55. In these conditions, PP2A/B55 is active and counteracts CDK activity; thus, mitotic entry is delayed, and cells divide with a large size. In nitrogen-poor media, TORC1 activity drops, leading to Greatwall-Endosulfine activation and PP2A/B55 inhibition. Reduced PP2A/B55 activity enables cells to divide with a smaller size. These results showed that the Greatwall-Endosulfine-PP2/B55 pathway regulates the G2/M transition and cell size at division upon nutritional shift-down. In this work, we have shown that the Greatwall-Endosulfine-PP2/B55 pathway is also relevant for the pre-quiescence response induced by nitrogen starvation. We have observed that cells lacking either Greatwall (*cek1Δ ppk18Δ*) or Endosulfine (*igo1Δ*) are unable to arrest in G1 and displayed a larger cell size than the wild-type under nitrogen starvation (Figures I.1 and I.17). Remarkably, deletion of *ppa2⁺* or repression of *pab1⁺* expression, which encode the catalytic and regulatory subunits of PP2A/B55, respectively, rescued the pre-quiescence defects of the *igo1Δ* mutant (Figure I.3). Our data is consistent with published results from other laboratories which reported that the Greatwall-Endosulfine-PP2A/B55 pathway is required to trigger the last two successive cell divisions and for G1 arrest in the absence of nitrogen (Aono et al., 2019). Interestingly, in budding yeast, the Greatwall orthologue, Rim15, is also involved in the pre-quiescence response (Pedruzzi et al., 2003; Watanabe et al., 2012). Cells deleted for *RIM15* were defective for proper G1 arrest following TORC1 inactivation by rapamycin (Pedruzzi et al., 2003). Hence, in both fission and budding yeasts, the Greatwall-Endosulfine module is essential for the pre-quiescence response.

2. Regulation of the sexual differentiation response by the Greatwall-Endosulfine-PP2A/B55 pathway

In *S. pombe*, nitrogen controls the transition from cell growth and division to cell differentiation. In the presence of nitrogen, fission yeast cells proliferate. Only when nitrogen concentration drops below a certain level, they initiate the differentiation response and undergo mating, meiosis and sporulation (Yamamoto, 1996). TORC1 and TORC2 complexes regulate this

transition. Whereas TORC1 is activated by nitrogen and promotes cell growth (reviewed in Laplante and Sabatini, 2012), TORC2 becomes active under nitrogen starvation and is required for cell differentiation (reviewed in Weisman, 2016). Recent work has described that TORC1 regulates the cell differentiation response through PP2A/B55 phosphatase (Laboucarié et al., 2017; Martín et al., 2017). In nitrogen-rich media, TORC1 allows activation of PP2A/B55 by inhibiting the Greatwall-Endosulfine module. Active PP2A/B55 opposes TORC2 phosphorylation of Gad8, preventing Gad8 activation and the initiation of the cell differentiation programme (Martín et al., 2017). According to this, the transcriptional profiles of thermosensitive *tor2-ts6* mutant significantly overlaps with the profile of *pab1Δ* cells (Martín et al., 2017; Matsuo et al., 2007). Greatwall and Endosulfine also play a positive role in regulating the differentiation response, since cells deleted for either of these genes (*cek1Δ ppk18Δ* or *igo1Δ*) showed low mating efficiency (Figure I.6). Furthermore, transcriptional analysis of *cek1Δ ppk18Δ* and *igo1Δ* mutants revealed that genes involved in the sexual differentiation response were down-regulated in these cells compared to wild-type (Vázquez-Bolado et al., unpublished data). By contrast, PP2A/B55 negatively regulated mating as cells lacking *ppa2⁺* or expressing low levels *pab1⁺* were hyperfertile and rescued the sporulation defect of *igo1Δ* mutant (Figure I.7). Remarkably, cells deleted for *pab1⁺* exhibited high levels of expression of genes implicated in conjugation or meiosis (Laboucarié et al., 2017) due to hyperphosphorylation and hyperactivation of Gad8 (Martín et al., 2017). Moreover, the SAGA complex participates in the control of the differentiation response. When nutrients are plentiful, the acetyltransferase Gcn5, which is part of the SAGA, downregulates *ste11⁺* expression (Helmlinger et al., 2008), an HMG-box transcription factor essential for the differentiation pathway (Mata and Bähler, 2006; Sugimoto et al., 1991). Interestingly, deletion of *gcn5⁺* restores *ste11⁺* expression in the *igo1Δ* mutant (Laboucarié et al., 2017). Other components of SAGA are also involved in the regulation of *ste11⁺* expression. Specifically, Taf12 and Spt8 subunits are required for *ste11⁺* induction in the absence of nitrogen (Helmlinger et al., 2008). Whereas PP2A/B55 dephosphorylates Taf12 in nitrogen-rich media, Gad8 phosphorylates it under nitrogen starvation (Laboucarié et al., 2017).

In *S. cerevisiae*, TORC1 and PKA complexes negatively regulate the differentiation response, which also requires Greatwall-Endosulfine-PP2A/B55 activity (Sarkar et al., 2014; Vidan and Mitchell, 1997). Cells deleted for *RIM15* or *IGO1* and *IGO2*, Greatwall and Endosulfine orthologues in budding yeast, respectively, undergo an inefficient pre-meiotic S phase and gametogenesis. Furthermore, the Rim15-Igo1/2 switch is required for pre-meiotic autophagy (Sarkar et al., 2014), which is essential for gametogenesis in budding (Tsukada and Ohsumi, 1993) and fission yeasts (reviewed in Mukaiyama et al., 2010). Nonetheless, the function of the Greatwall-Endosulfine-PP2A/B55 pathway seems to be restricted to the early stages of *S. cerevisiae* meiosis as phosphorylation of Igo1 on Ser64 increases at the beginning of meiosis and then disappears (Sarkar et al., 2014; Vidan and Mitchell, 1997). Hence, in both budding and fission yeasts, the Greatwall-Endosulfine module plays relevant roles in the sexual differentiation response through inhibition of PP2A/B55 phosphatase.

In metazoans, the Greatwall-Endosulfine-PP2A/B55 pathway has been involved in regulating gametogenesis in *Drosophila*, where Endosulfine is required for meiotic maturation and fertility (Drummond-Barbosa and Spradling, 2004; Von Stetina et al., 2008). Interestingly, the role of Endosulfine in gametogenesis might be conserved in mammals since ENSA, mammalian Endosulfine, is expressed in mouse oocytes. Moreover, ENSA expression rescued the Endosulfine mutant phenotype in flies (Von Stetina et al., 2008). On the other hand, mTORC1 regulation of the Greatwall-Endosulfine switch has not been reported in animal cells. However, overexpression of Greatwall promotes degradation of PH domain leucine-rich repeat protein phosphatase (PHLPP), resulting in hyperactivation of the Gad8 orthologue, Akt (Vera et al.,

2015). Although Greatwall regulates Akt activity independently of Endosulfine and PP2A in mammalian cells, both models share intriguing similarities.

3. The Greatwall-Endosulfine-PP2A/B55 pathway regulates cell survival under nitrogen starvation

Cellular quiescence is a conserved resting state in eukaryotes. The ability to exit from the cell cycle and enter this state is a key cellular strategy to ensure cell survival. When the environment is unfavourable for proliferation, most cells are capable of entering a non-dividing G_0 state, while retaining its ability to re-enter the cell cycle (Gray et al., 2004; Werner-Washburne et al., 1993). Quiescence is characterised by a reversible cell-cycle arrest in G1 with condensed chromatin, decreased transcription and translation, reduced cell size, increased resistance to stress, induction of autophagy and increased longevity (reviewed in Valcourt et al., 2012). Most of these G_0-features are shared by many organisms, suggesting that the core features of the quiescence programme are conserved (Gray et al., 2004; Kaeberlein, 2010). *S. pombe* is an excellent model to study quiescence as entry into and exit from G_0 are controlled by nitrogen (Mochida and Yanagida, 2006; Su et al., 1996). When fission yeast cells are starved for nitrogen, they divide twice without growth and arrest in G1 before entering into G_0. During this process, physiology and gene expression are significantly reprogrammed so that cells can adapt to adverse conditions (Marguerat et al., 2012; Sajiki et al., 2009; Takeda and Yanagida, 2010). Several studies have identified key processes involved in the regulation of quiescence, revealing that autophagy, RNA transcription and processing, vesicle transport, lipid biosynthesis and heterochromatin assembly are essential for G_0 (Oya et al., 2019; Sajiki et al., 2009, 2018; Sideri et al., 2015; Takeda and Yanagida, 2010). The nuclear organisation is also modified during quiescence. In fact, the nuclear volume decreases, the nucleus flattens, chromatin becomes hyper-condensed, and telomeres cluster close to the nuclear envelope (Maestroni et al., 2020; Su et al., 1996).

We have shown that the Greatwall-Endosulfine module becomes activated upon nitrogen starvation to inhibit PP2A/B55 phosphatase, allowing the last two cell divisions and G1 arrest prior to quiescence entry to occur. Since these results indicated that Greatwall and Endosulfine proteins are essential for the pre-quiescence response, we decided to study if the Greatwall-Endosulfine-PP2A/B55 pathway also plays a role in quiescence in fission yeast. In fact, results from this work proved that inactivation of PP2A/B55 by the Greatwall-Endosulfine switch in nitrogen-free medium (MM-N) is required for cell survival of quiescent cells. Accordingly, cells lacking Endosulfine (*igo1Δ*) lost viability dramatically after one week in MM-N (Figure I.8). Mutants deleted for Greatwall (*cek1Δ ppk18Δ*) or Endosulfine (*igo1Δ*) also showed defects in G_0 exit since quiescent cells could not resume proliferation after nitrogen replenishment (Figure I.12). Conversely, cells with reduced levels of Pab1, the B55 subunit of PP2A (*P41nmt1-GST-pab1⁺*), survived for a long time under nitrogen starvation, consistent with a negative role of PP2A/B55 in quiescence. Furthermore, down-regulation of PP2A/B55 rescued the lethality of *igo1⁺* deletion (Figure I.8), again suggesting that inhibition of PP2A/B55 phosphatase is essential for the proper establishment of the quiescent state in fission yeast. Nevertheless, *pab1⁺* repression only partially rescued the *igo1Δ* mutant defects to re-enter cell-cycle after nitrogen replenishment (Figure I.13), suggesting that PP2A/B55 activity might be required to maintain mitotic competence in the absence of Endosulfine.

As mentioned before, the Greatwall-Endosulfine-PP2A/B55 pathway connects TORC1 and TORC2 activities in order to regulate the differentiation programme in fission yeast. When nitrogen is abundant, TORC1 promotes the inhibition of Gad8, the main effector of TORC2, through the activation of PP2A/B55 phosphatase (Martín and López-Áviles, 2018; Martín et al.,

2017). As the Greatwall-Endosulfine-PP2A/B55 pathway acts through the TORC2-Gad8 axis to regulate the cell differentiation response, we decided to study if this crosstalk was also important for quiescence regulation. However, cells deleted for *gad8⁺* remained viable during quiescence (Figure I.18) and were also able to re-enter the cell cycle after nitrogen replenishment (Figures I.19 and I.20), suggesting that Ga8 is not required for quiescence in fission yeast. Accordingly, in budding yeast, it has not been described a connection between TORC2 signalling and quiescence. Surprisingly, the fission yeast TORC2-Gad8 axis is necessary for the pre-quiescence response since cells lacking either of the two genes (*tor1Δ* or *gad8Δ*) do not arrest in G1 under nitrogen starvation (Weisman and Choder, 2001; Weisman et al., 2007) (Figure I.17). These results suggest that *S. pombe* cells are capable of implementing the G_0 programme without previously arresting in G1. They also challenge the long-standing notion that G1 arrest is indispensable for the establishment of G_0.

Quiescence is associated with widespread transcriptional silencing, chromatin condensation and changes in nuclear architecture. In fission yeast, chromatin flattens, and the nuclear volume decreases during quiescence (Su et al., 1996). Interestingly, Figures I.14 and I.15 show that deletion of Endosulfine (*igo1Δ*) impaired nuclear integrity during quiescence. These nuclear defects might be the cause of the *igo1Δ* mutant lethality. Moreover, telomeric regions are modified during quiescence in fission yeast. Although the global transcription is reduced in quiescent cells, telomeric transcription is up-regulated (reviewed in Coulon and Vaurs, 2020). During quiescence, fission yeast telomeres cluster and attach to the nuclear envelope (Maestroni et al., 2020). This anchoring is important for heterochromatin establishment and telomeric transcription (reviewed in Coulon and Vaurs, 2020). Remarkably, telomere attrition is a common denominator of ageing (López-Otín et al., 2013). In fission yeast, telomere stability is also linked to cell survival in quiescence since deletion of telomerase (*ter1Δ*) decreases cell viability (Maestroni et al., 2017). Given this evidence, we studied telomere integrity in Greatwall and Endosulfine deletion mutants (*cek1Δ ppk18Δ* and *igo1Δ*) during quiescence by collaborating with Dr. Miguel Godinho Ferreira's group. Surprisingly, telomeres neither shortened nor fused in quiescent *cek1Δ ppk18Δ* and *igo1Δ* cells (Escandell et al., unpublished) (Figures 1A and 1B). However, genomic DNA was degraded after 20 days in MM-N (Figure 1C), which agrees with our results showing that *igo1Δ* cells were already dead at this time point (Figure I.8).

Work from other laboratories has also highlighted the relevance of the Greatwall-Endosulfine-PP2A pathway in fission yeast quiescence. A genome-wide screen identified Cek1 and Ppk18 as lifespan regulators (Chen et al., 2013a). Whereas cells lacking *ppk18⁺* showed reduced CLS, *cek1⁺* deletion did not affect lifespan, consistent with our results (Figures I.10). However, deletion of both genes caused greater defects that the single deletions, suggesting a partial redundancy between Ppk18 and Cek1 (Chica et al., 2016) (Figure I.10). Chen et al., 2013a also reported that the Pef1/Clg1 complex seemed to negatively regulate Cek1. They proposed that inhibition of this CDK complex promotes Cek1 activity, stimulating entry into quiescence. Interestingly, our group has demonstrated that Ppk18 and Cek1 were regulated by TORC1 activity (Chica et al., 2016). In the presence of Ppk18, Cek1 might be predominantly controlled by Pef1/Clg1, whereas TORC1 regulation of Cek1 may become relevant when Ppk18 is not present. Recently, another genome-wide screen identified *igo1⁺* as a G_0 essential gene (Sajiki et al., 2018). In agreement with our results, Aono et al., 2019 described that inhibition of PP2A/Pab1 by phosphorylated Endosulfine (Igo1-S64P) is required for long-term cell survival in quiescent fission yeast cells.

Notably, many of the mutations that extend lifespan decrease the activity of nutrient-signalling pathways. Calorie restriction (reduced nutrient intake) and down-regulation of TORC1 activity increase longevity in virtually all tested organisms, including yeast, flies, rodents and monkeys (Blagosklonny and Hall, 2009; Fontana et al., 2010). Moreover, deletion of the S6 kinase

orthologue, Sck2 in *S. pombe* and Sch9 in *S. cerevisiae*, that inhibits Greatwall, extends CLS (Chen and Runge, 2009; Fabrizio et al., 2001), while overexpression of *sck2⁺* reduces life span (Figure I.11). In budding yeast, Greatwall and Endosulfine orthologues, Rim15 and Igo1/2, respectively, integrate signals from TORC1, PKA and Pho85/Pho80 complexes and regulate several aspects of the quiescence programme (Swinnen et al., 2006). The Rim15-Igo1/2 module promotes G_0 entry and survival in stationary phase (Talarek et al., 2010; Wei et al., 2008) by inhibiting PP2A/B55 orthologue, PP2A/Cdc55 (Bontron et al., 2013). Inhibition of PP2A/Cdc55 triggers the stabilisation of mRNAs that are critical for survival in G_0 (Talarek et al., 2010), and stimulates the Gis1 and Msn2/4 transcription factors (Bontron et al., 2013), which are involved in the regulation of gene expression upon nutrient starvation (Boy-Marcotte et al., 1998; Causton et al., 2001; DeRisi et al., 1997; Gasch et al., 2000). Furthermore, Rim15 limits ROS levels and regulates the accumulation of storage carbohydrates during G_0 entry (Watanabe et al., 2012). Rim15 is also involved in the glucose-anabolic pathway as it is required for glycogen and trehalose synthesis and the accumulation of β-glucans. Deleting *RIM15* produces a defective G_0 entry, increases the fermentation rate and reduces the levels of β-glucans, trehalose and glycogen during sake fermentation (Watanabe et al., 2012, 2016). Interestingly, deletion of *CDC55* restores the fermentation rate of cells lacking *RIM15* (Watanabe et al., 2019). Remarkably, no connection between fermentation and fission yeast Greatwall has yet been established.

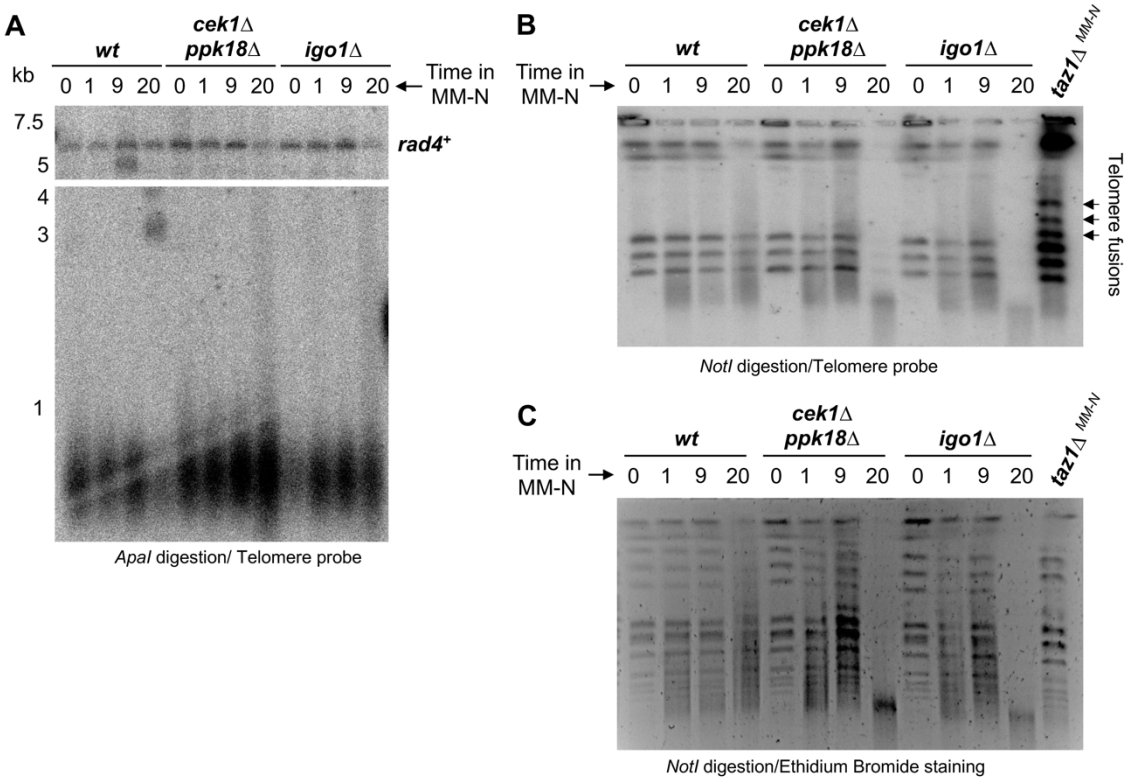

Figure 1. Telomere stability is maintained in *cek1Δ ppk18Δ* and i*go1Δ* mutants during quiescence. Cells were grown in MM, shifted to MM-N and kept under nitrogen starvation for 20 days. Cell samples were collected at the indicated time points after the shift and sent to Drs. José Escandell and Miguel Goudinho Ferreira for the telomere integrity analysis. **A, B.** Genomic DNA from wild-type, *igo1Δ* and *cek1Δ ppk18Δ* quiescent cells was digested with *ApaI* or *NotI* restriction enzymes and analysed by Southern blot with a telomere probe. **A.** Telomere length analysis. Neither the wild-type nor the mutant cells showed shortening of telomeres. **B.** Telomere fusion analysis. Only cells deleted for *taz1⁺*, a telomere regulator, showed telomere fusions (arrows). **C.** Genomic DNA from wild-type, *igo1Δ* and *cek1Δ ppk18Δ* quiescent cells was

digested with *NotI* and stained with ethidium bromide. *igo1Δ* and *cek1Δ ppk18Δ* genomic DNA was degraded after 20 days in MM-N.

Although the Greatwall-Endosulfine-PP2A/B55 pathway is highly conserved in eukaryotes: from yeast (Ppk18/Cek1-Igo1 in fission yeast, Rim15-Igo1/2 in budding yeast), *Drosophila*, and *Xenopus* (Greatwall-ENSA) to mammals (MastI-ENSA/Arpp19), there is still much to know about its functions and regulatory mechanisms. It will be important for the future to continue to investigate the role of this pathway in ageing and cell survival under nutritional stress conditions.

4. The Gretwall-Endosulfine-PP2A/B55 pathway integrates nutritional and cell-cycle cues in fission yeast

Cell-cycle progression is driven by the periodic activation and inactivation of CDK/Cyclin complexes. Oscillations in CDK/Cyclin activity depend on cyclin levels, the presence of CDK inhibitors and the phosphorylation status of the CDK (Morgan, 1997). CDK/Cyclin activity is low in G1, slightly rises in late G1 to trigger S phase entry, and continues to increase in G2 to promote entry into mitosis, peaking in metaphase (Coudreuse and Nurse, 2010). Several studies have recently highlighted the role of protein phosphatases in cell-cycle control (Cundell et al., 2013, 2016; Domingo-Sananes et al., 2011; Grallert et al., 2015). In fact, the phosphorylation status of CDK/Cyclin substrates depends on the balance between CDK/Cyclin kinase activity and its counteracting phosphatases (Cundell et al., 2016). In particular, PP2A phosphatase is essential for cell-cycle regulation as it is the main antagonist of CDK/Cyclin phosphorylation in animal cells (Mochida et al., 2009). Interestingly, substrate-specific CDK/Cyclin activity also plays a key role in cell-cycle progression (Swaffer et al., 2016): CDKs prefer serine residues and PP2A/B55 threonines. Consequently, serines are phosphorylated in the early phases of the cell cycle, whereas threonines tend to be phosphorylated late in the cell cycle (Godfrey et al., 2017; Kamenz and Ferrell, 2017).

Mitotic entry is the result of the balance between Cdk1/CyclinB protein kinase and PP2A/B55 protein phosphatase activities (Glover, 2012; Lorca and Castro, 2013). During interphase, PP2A/B55 activity is high (Mochida and Hunt, 2012) and dephosphorylates Wee1, promoting the phosphorylation of Cdk1 on Y15 (Mueller et al., 1995), which inactivates Cdk1/CyclinB complex. PP2A/B55 also ensures that Cdk1/CyclinB levels are low by dephosphorylating and inhibiting Cdc25 (Pal et al., 2008), that dephosphorylates Cdk1-Y15 and activates Cdk1/CyclinB complex (Coleman and Dunphy, 1994; Moreno et al., 1990). Moreover, PP2A/B55 dephosphorylates Cdk1/CyclinB substrates in G2, opposing Cdk1/CyclinB activity and delaying entry into mitosis until Cdk1/CyclinB activity levels increase above a certain threshold (Mochida et al., 2009). Hence, at the G2/M transition, PP2A/B55 must be inhibited before entry into mitosis. In *Xenopus*, the conserved Greatwall-Endosulfine module behaves as a molecular switch that inactivates PP2A/B55 (Glover, 2012; Lorca and Castro, 2013). In late G2, Greatwall phosphorylates Endosulfine, triggering its interaction with PP2A/B55 and the inhibition of the phosphatase complex (Gharbi-Ayachi et al., 2010; Mochida et al., 2010). In metazoans, the Greatwall-Endosulfine module is subjected to Cdk1/CyclinB regulation. At the G2/M transition, Cdk1/CyclinB complex phosphorylates Greatwall, which triggers the autophosphorylation of Greatwall and its full activation (Blake-Hodek et al., 2012; Vigneron et al., 2011). Once Greatwall is activated, it phosphorylates Endosulfine, that binds to and inhibits PP2A/B55 phosphatase. Therefore, Wee1 inhibition of Cdk1/CyclinB is relieved, mitotic substrates are phosphorylated, and mitosis is initiated.

TORC1 plays a central role in the regulation of cell growth and proliferation in eukaryotes. TORC1 senses the nutritional status of the cell and promotes cell growth. It positively regulates anabolic processes, including transcription and protein and lipid synthesis, while inhibiting

catabolic processes, such as autophagy (Alvarez and Moreno, 2006; Uritani et al., 2006; Matsuo et al., 2007; Saxton and Sabatini, 2017). Interestingly, in budding and fission yeasts, the Greatwall-Endosulfine switch is negatively regulated by TORC1 and connects TORC1 to the cell-cycle machinery through the regulation of PP2A/B55 phosphatase (Chica et al., 2016; Pedruzzi et al., 2003).

According to our theoretical model, the Greatwall-Endosulfine module integrates cell cycle and nutritional signals to down-regulate the activity of PP2A/B55 phosphatase in fission yeast (Figure II.1). TORC1 senses nitrogen and amino acids availability, becoming active when these nutrients are abundant, and inactive if they are scarce. We have recently shown that TORC1, through Sck2, the orthologue of S6K in *S. pombe*, regulates the G2/M transition and cell size at division by inhibiting the Greatwall-Endosulfine module (Chica et al., 2016; Pérez-Hidalgo and Moreno, 2016, 2017). Interestingly, the fission yeast Greatwall and Endosulfine orthologues, Ppk18 and Igo1, contain $(R/K)_2$-X-S/T or R/K-X-X-S/T sequences that fit the consensus for PKA phosphorylation sites (Figure II.2), suggesting that glucose levels might also control Greatwall-Endosulfine activity. Ppk18 and Igo1 also contain numerous S/T-P sequences that are targeted by Cdk1/CyclinB complexes. Ppk18 contains 24 of these sites, while Igo1 contains four (Figure II.2). We have mutated seven of the 24 putative Cdk1-phosphorylation sites in Ppk18 and found that Igo1-S64 phosphorylation was reduced in the *ppk18-7A* mutant (Pérez-Hidalgo et al., unpublished data), consistent with a reduction in Ppk18 activity. This preliminary data suggests that Ppk18-Igo1 activity could be positively regulated by Cdk1/CyclinB complex.

Given that PKA, TORC1 and Cdk1/CyclinB complexes have protein kinase activity, we decided to study the phosphorylation changes in Ppk18 and Igo1 proteins. Using 2D LC-MS/MS, we have identified several phosphorylated residues in Igo1 (Figure II.5). Notably, we detected that three serines, S31, S89 and S102, that fit the consensus for Cdk1 phosphorylation and two serines, S76 and S115, for PKA phosphorylation were phosphorylated *in vivo*. This data supported our hypothesis that the Greatwall-Endosulfine module is a hub for cell-cycle and nutritional cues. Then, we performed Cdk1 *in vitro* kinase assays to confirm that Igo1 was a direct target of Cdk1/CyclinB in fission yeast, finding that Cdk1/CyclinB was able to phosphorylate Igo1 but not Igo1-4A protein (Figures II.7 and II.8). In the *igo1-4A* mutant, serines 31, 89, 102 and 118 were substituted for alanines (Figure II.6), producing a non-phosphorylatable version of the Igo1 protein for all Cdk1 putative sites. Although phosphorylation of serine 118 was not detected in our mass spectrometry analysis, we decided to also mutate this residue to alanine. In animal cells, Cdk1/CyclinB promotes Greatwall-Endosulfine activity (Blake-Hodek et al., 2012; Vigneron et al., 2011). To test whether Cdk1/CyclinB also stimulates Greatwall-Endosulfine activity in fission yeast, we analysed the cell size of cells expressing the Igo1-4A version of the protein instead of Igo1. When fission yeast cells are transferred from nitrogen-rich media to nitrogen-poor media, they shorten G2 and divide with a reduced cell size. We have shown that cells deleted for *igo1⁺* are larger than the wild-type, even in nitrogen-rich media (Chica et al., 2016) (Figure II.9). In the *igo1Δ* mutant, PP2A/B55 activity levels are high, opposing Cdk1/CyclinB activity. As a result, entry into mitosis is delayed, and cells divide with a larger cell size. Interestingly, *igo1-4A* cells were also larger than the wild-type in nitrogen-rich media (MM) (Figure II.9), consistent with a reduction in Igo1 activity and suggesting that Cdk1/CyclinB positively regulates Igo1. Nevertheless, *igo1Δ* cells remained larger when grown in MMF, whereas *igo1-4A* mutant reduced cell size, behaving like wild-type cells (Figure II.9). These results suggested that Cdk1/CyclinB phosphorylation of Igo1 is relevant in nitrogen-rich media (MM), when Ppk18 is inactive. By contrast, in nitrogen-poor media (MMF), Ppk18 is active and phosphorylates Igo1 at serine 64, triggering PP2A/B55 inhibition, and therefore, cell size reduction (Chica et al., 2016).

The aforementioned results are consistent with our theoretical model, in which the Greatwall-Endosulfine switch integrates cell-cycle and environmental signals. We have shown

that Cdk1/CyclinB phosphorylates fission yeast Endosulfine, Igo1, promoting its activity. Nevertheless, the analysis of *igo1-4E* mutant, expressing a phosphomimetic version of Igo1 for all Cdk1 sites, will be necessary to complete our research on Igo1 cell-cycle dependent regulation. Interestingly, our data is consistent with studies carried out in other biological models. In metazoans, Cdk1/CyclinB feedback triggers Greatwall activation (reviewed in Castro and Lorca, 2018); therefore, promoting Greatwall-Endosulfine activity. Although our work shows that Cdk1/CyclinB acts through Endosulfine in fission yeast, both models share intriguing similarities. Furthermore, we could not rule out that Cdk1/CyclinB also regulates Greatwall since we could not map the phosphorylation sites in Ppk18. In fact, preliminary results from our laboratory supports (Pérez-Hidalgo, unpublished data). In *S. cerevisiae*, where no connection has yet been established between Cdk1/CyclinB and Greatwall-Endosulfine activity, TORC1 and PKA negatively regulate the Greatwall-Endosulfine module (Pedruzzi et al., 2003). Interestingly, our mass spectrometry analysis identified two potential PKA phosphorylation sites in Igo1 that were phosphorylated *in vivo*. This data supports previous results that suggest that the Greatwall-Endosulfine-PP2A/B55 pathway is negatively regulated by PKA (Chica and Rozalén, unpublished data) and that PKA regulation of Greatwall-Endosulfine activity might also be conserved in fission yeast. However, further work will be needed to better comprehend the connection between PKA and Greatwall-Endosulfine-PP2A/B55 activity in *S. pombe*.

5. New targets of the Gretwall-Endosulfine-PP2A/B55 pathway in *S. pombe*

We have previously reported that TORC1 signalling pathway modulates entry into mitosis and cell size at division (Chica et al., 2016). Upon nutritional shift-down, TORC1 activity decreases, promoting the activation of the Greatwall-Endosulfine switch and PP2A/B55 inhibition. Low levels of PP2A/B55 phosphatase activity enables cells to enter mitosis with reduced Cdk1/CyclinB activity and hence, cells divide with a reduced size. Moreover, we have shown that down-regulation of PP2A/B55 by Greatwall and Endosulfine proteins is also essential under nitrogen starvation. In these conditions, the Greatwall-Endosulfine pathway inhibits PP2A/B55 to trigger the pre-quiescence and sexual differentiation responses (Laboucarié et al., 2017; Martín et al., 2017) (Figures I.3 and I.7) and to maintain the CLS of fission yeast cells (Aono et al., 2019) (Figure I.12).

In this work, we were interested in identifying proteins that interacted *in vivo* with the Greatwall-Endosulfine-PP2A/B55 pathway to better comprehend its physiological role. In collaboration with Prof. Kathleen Gould at Vanderbilt University, we carried out pull-down experiments of GFP-tagged Igo1 and GFP-tagged Pab1 proteins followed by mass spectrometry analysis in cells cultured in MM and MM-N (Figure III.1). Using this proteomic approach, we were able to obtain Igo1 and Pab1 interactomes in both media (Tables III.S1-S4). Both Igo1 and Pab1 interacted with more proteins in MM-N than in MM, suggesting that the interactome networks became more intricate under nitrogen starvation. Interestingly, the Igo1 interactome showed over-representation of five GO biological processes: ‘Ribosome biogenesis’, ‘Translation’, ‘Retrograde vesicle-mediated transport, Golgi to ER’, ‘rRNA-containing ribonucleoprotein complex export from nucleus’ and ‘ribosome localization’ (Figure III.2). By contrast, the number of over-represented GO biological processes was higher in the Pab1 interactome, consistent with the role of PP2A/B55 phosphatase in multiple cellular processes (reviewed in Wurzenberger and Gerlich, 2011). Some of these GO biological processes included ‘Cytoplasmatic transport’, ‘Protein localization’, ‘Regulation of mitotic nuclear division’ or ‘Regulation of intracellular signal transduction’ (Figure III.3).

Previous data from our group showed that high PP2A/B55 activity during nitrogen starvation in cells lacking Greatwall (*ppk18Δ cek1Δ*) or Endosulfine (*igo1Δ*) results in drastic upregulation of the expression of subtelomeric genes and Tf2 retrotransposons (Vázquez-Bolado

et al., unpublished data), a common phenotype of mutants with silencing defects. These results suggest that the Greatwall-Endosulfine-PP2A/B55 pathway might be implicated in the epigenetic control of silencing. Interestingly, both Igo1 and Pab1 interacted with chromatin-related proteins (Tables III.S1-S4), supporting the idea of a role of the pathway in chromatin regulation and gene silencing. In yeasts and mammals, G_0 entry involves changes in global histones marks and chromatin compaction. In budding yeast, nucleosome density increases during quiescence entry and deacetylation of chromatin is critical for G_0 (McKnight et al., 2015). In mammalian cells, the distribution of H4K20 and H3K9 methylations (H4K20me and H3K9me) changes during quiescence (Boonsanay et al., 2016; Evertts et al., 2013; Grigoryev et al., 2004). In fission yeast, regulation of heterochromatin is also essential during quiescence. In fact, mutants in the RNAi pathway, which is involved in heterochromatin formation, lose viability during quiescence (Joh et al., 2016; Roche et al., 2016). Intriguingly, TORC1 is involved in epigenetic control in budding yeast and mammalian cells (reviewed in Laribee and Weisman, 2020). For example, histone acetylation and methylation are linked to the TORC1 signalling pathway in both models (reviewed in Laribee and Weisman, 2020), whereas the RSC and Ino80 chromatin remodelling complexes contribute to TORC1-dependent transcriptional regulation in *S. cerevisiae* (Angus-Hill et al., 2001; Beckwith et al., 2018; Damelin et al., 2002; Gowans et al., 2018). In fission yeast, a recent study shows that TORC1 targets the RNA elimination network to silence gametogenic genes by promoting RNA decay and facultative heterochromatin assembly (Wei et al., 2021). This data together with our mass spectrometry results suggest that the role of the TORC1-Greatwall-Endosulfine-PP2A/B55 pathway in epigenetic control might be conserved in fission yeast.

Among Igo1-associated proteins were histone H2B Htb1 and Ies6, a subunit of Ino80 complex (Tables III.S1 and S2). The nucleosome remodeller Ino80 is involved in several functions, including transcriptional regulation, DNA replication and DNA repair (reviewed in Poli et al., 2017). Its interaction with Igo1 might explain the upregulated expression of certain genome regions in *ppk18Δ cek1Δ* and *igo1Δ* cells. Furthermore, Pkc1, the PKC orthologue in *S. pombe*, was found in the Igo1 interactome (Tables III.2, III.S1 and III.S2). Notably, budding yeast Pkc1 induces Endosulfine dissociation from PP2A/B55, and therefore, promotes PP2A/B55 activation (Steph D. et al., 2012; Thai et al., 2017). This result suggests that PKC regulation of the Greatwall-Endosulfine-PP2A/B55 pathway may be conserved in *S. pombe*. Three transcription elongation factors were also identified in the Igo1 interactome (Tables III.1-III.S2), suggesting a possible role of the pathway in transcription regulation, a widely known function of TORC1 (reviewed in Laribee and Weisman, 2020).

Regarding Pab1, several protein complexes involved in chromatin condensation, chromatin remodelling and histone modification, including the Mst2 histone acetyl transferase complex, the Clr3 and Clr6 histone deacetylases and the SWI/SNF-type RSC complex, were present in the Pab1 interactome (Tables III.S3 and S4), again supporting a role of PP2A/B55 in regulating chromatin condensation and silencing during nitrogen starvation. Recent reports in *S. cerevisiae* indicate that condensins play a key role in chromatin compaction and transcription repression in quiescent cells (Swygert et al., 2019). Intriguingly, among Pab1-interacting proteins we identified two condensin subunits, Cut3 and Cut14, opening the possibility for condensin to also participate in chromatin compaction in fission yeast quiescent cells. A second complex with HAT activity, the SAGA complex, also interacted with Pab1. Specifically, four SAGA subunits were found in the Pab1 interactome, including Taf12, which has already been connected to PP2A/B55 activity (Laboucarié et al., 2017). Another result that supports a role of PP2A/B55 in chromatin silencing is the presence of multiple nucleoporins in the Pab1 interactome (Tables III.3-III.S4) since they are essential for heterochromatin clustering and epigenetic inheritance (Iglesias et al., 2020). Furthermore, the mass spectrometry analysis identified Atg6 and Atg14, the fission yeast orthologues of Beclin1 and Atg14L, in the Pab1 interactome (Tables III.S3 and III.S4). Atg6

and Atg14 are components of the class III PI3K complex I (Sun et al., 2013; Yu et al., 2020), which promotes autophagosome formation. These interactions supported previous data from our laboratory that showed that the Greatwall-Endosulfine-PP2A/B55 pathway modulates autophagy in fission yeast (Vázquez-Bolado et al., unpublished data). Accordingly, the autophagic flux is reduced in cells lacking *igo1⁺*, and deletion of *ppa2⁺* rescued the *igo1Δ* autophagic defects. The PP2A/B55 and Beclin1 connection has also been observed in mammals. Beclin1 phosphorylation at Ser90 is increased is cells treated with okadaic acid, an inhibitor of PP2A/B55α activity (Fujiwara et al., 2016). Moreover, many subunits of the SEA complex (GATOR1-GATOR2) copurified with Pab1. In yeasts, GATOR1, SEACIT in budding yeast, functions as a GAP of the Gtr1-Gtr2 GTPases, and therefore, controls TORC1 activity (Chia et al., 2017; Dokudovskaya and Rout, 2015). In *S. cerevisiae*, PP2A regulates the SEA complex (Laxman et al., 2014; Sutter et al., 2013). When sulphur is abundant, PP2A is methylated by Ppm1, becoming activated. Active PP2A dephosphorylates and inhibits the SEACIT subcomplex, promoting TORC1 activity. Our results suggest that this mechanism may be conserved in fission yeast. Several proteins involved in tRNA metabolism were also found among Pab1-interacting proteins (Tables III.S3 and III.S4). TORC1 promotes tRNA transcription by inhibiting the conserved Maf1 factor, which inhibits RNA Pol III (Cai and Wei, 2015; Graczyk et al., 2018; Michels et al., 2010; Shor et al., 2010; Wei et al., 2009). Interestingly, recent studies showed that RNA Pol III activity limits the lifespan downstream of TORC1 and that Maf1 is required for lifespan extension in fission yeast (Filer et al., 2017; Shetty et al., 2019). Furthermore, PP2A and PP4 phosphatases promote Maf1 dephosphorylation and activation (Zhang et al., 2018). Importantly, the Pab1 interactome was performed in cells overexpressing *pab1⁺* (*P41nm1:GFP:pab1⁺*), which could enhance some of the interactions mentioned above. Nonetheless, deletion of *igo1⁺* leads to an hyperactive PP2A/B55 phosphatase. Hence, some Pab1-interacting proteins could cause the phenotypes observed in *igo1Δ* mutant.

Several subunits of the Mst2 complex were included in the Pab1 interactome. The Mst2 complex is a histone acetyltransferase that functions redundantly with the Gcn5 subunit of the SAGA complex to control global levels of H3K14 acetylation (Nugent et al., 2010; Wang et al., 2012). Histone acetylation is implicated in multiple cellular processes such as DNA repair, gene expression or recombination. Histone H3 is primarily acetylated at K9 and K14, which are located at euchromatic regions (Pokholok et al., 2005; Wang et al., 2008). Mst2 also promotes gene expression by acetylating Brl1, a member of the histone H2B ubiquitin ligase complex (Flury et al., 2017). Brl1 ubiquitylates H2B at K119. Mst2 complex is composed of Mst2, Pdp3, Nto1, Eaf6, Tfg3, Ptf1 and Ptf2 (Wang et al., 2012). Surprisingly, all the subunits of the Mst2 complex except for Pdp3 were found in the Pab1 interactome (Tables III.4, III.S3 and III.S4). Pdp3 recruits the Mst2 complex to highly transcribed regions through its interaction with H3K36me3 (Flury et al., 2017). Interestingly, cells deleted for *pdp3⁺* showed silencing defects due to ectopic location of the Mst2 complex at heterochromatic regions (Flury et al., 2017) (Figure III.4). Since Mst2 subunit was found among proteins with the highest spectrum count (Table III.4), we decided to focus on Pab1 and Mst2 interaction. According to our theoretical model, PP2A/B55 regulates the recruitment of the Mst2 complex to active genes. When PP2A/B55 activity levels are high, it dephosphorylates Mst2 subunit, promoting the dissociation of the Mst2 complex from Pdp3. By contrast, when PP2A/B55 activity drops, Mst2 is phosphorylated and anchored to Pdp3-H3K36me3 regions, preventing ectopic location of the Mst2 complex and the activation of heterochromatin. Our results suggest that cells deleted for *igo1⁺* in nitrogen-poor or nitrogen-free media could be analogous to cells lacking *pdp3⁺*. In *igo1Δ* mutant, the Mst2 complex might lose its interaction with Pdp3 due to high levels of PP2A/B55 activity, ectopically locating at heterochromatic regions where it could activate the expression of normally silenced genes (Figure III.4). Loss of Pdp3 anchoring might explain the silencing defects of *igo1Δ* cells (Vázquez-Bolado et al., unpublished data). To test this hypothesis, we studied the phenotype of quiescent cells

lacking *igo1⁺* and *mst2⁺* (*igo1Δ mst2Δ*) to search for genetic interactions between these genes. We observed that deletion of *mst2⁺* slightly increased the cell survival of *igo1Δ* mutant (Figure III.7), suggesting that Mst2 activity might account for part of *igo1Δ* phenotype and supporting our hypothesis. Moreover, we also performed Pab1 and Mst2 coimmunoprecipitation assays to confirm its interaction. Unfortunately, we were unable to copurify them (Figure III.5). Future experiments will be required to verify the *in vivo* interaction between PP2A/B55 and Mst2 complexes and to test the hypothesis that deregulated Mst2 activity could be the cause of the *igo1Δ* silencing defects.

Conclusions

I. The Greatwall-Endosulfine-PP2A/B55 pathway plays a crucial role in the regulation of the nitrogen starvation response. Greatwall and Endosulfine proteins down-regulate PP2A/B55 activity, allowing cell size reduction and proper G1 arrest in the absence of nitrogen.

II. The Greatwall-Endosulfine-PP2A/B55 pathway regulates the sexual differentiation response. Upon nitrogen starvation, the Greatwall-Endosulfine module is activated and inhibits PP2A/B55 phosphatase complex to promote sexual differentiation.

III. Greatwall and Endosulfine proteins promote G_0 entry, cell survival and correct chromatin dynamics during quiescence. Inactivation of PP2A/B55 by the Greatwall-Endosulfine switch is required for cell survival in the G_0 phase induced by nitrogen starvation. Interestingly, the TORC2-Gad8 molecular axis, which is essential for the pre-quiescence response, is not involved in maintaining cell survival of quiescent cells under nitrogen deprivation.

IV. The Greatwall-Endosulfine switch is a hub for nutritional and cell cycle cues that regulates PP2A/B55 activity. Several protein kinases phosphorylate Endosulfine *in vivo*, including Cdk1 and PKA. Cdk1/CyclinB phosphorylation on serines 31, 89, 102 and 118 promotes Endosulfine activity during the cell cycle in nitrogen-rich media.

V. The interactomic assays identified multiple binding partners of Endosulfine and B55 proteins. B55 interacted with several protein complexes involved in chromatin condensation, chromatin remodelling and histone modification, such as the Mst2 complex, supporting a role of PP2A/B55 in regulating chromatin architecture and gene silencing during entry into quiescence.

References

Allshire, R.C., and Ekwall, K. (2015). Epigenetic regulation of chromatin states in *Schizosaccharomyces pombe*. Cold Spring Harb. Perspect. Biol. *7*, 1–25.

Alvarez, B., and Moreno, S. (2006). Fission yeast Tor2 promotes cell growth and represses cell differentiation. J. Cell Sci. *119*, 4475–4485.

Angus-Hill, M.L., Schlichter, A., Roberts, D., Erdjument-Bromage, H., Tempst, P., and Cairns, B.R. (2001). A Rsc3/Rsc30 zinc cluster dimer reveals novel roles for the chromatin remodeler RSC in gene expression and cell cycle control. Mol. Cell *7*, 741–751.

Aono, S., Haruna, Y., Watanabe, Y. hei, Mochida, S., and Takeda, K. (2019). The fission yeast Greatwall–Endosulfine pathway is required for proper quiescence/G0 phase entry and maintenance. Genes to Cells *24*, 172–186.

Bähler, J., Wu, J.Q., Longtine, M.S., Shah, N.G., McKenzie, A., Steever, A.B., Wach, A., Philippsen, P., and Pringle, J.R. (1998). Heterologous modules for efficient and versatile PCR-based gene targeting in *Schizosaccharomyces pombe*. Yeast *14*, 943–951.

Bar-Peled, L., Schweitzer, L.D., Zoncu, R., and Sabatini, D.M. (2012). Ragulator is a GEF for the rag GTPases that signal amino acid levels to mTORC1. Cell *150*, 1196–1208.

Bar-Peled, L., Chantranupong, L., Cherniack, A.D., Chen, W.W., Ottina, K.A., Grabiner, B.C., Spear, E.D., Carter, S.L., Meyerson, M., and Sabatini, D.M. (2013). A tumor suppressor complex with GAP activity for the Rag GTPases that signal amino acid sufficiency to mTORC1. Science *340*, 1100–1106.

Barford, D., Das, A.K., and Egloff, M.P. (1998). The structure and mechanism of protein phosphatases: insights into catalysis and regulation. Annu. Rev. Biophys. Biomol. Struct. *13*, 133–164.

Beckwith, S.L., Schwartz, E.K., García-Nieto, P.E., King, D.A., Gowans, G.J., Wong, K.M., Eckley, T.L., Paraschuk, A.P., Peltan, E.L., Lee, L.R., et al. (2018). The INO80 chromatin remodeler sustains metabolic stability by promoting TOR signaling and regulating histone acetylation. PLoS Genet. *14*, e1007216.

Binda, M., Péli-Gulli, M.P., Bonfils, G., Panchaud, N., Urban, J., Sturgill, T.W., Loewith, R., and De Virgilio, C. (2009). The Vam6 GEF controls TORC1 by activating the EGO complex. Mol. Cell *35*, 563–573.

Blackburn, E.H., Greider, C.W., and Szostak, J.W. (2006). Telomeres and telomerase: the path from maize, *Tetrahymena* and yeast to human cancer and aging. Nat. Med. *12*, 1133–1138.

Blagosklonny, M. V., and Hall, M.N. (2009). Growth and aging: a common molecular mechanism. Aging *1*, 357–362.

Blake-Hodek, K.A., Williams, B.C., Zhao, Y., Castilho, P. V., Chen, W., Mao, Y., Yamamoto, T.M., and Goldberg, M.L. (2012). Determinants for activation of the atypical AGC kinase Greatwall during M phase entry. Mol. Cell. Biol. *38*, 1337–1353.

Bloom, J., and Cross, F.R. (2007). Multiple levels of cyclin specificity in cell-cycle control. Nat. Rev. Mol. Cell Biol. *8*, 149–160.

Bontron, S., Jaquenoud, M., Vaga, S., Talarek, N., Bodenmiller, B., Aebersold, R., and De Virgilio, C. (2013). Yeast Endosulfines control entry intoquiescence and chronological lfe span by inhibiting protein phosphatase 2A. Cell Rep. *3*, 16–22.

Boonsanay, V., Zhang, T., Georgieva, A., Kostin, S., Qi, H., Yuan, X., Zhou, Y., and Braun, T. (2016). Regulation of skeletal muscle stem cell quiescence by Suv4-20h1-dependent facultative heterochromatin formation. Cell Stem Cell *18*, 229–242.

Boy-Marcotte, E., Perrot, M., Bussereau, F., Boucherie, H., and Jacquet, M. (1998). Msn2p and Msn4p control a large number of genes induced at the diauxic transition which are repressed by cyclic AMP in *Saccharomyces cerevisiae*. J. Bacteriol. *180*, 1044–1052.

Brown, E.J., Albers, M.W., Bum Shin, T., Ichikawa, K., Keith, C.T., Lane, W.S., and Schreiber,

S.L. (1994). A mammalian protein targeted by G1-arresting rapamycin-receptor complex. Nature *369*, 756–768.

Brunner, D., and Nurse, P. (2000). New concepts in fission yeast morphogenesis. Philos Trans R Soc L. B Biol Sci *355*, 873–877.

Bueno, A., Richardson, H., Reed, S.I., and Russell, P. (1991). A fission yeast B-type cyclin functioning early in the cell cycle. Cell *66*, 149–159.

Burkewitz, K., Zhang, Y., and Mair, W.B. (2014). AMPK at the nexus of energetics and aging. Cell Metab. *20*, 10–25.

Cafferkey, R., Young, P.R., McLaughlin, M.M., Bergsma, D.J., Koltin, Y., Sathe, G.M., Faucette, L., Eng, W.K., Johnson, R.K., and Livi, G.P. (1993). Dominant missense mutations in a novel yeast protein related to mammalian phosphatidylinositol 3-kinase and VPS34 abrogate rapamycin cytotoxicity. Mol. Cell. Biol. *13*, 6012–6023.

Cai, Y., and Wei, Y.H. (2015). Distinct regulation of Maf1 for lifespan extension by Protein kinase A and Sch9. Aging. *7*, 133–143.

Carlson, C.R., Grallert, B., Stokke, T., and Boye, E. (1999). Regulation of the start of DNA replication in *Schizosaccharomyces pombe*. J. Cell Sci. *112*, 939–946.

Castro, A., and Lorca, T. (2018). Greatwall kinase at a glance. J. Cell Sci. *138*, jcs222364.

Causton, H.C., Ren, B., Sang Seok Koh, Harbison, C.T., Kanin, E., Jennings, E.G., Tong Ihn Lee, True, H.L., Lander, E.S., and Young, R.A. (2001). Remodeling of yeast genome expression in response to environmental changes. Mol. Biol. Cell *12*, 323–327.

Chantranupong, L., Wolfson, R.L., Orozco, J.M., Saxton, R.A., Scaria, S.M., Bar-Peled, L., Spooner, E., Isasa, M., Gygi, S.P., and Sabatini, D.M. (2014). The sestrins interact with GATOR2 to negatively regulate the amino-acid-sensing pathway upstream of mTORC1. Cell Rep. *9*, 1–8.

Chantranupong, L., Scaria, S.M., Saxton, R.A., Gygi, M.P., Shen, K., Wyant, G.A., Wang, T., Harper, J.W., Gygi, S.P., and Sabatini, D.M. (2016). The CASTOR proteins are arginine sensors for the mTORC1 pathway. Cell *165*, 154–164.

Chen, B.R., and Runge, K.W. (2009). A new *Schizosaccharomyces pombe* chronological lifespan assay reveals that caloric restriction promotes efficient cell cycle exit and extends longevity. Exp. Gerontol. *44*, 493–502.

Chen, B.R., Li, Y., Eisenstatt, J.R., and Runge, K.W. (2013a). Identification of a lifespan extending mutation in the *Schizosaccharomyces pombe* cyclin gene *clg1*$^{+}$ by direct selection of long-lived mutants. PLoS One *8*, 1–18.

Chen, J.S., Broadus, M.R., McLean, J.R., Feoktistova, A., Ren, L., and Gould, K.L. (2013b). Comprehensive proteomics analysis reveals new substrates and regulators of the fission yeast Clp1/Cdc14 phosphatase. Mol. Cell. Proteomics *12*, 1074–1086.

Chia, K.H., Fukuda, T., Sofyantoro, F., Matsuda, T., Amai, T., and Shiozaki, K. (2017). Ragulator and GATOR1 complexes promote fission yeast growth by attenuating TOR complex 1 through rag GTPases. Elife *6*, e30880.

Chica, N., Rozalén, A.E., Pérez-Hidalgo, L., Rubio, A., Novak, B., and Moreno, S. (2016). Nutritional control of cell size by the Greatwall-Endosulfine-PP2A·B55 pathway. Curr. Biol. *26*, 319–330.

Codega, P., Silva-Vargas, V., Paul, A., Maldonado-Soto, A.R., DeLeo, A.M., Pastrana, E., and Doetsch, F. (2014). Prospective identification and purification of quiescent adult neural stem cells from their in vivo niche. Neuron *82*, 545–559.

Cohen, A., Kupiec, M., and Weisman, R. (2016). TORC2-Gad8 is found in the nucleus where it interacts with the MBF transcriptional complex to regulate the response to DNA replication stress. J. Biol. Chem. *291*, 9371–9381.

Coleman, T.R., and Dunphy, W.G. (1994). Cdc2 regulatory factors. Curr. Opin. Cell Biol. *6*, 877–

882.

Colman, R.J., Anderson, R.M., Johnson, S.C., Kastman, E.K., Kosmatka, K.J., Beasley, T.M., Allison, D.B., Cruzen, C., Simmons, H.A., Kemnitz, J.W., et al. (2009). Caloric restriction delays disease onset and mortality in rhesus monkeys. Science *325*, 201–204.

Costello, G., Rodgers, L., and Beach, D. (1986). Fission yeast enters the stationary phase G0 state from either mitotic G1 or G2. Curr. Genet. *11*, 119–125.

Coudreuse, D., and Nurse, P. (2010). Driving the cell cycle with a minimal CDK control network. Nature *468*, 1074–1079.

Coulon, S., and Vaurs, M. (2020). Telomeric transcription and telomere rearrangements in quiescent cells. J. Mol. Biol. *432*, 4220–4231.

Cundell, M.J., Bastos, R.N., Zhang, T., Holder, J., Gruneberg, U., Novak, B., and Barr, F.A. (2013). The BEG (PP2A-B55/ENSA/Greatwall) pathway ensures cytokinesis follows chromosome separation. Mol. Cell *52*, 393–405.

Cundell, M.J., Hutter, L.H., Bastos, R.N., Poser, E., Holder, J., Mohammed, S., Novak, B., and Barr, F.A. (2016). A PP2A-B55 recognition signal controls substrate dephosphorylation kinetics during mitotic exit. J. Cell Biol. *214*, 539–554.

Damelin, M., Simon, I., Moy, T.I., Wilson, B., Komili, S., Tempst, P., Roth, F.P., Young, R.A., Cairns, B.R., and Silver, P.A. (2002). The genome-wide localization of Rsc9, a component of the RSC chromatin-remodeling complex, changes in response to stress. Mol. Cell *9*, 563–573.

De Souza, C.P.C., and Osmani, S.A. (2007). Mitosis, not just open or closed. Eukaryot. Cell *6*, 1521–1527.

De Virgilio, C. (2012). The essence of yeast quiescence. FEMS Microbiol. Rev. *36*, 306–339.

Dephoure, N., Gould, K.L., Gygi, S.P., and Kellogg, D.R. (2013). Mapping and analysis of phosphorylation sites: a quick guide for cell biologists. Mol. Biol. Cell 24, 535–542.

DeRisi, J.L., Iyer, V.R., and Brown, P.O. (1997). Exploring the metabolic and genetic control of gene expression on a genomic scale. Science *278*, 680–686.

Dey, G., Culley, S., Curran, S., Schmidt, U., Henriques, R., Kukulski, W., and Baum, B. (2020). Closed mitosis requires local disassembly of the nuclear envelope. Nature *585*, 119–123.

Dhawan, J., and Laxman, S. (2015). Decoding the stem cell quiescence cycle - Lessons from yeast for regenerative biology. J. Cell Sci. *128*, 4467–4474.

Dibble, C.C., and Cantley, L.C. (2015). Regulation of mTORC1 by PI3K signaling. Trends Cell Biol. *25*, 545–555.

Dibble, C.C., Elis, W., Menon, S., Qin, W., Klekota, J., Asara, J.M., Finan, P.M., Kwiatkowski, D.J., Murphy, L.O., and Manning, B.D. (2012). TBC1D7 is a third subunit of the TSC1-TSC2 complex upstream of mTORC1. Mol. Cell *47*, 535–546.

Dixon, S.J., Fedyshyn, Y., Koh, J.L.Y., Prasad, T.S.K., Chahwan, C., Chua, G., Toufighi, K., Baryshnikova, A., Hayles, J., Hoe, K.L., et al. (2008). Significant conservation of synthetic lethal genetic interaction networks between distantly related eukaryotes. Proc. Natl. Acad. Sci. U.S.A. *105*, 16653–16658.

Dokudovskaya, S., and Rout, M.P. (2015). SEA you later alli-GATOR - a dynamic regulator of the TORC1 stress response pathway. J. Cell Sci. *128*, 2219–2228.

Domingo-Sananes, M.R., Kapuy, O., Hunt, T., and Novak, B. (2011). Switches and latches: a biochemical tug-of-war between the kinases and phosphatases that control mitosis. Philos. Trans. R. Soc. B Biol. Sci. *366*, 3584–3594.

Drummond-Barbosa, D., and Spradling, A.C. (2004). α-Endosulfine, a potential regulator of insulin secretion, is required for adult tissue growth control in *Drosophila*. Dev. Biol. *266*, 310–321.

Dunham, W.H., Mullin, M., and Gingras, A.C. (2012). Affinity-purification coupled to mass spectrometry: basic principles and strategies. Proteomics *12*, 1576–1590.

Eichhorn, P.J.A., Creyghton, M.P., and Bernards, R. (2009). Protein phosphatase 2A regulatory subunits and cancer. Biochim. Biophys. Acta Rev. Cancer *1795*, 1–15.

Eltschinger, S., and Loewith, R. (2016). TOR complexes and the maintenance of cellular homeostasis. Trends Cell Biol. *26*, 148–159.

Eng, C.P., Sehgal, S.N., and Vézina, C. (1984). Activity of rapamycin (AY-22,989) against transplanted tumors. J. Antibiot. *37*, 1231–1237.

Enns, L.C., and Ladiges, W. (2010). Protein kinase A signaling as an anti-aging target. Ageing Res. Rev. *9*, 269–272.

Everetts, A.G., Manning, A.L., Wang, X., Dyson, N.J., Garcia, B.A., and Coller, H.A. (2013). H4K20 methylation regulates quiescence and chromatin compaction. Mol. Biol. Cell *24*, 3025–3037.

Fabrizio, P., and Longo, V.D. (2003). The chronological life span of *Saccharomyces cerevisiae*. Aging Cell *371*, 371, 89–95.

Fabrizio, P., Pozza, F., Pletcher, S.D., Gendron, C.M., and Longo, V.D. (2001). Regulation of longevity and stress resistance by Sch9 in yeast. Science *292*, 288–290.

Fantes, P. (1977). Control of cell size and cycle time in *Schizosaccharomyces pombe*. J. Cell Sci. *24*, 51–67.

Fantes, P., and Nurse, P. (1977). Control of cell size at division in fission yeast by a growth-modulated size control over nuclear division. Exp. Cell Res. *107*, 377–386.

Filer, D., Thompson, M.A., Takhaveev, V., Dobson, A.J., Kotronaki, I., Green, J.W.M., Heinemann, M., Tullet, J.M.A., and Alic, N. (2017). RNA polymerase III limits longevity downstream of TORC1. Nature *552*, 263–267.

Flury, V., Georgescu, P.R., Iesmantavicius, V., Shimada, Y., Kuzdere, T., Braun, S., and Bühler, M. (2017). The histone acetyltransferase Mst2 protects active chromatin from epigenetic silencing by acetylating the ubiquitin ligase Brl1. Mol. Cell *67*, 294–307.

Foiani, M., Marini, F., Gamba, D., Lucchini, G., and Plevani, P. (1994). The B subunit of the DNA polymerase α-primase complex in *Saccharomyces cerevisiae* executes an essential function at the initial stage of DNA replication. Mol Cell Biol *14*, 923–933.

Fontana, L., Partridge, L., and Longo, V.D. (2010). Extending healthy life span - From yeast to humans. Science *328*, 321–326.

Fujiwara, N., Usui, T., Ohama, T., and Sato, K. (2016). Regulation of beclin 1 protein phosphorylation and autophagy by protein phosphatase 2A (PP2A) and death-associated protein kinase 3 (DAPK3). J. Biol. Chem. *291*, 10858–10866.

Fukada, S., Uezumi, A., Ikemoto, M., Masuda, S., Segawa, M., Tanimura, N., Yamamoto, H., Miyagoe-Suzuki, Y., and Takeda, S. (2007). Molecular signature of quiescent satellite cells in adult skeletal muscle. Stem Cells *25*, 2448–2459.

Garami, A., Zwartkruis, F.J.T., Nobukuni, T., Joaquin, M., Roccio, M., Stocker, H., Kozma, S.C., Hafen, E., Bos, J.L., and Thomas, G. (2003). Insulin activation of Rheb, a mediator of mTOR/S6K/4E-BP signaling, is inhibited by TSC1 and 2. Mol. Cell *11*, 1457–1466.

García-Blanco, N., Vázquez-Bolado, A., and Moreno, S. (2019). Greatwall-Endosulfine: a molecular switch that regulates PP2A/B55 protein phosphatase activity in dividing and quiescent cells. Int. J. Mol. Sci. *20*, 6228.

García-Martínez, J.M., and Alessi, D.R. (2008). mTOR complex 2 (mTORC2) controls hydrophobic motif phosphorylation and activation of serum- and glucocorticoid-induced protein kinase 1 (SGK1). Biochem. J. *416*, 375–385.

Gasch, A.P., Spellman, P.T., Kao, C.M., Carmel-Harel, O., Eisen, M.B., Storz, G., Botstein, D.,

and Brown, P.O. (2000). Genomic expression programs in the response of yeast cells to environmental changes. Mol. Biol. Cell *11*, 4241–4257.

Gaubitz, C., Oliveira, T.M., Prouteau, M., Leitner, A., Karuppasamy, M., Konstantinidou, G., Rispal, D., Eltschinger, S., Robinson, G.C., Thore, S., et al. (2015). Molecular basis of the rapamycin insensitivity of Target of rapamycin complex 2. Mol. Cell *58*, 977–988.

Gharbi-Ayachi, A., Labbé, J.-C., Burgess, A., Vigneron, S., Strub, J.-M., Brioudes, E., Van-Dorsselaer, A., Castro, A., and Lorca, T. (2010). The substrate of Greatwall kinase, Arpp19, controls mitosis by inhibiting protein phosphatase 2A. Science *330*, 1673–1677.

Glover, D.M. (2012). The overlooked greatwall: A new perspective on mitotic control. Open Biol. *2*, 120023.

Godfrey, M., Touati, S.A., Kataria, M., Jones, A., Snijders, A.P., and Uhlmann, F. (2017). PP2ACdc55 phosphatase imposes ordered cell-cycle phosphorylation by opposing threonine phosphorylation. Mol. Cell *65*, 393–402.

Gould, K.L., and Nurse, P. (1989). Tyrosine phosphorylation of the fission yeast *cdc2+* protein kinase regulates entry into mitosis. Nature *342*, 39–45.

Gowans, G.J., Schep, A.N., Wong, K.M., King, D.A., Greenleaf, W.J., and Morrison, A.J. (2018). INO80 chromatin remodeling coordinates metabolic homeostasis with cell division. Cell Rep. *22*, 611–623.

Goyal, A., and Simanis, V. (2012). Characterization of *ypa1* and *ypa2*, the *Schizosaccharomyces pombe* orthologs of the peptidyl proyl isomerases that activate PP2A, reveals a role for Ypa2p in the regulation of cytokinesis. Genetics *190*, 1235–1250.

Graczyk, D., Cieśla, M., and Boguta, M. (2018). Regulation of tRNA synthesis by the general transcription factors of RNA polymerase III - TFIIIB and TFIIIC, and by the MAF1 protein. Biochim. Biophys. Acta Gene Regul. Mech. *1861*, 320–329.

Grallert, A., Boke, E., Hagting, A., Hodgson, B., Connolly, Y., Griffiths, J.R., Smith, D.L., Pines, J., and Hagan, I.M. (2015). A PP1-PP2A phosphatase relay controls mitotic progression. Nature *517*, 94–98.

Gray, J. V., Petsko, G.A., Johnston, G.C., Ringe, D., Singer, R.A., and Werner-Washburne, M. (2004). "Sleeping Beauty": quiescence in *Saccharomyces cerevisiae*. Microbiol. Mol. Biol. Rev. *68*, 187–206.

Green, D.R., Galluzzi, L., and Kroemer, G. (2011). Mitochondria and the autophagy-inflammation-cell death axis in organismal aging. Science *333*, 1109–1112.

Gregg, S.Q., Gutiérrez, V., Rasile Robinson, A., Woodell, T., Nakao, A., Ross, M.A., Michalopoulos, G.K., Rigatti, L., Rothermel, C.E., Kamileri, I., et al. (2012). A mouse model of accelerated liver aging caused by a defect in DNA repair. Hepatology *55*, 609–621.

Grigoryev, S.A., Nikitina, T., Pehrson, J.R., Singh, P.B., and Woodcock, C.L. (2004). Dynamic relocation of epigenetic chromatin markers reveals an active role of constitutive heterochromatin in the transition from proliferation to quiescence. J. Cell Sci. *117*, 6153–6162.

Hagan, I., Hayles, J., and Nurse, P. (1988). Cloning and sequencing of the cyclin-related *cdc13+* gene and a cytological study of its role in fission yeast mitosis. J. Cell Sci. *91*, 587–595.

Hara, K., Maruki, Y., Long, X., Yoshino, K. ichi, Oshiro, N., Hidayat, S., Tokunaga, C., Avruch, J., and Yonezawa, K. (2002). Raptor, a binding partner of target of rapamycin (TOR), mediates TOR action. Cell *110*, 177–189.

Hara, M., Abe, Y., Tanaka, T., Yamamoto, T., Okumura, E., and Kishimoto, T. (2012). Greatwall kinase and cyclin B-Cdk1 are both critical constituents of M-phase-promoting factor. Nat. Commun. *3*, 1059.

Hartwell, L.H., and Weinert, T. a (1989). Checkpoints: controls that ensure the order of cell cycle

events. Science *246*, 629–634.

Hatakeyama, R., Péli-Gulli, M.P., Hu, Z., Jaquenoud, M., Garcia Osuna, G.M., Sardu, A., Dengjel, J., and De Virgilio, C. (2019). Spatially distinct pools of TORC1 balance protein homeostasis. Mol. Cell *15*, 561–564.

He, C., and Kennedy, B.K. (2015). Aging in the single-celled eukaryote, *S. cerevisiae*. In Stem Cell Aging: Mechanisms, Consequences, Rejuvenation, pp. 19–49.

Heitman, J., Movva, N.R., and Hall, M.N. (1991). Targets for cell cycle arrest by the immunosuppressant rapamycin in yeast. Science *253*, 905–909.

Helmlinger, D., Marguerat, S., Villén, J., Gygi, S.P., Bähler, J., and Winston, F. (2008). The *S. pombe* SAGA complex controls the switch from proliferation to sexual differentiation through the opposing roles of its subunits Gcn5 and Spt8. Genes Dev. *22*, 3184–3195.

Hentges, P.N., Van Driessche, B., Tafforeau, L., Vandenhaute, J., and Carr, A.M. (2005). Three novel antibiotic marker cassettes for gene disruption and marker switching in *Schizosaccharomyces pombe*. Yeast *22*, 1013–1019.

Hiraoka, Y., Toda, T., and Yanagida, M. (1984). The *NDA3* gene of fission yeast encodes β-tubulin: a cold-sensitive *nda3* mutation reversibly blocks spindle formation and chromosome movement in mitosis. Cell *30*, 349–358.

Hoffman, C.S., Wood, V., and Fantes, P.A. (2015). An ancient yeast for young geneticists: a primer on the *Schizosaccharomyces pombe* model system. Genetics *201*, 403–423.

Holmes, D.S., and Quigley, M. (1981). A rapid boiling method for the preparation of bacterial plasmids. Anal. Biochem. *114*, 193–197.

Holz, M.K., Ballif, B.A., Gygi, S.P., and Blenis, J. (2005). mTOR and S6K1 mediate assembly of the translation preinitiation complex through dynamic protein interchange and ordered phosphorylation events. Cell *123*, 569–580.

Hsu, P.P., Kang, S.A., Rameseder, J., Zhang, Y., Ottina, K.A., Lim, D., Peterson, T.R., Choi, Y., Gray, N.S., Yaffe, M.B., et al. (2011). The mTOR-regulated phosphoproteome reveals a mechanism of mTORC1-mediated inhibition of growth factor signaling. Science *332*, 1317–1322.

Hunter, T. (1995). Protein kinases and phosphatases: the Yin and Yang of protein phosphorylation and signaling. Cell *80*, 225–236.

Iglesias, N., Paulo, J.A., Tatarakis, A., Wang, X., Edwards, A.L., Bhanu, N. V., Garcia, B.A., Haas, W., Gygi, S.P., and Moazed, D. (2020). Native chromatin proteomics reveals a role for specific nucleoporins in heterochromatin organization and maintenance. Mol. Cell *77*, 51–66.

Ikai, N., Nakazawa, N., Hayashi, T., and Yanagida, M. (2011). The reverse, but coordinated, roles of Tor2 (TORC1) and Tor1 (TORC2) kinases for growth, cell cycle and separase-mediated mitosis in Schizosaccharomyces pombe. Open Biol. *1*, 110007.

Ikeda, K., Morigasaki, S., Tatebe, H., Tamanoi, F., and Shiozaki, K. (2008). Cell cycle fission yeast TOR complex 2 activates the AGC-family Gad8 kinase essential for stress resistance and cell cycle control. Cell Cycle Landes Biosci. Cell Cycle *73*, 1–7.

Inoki, K., Zhu, T., and Guan, K.L. (2003). TSC2 mediates cellular energy response to control cell growth and survival. Cell *115*, 577–590.

Inoue, H., Nojima, H., and Okayama, H. (1990). High efficiency transformation of *Escherichia coli* with plasmids. Gene *96*, 23–28.

Jacinto, E., Loewith, R., Schmidt, A., Lin, S., Rüegg, M.A., Hall, A., and Hall, M.N. (2004). Mammalian TOR complex 2 controls the actin cytoskeleton and is rapamycin insensitive. Nat. Cell Biol. *6*, 1122–1128.

Janssens, V., and Goris, J. (2001). Protein phosphatase 2A: a highly regulated family of serine/threonine phosphatases implicated in cell growth and signalling. Biochem. J. *353*,

417–439.

Jeffrey, P.D., Russo, A.A., Polyak, K., Gibbs, E., Hurwitz, J., Massagué, J., and Pavletich, N.P. (1995). Mechanism of CDK activation revealed by the structure of a CyclinA-CDK2 complex. Nature *376*, 313–320.

Jiang, W., and Hallberg, R.L. (2000). Isolation and characterization of *par1⁺* and *par2⁺*: two *Schizosaccharomyces pombe* genes encoding B' subunits of protein phosphatase 2A. Genetics *154*, 1025–1038.

Jiang, W., and Hallberg, R.L. (2001). Correct regulation of the septation initiation network in *Schizosaccharomyces pombe* requires the activities of *par1* and *par2*. Genetics *158*, 1413–1429.

Joh, R.I., Khanduja, J.S., Calvo, I.A., Mistry, M., Palmieri, C.M., Savol, A.J., Ho Sui, S.J., Sadreyev, R.I., Aryee, M.J., and Motamedi, M. (2016). Survival in quiescence requires the euchromatic deployment of Clr4/SUV39H by Argonaute-associated small RNAs. Mol. Cell *64*, 1088–1101.

Johnson, S.C., Rabinovitch, P.S., and Kaeberlein, M. (2013). MTOR is a key modulator of ageing and age-related disease. Nature *483*, 338–345.

Kaeberlein, M. (2006). Longevity and aging in budding yeast. In Handbook of Models for Human Aging, pp. 207–217.

Kaeberlein, M. (2010). Lessons on longevity from budding yeast. Nature *464*, 513–519.

Kamenz, J., and Ferrell, J.E. (2017). The temporal ordering of cell-cycle phosphorylation. Mol. Cell *65*, 371–373.

Kanoh, J., and Yanagida, M. (2010). Structure of TOR complexes in fission yeast. In Enzymes, pp. 271–284.

Kawai, M., Nakashima, A., Ueno, M., Ushimaru, T., Aiba, K., Doi, H., and Uritani, M. (2001). Fission yeast Tor1 functions in response to various stresses including nitrogen starvation, high osmolarity, and high temperature. Curr. Genet. *39*, 166–174.

Kim, D.H., Sarbassov, D.D., Ali, S.M., King, J.E., Latek, R.R., Erdjument-Bromage, H., Tempst, P., and Sabatini, D.M. (2002). mTOR interacts with Raptor to form a nutrient-sensitive complex that signals to the cell growth machinery. Cell *110*, 163–175.

Kim, D.H., Sarbassov, D.D., Ali, S.M., Latek, R.R., Guntur, K.V.P., Erdjument-Bromage, H., Tempst, P., and Sabatini, D.M. (2003). GβL, a positive regulator of the rapamycin-sensitive pathway required for the nutrient-sensitive interaction between Raptor and mTOR. Mol. Cell *11*, 895–904.

King, J., and Laemmli, U.K. (1971). Polypeptides of the tail fibres of bacteriophage T4. J. Mol. Biol. *62*, 465–477.

Kinoshita, K., Nemoto, T., Nabeshima, K., Kondoh, H., Niwa, H., and Yanagida, M. (1996). The regulatory subunits of fission yeast protein phosphatase 2A (PP2A) affect cell morphogenesis, cell wall synthesis and cytokinesis. Genes to Cells *1*, 29–45.

Kinoshita, N., Ohkura, H., and Yanagida, M. (1990). Distinct, essential roles of type 1 and 2A protein phosphatases in the control of the fission yeast cell division cycle. Cell *63*, 405–415.

Kira, S., Tabata, K., Shirahama-Noda, K., Nozoe, A., Yoshimori, T., and Noda, T. (2014). Reciprocal conversion of Gtr1 and Gtr2 nucleotidebinding states by Npr2-Npr3 inactivates TORC1 and induces autophagy. Autophagy *10*, 1565–1578.

Kira, S., Kumano, Y., Ukai, H., Takeda, E., Matsuura, A., and Noda, T. (2016). Dynamic relocation of the TORC1-Gtr1/2-Ego1/2/3 complex is regulated by Gtr1 and Gtr2. Mol. Biol. Cell *27*, 382–396.

Kitajima, T.S., Sakuno, T., Ishiguro, K.I., Iemura, S.I., Natsume, T., Kawashima, S.A., and Watanabe, Y. (2006). Shugoshin collaborates with protein phosphatase 2A to protect

cohesin. Nature *441*, 46–52.

Knutsen, J.H.J., da Rein, I., Rothe, C., Stokke, T., Grallert, B., and Boye, E. (2011). Cell-cycle analysis of fission yeast cells by flow cytometry. PLoS One *6*, e17175.

Kohda, T.A., Tanaka, K., Konomi, M., Sato, M., Osumi, M., and Yamamoto, M. (2007). Fission yeast autophagy induced by nitrogen starvation generates a nitrogen source that drives adaptation processes. Genes to Cells *12*, 155–170.

Kominami, K.I., Ochotorena, I., and Toda, T. (1998). Two F-box/WD-repeat proteins Pop1 and Pop2 form hetero- and homo-complexes together with cullin-1 in the fission yeast SCF (Skp1-Cullin-1-F- box) ubiquitin ligase. Genes to Cells *3*, 721–735.

Kunz, J., Henriquez, R., Schneider, U., Deuter-Reinhard, M., Movva, N.R., and Hall, M.N. (1993). Target of rapamycin in yeast, TOR2, is an essential phosphatidylinositol kinase homolog required for G1 progression. Cell *73*, 585–596.

Kupiec, M., and Weisman, R. (2012). TOR links starvation responses to telomere length maintenance. Cell Cycle *11*, 2268–2271.

Kushner, S. (1978). An improved method for transformation of *Escherichia coli* with colEI derived plasmid. In Genetic engineering, pp. 17–23.

Laboucarié, T., Detilleux, D., Rodriguez-Mias, R.A., Faux, C., Romeo, Y., Franz-Wachtel, M., Krug, K., Maček, B., Villén, J., Petersen, J., et al. (2017). TORC1 and TORC2 converge to regulate the SAGA co-activator in response to nutrient availability. EMBO Rep. *18*, 2197–2218.

Lahoz, A., Alcaide-Gavilán, M., Daga, R.R., and Jimenez, J. (2010). Antagonistic roles of PP2A-Pab1 and Etd1 in the control of cytokinesis in fission yeast. Genetics *186*, 1261–1270.

Laor, D., Cohen, A., Pasmanik-Chor, M., Oron-Karni, V., Kupiec, M., and Weisman, R. (2014). Isp7 is a novel regulator of amino acid uptake in the TOR signaling pathway. Mol. Cell. Biol. *34*, 794–806.

Laplante, M., and Sabatini, D.M. (2012). mTOR signaling in growth control and disease. Cell *149*, 274–293.

Laribee, N.R., and Weisman, R. (2020). Nuclear functions of TOR: impact on transcription and the epigenome. Genes *11*, 641.

Laxman, S., Sutter, B.M., and Tu, B.P. (2014). Methionine is a signal of amino acid sufficiency that inhibits autophagy through the methylation of PP2A. Autophagy *10*, 386–387.

Li, B., Jog, S., Candelario, J., Reddy, S., and Comai, L. (2009). Altered nuclear functions in progeroid syndromes: a paradigm for aging research. Sci. World J. *16*, 1449–1462.

Liu, P., Gan, W., Chin, Y.R., Ogura, K., Guo, J., Zhang, J., Wang, B., Blenis, J., Cantley, L.C., Toker, A., et al. (2015). Ptdins(3,4,5)P_3-dependent activation of the mTORC2 kinase complex. Cancer Discov. *5*, 1194–1209.

Loewith, R., and Hall, M.N. (2011). Target of rapamycin (TOR) in nutrient signaling and growth control. Genetics 189, 1177–1201.

Loewith, R., Jacinto, E., Wullschleger, S., Lorberg, A., Crespo, J.L., Bonenfant, D., Oppliger, W., Jenoe, P., and Hall, M.N. (2002). Two TOR complexes, only one of which is rapamycin sensitive, have distinct roles in cell growth control. Mol. Cell *10*, 457–468.

Long, X., Lin, Y., Ortiz-Vega, S., Yonezawa, K., and Avruch, J. (2005). Rheb binds and regulates the mTOR kinase. Curr. Biol. *15*, 702–713.

Loog, M., and Morgan, D.O. (2005). Cyclin specificity in the phosphorylation of cyclin-dependent kinase substrates. Nature *434*, 104–108.

López-Otín, C., Blasco, M.A., Partridge, L., Serrano, M., and Kroemer, G. (2013). The hallmarks of aging. Cell *153*, 1194–1217.

Lorca, T., and Castro, A. (2013). The Greatwall kinase: a new pathway in the control of the cell

cycle. Oncogene *32*, 537–543.

Ma, N., Liu, Q., Zhang, L., Henske, E.P., and Ma, Y. (2013). TORC1 signaling is governed by two negative regulators in fission yeast. Genetics *195*, 457–568.

Ma, N., Ma, Y., Nakashima, A., Kikkawa, U., and Furuyashiki, T. (2016). The loss of Lam2 and Npr2-Npr3 diminishes the vacuolar localization of Gtr1-Gtr2 and disinhibits TORC1 activity in fission yeast. PLoS One *11*, e0156239.

Ma, X.M., Yoon, S.O., Richardson, C.J., Jülich, K., and Blenis, J. (2008). SKAR links pre-mRNA splicing to mTOR/S6K1-mediated enhanced translation efficiency of spliced mRNAs. Cell *133*, 303–313.

Mach, K.E., Furge, K.A., and Albright, C.F. (2000). Loss of Rhb1, a Rheb-related GTPase in fission yeast, causes growth arrest with a terminal phenotype similar to that caused by nitrogen starvation. Genetics *155*, 611–622.

Maestroni, L., Audry, J., Matmati, S., Arcangioli, B., Géli, V., and Coulon, S. (2017). Eroded telomeres are rearranged in quiescent fission yeast cells through duplications of subtelomeric sequences. Nat. Commun. *8*, 1684.

Maestroni, L., Reyes, C., Vaurs, M., Gachet, Y., Tournier, S., Géli, V., and Coulon, S. (2020). Nuclear envelope attachment of telomeres limits TERRA and telomeric rearrangements in quiescent fission yeast cells. Nucleic Acids Res. *48*, 3029–3041.

Malumbres, M. (2014). Cyclin-dependent kinases. Genome Biol. *15*, 122.

Manning, B.D., and Toker, A. (2017). AKT/PKB signaling: navigating the network. Cell *169*, 381–405.

Marguerat, S., Schmidt, A., Codlin, S., Chen, W., Aebersold, R., and Bähler, J. (2012). Quantitative analysis of fission yeast transcriptomes and proteomes in proliferating and quiescent cells. Cell *151*, 671–683.

Martel, R.R., Klicius, J., and Galet, S. (1977). Inhibition of the immune response by rapamycin, a new antifungal antibiotic. Can. J. Physiol. Pharmacol. *55*, 48–51.

Martín-Castellanos, C., Labib, K., and Moreno, S. (1996). B-type cyclins regulate G1 progression in fission yeast in opposition to the p25^{rum1} cdk inhibitor. EMBO J. *15*, 839–849.

Martín-Castellanos, C., Blanco, M.A., De Prada, J.M., and Moreno, S. (2000). The puc1 cyclin regulates the G1 phase of the fission yeast cell cycle in response to cell size. Mol. Biol. Cell *11*, 543–554.

Martín, R., and López-Áviles, S. (2018). Express yourself: how PP2A-B55^{Pab1} helps TORC1 talk to TORC2. Curr. Genet. *64*, 43–51.

Martín, R., Portantier, M., Chica, N., Nyquist-Andersen, M., Mata, J., and López-Áviles, S. (2017). A PP2A-B55-mediated crosstalk between TORC1 and TORC2 regulates the differentiation response in fission yeast. Curr. Biol. *27*, 175–188.

Mata, J., and Bähler, J. (2006). Global roles of Ste11p, cell type, and pheromone in the control of gene expression during early sexual differentiation in fission yeast. Proc. Natl. Acad. Sci. U.S.A. *103*, 15517–15522.

Matsumoto, S., Bandyopadhyay, A., Kwiatkowski, D.J., Maitra, U., and Matsumoto, T. (2002). Role of the Tsc1-Tsc2 complex in signaling and transport across the cell membrane in the fission yeast *Schizosaccharomyces pombe*. Genetics *161*, 1053–1063.

Matsuo, T., Kubo, Y., Watanabe, Y., and Yamamoto, M. (2003). *Schizosaccharomyces pombe* AGC family kinase Gad8p forms a conserved signaling module with TOR and PDK1-like kinases. EMBO J. *22*, 3073–3083.

Matsuo, T., Otsubo, Y., Urano, J., Tamanoi, F., and Yamamoto, M. (2007). Loss of the TOR kinase Tor2 mimics nitrogen starvation and activates the sexual development pathway in fission yeast. Mol. Cell. Biol. *27*, 3154–3164.

Mattison, J.A., Roth, G.S., Mark Beasley, T., Tilmont, E.M., Handy, A.M., Herbert, R.L., Longo, D.L., Allison, D.B., Young, J.E., Bryant, M., et al. (2012). Impact of caloric restriction on health and survival in rhesus monkeys from the NIA study. Nature *489*, 318–321.

Maundrell, K. (1990). nmt1 of fission yeast. A highly transcribed gene completely repressed by thiamine. J. Biol. Chem. *265*, 10857–10864.

McKnight, J.N., Boerma, J.W., Breeden, L.L., and Tsukiyama, T. (2015). Global promoter targeting of a conserved lysine deacetylase for transcriptional shutoff during quiescence entry. Mol. Cell *59*, 732–743.

Michels, A.A., Robitaille, A.M., Buczynski-Ruchonnet, D., Hodroj, W., Reina, J.H., Hall, M.N., and Hernandez, N. (2010). mTORC1 directly phosphorylates and regulates human MAF1. Mol. Cell. Biol. *30*, 3749–3757.

Mochida, S., and Hunt, T. (2012). Protein phosphatases and their regulation in the control of mitosis. EMBO Rep. *13*, 197–203.

Mochida, S., and Yanagida, M. (2006). Distinct modes of DNA damage response in *S. pombe* G0 and vegetative cells. Genes to Cells *11*, 13–27.

Mochida, S., Ikeo, S., Gannon, J., and Hunt, T. (2009). Regulated activity of PP2A-B55 δ is crucial for controlling entry into and exit from mitosis in *Xenopus* egg extracts. EMBO J. *28*, 2777–2785.

Mochida, S., Maslen, S.L., Skehel, M., and Hunt, T. (2010). Greatwall phosphorylates an inhibitor of protein phosphatase 2A that is essential for mitosis. Science *330*, 1670–1673.

Mondesert, O., McGowan, C.H., and Russell, P. (1996). Cig2, a B-type cyclin, promotes the onset of S in *Schizosaccharomyces pombe*. Mol. Cell. Biol. *16*, 1527–1533.

Moreno, S., and Nurse, P. (1994). Regulation of progression through the Gl phase of the cell cycle by the *rum1⁺* gene. Nature *367*, 236–242.

Moreno, S., Hayles, J., and Nurse, P. (1989). Regulation of p34cdc2 protein kinase during mitosis. Cell *58*, 361–372.

Moreno, S., Nurse, P., and Russell, P. (1990). Regulation of mitosis by cyclic accumulation of p80^{cdc25} mitotic inducer in fission yeast. Nature *344*, 549–552.

Moreno, S., Klar, A., and Nurse, P. (1991). Molecular genetic analysis of fission yeast *Schizosaccharomyces pombe*. Methods Enzymol. *194*, 795–823.

Morgan, D.O. (1997). Cyclin-dependent kinases: engines, clocks, and microprocessors. Annu. Rev. Cell Dev. Biol. *13*, 261–291.

Morrison, S.J., and Weissman, I.L. (1994). The long-term repopulating subset of hematopoietic stem cells is deterministic and isolatable by phenotype. Immunity *1*, 661–637.

Mortimer, R.K., and Johnston, J.R. (1959). Life span of individual yeast cells. Nature *183*, 1751–1752.

Moser, B.A., and Russell, P. (2000). Cell cycle regulation in *Schizosaccharomyces pombe*. Curr. Opin. Microbiol. *3*, 631–636.

Moskalev, A.A., Shaposhnikov, M. V., Plyusnina, E.N., Zhavoronkov, A., Budovsky, A., Yanai, H., and Fraifeld, V.E. (2013). The role of DNA damage and repair in aging through the prism of Koch-like criteria. Ageing Res. Rev. *12*, 661–684.

Mueller, P.R., Coleman, T.R., and Dunphy, W.G. (1995). Cell cycle regulation of a *Xenopus* Wee1-like kinase. Mol. Biol. Cell *344*, 549–552.

Mukaiyama, H., Nakase, M., Nakamura, T., Kakinuma, Y., and Takegawa, K. (2010). Autophagy in the fission yeast *Schizosaccharomyces pombe*. FEBS Lett. *584*, 1327–1334.

Nasmyth, K., Nurse, P., and Fraser, R.S.S. (1979). The effect of cell mass on the cell cycle timing and duration of S-phase in fission yeast. J. Cell Sci. *39*, 215–233.

Nugent, R.L., Johnsson, A., Fleharty, B., Gogol, M., Xue-Franzén, Y., Seidel, C., Wright, A.P.H., and Forsburg, S.L. (2010). Expression profiling of *S. pombe* acetyltransferase mutants identifies redundant pathways of gene regulation. BMC Genomics *11*, 59.

Nurse, P. (1975). Genetic control of cell size at cell division in yeast. Nature *256*, 547–551.

Nurse, P. (1990). Universal control mechanism regulating onset of M-phase. Nature 344, 503–508.

Nurse, P., and Bissett, Y. (1981). Gene required in G1 for commitment to cell cycle and in G2 for control of mitosis in fission yeast. Nature *292*, 558–560.

Nurse, P., and Thuriaux, P. (1977). Controls over the timing of DNA replication during the cell cycle of fission yeast. Exp. Cell Res. *107*, 365–375.

Oberdoerffer, P., and Sinclair, D.A. (2007). The role of nuclear architecture in genomic instability and ageing. Nat. Rev. Mol. Cell Biol. *8*, 962–702.

Osorio, F.G., Varela, I., Lara, E., Puente, X.S., Espada, J., Santoro, R., Freije, J.M.P., Fraga, M.F., and López-Otín, C. (2010). Nuclear envelope alterations generate an aging-like epigenetic pattern in mice deficient in Zmpste24 metalloprotease. Aging Cell *9*, 947–957.

Oya, E., Durand-Dubief, M., Cohen, A., Maksimov, V., Schurra, C., Nakayama, J.I., Weisman, R., Arcangioli, B., and Ekwall, K. (2019). Leo1 is essential for the dynamic regulation of heterochromatin and gene expression during cellular quiescence. Epigenetics and Chromatin *12*, 45.

Painting, K., and Kirsop, B. (1990). A quick method for estimating the percentage of viable cells in a yeast population, using methylene blue staining. World J. Microbiol. Biotechnol. *6*, 346–347.

Pal, G., Paraz, M.T.Z., and Kellogg, D.R. (2008). Regulation of Mih1/Cdc25 by protein phosphatase 2A and casein kinase 1. J. Cell Biol. *180*, 931–945.

Panchaud, N., Péli-Gulli, M.P., and De Virgilio, C. (2013). Amino acid deprivation inhibits TORC1 through a GTPase-activating protein complex for the Rag family GTPase Gtr1. Sci. Signal. *6*, ra42.

Parmigiani, A., Nourbakhsh, A., Ding, B., Wang, W., Kim, Y.C., Akopiants, K., Guan, K.L., Karin, M., and Budanov, A. V. (2014). Sestrins inhibit mTORC1 kinase activation through the GATOR complex. Cell Rep. *9*, 1281–1291.

Pearce, L.R., Komander, D., and Alessi, D.R. (2010). The nuts and bolts of AGC protein kinases. Nat. Rev. Mol. Cell Biol. *11*, 9–22.

Pedruzzi, I., Dubouloz, F., Cameroni, E., Wanke, V., Roosen, J., Winderickx, J., and De Virgilio, C. (2003). TOR and PKA signaling pathways converge on the protein kinase Rim15 to control entry into G0. Mol. Cell *12*, 1607–1613.

Pérez-Hidalgo, L., and Moreno, S. (2016). Nutrients control cell size. Cell Cycle *15*, 1655–1666.

Pérez-Hidalgo, L., and Moreno, S. (2017). Coupling TOR to the cell cycle by the Greatwall-Endosulfine-PP2A-B55 pathway. Biomolecules *7*, 59.

Petersen, J., and Nurse, P. (2007). TOR signalling regulates mitotic commitment through the stress MAP kinase pathway and the Polo and Cdc2 kinases. Nat. Cell Biol. *9*, 1263–1272.

Petersen, J., Weilguny, D., Egel, R., and Nielsen, O. (1995). Characterization of fus1 of *Schizosaccharomyces pombe*: a developmentally controlled function needed for conjugation. Mol. Cell. Biol. *15*, 3697–3707.

Pokholok, D.K., Harbison, C.T., Levine, S., Cole, M., Hannett, N.M., Tong, I.L., Bell, G.W., Walker, K., Rolfe, P.A., Herbolsheimer, E., et al. (2005). Genome-wide map of nucleosome acetylation and methylation in yeast. Cell *122*, 517–527.

Poli, J., Gasser, S.M., and Papamichos-Chronakis, M. (2017). The INO80 remodeller in transcription, replication and repair. Philos. Trans. R. Soc. B Biol. Sci. *372*, 20160290.

Poulose, N., and Raju, R. (2015). Sirtuin regulation in aging and injury. Biochim. Biophys. Acta Mol. Basis Dis. *1852*, 2442–2455.

Powers, T. (2007). TOR signaling and S6 kinase 1: yeast catches up. Cell Metab. *6*, 1–2.

Powers, E.T., Morimoto, R.I., Dillin, A., Kelly, J.W., and Balch, W.E. (2009). Biological and chemical approaches to diseases of proteostasis deficiency. Annu. Rev. Biochem. *78*, 959–991.

Powis, K., Zhang, T., Panchaud, N., Wang, R., De Virgilio, C., and Ding, J. (2015). Crystal structure of the Ego1-Ego2-Ego3 complex and its role in promoting Rag GTPase-dependent TORC1 signaling. Cell Res. *25*, 1043–1059.

Reinders, A., Bürckert, N., Boller, T., Wiemken, A., and De Virgilio, C. (1998). S*accharomyces cerevisiae* cAMP-dependent protein kinase controls entry into stationary phase through the Rim15p protein kinase. Genes Dev. *12*, 2943–2955.

Roberts-Galbraith, R.H., Chen, J.S., Wang, J., and Gould, K.L. (2009). The SH3 domains of two PCH family members cooperate in assembly of the *Schizosaccharomyces pombe* contractile ring. J. Cell Biol. *184*, 113–127.

Roche, B., Arcangioli, B., and Martienssen, R.A. (2016). RNA interference is essential for cellular quiescence. Science *354*, aah5651.

Roelants, F.M., Leskoske, K.L., Marshall, M.N.M., Locke, M.N., and Thorner, J. (2017). The TORC2-dependent signaling network in the yeast *Saccharomyces cerevisiae*. Biomolecules *28*, 196–210.

Rubio, A., García-Blanco, N., Vázquez-Bolado, A., Suárez, M.B., and Moreno, S. (2018). Nutritional cell cycle reprogramming reveals that inhibition of Cdk1 is required for proper MBF-dependent transcription. J. Cell Sci. *131*, jcs218743.

Russell, S.J., and Kahn, C.R. (2007). Endocrine regulation of ageing. Nat. Rev. Mol. Cell Biol. *8*, 681–691.

Sabatini, D.M., Erdjument-Bromage, H., Lui, M., Tempst, P., and Snyder, S.H. (1994). RAFT1: A mammalian protein that binds to FKBP12 in a rapamycin-dependent fashion and is homologous to yeast TORs. Cell *78*, 35–43.

Sabers, C.J., Martin, M.M., Brunn, G.J., Williams, J.M., Dumont, F.J., Wiederrecht, G., and Abraham, R.T. (1995). Isolation of a protein target of the FKBP12-rapamycin complex in mammalian cells. J. Biol. Chem. *270*, 815–822.

Sajiki, K., Hatanaka, M., Nakamura, T., Takeda, K., Shimanuki, M., Yoshida, T., Hanyu, Y., Hayashi, T., Nakaseko, Y., and Yanagida, M. (2009). Genetic control of cellular quiescence in *S. pombe*. J. Cell Sci. *122*, 1418–1429.

Sajiki, K., Pluskal, T., Shimanuki, M., and Yanagida, M. (2013). Metabolomic analysis of fission yeast at the onset of nitrogen starvation. Metabolites *3*, 1118–1129.

Sajiki, K., Tahara, Y., Uehara, L., Sasaki, T., Pluskal, T., and Yanagida, M. (2018). Genetic regulation of mitotic competence in G0 quiescent cells. Sci. Adv. 1–9.

Sambrook J, Fritsch EF, M.T. (1989). Molecular cloning: a laboratory manual. 2nd Ed. Cold Spring Harbor, NY. Cold Spring Harbor Laboratory Press.

Sancak, Y., Bar-Peled, L., Zoncu, R., Markhard, A.L., Nada, S., and Sabatini, D.M. (2010). Ragulator-rag complex targets mTORC1 to the lysosomal surface and is necessary for its activation by amino acids. Cell *141*, 290–303.

Sarbassov, D.D., Guertin, D.A., Ali, S.M., and Sabatini, D.M. (2005). Phosphorylation and regulation of Akt/PKB by the rictor-mTOR complex. Science *307*, 1098–1101.

Sarbassov, D.D., Ali, S.M., Kim, D., Guertin, D.A., Latek, R.R., Erdjument-Bromage, H., Tempst, P., and Sabatini, D.M. (2004). Rictor, a novel binding partner of mTOR, defines a rapamycin-insensitive and Raptor-independent pathway that regulates the cytoskeleton. Curr. Biol. *14*, 1296–1302.

Sarkar, S., Dalgaard, J.Z., Millar, J.B.A., and Arumugam, P. (2014). The Rim15-Endosulfine-PP2A^{Cdc55} signalling module regulates entry into gametogenesis and quiescence via distinct mechanisms in budding yeast. PLoS Genet. *10*, e1004456.

Sato, M., Dhut, S., and Toda, T. (2005). New drug-resistant cassettes for gene disruption and epitope tagging in *Schizosaccharomyces pombe*. Yeast *22*, 583–591.

Saxton, R.A., and Sabatini, D.M. (2017). mTOR Signaling in growth, metabolism, and disease. Cell 168, 960–976.

Saxton, R.A., Chantranupong, L., Knockenhauer, K.E., Schwartz, T.U., and Sabatini, D.M. (2016). Mechanism of arginine sensing by CASTOR1 upstream of mTORC1. Nature *536*, 229–233.

Sazer, S., and Sherwood, S.W. (1990). Mitochondrial growth and DNA synthesis occur in the absence of nuclear DNA replication in fission yeast. J. Cell Sci. *97*, 509–516.

Schmidt, A., Kunz, J., and Hall, M.N. (1996). TOR2 is required for organization of the actin cytoskeleton in yeast. Proc. Natl. Acad. Sci. U.S.A. *93*, 13780–13785.

Sekiguchi, T., Hirose, E., Nakashima, N., Ii, M., and Nishimoto, T. (2001). Novel G proteins, Rag C and Rag D, interact with GTP-binding proteins, Rag A and Rag B. J. Biol. Chem. *276*, 7246–7257.

Shetty, M., Noguchi, C., Wilson, S., Martinez, E., Shiozaki, K., Sell, C., Mell, J.C., and Noguchi, E. (2019). Maf1-dependent transcriptional regulation of tRNAs prevents genomic instability and is associated with extended lifespan. Aging Cell *19*, e13068.

Shimanuki, M., Chung, S.Y., Chikashige, Y., Kawasaki, Y., Uehara, L., Tsutsumi, C., Hatanaka, M., Hiraoka, Y., Nagao, K., and Yanagida, M. (2007). Two-step, extensive alterations in the transcriptome from G0 arrest to cell division in *Schizosaccharomyces pombe*. Genes to Cells *12*, 677–692.

Shor, B., Wu, J., Shakey, Q., Toral-Barza, L., Shi, C., Follettie, M., and Yu, K. (2010). Requirement of the mTOR kinase for the regulation of Maf1 phosphorylation and control of RNA polymerase III-dependent transcription in cancer cells. J. Biol. Chem. *285*, 15380–15392.

Shumaker, D.K., Dechat, T., Kohlmaier, A., Adam, S.A., Bozovsky, M.R., Erdos, M.R., Eriksson, M., Goldman, A.E., Khuon, S., Collins, F.S., et al. (2006). Mutant nuclear lamin A leads to progressive alterations of epigenetic control in premature aging. Proc. Natl. Acad. Sci. U.S.A. *103*, 8703–8708.

Sideri, T., Rallis, C., Bitton, D.A., Lages, B.M., Suo, F., Rodríguez-López, M., Du, L.L., and Bähler, J. (2015). Parallel profiling of fission yeast deletion mutants for proliferation and for lifespan during long-term quiescence. G3 (Bethesda) *5*, 145–155.

Sipiczki, M. (2000). Where does fission yeast sit on the tree of life? Genome Biol. *1*, reviews1011.1.

Steph D., A., Nguyen, D.L., Thai, V., Meloy, M., MacDonough, T., and Kellogg, D.R. (2012). A link between mitotic entry and membrane growth suggests a novel model for cell size control. J. Cell Biol. *197*, 89–104.

Stern, B., and Nurse, P. (1998). Cyclin B proteolysis and the cyclin-dependent kinase inhibitor rum1p are required for pheromone-induced G1 arrest in fission yeast. Mol. Biol. Cell *9*, 1309–1321.

Von Stetina, J.R., Tranguch, S., Dey, S.K., Lee, L.A., Cha, B., and Drummond-Barbosa, D. (2008). α-Endosulfine is a conserved protein required for oocyte meiotic maturation in *Drosophila*. Development *135*, 3697–3706.

Su, S.S.Y., Tanaka, Y., Samejima, I., Tanaka, K., and Yanagida, M. (1996). A nitrogen starvation-induced dormant G0 state in fission yeast: the establishment from uncommitted G1 state and its delay for return to proliferation. J. Cell Sci. *109*, 1347–1357.

Sugimoto, A., Iino, Y., Maeda, T., Watanabe, Y., and Yamamoto, M. (1991). Schizosaccharomyces pombe *ste11*$^{+}$ encodes a transcription factor with an HMG motif that is a critical regulator of sexual development. Genes Dev. *5*, 1990–1999.

Sun, L.L., Li, M., Suo, F., Liu, X.M., Shen, E.Z., Yang, B., Dong, M.Q., He, W.Z., and Du, L.L. (2013). Global analysis of fission yeast mating genes reveals new autophagy factors. PLoS Genet. *9*, e1003715.

Sunnerhagen, P. (2002). Prospects for functional genomics in *Schizosaccharomyces pombe*. Curr. Genet. *42*, 73–84.

Sutter, B.M., Wu, X., Laxman, S., and Tu, B.P. (2013). Methionine inhibits autophagy and promotes growth by inducing the SAM-responsive methylation of PP2A. Cell *4*, 403–415.

Sveiczer, Á., and Horváth, A. (2017). How do fission yeast cells grow and connect growth to the mitotic cycle? Curr. Genet. *63*, 165–173.

Swaffer, M.P., Jones, A.W., Flynn, H.R., Snijders, A.P., and Nurse, P. (2016). CDK substrate phosphorylation and ordering the cell cycle. Cell *167*, 1750–1761.

Swinnen, E., Wanke, V., Roosen, J., Smets, B., Dubouloz, F., Pedruzzi, I., Cameroni, E., De Virgilio, C., and Winderickx, J. (2006). Rim15 and the crossroads of nutrient signalling pathways in *Saccharomyces cerevisiae*. Cell Div. *1*, 3.

Swygert, S.G., Kim, S., Wu, X., Fu, T., Hsieh, T.H., Rando, O.J., Eisenman, R.N., Shendure, J., McKnight, J.N., and Tsukiyama, T. (2019). Condensin-dependent chromatin compaction represses transcription globally during quiescence. Mol. Cell *73*, 533–564.

Tagwerker, C., Flick, K., Cui, M., Guerrero, C., Dou, Y., Auer, B., Baldi, P., Huang, L., and Kaiser, P. (2006). A tandem affinity tag for two-step purification under fully denaturing conditions: Application in ubiquitin profiling complex identification combined with in vivo cross-linking. Mol. Cell. Proteomics *5*, 737–748.

Takeda, K., and Yanagida, M. (2010). In quiescence of fission yeast, autophagy and the proteasome collaborate for mitochondrial maintenance and longevity. Autophagy *6*, 564–565.

Takeda, K., Yoshida, T., Kikuchi, S., Nagao, K., Kokubu, A., Pluskal, T., Villar-Briones, A., Nakamura, T., and Yanagida, M. (2010). Synergistic roles of the proteasome and autophagy for mitochondrial maintenance and chronological lifespan in fission yeast. Proc. Natl. Acad. Sci. U.S.A. *7*, 3540–3545.

Talarek, N., Cameroni, E., Jaquenoud, M., Luo, X., Bontron, S., Lippman, S., Devgan, G., Snyder, M., Broach, J.R., and De Virgilio, C. (2010). Initiation of the TORC1-regulated G0 program requires Igo1/2, which license specific mRNAs to evade degradation via the 5′-3′ mRNA decay pathway. Mol. Cell *38*, 345–355.

Tanny, J.C., Erdjument-Bromage, H., Tempst, P., and Allis, C.D. (2007). Ubiquitylation of histone H2B controls RNA polymerase II transcription elongation independently of histone H3 methylation. Genes Dev. *21*, 835–847.

Tee, A.R., Manning, B.D., Roux, P.P., Cantley, L.C., and Blenis, J. (2003). Tuberous Sclerosis Complex gene products, Tuberin and Hamartin, control mTOR signaling by acting as a GTPase-activating protein complex toward Rheb. Curr. Biol. *13*, 1259–1268.

Thai, V., Dephoure, N., Weiss, A., Ferguson, J., Leitao, R., Gygi, S.P., and Kellogg, D.R. (2017). Protein kinase C controls binding of Igo/ENSA proteins to protein phosphatase 2A in budding yeast. J. Biol. Chem. *292*, 4925–4941.

Toda, T., Yamamoto, M., and Yanagida, M. (1981). Sequential alterations in the nuclear chromatin region during mitosis of the fission yeast *Schizosaccharomyces pombe*: video fluorescence microscopy of synchronously growing wild type and cold sensitive cdc mutants by using a DNA-binding fluorescent probe. J. Cell Sci. *52*, 271–287.

Tsukada, M., and Ohsumi, Y. (1993). Isolation and characterization of autophagy-defective mutants of Saccharomyces cerevisiae. FEBS Lett. *333*, 169–174.

Tsurumi, A., and Li, W.X. (2012). Global heterochromatin loss: a unifying theory of aging? Epigenetics *7*, 680–688.

Uhlmann, F., Bouchoux, C., and López-Avilés, S. (2011). A quantitative model for cyclin-dependent kinase control of the cell cycle: Revisited. Philos. Trans. R. Soc. B Biol. Sci. *366*, 3572–3583.

Uritani, M., Hidaka, H., Hotta, Y., Ueno, M., Ushimaru, T., and Toda, T. (2006). Fission yeast Tor2 links nitrogen signals to cell proliferation and acts downstream of the Rheb GTPase. Genes to Cells *11*, 1367–1379.

Valbuena, N., and Moreno, S. (2012). AMPK phosphorylation by Ssp1 is required for proper sexual differentiation in fission yeast. J. Cell Sci. *125*, 2655–2664.

Valcourt, J.R., Lemons, J.M.S., Haley, E.M., Kojima, M., Demuren, O.O., and Coller, H.A. (2012). Staying alive: metabolic adaptations to quiescence. Cell Cycle *11*, 1680–1696.

Van Slegtenhorst, M., Carr, E., Stoyanova, R., Kruger, W.D., and Henske, E.P. (2004). *tsc1*$^{+}$ and *tsc2*$^{+}$ regulate arginine uptake and metabolism in *Schizosaccharomyces pombe*. J. Biol. Chem. *279*, 12706–12713.

Vera, J., Lartigue, L., Vigneron, S., Gadea, G., Gire, V., Del Rio, M., Soubeyran, I., Chibon, F., Lorca, T., and Castro, A. (2015). Greatwall promotes cell transformation by hyperactivating AKT in human malignancies. Elife *4*, e10115.

Vézina, C., and Kudelski, A. (1975). Rapamycin (AY-22,989), a new antifungal antibiotic. I. taxonomy of the producing streptomycete and isolation of the active principle. J. Antibiot. *28*, 721–726.

Vidan, S., and Mitchell, A.P. (1997). Stimulation of yeast meiotic gene expression by the glucose-repressible protein kinase Rim15p. Mol. Cell. Biol. *17*, 2688–2697.

Vigneron, S., Gharbi-Ayachi, A., Raymond, A.-A., Burgess, A., Labbe, J.-C., Labesse, G., Monsarrat, B., Lorca, T., and Castro, A. (2011). Characterization of the mechanisms controlling greatwall activity. Mol. Cell. Biol. *31*, 2262–2275.

Voets, E., and Wolthuis, R.M.F. (2010). MASTL is the human orthologue of Greatwall kinase that facilitates mitotic entry, anaphase and cytokinesis. Cell Cycle *9*, 3591–3601.

Wang, Y., Kallgren, S.P., Reddy, B.D., Kuntz, K., López-Maury, L., Thompson, J., Watt, S., Chun, M., Hou, H., Shi, Y., et al. (2012). Histone H3 lysine 14 acetylation is required for activation of a DNA damage checkpoint in fission yeast. J. Biol. Chem. *287*, 4386–4393.

Wang, Z., Zang, C., Rosenfeld, J.A., Schones, D.E., Barski, A., Cuddapah, S., Cui, K., Roh, T.Y., Peng, W., Zhang, M.Q., et al. (2008). Combinatorial patterns of histone acetylations and methylations in the human genome. Nat. Genet. *40*, 897–903.

Watanabe, D., Araki, Y., Zhou, Y., Maeya, N., Akao, T., and Shimoi, H. (2012). A Loss-of-function mutation in the PAS kinase Rim15p is related to defective quiescence entry and high fermentation rates of *Saccharomyces cerevisiae* sake yeast strains. Appl. Environ. Microbiol. *78*, 4008–4016.

Watanabe, D., Zhou, Y., Hirata, A., Sugimoto, Y., Takagi, K., Akao, T., Ohya, Y., Takagi, H., and Shimoi, H. (2016). Inhibitory role of greatwall-like protein kinase Rim15p in alcoholic fermentation via upregulating the UDP-glucose synthesis pathway in *Saccharomyces cerevisiae*. Appl. Environ. Microbiol. *82*, 340–351.

Watanabe, D., Kajihara, T., Sugimoto, Y., Takagi, K., Mizuno, M., Zhou, Y., Chen, J., Takeda, K., Tatebe, H., Shiozaki, K., et al. (2019). Nutrient signaling via the TORC1-Greatwall-PP2AB55d pathway is responsible for the high initial rates of alcoholic fermentation in sake yeast strains of *Saccharomyces cerevisiae*. Appl. Environ. Microbiol. *85*, e02083–18.

Watson, J.D., Baker, T.A., Bell, S.P., Grann, A., Levine, M., and Losick, R. (2015). Molecular biology of the gene. 7th Ed. Pearson.

Wei, M., Fabrizio, P., Hu, J., Ge, H., Cheng, C., Li, L., and Longo, V.D. (2008). Life span extension by calorie restriction depends on Rim15 and transcription factors downstream of Ras/PKA, Tor, and Sch9. PLoS Genet. *4*, 0139–0149.

Wei, Y., Tsang, C.K., and Zheng, X.F.S. (2009). Mechanisms of regulation of RNA polymerase III-dependent transcription by TORC1. EMBO J. *28*, 2220–2230.

Wei, Y., Lee, N.N., Pan, L., Dhakshnamoorthy, J., Sun, L.-L., Zofall, M., Wheeler, D., and Grewal, S.I.S. (2021). TOR targets an RNA processing network to regulate facultative heterochromatin, developmental gene expression and cell proliferation. Nat. Cell Biol. *23*, 243–256.

Weisman, R. (2016). Target of Rapamycin (TOR) regulates growth in response to nutritional signals. Microbiol. Spectr. *4*.

Weisman, R., and Choder, M. (2001). The fission yeast TOR nomolog, *tor1+*, is required for the response to starvation and other stresses via a conserved serine. J. Biol. Chem. *276*, 7027–7032.

Weisman, R., Roitburg, I., Schonbrun, M., Harari, R., and Kupiec, M. (2007). Opposite effects of Tor1 and Tor2 on nitrogen starvation responses in fission yeast. Genetics *175*, 1153–1162.

Werner-Washburne, M., Braun, E., Johnston, G.C., and Singer, R.A. (1993). Stationary phase in the yeast *Saccharomyces cerevisiae*. Microbiol. Rev. *57*, 383–401.

Wodak, S.J., Vlasblom, J., Turinsky, A.L., and Pu, S. (2013). Protein-protein interaction networks: The puzzling riches. Curr. Opin. Struct. Biol. 23, 941–953.

Wolfson, R.L., Chantranupong, L., Wyant, G.A., Gu, X., Orozco, J.M., Shen, K., Condon, K.J., Petri, S., Kedir, J., Scaria, S.M., et al. (2017). KICSTOR recruits GATOR1 to the lysosome and is necessary for nutrients to regulate mTORC1. Nature *543*, 438–442.

Wood, V., Gwilliam, R., Rajandream, M.A., Lyne, M., Lyne, R., Stewart, A., Sgouros, J., Peat, N., Hayles, J., Baker, S., et al. (2002). The genome sequence of *Schizosaccharomyces pombe*. Nature *415*, 871–880.

Wurzenberger, C., and Gerlich, D.W. (2011). Phosphatases: providing safe passage through mitotic exit. Nat. Rev. Mol. Cell Biol. *12*, 469–482.

Xing, Y., Xu, Y., Chen, Y., Jeffrey, P.D., Chao, Y., Lin, Z., Li, Z., Strack, S., Stock, J.B., and Shi, Y. (2006). Structure of protein phosphatase 2A core enzyme bound to tumor-inducing toxins. Cell *127*, 341–353.

Xu, Y., Xing, Y., Chen, Y., Chao, Y., Lin, Z., Fan, E., Yu, J.W., Strack, S., Jeffrey, P.D., and Shi, Y. (2006). Structure of the protein phosphatase 2A holoenzyme. Cell *127*, 1239–1251.

Yamamoto, M. (1996). The molecular control mechanisms of meiosis in fission yeast. Trends Biochem. Sci. *21*, 18–22.

Yanagida, M. (2009). Cellular quiescence: are controlling genes conserved? Trends Cell Biol. *19*, 705–715.

Yang, G., Murashige, D.S., Humphrey, S.J., and James, D.E. (2015). A positive feedback loop between Akt and mTORC2 via SIN1 phosphorylation. Cell Rep. *12*, 937–943.

Yao, G. (2014). Modelling mammalian cellular quiescence. Interface Focus *4*, 20130074.

Yu, J., Zhao, Y., Li, Z.X., Galas, S., and Goldberg, M.L. (2006). Greatwall kinase participates in the Cdc2 autoregulatory loop in *Xenopus* egg extracts. Mol. Cell *22*, 83–91.

Yu, Y., Yoon, S.O., Poulogiannis, G., Yang, Q., Ma, X.M., Villén, J., Kubica, N., Hoffman, G.R., Cantley, L.C., Gygi, S.P., et al. (2011). Phosphoproteomic analysis identifies Grb10 as an mTORC1 substrate that negatively regulates insulin signaling. Science *332*, 1322–1326.

Yu, Z.Q., Sun, L.L., Jiang, Z. Di, Liu, X.M., Zhao, D., Wang, H.T., He, W.Z., Dong, M.Q., and Du,

L.L. (2020). Atg38-Atg8 interaction in fission yeast establishes a positive feedback loop to promote autophagy. Autophagy *16*, 2036–2051.

Zetterberg, A., and Larsson, O. (1985). Kinetic analysis of regulatory events in G1 leading to proliferation or quiescence of Swiss 3T3 cells. Proc. Natl. Acad. Sci. U.S.A. *82*, 5365–5369.

Zhang, N., and Cao, L. (2017). Starvation signals in yeast are integrated to coordinate metabolic reprogramming and stress response to ensure longevity. Curr. Genet. *63*, 839–843.

Zhang, G., Li, J., Purkayastha, S., Tang, Y., Zhang, H., Yin, Y., Li, B., Liu, G., and Cai, D. (2013). Hypothalamic programming of systemic ageing involving IKK-β, NF-κB and GnRH. Nature *497*, 211–216.

Zhang, S., Li, X., Wang, H.Y., and Steven Zheng, X.F. (2018). Beyond regulation of pol III: role of MAF1 in growth, metabolism, aging and cancer. Biochim. Biophys. Acta Gene Regul. Mech. *1861*, 338–343.

Zhang, T., Péli-Gulli, M.P., Yang, H., De Virgilio, C., and Ding, J. (2012). Ego3 functions as a homodimer to mediate the interaction between Gtr1-Gtr2 and Ego1 in the EGO complex to activate TORC1. Structure *20*, 2151–2160.

Zofall, M., and Grewal, S.I.S. (2007). HULC, a histone H2B ubiquitinating complex, modulates heterochromatin independent of histone methylation in fission yeast. J. Biol. Chem. *282*, 14065–14072.

Zoncu, R., Bar-Peled, L., Efeyan, A., Wang, S., Sancak, Y., and Sabatini, D.M. (2011). mTORC1 senses lysosomal amino acids through an inside-out mechanism that requires the vacuolar H^+-ATPase. Science *334*, 678–683.

Supplemental information

Table II.S1. List of the Igo1 phosphorylation sites identified in MM in the mass spectrometry analysis.

Site	Modification	Best ascore	Localisation probability	Spectral count
S17	Phospho	17,14	100%	1
S17	Dehydrated	15,9	98%	1
S18	Dehydrated	19,27	100%	1
S18	Phospho	18	98%	1
S19	Dehydrated	20,41	100%	2
S31	Dehydrated	1.000,00	100%	4
S64	Dehydrated	100	100%	14
S64	Phospho	69,9	100%	13
T81	Phospho	53,53	100%	6
S99	Dehydrated	32,97	100%	1
S102	Dehydrated	19,54	90%	1
S108	Dehydrated	38,27	100%	1
S115	Dehydrated	41,64	100%	1

Table II.S2. List of the Igo1 phosphorylation sites identified in MM-N in the mass spectrometry analysis.

Site	Modification	Best ascore	Localisation probability	Spectral count
S31	Dehydrated	1.000,00	100%	1
S64	Dehydrated	100	100%	13
S64	Phospho	76,14	100%	10
T81	Phospho	59,1	100%	3
S99	Dehydrated	43,48	100%	2
S108	Dehydrated	68,31	100%	1
S31	Dehydrated	1.000,00	100%	1

Table II.S1. List of proteins identified from Igo1:GFP pull-down in MM.

Systematic name	Protein	Description	Total spectrum count	Percentage sequence coverage
SPAC10F6.16	**Mug134**	**mRNA stability protein Igo1 (predicted)**	**443**	**55,40%**
SPCC16C4.13c, SPCC31H12.04c	**Rpl1201**	60S ribosomal protein L12.1/L12A	61	40,60%
SPAC25G10.06	**Rps2801**	40S ribosomal protein S28 (predicted)	25	41,20%
SPAC1250.05	**Rpl3002**	60S ribosomal protein L30 (predicted)	20	20,50%
SPCC794.09c	**Tef101**	translation elongation factor EF-1 alpha Ef1a-a	18	21,30%
SPAC1F7.13c, SPBC2F12.07c, SPBC839.04	**Rpl801**	60S ribosomal protein L8 (predicted)	15	15,40%
SPAC664.04c, SPBC18H10.14	**Rps1602**	40S ribosomal protein S16 (predicted)	15	35,00%
SPAC3H5.05c, SPBC18H10.13	**Rps1401**	40S ribosomal protein S14 (predicted)	14	41,70%
SPBC16D10.11c, SPCC1259.01c	**Rps1801**	40S ribosomal protein S18 (predicted)	14	29,60%
SPCC576.07	**Ret3**	coatomer zeta subunit (predicted)	14	21,60%
SPAC3G9.03, SPCC1322.11	**Rpl2301**	60S ribosomal protein L23	11	20,10%
SPCC285.08	**Ret2**	coatomer delta subunit Ret2 (predicted)	11	24,60%
SPAC23A1.08c	**Rpl3401**	60S ribosomal protein L34	10	25,00%
SPAC19B12.04, SPBC19G7.03c	**Rps3001**	40S ribosomal protein S30 (predicted)	9	21,30%
SPAC521.05	**Rps802**	40S ribosomal protein S8 (predicted)	9	27,00%
SPBC11G11.03	**Mrt4**	mRNA turnover and ribosome assembly protein Mrt4 (predicted)	9	31,10%
SPBC146.14c	**Sec26**	coatomer beta subunit (predicted)	8	5,85%

SPAC17A5.03, SPAPB8E5.06c	**Rpl301**	60S ribosomal protein L3	7	10,60%
SPAC57A7.10c	**Sec21**	coatomer gamma subunit Sec21 (predicted)	7	6,85%
SPAC694.05c	**Rps2502**	40S ribosomal protein S25 (predicted)	7	22,50%
SPAPB2C8.01	**Spapb2C8.01**	cell surface glycoprotein, adhesion molecule (predicted)	7	1,97%
SPBPJ4664.04	**Cop1**	coatomer alpha subunit Cop1 (predicted)	7	5,55%
SPCC1223.02	**Nmt1**	4-amino-5-hydroxymethyl-2-methylpyrimidine phosphate synthase Nmt1	7	12,40%
SPCC364.07	**Ser3**	D-3 phosphoglycerate dehydrogenase Ser3 (predicted)	7	17,80%
SPAC1783.08c, SPCC576.11	**Rpl1502**	60S ribosomal protein L15b (predicted)	4	10,90%
SPAC17G8.14c	**Pck1**	protein kinase C (PKC)-like Pck1	4	1,62%
SPAC959.07, SPBC19F8.08	**Rps403**	40S ribosomal protein S4 (predicted)	4	8,78%
SPBC26H8.01	**Thi2**	thiazole biosynthetic enzyme	4	11,60%
SPAC1610.02c	**Mrpl1**	mitochondrial ribosomal protein subunit L1 (predicted)	3	10,70%
SPAC23H4.10c	**Thi4**	bifunctional thiamine-phosphate dipyrophosphorylase/hydroxyethylthiazole kinase	3	8,49%
SPAC3A12.14	**Cam1**	calmodulin Cam1	3	29,30%
SPBC28F2.11	**Hmo1**	HMG box protein Hmo1	3	8,39%
SPCC1682.14	**Rpl1902**	60S ribosomal protein L19	3	15,00%
SPCC23B6.02c	**Spcc23B6.02C**	pre-ribosomal factor (predicted)	3	17,10%
SPAC140.02	**Gar2**	nucleolar protein required for rRNA processing	2	4,60%
SPAC22H12.02	**Tfg3**	transcription factor TFIIF complex subunit Tfg3	2	12,00%
SPAC26A3.04, SPAC3A12.10	**Rpl2002**	60S ribosomal protein L20 (predicted)	2	11,90%
SPAC31G5.17c	**Rps1001**	40S ribosomal protein S10 (predicted)	2	19,40%
SPCC622.09	**Htb1**	histone H2B Htb1	2	18,30%

Table III.S2. List of proteins identified from Igo1:GFP pull-down in MM-N.

Systematic name	Protein	Description	Total spectrum count	Percentage sequence coverage
SPAC10F6.16	**Mug134**	**mRNA stability protein Igo1 (predicted)**	398	56,10%
SPCC16C4.13c, SPCC31H12.04c	**Rpl1201**	60S ribosomal protein L12.1/L12A	243	52,10%
SPAC23A1.10, SPBC839.15c	**Tef102**	translation elongation factor EF-1 alpha Ef1a-b	69	34,80%
SPCC970.05	**Rpl3601**	60S ribosomal protein L36	60	16,20%
SPAC25G10.06, SPCC285.15c	**Rps2801**	40S ribosomal protein S28 (predicted)	53	41,20%
SPAC57A7.10c	**Sec21**	coatomer gamma subunit Sec21 (predicted)	53	25,70%
SPBC146.14c	**Sec26**	coatomer beta subunit (predicted)	52	20,40%
SPAC17G8.14c	**Pck1**	protein kinase C (PKC)-like Pck1	42	10,40%
SPBPJ4664.04	**Cop1**	coatomer alpha subunit Cop1 (predicted)	35	19,60%
SPAC664.04c, SPBC18H10.14	**Rps1602**	40S ribosomal protein S16 (predicted)	31	52,10%
SPAC3G9.03, SPCC1322.11	**Rpl2301**	60S ribosomal protein L23	28	34,50%
SPCC285.08	**Ret2**	coatomer delta subunit Ret2 (predicted)	27	23,30%
SPAPB2C8.01	**Spapb2C8.01**	cell surface glycoprotein, adhesion molecule (predicted)	24	1,97%
SPAC23A1.08c	**Rpl3401**	60S ribosomal protein L34	23	34,80%
SPAC3H5.05c, SPBC18H10.13	**Rps1401**	40S ribosomal protein S14 (predicted)	23	43,20%
SPAC1250.05	**Rpl3002**	60S ribosomal protein L30 (predicted)	22	35,00%
SPBC16D10.11c, SPCC1259.01c	**Rps1801**	40S ribosomal protein S18 (predicted)	22	35,50%
SPAC1F7.13c, SPBC2F12.07c, SPBC839.04	**Rpl801**	60S ribosomal protein L8 (predicted)	21	25,70%

SPAC23C11.02c, SPBP4H10.13	**Rps23**	40S ribosomal protein S23 (predicted)	20	34,30%
SPAC23H4.10c	**Thi4**	bifunctional thiamine-phosphate dipyrophosphorylase/hydroxyethylthiazole kinase	20	26,80%
SPBC11G11.05	**Rpa34**	DNA-directed RNA polymerase I complex subunit Rpa34 (predicted)	20	23,50%
SPBC11G11.03	**Mrt4**	mRNA turnover and ribosome assembly protein Mrt4 (predicted)	19	48,10%
SPBC26H8.01	**Thi2**	thiazole biosynthetic enzyme	19	20,70%
SPAC1F5.03c	**Spac1F5.03C**	FAD-dependent oxidoreductase involved in late endosome to Golgi transport (predicted)	18	27,70%
SPAC4F10.14c	**Btf3**	nascent polypeptide-associated complex beta subunit	17	40,40%
SPAC22A12.04c, SPAC5D6.01	**Rps2201**	40S ribosomal protein S15a (predicted)	16	31,50%
SPBC18E5.06	**Rps21**	40S ribosomal protein S21	16	42,50%
SPBC24C6.05	**Sec28**	coatomer epsilon subunit (predicted)	16	21,20%
SPAC1782.10c	**Nhp2**	box H/ACA snoRNP complex subunit Nhp2	15	24,70%
SPAC26A3.04, SPAC3A12.10	**Rpl2002**	60S ribosomal protein L20 (predicted)	15	29,50%
SPCC576.07	**Ret3**	coatomer zeta subunit (predicted)	15	30,50%
SPAC19B12.04, SPBC19G7.03c	**Rps3001**	40S ribosomal protein S30 (predicted)	14	21,30%
SPACUNK4.11c	**Mpp6**	nuclear exosome-associated RNA binding protein Mpp6	11	21,30%
SPBC1539.10	**Nop16**	ribosome biogenesis protein Nop16 (predicted)	11	22,00%
SPAC513.01c, SPCP31B10.07	**Eft201**	translation elongation factor 2 (EF-2) Eft2,A	10	7,60%
SPCC1223.02	**Nmt1**	4-amino-5-hydroxymethyl-2-methylpyrimidine phosphate synthase Nmt1	10	22,00%
SPCC364.07	**Ser3**	D-3 phosphoglycerate dehydrogenase Ser3 (predicted)	10	12,90%
SPAC26A3.07c,SPBC17G9.10	**Rpl1101**	60S ribosomal protein L11 (predicted)	9	14,40%
SPAP27G11.13c	**Nop10**	snoRNP pseudouridylase box H/ACA snoRNP complex protein (predicted)	9	40,60%
SPCC1682.14	**Rpl1902**	60S ribosomal protein L19	9	23,80%
SPAC17H9.05	**Ebp2**	rRNA processing protein Ebp2 (predicted)	8	13,50%

SPAC18G6.07c	**Mra1**	rRNA (pseudouridine) methyltransferase Mra1	8	12,00%
SPAC144.11, SPAC31G5.03	**Rps1102**	40S ribosomal protein S11 (predicted)	7	32,90%
SPAC1610.02c	**Mrpl1**	mitochondrial ribosomal protein subunit L1 (predicted)	7	20,90%
SPBC20F10.01	**Gar1**	snoRNP pseudouridylase box H/ACA snoRNP complex protein Gar1	7	13,40%
SPBC28F2.11	**Hmo1**	HMG box protein Hmo1	7	19,70%
SPBC29A10.12	**Spbc29A10.12**	DUF1014 family protein, HMG-box clan member	7	16,90%
SPBC2D10.19c	**Alb1**	pre-60S shuttling factor Alb1 (predicted)	7	33,30%
SPBC365.04c	**Spbc365.04C**	RNA-binding protein, involved in ribosome biogenesis (predicted)	7	21,00%
SPBC3F6.03	**Trr1**	thioredoxin reductase Trr1	7	25,20%
SPBC4C3.07	**Eif6**	translation initiation factor eIF3f	7	17,90%
SPCC622.09	**Htb1**	histone H2B Htb1	7	27,80%
SPAC222.04c	**Ies6**	Ino80 complex subunit Ies6	6	26,50%
SPCC1919.09	**Tif6**	translation initiation factor-like ribosome biogenesis protein	6	22,10%
SPCC736.10c	**Mrps8**	mitochondrial ribosomal protein subunit S8 (predicted)	6	38,80%
SPAC22H12.02	**Tfg3**	transcription factor TFIIF complex subunit Tfg3	5	22,40%
SPAC3A12.14	**Cam1**	calmodulin Cam1	5	29,30%
SPAC56F8.05c	**Mug64**	BAR domain protein (predicted)	5	13,30%
SPAC694.05c	**Rps2502**	40S ribosomal protein S25 (predicted)	5	12,40%
SPAP8A3.09c	**Paa1**	protein phosphatase regulatory subunit Paa1	5	4,75%
SPBC215.09c	**Erg10**	acetyl-CoA C-acetyltransferase Erg10 (predicted)	5	8,10%
SPBC4B4.11	**Spbc4B4.11**	conserved fungal protein	5	21,20%
SPCC1442.19	**Mrp49**	mitochondrial ribosomal protein Mrp49 (predicted)	5	20,00%
SPCC1682.04	**Cdc31**	centrin	5	21,60%
SPAC31G5.17c	**Rps1001**	40S ribosomal protein S10 (predicted)	4	29,90%

SPBC1709.09	**Rrf1**	mitochondrial translation termination factor Rrf1	4	11,10%
SPBC23G7.05	**Sui1**	translation initiation factor eIF1	4	21,10%
SPBC23G7.15c	**Rpp202**	60S acidic ribosomal protein A4	4	70,00%
SPCC23B6.02c	**Spcc23B6.02C**	pre-ribosomal factor (predicted)	4	17,10%
SPAC13G7.03	**Upf3**	up-frameshift suppressor 3 family protein (predicted)	3	12,20%
SPAC1952.14c	**Mrpl25**	mitochondrial ribosomal protein subunit L25 (predicted)	3	17,20%
SPAC23C11.11	**Cka1**	serine/threonine protein kinase Cka1	3	8,43%
SPAC26A3.05	**Chc1**	clathrin heavy chain Chc1 (predicted)	3	2,04%
SPAC4F8.06	**Mrps12**	mitochondrial ribosomal protein subunit MrpS12 (predicted)	3	21,60%
SPBC4B4.04	**Eif21**	translation initiation factor eIF2A (predicted)	3	4,69%
SPBP22H7.08	**Rps1002**	40S ribosomal protein S10 (predicted)	3	29,30%
SPAC140.02	**Gar2**	nucleolar protein required for rRNA processing	2	7,00%
SPAC1F3.01	**Rrp6**	exosome 3'-5' exoribonuclease subunit Rrp6 (predicted)	2	3,47%
SPAC227.07c	**Pab1**	protein phosphatase regulatory subunit Pab1	2	7,99%
SPAC24C9.11	**Sgd1**	ribosome small subunit biogenesis protein Sgd1 (predicted)	2	2,58%
SPAC4F10.20	**Grx1**	glutaredoxin Grx1	2	23,80%
SPBC106.14c	**Sda1**	SDA1 family protein (predicted)	2	3,62%
SPBC13E7.07	**Spbc13E7.07**	Schizosaccharomyces specific protein	2	4,76%
SPBC16A3.05c	**Rae1**	RNA export factor, nucleoporin Rae1	2	7,10%
SPBC23G7.07c	**Cms1**	U3-containing 90S preribosome complex subunit Cms1 (predicted)	2	10,50%
SPBC2G2.06c	**Apl1**	AP-2 adaptor complex subunit Apl1 (predicted)	2	4,14%
SPBC32H8.05	**Spbc32H8.05**	conserved fungal protein	2	25,60%
SPBC651.01c	**Nog1**	GTP binding protein Nog1 (predicted)	2	4,36%

Table III.S3. List of proteins identified from Pab1:GFP pull-down in MM.

Systematic name	Protein	Description	Total spectrum count	Percentage sequence coverage
SPAC227.07c	**Pab1**	protein phosphatase regulatory subunit Pab1	**441**	**65,9%**
SPAP8A3.09c	**Paa1**	protein phosphatase regulatory subunit Paa1	61	34,9%
SPBC16H5.07c	**Ppa2**	serine/threonine protein phosphatase Ppa2	39	42,2%
SPCC162.08c	**Nup211**	nucleoporin nup211	27	15,2%
SPBPJ4664.04	**Cop1**	coatomer alpha subunit Cop1 (predicted)	22	19,0%
SPCC965.04c	**Yme1**	mitochondrial inner membrane i-AAA protease complex subunit Yme1 (predicted)	22	22,8%
SPAC823.15	**Ppa1**	minor serine/threonine protein phosphatase Ppa1	19	25,2%
SPAC19E9.01c	**Nup40**	nucleoporin Nup40	18	32,3%
SPAC57A7.10c	**Sec21**	coatomer gamma subunit Sec21 (predicted)	18	21,7%
SPBC646.11	**Cct6**	chaperonin-containing T-complex zeta subunit Cct6	18	32,5%
SPBC146.14c	**Sec26**	coatomer beta subunit (predicted)	17	16,8%
SPBC30B4.03c	**Adn1**	adhesion defective protein	15	37,3%
SPBC26H8.01	**Thi2**	thiazole biosynthetic enzyme	13	27,1%
SPCC4G3.14	**Mdj1**	mitochondrial DNAJ domain protein Mdj1 (predicted)	11	17,8%
SPBC36.07	**Elp1**	elongator subunit Elp1 (predicted)	10	8,6%
SPCC1902.02	**Mug72**	oxidoreductase (predicted)	10	18,5%
SPCC970.01	**Rad16**	DNA repair endonuclease XPF	10	10,4%
SPAC12G12.01c	**Sea4**	SEA complex subunit, ubiquitin-protein ligase E3, Sea4 (predicted)	9	8,7%
SPAC521.05	**Rps802**	40S ribosomal protein S8 (predicted)	9	37,0%
SPBC14F5.13c	**Pho8**	vacuolar membrane alkaline phosphatase (predicted)	9	16,9%
SPAC1486.04c	**Alm1**	medial ring protein Alm1	8	6,5%

SPAC1834.11c	**Sec18**	secretory pathway protein Sec18 (predicted)	8	12,0%
SPBC2G5.06c	**Hmt2**	sulfide-quinone oxidoreductase	8	14,4%
SPAC29A4.20	**Elp3**	elongator complex subunit Elp3 (predicted)	7	17,5%
SPBC119.07	**Ppk19**	serine/threonine protein kinase Ppk19	7	3,9%
SPBC24C6.05	**Sec28**	coatomer epsilon subunit (predicted)	7	17,7%
SPBC2G2.08	**Ade9**	C-1-tetrahydrofolatesynthase/methylenetetrahydrof olatedehydrogenase/ methylenetetrahydrofolatecyclohydrolase/ formyltetrahydrofolatesynthetase (predicted)	7	7,7%
SPCC1682.04	**Cdc31**	centrin	7	33,0%
SPCC285.08	**Ret2**	coatomer delta subunit Ret2 (predicted)	7	16,7%
SPAC17G6.10	**Ssr1**	SWI/SNF and RSC complex subunit Ssr1	6	11,6%
SPAC20G8.06	**Not1**	CCR4-Not complex subunit Not1 (predicted)	6	3,9%
SPAC1A6.07	**Sle1**	eisosome assembly protein Seg1	5	11,6%
SPAC20G8.02	**Spac20G8.02**	mitochondrial	5	0,0%
SPAC25G10.06	**Rps2801**	40S ribosomal protein S28 (predicted)	5	36,8%
SPAC2G11.10c	**Uba42**	thiosulfate sulfurtransferase, URM1 activating enzyme E1-type Uba42 (predicted)	5	15,2%
SPAC31G5.04	**Lys12**	homoisocitrate dehydrogenase Lys12	5	14,6%
SPAC821.07c	**Moc3**	transcription factor Moc3	5	12,2%
SPBC17D11.04c	**Nto1**	histone acetyltransferase complex subunit Nto1 (predicted)	5	6,0%
SPBC19C2.07	**Fba1**	fructose-bisphosphate aldolase Fba1	5	19,3%
SPBC27B12.04c	**Far11**	SIP/FAR complex subunit, Far11/Csc2	5	6,5%
SPBP4H10.06c	**Cut14**	condensin complex SMC subunit Smc2	5	6,7%
SPCC1223.02	**Nmt1**	4-amino-5-hydroxymethyl-2-methylpyrimidine phosphate synthase Nmt1	5	15,9%
SPAC140.02	**Gar2**	nucleolar protein required for rRNA processing	4	9,2%
SPAC15F9.02	**Seh1**	Seh1-associated complex subunit Seh1	4	12,4%
SPAC16.04	**Dus3**	tRNA dihydrouridine synthase Dus3 (predicted)	4	7,1%

SPAC1F7.09c	**Spac1F7.09C**	allantoicase	4	0,0%
SPAC23C11.11	**Cka1**	serine/threonine protein kinase Cka1	4	16,0%
SPAC23C11.16	**Plo1**	Polo kinase Plo1	4	7,0%
SPAC23C4.19	**Spt5**	DSIF transcription elongation factor complex subunit Spt5	4	6,8%
SPAC9G1.02	**Wis4**	MAP kinase kinase kinase Wis4	4	4,2%
SPBC1711.05	**Spbc1711.05**	nucleoc	4	0,0%
SPBC1773.01	**Far8**	SIP/FAR complex striatin subunit, Far8/Csc3	4	6,4%
SPBC26H8.04c	**Iml1**	GTPase-activating protein subunit of SEA and Iml1p complexes Iml1 (predicted)	4	4,0%
SPBC365.06	**Pmt3**	SUMO	4	23,9%
SPBC409.16c	**Saw1**	recombination protein Saw1 (predicted)	4	29,2%
SPBC839.10	**Usp107**	U1 snRNP-associated protein Usp107	4	8,2%
SPBP22H7.08	**Rps1002**	40S ribosomal protein S10 (predicted)	4	29,3%
SPCC1450.11c	**Cek1**	serine/threonine protein kinase Cek1	4	3,7%
SPAC1006.05c	**Och1**	alpha-1,6-mannosyltransferase Och1	3	10,9%
SPAC1782.10c	**Nhp2**	box H/ACA snoRNP complex subunit Nhp2	3	25,3%
SPAC17H9.05	**Ebp2**	rRNA processing protein Ebp2 (predicted)	3	8,7%
SPAC17H9.12c	**Spac17H9.12C**	mitoch	3	0,0%
SPAC1834.08	**Mak1**	histidine kinase Mak1	3	2,5%
SPAC1A6.10	**Tcd1**	tRNA threonylcarbamoyladenosine dehydratase Tcd1 (predicted)	3	8,7%
SPAC23H4.10c	**Thi4**	bifunctional thiamine-phosphate dipyrophosphorylase/hydroxyethylthiazole kinase	3	13,3%
SPAC2F3.10	**Vps54**	GARP complex subunit Vps54 (predicted)	3	4,3%
SPAC31G5.17c	**Rps1001**	40S ribosomal protein S10 (predicted)	3	29,9%
SPAC343.09	**Ubx3**	UBX domain protein Ubx3, Cdc48 cofactor	3	8,5%
SPAC3A12.14	**Cam1**	calmodulin Cam1	3	18,7%

SPAC7D4.03c	**Spac7D4.03C**	conserved	3	0,0%
SPBC11G11.02c	**End3**	actin cortical patch component End3 (predicted)	3	9,3%
SPBC1539.10	**Nop16**	ribosome biogenesis protein Nop16 (predicted)	3	14,4%
SPBC1685.02c	**Rps1202**	40S ribosomal protein S12 (predicted)	3	16,2%
SPBC16H5.06	**Rip1**	ubiquinol-cytochrome-c reductase complex subunit 5	3	15,8%
SPBC19G7.05c	**Bgs1**	1,3-beta-glucan synthase catalytic subunit Bgs1	3	2,0%
SPBC1A4.05	**Blt1**	ubiquitin domain-like protein Blt1	3	5,7%
SPBC23G7.15c	**Rpp202**	60S acidic ribosomal protein A4	3	20,9%
SPBC4C3.07	**Eif6**	translation initiation factor eIF3f	3	13,9%
SPBC543.04	**Npr3**	SEA/Iml1/Npr2/3 complex subunit Npr3 (predicted)	3	7,0%
SPBP8B7.16c	**Dbp2**	ATP-dependent RNA helicase Dbp2	3	4,2%
SPCC1827.05c	**Spcc1827.05C**	nucleolar	3	0,0%
SPCC576.07	**Ret3**	coatomer zeta subunit (predicted)	3	16,3%
SPCC895.07	**Alp14**	TOG/XMAP14 family protein Alp14	3	6,3%
SPAC1071.02	**Mms19**	Dos2 silencing complex subunit Mms19	2	3,1%
SPAC1071.07c	**Rps1502**	40S ribosomal protein S15 (predicted)	2	9,7%
SPAC11E3.05	**Sea3**	ubiquitin-protein ligase E3, coatamer related complex subunit Sea3 (predicted)	2	2,6%
SPAC1250.05	**Rpl3002**	60S ribosomal protein L30 (predicted)	2	19,7%
SPAC1687.01	**Rpc19**	DNA-directed RNA polymerase I and III subunit Rpc19	2	23,2%
SPAC17G8.13c	**Mst2**	histone acetyltransferase Mst2	2	7,1%
SPAC1B3.18c	**Mrps18**	mitochondrial ribosomal protein subunit S18 (predicted)	2	13,0%
SPAC222.09	**Seb1**	RNA-binding protein Seb1	2	2,6%
SPAC23A1.08c	**Rpl3401**	60S ribosomal protein L34	2	12,5%
SPAC25A8.02	**Atg14**	autophagy protein Atg14	2	8,0%

SPAC25G10.09c	**Pan1**	actin cortical patch component, with EF hand and WH2 motif Panl (predicted)	2	1,6%
SPAC26A3.15c	**Nsp1**	nucleoporin Nsp1	2	5,4%
SPAC323.04	**Spac323.04**	mitochondr	2	0,0%
SPAC3A12.15	**Vps53**	GARP complex subunit Vps53 (predicted)	2	3,4%
SPAC3H8.04	**Spac3H8.04**	possible	2	0,0%
SPAC4F8.11	**Sea2**	SEA complex subunit, human WDR24 family, Sea2 (predicted)	2	2,8%
SPAC644.16	**Rna15**	RNA-binding protein Rna15	2	6,2%
SPAC694.02	**Spac694.02**	DEAD/DEAH	2	0,0%
SPAC6F12.02	**Rst2**	transcription factor Rst2	2	2,5%
SPAC6F6.09	**Eaf6**	Mst2/NuA4 histone acetyltransferase complex subunit Eaf6	2	19,6%
SPAC9.07c	**Spac9.07C**	GTPase	2	0,0%
SPAC9.09	**Met26**	homocysteine methyltransferase Met26	2	2,1%
SPAC959.08	**Rpl2102**	60S ribosomal protein L21 (predicted)	2	24,4%
SPBC13G1.01c	**Nam9**	mitochondrial ribosomal protein subunit S4 (predicted)	2	8,0%
SPBC146.03c	**Cut3**	condensin complex SMC subunit Smc4	2	2,0%
SPBC1604.20c	**Tea2**	kinesin-like protein Tea2	2	4,3%
SPBC1677.03c	**Tda1**	threonine ammonia-lyase Tda1	2	5,3%
SPBC16G5.11c	**Bag101**	BAG family molecular chaperone regulator Bag101 (predicted)	2	5,6%
SPBC16G5.13	**Ptf2**	Mst2 histone acetytransferase acytyltransferase complex subunit	2	18,3%
SPBC18E5.06	**Rps21**	40S ribosomal protein S21	2	29,9%
SPBC21C3.16c	**Spt4**	DSIF transcription elongation factor complex subunit Spt4	2	24,8%
SPBC21H7.02	**Taf10**	SAGA complex/transcription factor TFIID complex subunit Taf10	2	13,0%
SPBC29A3.18	**Cyt1**	cytochrome c1 Cyt1 (predicted)	2	7,2%
SPBC354.14c	**Vac8**	vacuolar protein Vac8 (predicted)	2	6,6%

SPBC409.07c	**Wis1**	MAP kinase kinase Wis1	2	4,5%
SPBC577.06c	**Stt4**	1-phosphatidylinositol 4-kinase Stt4 (predicted)	2	1,4%
SPBC691.04	**Mss116**	mitochondrial ATP-dependent RNA helicase Mss116 (predicted)	2	6,0%
SPBC8D2.17	**Gmh4**	alpha-1,2-galactosyltransferase (predicted)	2	4,6%
SPCC1393.03	**Rps1501**	40S ribosomal protein S15 (predicted)	2	9,8%
SPCC162.07	**Ent1**	epsin	2	4,7%
SPCC16C4.18c	**Taf6**	histone H4-like TAF Taf6, SAGA complex subunit	2	6,0%
SPCC18.06c	**Caf1**	CCR4-Not complex CAF1 family ribonuclease subunit Caf1	2	8,7%
SPCC18B5.04	**Rsm18**	mitochondrial ribosomal protein subunit S18 (predicted)	2	13,9%
SPCC736.10c	**Mrps8**	mitochondrial ribosomal protein subunit S8 (predicted)	2	21,1%
SPCC737.08	**Spcc737.08**	midasin	2	0,0%

Table III.S4. List of proteins identified from Pab1:GFP pull-down in MM-N.

Systematic name	Protein	Description	Exclusive spectrum count	Percentage sequence coverage
SPAC227.07c	**Pab1**	**protein phosphatase regulatory subunit Pab1**	**5547**	**79,90%**
SPAP8A3.09c	**Paa1**	protein phosphatase regulatory subunit Paa1	1427	82,00%
SPBC16H5.07c	**Ppa2**	serine/threonine protein phosphatase Ppa2	897	88,20%
SPCC794.09c	**Tef101**	translation elongation factor EF-1 alpha Ef1a-a	552	56,70%
SPBPJ4664.04	**Cop1**	coatomer alpha subunit Cop1 (predicted)	174	47,00%
SPAC823.15	**Ppa1**	minor serine/threonine protein phosphatase Ppa1	146	63,40%
SPBC146.14c	**Sec26**	coatomer beta subunit (predicted)	132	47,60%
SPCC965.04c	**Yme1**	mitochondrial inner membrane i-AAA protease complex subunit Yme1 (predicted)	122	46,30%
SPBC26H8.01	**Thi2**	thiazole biosynthetic enzyme	112	40,50%

SPBC119.07	**Ppk19**	serine/threonine protein kinase Ppk19	109	32,20%
SPCC162.08c	**Nup211**	nucleoporin nup211	106	44,00%
SPAC1486.04c	**Alm1**	medial ring protein Alm1	96	38,00%
SPAC57A7.10c	**Sec21**	coatomer gamma subunit Sec21 (predicted)	96	43,40%
SPBC646.11	**Cct6**	chaperonin-containing T-complex zeta subunit Cct6	93	56,80%
SPAC821.07c	**Moc3**	transcription factor Moc3	77	28,90%
SPAC1F7.09c	**Spac1F7.09C**	allantoicase (predicted)	72	77,80%
SPBC36.07	**Elp1**	elongator subunit Elp1 (predicted)	72	33,40%
SPCC970.01	**Rad16**	DNA repair endonuclease XPF	69	27,70%
SPAC1834.11c	**Sec18**	secretory pathway protein Sec18 (predicted)	60	45,30%
SPCC1902.02	**Mug72**	oxidoreductase (predicted)	58	44,80%
SPAC17G8.13c	**Mst2**	histone acetyltransferase Mst2	57	52,60%
SPBC19C7.06	**Prs1**	cytoplasmic proline-tRNA ligase Prs1 (predicted)	54	42,50%
SPAC458.05	**Pik3**	phosphatidylinositol 3-kinase Pik3	52	32,10%
SPCC4G3.14	**Mdj1**	mitochondrial DNAJ domain protein Mdj1 (predicted)	52	31,60%
SPBC14F5.13c	**Pho8**	vacuolar membrane alkaline phosphatase (predicted)	50	35,90%
SPBC839.10	**Usp107**	U1 snRNP-associated protein Usp107	47	43,30%
SPAC20G8.06	**Not1**	CCR4-Not complex subunit Not1 (predicted)	45	19,40%
SPBC26H8.04c	**Iml1**	GTPase-activating protein subunit of SEA and Iml1p complexes Iml1 (predicted)	45	22,20%
SPBC2G5.06c	**Hmt2**	sulfide-quinone oxidoreductase	44	39,70%
SPAC29A4.20	**Elp3**	elongator complex subunit Elp3 (predicted)	43	45,80%
SPAC521.05	**Rps802**	40S ribosomal protein S8 (predicted)	40	57,00%
SPAC11E3.05	**Sea3**	ubiquitin-protein ligase E3, coatamer related complex subunit Sea3 (predicted)	38	22,00%
SPAC25G10.06	**Rps2801**	40S ribosomal protein S28 (predicted)	38	36,80%

SPCC285.08	**Ret2**	coatomer delta subunit Ret2 (predicted)	37	27,50%
SPCC737.08	**Spcc737.08**	midasin (predicted)	37	8,84%
SPBC30B4.03c	**Adn1**	adhesion defective protein	36	58,80%
SPAC23H4.10c	**Thi4**	bifunctional thiamine-phosphate dipyrophosphorylase/hydroxyethylthiazole kinase	35	53,50%
SPBC24C6.05	**Sec28**	coatomer epsilon subunit (predicted)	35	58,30%
SPAC323.04	**Spac323.04**	mitochondrial ATPase (predicted)	31	40,20%
SPAC19E9.01c	**Nup40**	nucleoporin Nup40	30	39,10%
SPAC4F8.11	**Sea2**	SEA complex subunit, human WDR24 family, Sea2 (predicted)	30	27,70%
SPBC17D11.04c	**Nto1**	histone acetyltransferase complex subunit Nto1 (predicted)	30	22,90%
SPBC27.08c	**Sua1**	sulfate adenylyltransferase	29	39,40%
SPCC16A11.13	**Luc7**	U1 snRNP-associated protein Luc7	29	50,80%
SPCC1840.03	**Sal3**	karyopherin Sal3	29	21,30%
SPAC11D3.15	**Spac11D3.15**	5-oxoprolinase (ATP-hydrolizing) (predicted)	28	20,20%
SPAC12G12.01c	**Sea4**	SEA complex subunit, ubiquitin-protein ligase E3, Sea4 (predicted)	28	28,10%
SPBP22H7.08	**Rps1002**	40S ribosomal protein S10 (predicted)	28	46,90%
SPCC1223.02	**Nmt1**	4-amino-5-hydroxymethyl-2-methylpyrimidine phosphate synthase Nmt1	28	31,20%
SPCC576.07	**Ret3**	coatomer zeta subunit (predicted)	28	41,10%
SPAC20G8.10c	**Atg6**	**autophagy associated beclin family protein Atg6**	**27**	**33,60%**
SPAC23G3.11	**Rpn6**	19S proteasome regulatory subunit Rpn6 (predicted)	26	36,80%
SPAC6G10.05c	**Trs120**	TRAPP complex subunit Trs120 (predicted)	26	18,20%
SPBC1773.01	**Far8**	SIP/FAR complex striatin subunit, Far8/Csc3	26	27,80%
SPBC17D11.07c	**Rpn2**	19S proteasome regulatory subunit Rpn2 (predicted)	26	20,20%
SPCC1393.03	**Rps1501**	40S ribosomal protein S15 (predicted)	26	47,70%
SPAC15F9.02	**Seh1**	Seh1-associated complex subunit Seh1	25	48,70%

SPAC25G10.09c	**Pan1**	actin cortical patch component, with EF hand and WH2 motif Panl (predicted)	25	13,30%
SPBC19C2.07	**Fba1**	fructose-bisphosphate aldolase Fba1	25	45,00%
SPBC21C3.15c	**Spbc21C3.15C**	aldehyde dehydrogenase (predicted)	25	24,70%
SPBC409.16c	**Saw1**	recombination protein Saw1 (predicted)	25	75,80%
SPAC4D7.13	**Usp104**	U1 snRNP-associated protein Usp104	24	22,60%
SPBC11G11.03	**Mrt4**	mRNA turnover and ribosome assembly protein Mrt4 (predicted)	24	41,50%
SPBC577.06c	**Stt4**	1-phosphatidylinositol 4-kinase Stt4 (predicted)	24	10,80%
SPCC1682.04	**Cdc31**	centrin	24	44,30%
SPCC285.14	**Trs130**	TRAPP complex subunit Trs130 (predicted)	24	16,80%
SPCC330.14c	**Rpl2402**	60S ribosomal protein L24 (predicted)	24	34,20%
SPAC13G6.07c	**Rps601**	40S ribosomal protein S6	23	44,40%
SPAC20G8.02	**Spac20G8.02**	mitochondrial DDHD family phospholipase (predicted)	23	20,50%
SPAC2F3.10	**Vps54**	GARP complex subunit Vps54 (predicted)	23	20,10%
SPBC27B12.04c	**Far11**	SIP/FAR complex subunit, Far11/Csc2	23	21,30%
SPAC22H12.02	**Tfg3**	transcription factor TFIIF complex subunit Tfg3	22	45,60%
SPBC29A3.18	**Cyt1**	cytochrome c1 Cyt1 (predicted)	22	35,80%
SPAC23A1.08c	**Rpl3401**	60S ribosomal protein L34	21	42,00%
SPBC16A3.01	**Spn3**	mitotic septin Spn3	21	47,30%
SPAC22H10.04	**Ppa3**	protein phosphatase type 2A Ppa1	20	49,80%
SPAC26A3.05	**Chc1**	clathrin heavy chain Chc1 (predicted)	20	18,40%
SPBC27B12.13	**Tom40**	mitochondrial TOM complex subunit Tom40 (predicted)	20	37,50%
SPBC646.09c	**Int6**	eIF3e subunit Int6	20	35,30%
SPCC162.02c	**Spcc162.02C**	AMP-binding dehydrogenase (predicted)	20	18,30%
SPCC70.03c	**Spcc70.03C**	proline dehydrogenase (predicted)	20	27,40%

SPCC736.06	**Dar2**	mitochondrial aspartate-tRNA ligase Dar2 (predicted)	20	23,90%
SPAC4F10.14c	**Btf3**	nascent polypeptide-associated complex beta subunit	19	58,30%
SPBC4C3.07	**Eif6**	translation initiation factor eIF3f	19	36,40%
SPCC1020.13c	**Spcc1020.13C**	DDHD family phospholipase (predicted)	19	25,40%
SPBC119.01	**Rpn3**	19S proteasome regulatory subunit Rpn3	18	20,90%
SPBC18E5.06	**Rps21**	40S ribosomal protein S21	18	62,10%
SPCC1442.10c	**Rpb3**	RNA polymerase II subunit 3	18	32,00%
SPAC1250.05	**Rpl3002**	60S ribosomal protein L30 (predicted)	17	35,00%
SPAC890.06	**Nup155**	nucleoporin Nup155	17	13,70%
SPBC146.03c	**Cut3**	condensin complex SMC subunit Smc4	17	11,90%
SPBC947.15c	**Nde1**	mitochondrial NADH dehydrogenase (ubiquinone) Nde1 (predicted)	17	25,40%
SPAC1834.08	**Mak1**	histidine kinase Mak1	16	11,20%
SPAC343.05	**Vma1**	V-type ATPase V1 domain, subunit A	16	27,90%
SPBC16C6.02c	**Vps1302**	chorein homolog Vps1302 (predicted)	16	6,62%
SPBC543.04	**Npr3**	SEA/Iml1/Npr2/3 complex subunit Npr3 (predicted)	16	19,30%
SPCC576.11	**Rpl15**	60S ribosomal protein L15 (predicted)	16	36,80%
SPAC16.04	**Dus3**	tRNA dihydrouridine synthase Dus3 (predicted)	15	18,00%
SPAC23C11.11	**Cka1**	serine/threonine protein kinase Cka1	15	29,20%
SPAC3A12.15	**Vps53**	GARP complex subunit Vps53 (predicted)	15	19,60%
SPAC9.07c	**Spac9.07C**	GTPase Rbg1 (predicted)	15	35,20%
SPBC29A10.16c	**Spbc29A10.16C**	cytochrome b5 (predicted)	15	65,30%
SPCC330.06c	**Pmp20**	thioredoxin peroxidase Pmp20	15	44,20%
SPCC970.05	**Rpl3601**	60S ribosomal protein L36	15	24,20%
SPAC24C9.10c	**Mrp4**	mitochondrial ribosomal protein subunit S2 (predicted)	14	28,50%

SPAC56F8.03	**Spac56F8.03**	translation initiation factor IF2 (predicted)	14	10,10%
SPAC8F11.08c	**Spac8F11.08C**	esterase/lipase (predicted)	14	30,90%
SPAC9.09	**Met26**	homocysteine methyltransferase Met26	14	16,00%
SPAC922.07c	**Atd2**	aldehyde dehydrogenase (predicted)	14	22,40%
SPAC9G1.02	**Wis4**	MAP kinase kinase kinase Wis4	14	14,80%
SPBC1A4.05	**Blt1**	ubiquitin domain-like protein Blt1	14	20,70%
SPBC3H7.13	**Far10**	SIP/FAR complex FHA domain subunit Far10/Csc1	14	34,60%
SPAC1006.09	**Win1**	MAP kinase kinase kinase Win1	13	7,45%
SPAC1782.10c	**Nhp2**	box H/ACA snoRNP complex subunit Nhp2	13	25,30%
SPAC30.01c	**Sec72**	Sec7 domain protein, ARF GEF Sec72	13	6,48%
SPAC31G5.04	**Lys12**	homoisocitrate dehydrogenase Lys12	13	25,40%
SPAC3H8.04	**Spac3H8.04**	possible chromosome segregation protein (predicted)	13	31,10%
SPAC4D7.09	**Tif223**	translation initiation factor eIF2B gamma subunit (predicted)	13	22,90%
SPBC215.09c	**Erg10**	acetyl-CoA C-acetyltransferase Erg10 (predicted)	13	32,20%
SPBC354.14c	**Vac8**	vacuolar protein Vac8 (predicted)	13	23,30%
SPBC691.04	**Mss116**	mitochondrial ATP-dependent RNA helicase Mss116 (predicted)	13	22,40%
SPBC776.02c	**Dis2**	serine/threonine protein phosphatase PP1 subfamily, Dis2	13	22,30%
SPBP4H10.06c	**Cut14**	condensin complex SMC subunit Smc2	13	13,20%
SPCC1450.11c	**Cek1**	serine/threonine protein kinase Cek1	13	7,03%
SPCC16A11.17	**Mcm4**	MCM complex subunit Mcm4/Cdc21	13	13,40%
SPAC11D3.14c	**Spac11D3.14C**	5-oxoprolinase (ATP-hydrolizing) (predicted)	12	12,90%
SPAC1805.17	**Crm1**	importin family nuclear export receptor Crm1	12	11,00%
SPAC23C4.19	**Spt5**	DSIF transcription elongation factor complex subunit Spt5	12	11,50%
SPAC23D3.09	**Arp42**	SWI/SNF and RSC complex subunit Arp42	12	33,00%

SPAC23D3.11	**Ayr1**	1-acyldihydroxyacetone phosphate reductase (predicted)	12	41,90%
SPAC29A4.03c	**Spac29A4.03C**	mitochondrial ribosomal protein subunit Mrps9 (predicted)	12	18,10%
SPAC644.16	**Rna15**	RNA-binding protein Rna15	12	17,50%
SPAC694.02	**Spac694.02**	DEAD/DEAH box helicase	12	9,32%
SPAC7D4.03c	**Spac7D4.03C**	conserved fungal family	12	10,70%
SPAPB2C8.01	**Spapb2C8.01**	cell surface glycoprotein, adhesion molecule (predicted)	12	1,97%
SPCC1322.16	**Phb2**	prohibitin Phb2 (predicted)	12	28,10%
SPCC613.06	**Rpl902**	60S ribosomal protein L9	12	51,90%
SPCC736.10c	**Mrps8**	mitochondrial ribosomal protein subunit S8 (predicted)	12	39,50%
SPCC790.02	**Pep3**	HOPS/CORVET complex subunit, ubiquitin-protein ligase E3 (predicted)	12	16,20%
SPAC17H9.12c	**Spac17H9.12C**	mitochondrial cytochrome c-heme linkage protein Cyc2 (predicted)	11	45,90%
SPAC19B12.03	**Bgs3**	1,3-beta-glucan synthase subunit Bgs3	11	7,78%
SPAC1B1.02c	**Spac1B1.02C**	NAD/NADH kinase (predicted)	11	11,00%
SPAC3A12.18	**Zwf1**	glucose-6-phosphate 1-dehydrogenase (predicted)	11	17,00%
SPAC3F10.11c	**Abc2**	glutathione S-conjugate-exporting ATPase Abc2	11	11,90%
SPAC56F8.05c	**Mug64**	BAR domain protein (predicted)	11	25,50%
SPAC821.06	**Spn2**	mitotic and meiotic (sporulation) septin Spn2	11	29,30%
SPAC824.05	**Vps16**	HOPS/CORVET complex subunit Vps16 (predicted)	11	7,78%
SPBC15D4.09c	**Spbc15D4.09C**	cystathionine gamma-synthase Met3 (predicted)	11	15,90%
SPBC16G5.13	**Ptf2**	Mst2 histone acetytransferase acytyltransferase complex subunit	11	59,50%
SPBC1703.02	**Rsc9**	RSC complex subunit Rsc9	11	7,31%
SPBC19C7.07c	**Sen34**	tRNA-splicing endonuclease catalytic subunit Sen34 (predicted)	11	29,60%
SPBC19G7.05c	**Bgs1**	1,3-beta-glucan synthase catalytic subunit Bgs1	11	6,25%
SPCC18.06c	**Caf1**	CCR4-Not complex CAF1 family ribonuclease subunit Caf1	11	20,00%

SPCC1919.09	**Tif6**	translation initiation factor-like ribosome biogenesis protein	11	48,80%
SPAC11D3.18c	**Spac11D3.18C**	plasma membrane nicotinic acid transmembrane transporter (predicted)	10	11,40%
SPAC140.02	**Gar2**	nucleolar protein required for rRNA processing	10	14,00%
SPAC1782.01	**Ecm29**	proteasome assembly chaperone Ecm29	10	5,90%
SPAC1A6.10	**Tcd1**	tRNA threonylcarbamoyladenosine dehydratase Tcd1 (predicted)	10	31,50%
SPAC23C11.16	**Plo1**	Polo kinase Plo1	10	16,00%
SPAC25H1.08c	**Spac25H1.08C**	ribosome assembly protein Sqt1 (predicted)	10	21,60%
SPAC27F1.07	**Ost1**	dolichyl-diphospho-oligosaccharide-protein glycosyltransferase Ost1 (predicted)	10	19,10%
SPAC3A11.07	**Nde2**	mitochondrial NADH dehydrogenase (ubiquinone) Nde2 (predicted)	10	17,10%
SPAC922.06	**Spac922.06**	3-oxoacyl-[acyl-carrier-protein]reductase (predicted)	10	31,00%
SPAPJ698.03c	**Prp12**	U2 snRNP-associated protein Sap130	10	12,90%
SPBC13A2.02	**Nup82**	nucleoporin Nup82	10	12,20%
SPBC1861.05	**Spbc1861.05**	pseudouridine-metabolizing bifunctional protein (predicted)	10	12,70%
SPBC18H10.19	**Vps38**	phophatidylinositol 3-kinase complex subunit Vps38	10	20,00%
SPBC2G2.08	**Ade9**	C-1-tetrahydrofolatesynthase/methylenetetrahydrofolatedehydrogenase/ methylenetetrahydrofolatecyclohydrolase/formyltetrahydrofolatesynthetase (predicted)	10	13,40%
SPBC409.07c	**Wis1**	MAP kinase kinase Wis1	10	17,40%
SPBC543.02c	**Spbc543.02C**	DNAJ/TPR domain protein DNAJC7 family	10	31,10%
SPCC1682.10	**Rpn8**	19S proteasome regulatory subunit Rpn8 (predicted)	10	23,50%
SPCC338.15	**Wbp1**	dolichyl-di-phosphooligosaccharide-protein glycotransferase subunit Wbp1 (predicted)	10	27,70%
SPCC548.06c	**Ght8**	hexose transmembrane transporter Ght8 (predicted)	10	12,20%
SPAC1687.01	**Rpc19**	DNA-directed RNA polymerase I and III subunit Rpc19	9	54,40%
SPAC17G6.11c	**Spac17G6.11C**	glucosidase (predicted)	9	4,40%
SPAC1851.03	**Ckb1**	CK2 family regulatory subunit Ckb1	9	23,80%
SPAC1B2.03c	**Spac1B2.03C**	GNS1/SUR4 family protein (predicted)	9	20,10%

SPAC222.08c	**Sno1**	glutamine aminotransferase subunit Sno1 (predicted)	9	32,90%
SPAC222.14c	**Sey1**	GTP binding protein Sey1 (predicted)	9	12,10%
SPAC25A8.02	**Atg14**	autophagy protein Atg14	9	17,20%
SPAC2C4.10c	**Csc4**	SIP/FAR complex subunit, Csc4	9	28,30%
SPAC2G11.10c	**Uba42**	thiosulfate sulfurtransferase, URM1 activating enzyme E1-type Uba42 (predicted)	9	16,70%
SPAC31G5.17c	**Rps1001**	40S ribosomal protein S10 (predicted)	9	41,00%
SPAC4H3.11c	**Ppc89**	spindle pole body protein Ppc89	9	13,00%
SPAC5H10.01	**Spac5H10.01**	DUF1445 family mitochondrial protein (predicted)	9	28,60%
SPAC637.04	**Ypp1**	cargo-transport protein Ypp1 (predicted)	9	12,60%
SPAC959.02	**Sec17**	alpha SNAP (predicted)	9	27,70%
SPAC977.14c	**Spac977.14C**	aldo/keto reductase, predicted calcium channel regulator	9	24,80%
SPBC11G11.05	**Rpa34**	DNA-directed RNA polymerase I complex subunit Rpa34 (predicted)	9	17,10%
SPBC365.06	**Pmt3**	SUMO	9	31,60%
SPBC582.07c	**Rpn7**	19S proteasome regulatory subunit Rpn7	9	18,80%
SPBP8B7.18c	**Spbp8B7.18C**	phosphomethylpyrimidine kinase (predicted)	9	22,70%
SPCC550.11	**Spcc550.11**	karyopherin (predicted)	9	12,30%
SPCC622.09	**Htb1**	histone H2B Htb1	9	27,00%
SPAC13G6.11c	**Erg12**	mevalonate kinase Erg12 (predicted)	8	17,80%
SPAC1B3.12c	**Rpb10**	DNA-directed RNA polymerase I, II, and III subunit Rpb10	8	63,40%
SPAC26A3.15c	**Nsp1**	nucleoporin Nsp1	8	12,40%
SPAC26H5.07c	**Spac26H5.07C**	seven transmembrane receptor protein (predicted)	8	8,91%
SPAC3G6.10c	**Vps51**	GARP complex subunit Vps51 (predicted)	8	52,20%
SPAC6F6.03c	**Spac6F6.03C**	ribosome export GTPase (predicted)	8	21,20%
SPAC6G9.06c	**Pcp1**	pericentrin Pcp1	8	6,46%

SPAC9G1.11c	**Spn4**	mitotic septin Spn4	8	25,00%
SPAPB1A10.08	**Spapb1A10.08**	Schizosaccharomyces specific protein	8	7,45%
SPBC1347.02	**Fkbp39**	FKBP-type peptidyl-prolyl cis-trans isomerase (predicted)	8	24,90%
SPBC13G1.01c	**Nam9**	mitochondrial ribosomal protein subunit S4 (predicted)	8	27,50%
SPBC1685.02c	**Rps1202**	40S ribosomal protein S12 (predicted)	8	37,80%
SPBC16G5.01	**Rpn12**	19S proteasome regulatory subunit Rpn12	8	34,80%
SPBC1709.09	**Rrf1**	mitochondrial translation termination factor Rrf1	8	26,60%
SPBC1921.05	**Ape2**	aminopeptidase Ape2 (predicted)	8	9,41%
SPBC21H7.07c	**His5**	imidazoleglycerol-phosphate dehydratase His5	8	27,30%
SPBC2F12.02c	**Mrpl7**	mitochondrial ribosomal protein subunit L7 (predicted)	8	17,80%
SPBC3B9.14c	**Mrpl3**	mitochondrial ribosomal protein subunit L3 (predicted)	8	10,10%
SPBC83.05	**Spbc83.05**	mitochondrial RNA-binding protein (predicted)	8	13,60%
SPCC1183.02	**Spcc1183.02**	glutathione S-transferase, translational elongation factor eEF1 (predicted)	8	18,20%
SPCC1442.16c	**Zta1**	NADPH quinone oxidoreductase/ARE-binding protein (predicted)	8	35,00%
SPCC1682.09c	**Ggc1**	mitochondrial guanine nucleotide transmembrane transporter Ggc1 (predicted)	8	27,00%
SPCC613.04c	**Rng3**	UCS-domain protein Rng3	8	11,00%
SPAC1635.01	**Spac1635.01**	mitochondrial outer membrane voltage-dependent anion-selective channel (predicted)	7	20,20%
SPAC1805.04	**Nup132**	nucleoporin Nup132	7	7,40%
SPAC23G3.02c	**Sib1**	ferrichrome synthetase Sib1	7	2,09%
SPAC23H3.03c	**Npr2**	SEA/Iml1/Npr2/3 complex subunit Npr2 (predicted)	7	11,20%
SPAC23H4.14	**Vam6**	guanyl-nucleotide exchange factor, HOPS complex subunit Vam6 (predicted)	7	7,51%
SPAC29A4.04c	**Cbf5**	pseudouridylate synthase Cbf5 (predicted)	7	12,40%
SPAC4F10.10c	**Mnn9**	mannosyltransferase complex subunit, Anp family Mnn9 (predicted)	7	15,10%
SPAC5H10.10	**Spac5H10.10**	NADPH dehydrogenase (predicted)	7	13,00%

SPAC607.05	**Rpn9**	19S proteasome regulatory subunit Rpn9	7	21,50%
SPAC637.10c	**Rpn10**	19S proteasome regulatory subunit Rpn10	7	28,40%
SPAC6F6.09	**Eaf6**	Mst2/NuA4 histone acetyltransferase complex subunit Eaf6	7	21,00%
SPAC869.02c	**Spac869.02C**	nitric oxide dioxygenase (predicted)	7	14,10%
SPAC9E9.04	**Spac9E9.04**	bcap family homolog (predicted)	7	26,10%
SPAP27G11.05c	**Vps41**	HOPS complex subunit Vps41 (predicted)	7	13,90%
SPAPB8E5.07c	**Rrp12**	rRNA processing protein Rrp12 (predicted)	7	6,88%
SPBC14F5.03c	**Kap123**	karyopherin Kap123	7	11,80%
SPBC1604.04	**Spbc1604.04**	mitochondrial thiamine pyrophosphate transmembrane transporter (predicted)	7	17,70%
SPBC211.04c	**Mcm6**	MCM complex subunit Mcm6	7	11,80%
SPBC28E12.06c	**Lvs1**	beige protein homolog Lvs1 (predicted)	7	3,76%
SPBC2G2.06c	**Apl1**	AP-2 adaptor complex subunit Apl1 (predicted)	7	5,91%
SPBC336.04	**Cdc6**	DNA polymerase delta catalytic subunit Cdc6	7	8,66%
SPBC660.08	**Spbc660.08**	Schizosaccharomyces specific protein	7	14,90%
SPBC839.07	**Ibp1**	Cdc25 family phosphatase Ibp1	7	34,10%
SPBP35G2.11c	**Spbp35G2.11C**	transcription related zf-ZZ type zinc finger protein	7	11,80%
SPCC126.05c	**Mrpl17**	mitochondrial ribosomal protein subunit L17 (predicted)	7	23,90%
SPCC1753.05	**Rsm1**	RNA export factor Rsm1	7	18,20%
SPCC1919.10c	**Myo52**	myosin type V	7	7,19%
SPCC24B10.07	**Gad8**	AGC family protein kinase Gad8	7	13,40%
SPCC4G3.06c	**Mrpl4**	mitochondrial ribosomal protein subunit L4 (predicted)	7	29,20%
SPCC663.04	**Rpl39**	60S ribosomal protein L39	7	43,10%
SPAC1039.07c	**Spac1039.07C**	aminotransferase class-III, possible transaminase, unknown specificity	6	15,80%
SPAC12B10.01c	**Spac12B10.01C**	HECT-type ubiquitin-protein ligase E3 (predicted)	6	2,91%

SPAC17H9.14c	**Pdi2**	protein disulfide isomerase	6	16,40%
SPAC1805.08	**Dlc1**	dynein light chain Dlc1	6	45,90%
SPAC18G6.07c	**Mra1**	rRNA (pseudouridine) methyltransferase Mra1	6	13,90%
SPAC27F1.09c	**Prp10**	U2 snRNP-associated protein Sap155	6	5,92%
SPAC343.14c	**Spac343.14C**	translation initiation factor eIF2B beta subunit (predicted)	6	10,90%
SPAC3A12.07	**Rpb11**	RNA polymerase II complex subunit Rpb11	6	40,70%
SPAC589.06c	**Spac589.06C**	pho88 family protein (predicted)	6	14,90%
SPAC630.03	**Arp3**	Arp2/3 protein complex, actin-like protein subunit Arp3	6	14,30%
SPAC823.12	**Vps11**	HOPs/CORVET complex biquitin protein ligase E3 subunit Vps11 (predicted)	6	6,95%
SPAC823.14	**Ptf1**	Mst2 histone acetytransferase acytyltransferase complex, predicted phosphoric monoester hydrolase Ptf1	6	24,50%
SPAC890.07c	**Rmt1**	type I protein arginine N-methyltransferase Rmt1	6	16,50%
SPAC926.08c	**Rpf2**	Brix domain ribosome biogenesis protein Rpf2	6	21,50%
SPAP7G5.06	**Per1**	plasma membrane amino acid permease Per1	6	10,50%
SPBC11G11.04	**Trs20**	TRAPP complex subunit Trs20 (predicted)	6	40,40%
SPBC1711.05	**Spbc1711.05**	nucleocytoplasmic transport chaperone Srp40 (predicted)	6	11,80%
SPBC1711.13	**His2**	histidinol dehydrogenase His2 (predicted)	6	15,00%
SPBC1718.04	**Spbc1718.04**	glycerol-3-phosphate O-acyltransferase (predicted)	6	9,33%
SPBC19G7.10c	**Pdc2**	topoisomerase II-associated deadenylation-dependent mRNA-decapping factor Pdc2 (predicted)	6	5,97%
SPBC20F10.01	**Gar1**	snoRNP pseudouridylase box H/ACA snoRNP complex protein Gar1	6	20,60%
SPBC21H7.02	**Taf10**	SAGA complex/transcription factor TFIID complex subunit Taf10	6	22,30%
SPBC28F2.12	**Rpb1**	RNA polymerase II large subunit Rpb1	6	5,25%
SPBC354.02c	**Sec61**	translocon alpha subunit Sec61	6	10,40%
SPBC365.04c	**Spbc365.04C**	RNA-binding protein, involved in ribosome biogenesis (predicted)	6	9,01%
SPBC582.08	**Rhp1602**	alanine aminotransferase Rhp1602 (predicted)	6	21,20%

SPBC660.07	**Ntp1**	alpha,alpha-trehalase Ntp1	6	6,39%
SPBC725.14	**Arg6**	acetylglutamate synthase Arg6 (predicted)	6	12,60%
SPBC8E4.03	**Spbc8E4.03**	agmatinase 2 (predicted)	6	15,70%
SPBP16F5.03c	**Tra1**	SAGA complex phosphatidylinositol pseudokinase Tra1	6	2,11%
SPCC1259.09c	**Pdx1**	pyruvate dehydrogenase protein x component, Pdx1 (predicted)	6	13,60%
SPCC1442.09	**Trp3**	anthranilate synthase component I (predicted)	6	18,00%
SPCC364.07	**Ser3**	D-3 phosphoglycerate dehydrogenase Ser3 (predicted)	6	16,70%
SPCC4B3.17	**Cbp3**	ubiquinol cytochrome-c reductase assembly protein Cbp3 (predicted)	6	14,50%
SPCC613.10	**Qcr2**	ubiquinol-cytochrome-c reductase complex core protein Qcr2 (predicted)	6	17,60%
SPCC622.12c	**Gdh1**	NADP-specific glutamate dehydrogenase Gdh1 (predicted)	6	13,50%
SPCC895.06	**Elp2**	elongator complex subunit Elp2 (predicted)	6	9,08%
SPCC962.03c	**Cut15**	karyopherin Cut15	6	11,30%
SPCC970.06	**Spcc970.06**	cargo receptor for soluble proteins (predicted)	6	18,90%
SPMIT.08	**Var1**	mitochondrial ribosomal small subunit Var1	6	19,80%
SPAC1071.02	**Mms19**	Dos2 silencing complex subunit Mms19	5	4,22%
SPAC10F6.09c	**Psm3**	mitotic cohesin complex subunit Psm3	5	6,95%
SPAC12G12.09	**Eti1**	conserved fungal protein associated with stress granule	5	9,01%
SPAC12G12.12	**Gms2**	UDP-galactose transmembrane transporter Gms2 (predicted)	5	10,80%
SPAC13A11.01c	**Rga8**	Rho-type GTPase activating protein Rga8	5	6,95%
SPAC1786.03	**Cut11**	spindle pole body docking protein Cut11	5	7,65%
SPAC17G6.10	**Ssr1**	SWI/SNF and RSC complex subunit Ssr1	5	8,35%
SPAC20G8.09c	**Nat10**	ribosome biogenesis ATPase	5	6,39%
SPAC21E11.06	**Tif224**	translation initiation factor eIF2B delta subunit (predicted)	5	13,90%
SPAC23C11.17	**Mdm28**	mitochondrial inner membrane protein involved in potassium ion transport Mdm28 (predicted)	5	5,57%

SPAC27E2.09	**Mak2**	histidine kinase Mak2	5	2,90%
SPAC27F1.06c	**Spac27F1.06C**	FKBP-type peptidyl-prolyl cis-trans isomerase (predicted)	5	13,00%
SPAC29A4.08c	**Prp19**	ubiquitin-protein ligase E4 Prp19	5	11,70%
SPAC2F3.02	**Spac2F3.02**	ER protein translocation subcomplex subunit (predicted)	5	18,80%
SPAC2F7.13c	**Wrs1**	cytoplasmic tryptophan-tRNA ligase Wrs1 (predicted)	5	13,90%
SPAC343.12	**Rds1**	conserved fungal protein	5	7,71%
SPAC3A12.14	**Cam1**	calmodulin Cam1	5	51,30%
SPAC4A8.04	**Isp6**	vacuolar serine protease Isp6	5	11,80%
SPAC4A8.05c	**Myp2**	myosin II heavy chain Myo3	5	3,90%
SPAC4D7.01c	**Sec71**	Sec7 domain protein, ARF GEF (predicted)	5	2,60%
SPAC56E4.03	**Spac56E4.03**	aromatic aminotransferase (predicted)	5	13,90%
SPAC56F8.10	**Met9**	methylenetetrahydrofolate reductase Met9	5	10,30%
SPAC607.03c	**Snu13**	U3 snoRNP-associated protein Snu13	5	27,20%
SPAC637.05c	**Vma2**	V-type ATPase V1 subunit B	5	14,50%
SPAC890.04c	**Spac890.04C**	ribosome biogenesis protein Ytm1 (predicted)	5	10,00%
SPAC9.10	**Thi9**	thiamine transmembrane transporter Thi9	5	8,97%
SPACUNK4.11c	**Mpp6**	nuclear exosome-associated RNA binding protein Mpp6	5	8,51%
SPAP14E8.03	**Bos1**	SNARE Bos1 (predicted)	5	15,70%
SPAP27G11.13c	**Nop10**	snoRNP pseudouridylase box H/ACA snoRNP complex protein (predicted)	5	40,60%
SPAP8A3.12c	**Tpp2**	tripeptidyl-peptidase II Tpp2	5	5,65%
SPBC14F5.02	**Trs65**	TRAPP complex subunit Trs65 (predicted)	5	13,60%
SPBC1604.05	**Pgi1**	glucose-6-phosphate isomerase (predicted)	5	10,00%
SPBC1604.20c	**Tea2**	kinesin-like protein Tea2	5	11,90%
SPBC1677.03c	**Tda1**	threonine ammonia-lyase Tda1	5	15,20%

SPBC16G5.11c	**Bag101**	BAG family molecular chaperone regulator Bag101 (predicted)	5	25,60%
SPBC1861.08c	**Lea1**	U2 snRNP-associated protein Lea1 (predicted)	5	27,80%
SPBC23E6.04c	**Utp10**	U3 snoRNP-associated protein Utp10 (predicted)	5	5,40%
SPBC23G7.05	**Sui1**	translation initiation factor eIF1	5	34,90%
SPBC25D12.04	**Suc22**	ribonucleotide reductase small subunit Suc22	5	16,40%
SPBC28F2.08c	**Hrd3**	HRD ubiquitin ligase complex subunit (predicted)	5	7,29%
SPBC2D10.14c	**Myo51**	myosin type V	5	5,17%
SPBC336.11	**Vps52**	GARP complex subunit Vps52 (predicted)	5	12,60%
SPBC337.14	**Rpb4**	DNA-directed RNA polymerase II complex subunit Rpb4	5	40,70%
SPBC36.05c	**Clr6**	histone deacetylase (class I) Clr6	5	15,10%
SPBC3B9.12	**Trs23**	TRAPP complex subunit Trs23 (predicted)	5	15,20%
SPBC3E7.11c	**Spbc3E7.11C**	DNAJ protein Caj1/Djp1-type (predicted)	5	12,40%
SPBC4.03c	**Spbc4.03C**	COPII-coated vesicle component Sfb3 (predicted)	5	7,18%
SPBC460.02c	**Spbc460.02C**	eukaryotic translation elongation factor, glutathione S-transferase (predicted)	5	20,50%
SPBC4C3.03	**Thr1**	homoserine kinase Thr1 (predicted)	5	19,20%
SPBC56F2.04	**Utp20**	U3 snoRNP protein Utp20 (predicted)	5	2,17%
SPBC660.13c	**Ssb1**	DNA replication factor A subunit Ssb1	5	12,20%
SPBC8D2.17	**Gmh4**	alpha-1,2-galactosyltransferase (predicted)	5	15,50%
SPCC1235.14	**Ght5**	hexose transmembrane transporter Ght5	5	10,30%
SPCC162.07	**Ent1**	epsin	5	7,41%
SPCC24B10.11c	**Tho7**	THO complex subunit Tho7 (predicted)	5	20,80%
SPCC285.17	**Spp27**	RNA polymerase I upstream activation factor complex subunit Spp27	5	13,30%
SPCC364.01	**Cif1**	calnexin independence factor Cif1	5	20,90%
SPCC5E4.03c	**Taf5**	SAGA complex subunit/TATA-binding protein associated factor/transcription factor TFIID complex subunit Taf5	5	11,40%

SPCP1E11.11	**Puf6**	Puf family RNA-binding protein Puf6 (predicted)	5	4,36%
SPAC1006.07	**Spac1006.07**	translation initiation factor eIF4A (predicted)	4	11,20%
SPAC11D3.02c	**Spac11D3.02C**	ELLA family acetyltransferase (predicted)	4	23,30%
SPAC12G12.03	**Cip2**	RNA-binding protein Cip2	4	4,86%
SPAC12G12.06c	**Rcl1**	rRNA processing protein Rcl1 (predicted)	4	15,70%
SPAC15A10.02	**Taf12**	transcription factor TFIID complex subunit A/ SAGA complex subunit Taf12	4	7,56%
SPAC1610.02c	**Mrpl1**	mitochondrial ribosomal protein subunit L1 (predicted)	4	24,50%
SPAC167.07c	**Hul5**	HECT-type ubiquitin-protein ligase E3 (predicted)	4	5,54%
SPAC1687.03c	**Rfc4**	DNA replication factor C complex subunit Rfc4 (predicted)	4	18,10%
SPAC16A10.04	**Rho4**	Rho family GTPase Rho4	4	18,20%
SPAC17A2.03c	**Vma6**	V-type ATPase V0 subunit d (predicted)	4	11,40%
SPAC17A5.06	**Ptr8**	transcription factor TFIIH complex ERCC-3 subunit Ptr8	4	6,47%
SPAC17C9.06	**Sam50**	mitochondrial sorting and assembly machinery complex subunit Sam50 (predicted)	4	7,79%
SPAC17D4.01	**Pex7**	peroxin-7 (predicted)	4	19,20%
SPAC17H9.05	**Ebp2**	rRNA processing protein Ebp2 (predicted)	4	8,71%
SPAC19G12.17	**Erh1**	enhancer of rudimentary homolog Erh1	4	35,60%
SPAC1B3.01c	**Spac1B3.01C**	uracil phosphoribosyltransferase (predicted)	4	22,80%
SPAC1F5.07c	**Hem14**	protoporphyrinogen oxidase Hem14 (predicted)	4	11,00%
SPAC222.09	**Seb1**	RNA-binding protein Seb1	4	4,84%
SPAC22G7.09c	**Nup45**	nucleoporin Nup45	4	10,80%
SPAC24H6.11c	**Spac24H6.11C**	sulfate transmembrane transporter (predicted)	4	5,53%
SPAC26H5.04	**Gid5**	GID complex armadillo repeat subunit Gid5 (predicted)	4	5,07%
SPAC29A4.18	**Prw1**	Clr6 histone deacetylase complex subunit Prw1	4	9,74%
SPAC2F7.05c	**Tif5**	translation initiation factor eIF5, Tif5(predicted)	4	18,50%

SPAC31A2.07c	**Dbp10**	ATP-dependent RNA helicase Dbp10 (predicted)	4	7,90%
SPAC31G5.19	**Abo1**	ATPase with bromodomain protein (predicted)	4	4,79%
SPAC3A12.05c	**Taf2**	TATA-binding protein associated factor Taf2 (predicted)	4	2,73%
SPAC3A12.11c	**Cwf2**	RNA-binding protein Cwf2	4	7,99%
SPAC3H1.05	**Spac3H1.05**	CAAX prenyl protease (predicted)	4	9,28%
SPAC4D7.04c	**Rer2**	cis-prenyltransferase	4	18,90%
SPAC589.04	**Spac589.04**	metaxin 1 (predicted)	4	19,20%
SPAC637.06	**Gmh5**	alpha-1,2-galactosyltransferase (predicted)	4	15,30%
SPAC806.02c	**Spac806.02C**	Par A family ATPase/WD repeat iron cluster assembly fusion protein (predicted)	4	12,80%
SPAP8A3.07c	**Spap8A3.07C**	phospho-2-dehydro-3-deoxyheptonate aldolase (predicted)	4	17,70%
SPAPYUG7.03c	**Mid2**	medial ring protein Mid2	4	6,37%
SPBC1198.02	**Dea2**	adenine deaminase Dea2	4	9,26%
SPBC1271.04c	**Spbc1271.04C**	eIF-5A-deoxyhypusine synthase (predicted)	4	18,30%
SPBC1271.12	**Kes1**	oxysterol binding protein (predicted)	4	8,25%
SPBC13G1.02	**Mpg2**	mannose-1-phosphate guanyltransferase (predicted)	4	12,10%
SPBC1539.04	**Tts1**	tetra spanning protein 1, Tts1	4	15,10%
SPBC1539.10	**Nop16**	ribosome biogenesis protein Nop16 (predicted)	4	13,90%
SPBC1604.21c	**Ptr3**	ubiquitin activating enzyme E1	4	5,04%
SPBC18H10.17c	**Spbc18H10.17C**	mitochondrial recombinase Mhr1 (predicted)	4	18,90%
SPBC1921.01c	**Rpl35B**	60S ribosomal protein L35a (predicted)	4	41,70%
SPBC211.05	**Sap10**	splicing factor 3B	4	41,20%
SPBC216.07c	**Tor2**	phosphatidylinositol kinase Tor2	4	1,33%
SPBC21B10.05c	**Pop3**	WD repeat protein Pop3	4	8,28%
SPBC21D10.09c	**Rkr1**	RQC complex ubiquitin-protein ligase E3 Rkr1 (predicted)	4	2,55%

SPBC26H8.08c	**Grn1**	GTPase Grn1	4	12,30%
SPBC36B7.03	**Sec63**	ER protein translocation subcomplex subunit Sec63 (predicted)	4	7,53%
SPBC36B7.09	**Gcn2**	eIF2 alpha kinase Gcn2	4	3,81%
SPBC3E7.05c	**Spbc3E7.05C**	human mitofilin ortholog (predicted)	4	6,91%
SPBC3H7.01	**Spo14**	GDP/GTP exchange factor, WD repeat protein Spo14	4	11,40%
SPBC3H7.04	**Spbc3H7.04**	supeoxide dismutase, mitochondrial ribosomal protein subunit (predicted)	4	11,40%
SPBC4B4.04	**Eif21**	translation initiation factor eIF2A (predicted)	4	5,73%
SPBC56F2.08c	**Spbc56F2.08C**	RNA-binding protein (predicted)	4	10,40%
SPBC577.10	**Pre4**	20S proteasome complex subunit beta 7, Pre4 (predicted)	4	21,80%
SPBC651.01c	**Nog1**	GTP binding protein Nog1 (predicted)	4	9,66%
SPBC713.02c	**Ubp15**	ubiquitin C-terminal hydrolase Ubp15	4	4,34%
SPBC800.03	**Clr3**	histone deacetylase (class II) Clr3	4	8,73%
SPBC839.16	**Thf1**	C1-5,6,7,8-tetrahydrofolate (THF) synthase, trifunctional enzyme Thf1	4	5,76%
SPBC887.17	**Spbc887.17**	transmembrane transporter (predicted)	4	5,92%
SPBC947.14c	**Cbp6**	mitochondrial respiratory chain complex assembly protein Cbp6 (predicted)	4	35,00%
SPCC1223.05c	**Rpl3702**	60S ribosomal protein L37 (predicted)	4	22,00%
SPCC126.15c	**Sec65**	signal recognition particle subunit Sec65 (predicted)	4	10,80%
SPCC1322.05c	**Spcc1322.05C**	leukotriene A-4 hydrolase (predicted)	4	4,41%
SPCC1442.06	**Pre8**	20S proteasome complex subunit alpha 2, Pre8 (predicted)	4	28,60%
SPCC162.09c	**Hmg1**	3-hydroxy-3-methylglutaryl-CoA reductase Hmg1	4	3,61%
SPCC1795.02c	**Vcx1**	CaCA proton/calcium exchanger (predicted)	4	6,31%
SPCC1840.08c	**Pdi5**	protein disulfide isomerase (predicted)	4	9,09%
SPCC188.06c	**Srp54**	signal recognition particle subunit Srp54	4	9,77%
SPCC584.15c	**Spcc584.15C**	arrestin involved in ubiquitin-dependent endocytosis	4	11,30%

SPCC74.06	**Mak3**	histidine kinase Mak3	4	2,22%
SPCC962.01	**Spcc962.01**	C2 domain endoplasmic reticulum membrane organization protein (predicted)	4	5,25%
SPCP1E11.05c	**Are2**	acyl-coA-sterol acyltransferase Are2 (predicted)	4	9,75%
SPAC1006.06	**Rgf2**	RhoGEF Rgf2	3	3,02%
SPAC12B10.02c	**Spac12B10.02C**	endoplasmic reticulum resident protein required for packaging into COPII vesicles (predicted)	3	15,70%
SPAC13D6.02c	**Byr3**	translational activator, zf-CCHC type zinc finger protein (predicted)	3	17,30%
SPAC13G6.03	**Gpi7**	GPI anchor biosynthesis protein Gpi7 (predicted)	3	4,75%
SPAC17A5.13	**Fol2**	GTP cyclohydrolase Fol2 (predicted)	3	16,20%
SPAC17G8.04c	**Arc5**	ARP2/3 actin-organizing complex subunit Arc5	3	20,40%
SPAC17G8.08c	**Spac17G8.08C**	human TMEM165 homolog, implicated in calcium tranport	3	13,60%
SPAC17G8.14c	**Pck1**	protein kinase C (PKC)-like Pck1	3	4,15%
SPAC1952.09c	**Spac1952.09C**	acetyl-CoA hydrolase (predicted)	3	5,18%
SPAC23C11.14	**Zhf1**	zinc ion transmembrane transporter Zhf1	3	6,46%
SPAC24H6.03	**Cul3**	cullin 3	3	3,95%
SPAC24H6.13	**Spac24H6.13**	DUF221 family protein implicated in Golgi to plasma membrane transport (predicted)	3	3,90%
SPAC25B8.03	**Psd2**	phosphatidylserine decarboxylase Psd2	3	11,00%
SPAC27D7.14c	**Tpr1**	RNA polymerase II associated Paf1 complex subunit Tpr1	3	4,14%
SPAC27E2.03c	**Spac27E2.03C**	Obg-Like ATPase (predicted)	3	14,80%
SPAC2G11.14	**Taf111**	transcription factor TFIID complex subunit Taf111	3	6,03%
SPAC30C2.02	**Mmd1**	deoxyhypusine hydroxylase (predicted)	3	16,70%
SPAC31A2.09c	**Apm4**	AP-2 adaptor complex subunit Apm4 (predicted)	3	8,07%
SPAC31A2.16	**Gef2**	RhoGEF Gef2	3	3,91%
SPAC3A11.10c	**Spac3A11.10C**	dipeptidyl peptidase (predicted)	3	13,90%
SPAC3A12.17c	**Cys12**	cysteine synthase-like protein Cys12	3	13,90%

SPAC3G6.03c	**Spac3G6.03C**	Maf-like protein	3	22,40%
SPAC4A8.07c	**Lcb4**	sphingoid long chain base kinase (predicted)	3	8,95%
SPAC4H3.03c	**Spac4H3.03C**	glucan 1,4-alpha-glucosidase (predicted)	3	6,16%
SPAC57A10.07	**Spac57A10.07**	conserved protein (fungal and protozoan)	3	12,50%
SPAC57A7.08	**Pzh1**	serine/threonine protein phosphatase Pzh1	3	6,80%
SPAC644.14c	**Rad51**	RecA family recombinase Rad51/Rhp51	3	15,90%
SPAC6F12.05c	**Tnr3**	thiamine diphosphokinase Tnr3/ Nudix hydrolase fusion protein	3	6,15%
SPAC8C9.12c	**Spac8C9.12C**	mitochondrial iron ion transmembrane transporter (predicted)	3	10,60%
SPAC926.06c	**Spac926.06C**	leucine-rich repeat protein, unknown role	3	9,34%
SPAP27G11.10c	**Nup184**	nucleoporin Nup184	3	1,85%
SPBC106.16	**Pre6**	20S proteasome complex subunit alpha 4 Pre6	3	21,20%
SPBC1105.01	**Spbc1105.01**	rRNA processing protein Rrp12-like (predicted)	3	4,80%
SPBC1105.03c	**Mrpl1601**	mitochondrial ribosomal protein subunit L16 (predicted)	3	13,50%
SPBC11B10.07c	**Ivn1**	CDC50 domain protein, implicated in signal transduction (predicted)	3	8,09%
SPBC11C11.02	**Imp2**	contractile ring protein Imp2	3	7,76%
SPBC1271.02	**Stt3**	oligosaccharyltransferase subunit Stt3	3	6,38%
SPBC12D12.01	**Sad1**	spindle pole body protein Sad1	3	8,75%
SPBC1347.05c	**Spbc1347.05C**	DNAJ domain protein Scj1 (predicted)	3	9,55%
SPBC1683.11c	**Spbc1683.11C**	isocitrate lyase (predicted)	3	8,88%
SPBC1685.14c	**Spbc1685.14C**	Vid27 family protein	3	4,62%
SPBC16E9.05	**Erg6**	sterol 24-C-methyltransferase Erg6	3	12,70%
SPBC16E9.10c	**Rix7**	AAA family ATPase Rix7 (predicted)	3	4,62%
SPBC16H5.06	**Rip1**	ubiquinol-cytochrome-c reductase complex subunit 5	3	12,30%
SPBC1703.15c	**Vps33**	HOPS/CORVET complex subunit, vacuolar sorting protein Vps33	3	7,26%

SPBC1706.03	**Fzo1**	mitochondrial dynamin family fusion GTPase protein (predicted)	3	7,12%
SPBC1709.17	**Spbc1709.17**	folylpolyglutamate synthase (predicted)	3	6,53%
SPBC17A3.01c	**Tim50**	TIM23 translocase complex subunit Tim50 (predicted)	3	9,51%
SPBC19C2.14	**Smd3**	Sm snRNP core protein Smd3	3	19,60%
SPBC19G7.14c	**Cog5**	Golgi transport complex subunit Cog5 (predicted)	3	7,79%
SPBC215.08c	**Arg4**	arginine specific carbamoyl-phosphate synthase Arg4 (predicted)	3	5,86%
SPBC23G7.15c	**Rpp202**	60S acidic ribosomal protein A4	3	43,60%
SPBC28F2.03	**Ppi1**	cyclophilin family peptidyl-prolyl cis-trans isomerase Cyp2	3	17,90%
SPBC28F2.11	**Hmo1**	HMG box protein Hmo1	3	13,50%
SPBC29B5.02c	**Isp4**	OPT oligopeptide transmembrane transporter family Isp4	3	4,84%
SPBC2G2.02	**Syj1**	inositol-polyphosphate 5-phosphatase (synaptojanin homolog 1)	3	5,30%
SPBC2G2.07c	**Mug178**	mitochondrial ribosomal protein subunit L51-b (predicted)	3	12,40%
SPBC2G2.12	**Hrs1**	mitochondrial and cytoplasmic histidine-tRNA ligase Hrs1 (predicted)	3	6,57%
SPBC30B4.05	**Kap109**	karyopherin Kap109	3	5,58%
SPBC354.15	**Fap1**	L-pipecolate oxidase	3	5,58%
SPBC359.03c	**Aat1**	amino acid transmembrane transporter Aat1	3	6,74%
SPBC365.12c	**Ish1**	LEA domain protein	3	8,33%
SPBC3E7.02c	**Hsp16**	heat shock protein Hsp16	3	14,70%
SPBC409.19c	**Spbc409.19C**	metaxin (predicted)	3	12,40%
SPBC428.05c	**Arg12**	argininosuccinate synthase Arg12	3	8,78%
SPBC428.14	**Spbc428.14**	1-acylglycerol-3-phosphate acyltransferase (predicted)	3	13,10%
SPBC4B4.02c	**Nca2**	mitochondrial protein Nca2 (predicted)	3	7,85%
SPBC4C3.10c	**Pre3**	20S proteasome complex subunit beta 1 Pre3 (predicted)	3	14,20%
SPBC577.04	**Spbc577.04**	human THOC5 ortholog (predicted)	3	15,50%

SPBC646.02	**Cwf11**	complexed with Cdc5 protein Cwf11	3	3,58%
SPBC646.12c	**Gap1**	GTPase activating protein Gap1	3	3,66%
SPBC651.11c	**Apm3**	AP-3 adaptor complex subunit Apm3 (predicted)	3	9,41%
SPBC691.02c	**Drp1**	RINT1 family protein (predicted)	3	7,67%
SPBC83.14c	**Rfc5**	DNA replication factor C complex subunit Rfc5 (predicted)	3	10,60%
SPBC8D2.14c	**Sed5**	SNARE Sed5 (predicted)	3	17,50%
SPBC8D2.15	**Lip5**	mitochondrial lipoic acid synthetase Lip5 (predicted)	3	7,84%
SPBPB2B2.01	**Spbpb2B2.01**	amino acid transmembrane transporter (predicted)	3	5,47%
SPCC1020.06c	**Tal1**	transaldolase (predicted)	3	14,00%
SPCC1442.05c	**Mic26**	MICOS complex subunit Mic26 (predicted)	3	14,70%
SPCC1442.19	**Mrp49**	mitochondrial ribosomal protein Mrp49 (predicted)	3	22,20%
SPCC1494.07	**Spcc1494.07**	tRNA 2'-O-methylase subunit Trm72 (predicted)	3	3,40%
SPCC16A11.14	**Sfh1**	RSC complex subunit Sfh1	3	17,50%
SPCC16C4.18c	**Taf6**	histone H4-like TAF Taf6, SAGA complex subunit	3	9,73%
SPCC1739.10	**Mug33**	Tea1-interacting protein involved in exocytosis	3	14,00%
SPCC1739.11c	**Cdc11**	SIN component scaffold protein, centriolin ortholog Cdc11	3	3,44%
SPCC1827.05c	**Spcc1827.05C**	nucleolar RNA-binding protein NIFK (predicted)	3	9,78%
SPCC1840.06	**Atp5**	F0-ATPase delta subunit (predicted)	3	18,10%
SPCC1840.07c	**Spcc1840.07C**	phosphoprotein phosphatase (predicted)	3	8,13%
SPCC188.08c	**Ubp5**	ubiquitin C-terminal hydrolase Ubp5	3	3,70%
SPCC18B5.05c	**Spcc18B5.05C**	phosphomethylpyrimidine kinase (predicted)	3	14,10%
SPCC290.03c	**Nup186**	nucleoporin Nup186	3	1,94%
SPCC364.05	**Vps3**	CORVET complex subunit, GTPase regulator Vps3 (predicted)	3	5,16%
SPCC4G3.12c	**Spcc4G3.12C**	ubiquitin-protein ligase E3 (predicted)	3	4,02%

SPCC553.09c	**Spb70**	DNA polymerase alpha B-subunit	3	9,06%
SPCC63.12c	**Pup3**	20S proteasome complex subunit beta 3, Pup3 (predicted)	3	13,20%
SPCC645.06c	**Rgf3**	RhoGEF Rgf3	3	3,92%
SPCC663.03	**Pmd1**	leptomycin transmembrane transporter Pmd1	3	3,60%
SPCC74.01	**Sly1**	SNARE binding protein Sly1 (predicted)	3	8,61%
SPCC757.15	**Cox14**	cytochrome c oxidase assembly protein Cox14 (predicted)	3	40,60%
SPCC830.11c	**Fap7**	nucleoside-triphosphatase involved in SSU-rRNA maturation Fap7 (predicted)	3	28,60%
SPCC970.09	**Sec8**	exocyst complex subunit Sec8	3	4,38%
SPCP1E11.07c	**Cwf18**	complexed with Cdc5 protein Cwf18	3	23,20%
SPAC10F6.13c	**Spac10F6.13C**	aspartate aminotransferase (predicted)	2	8,07%
SPAC1142.06	**Get3**	GET complex ATPase subunit Get3 (predicted)	2	7,90%
SPAC11H11.06	**Arp2**	ARP2/3 actin-organizing complex subunit Arp2	2	8,46%
SPAC13F5.06c	**Sec10**	exocyst complex subunit Sec10	2	4,93%
SPAC1486.07c	**Mrpl19**	mitochondrial ribosomal protein subunit L19 (predicted)	2	20,80%
SPAC1556.07	**Pmm1**	phosphomannomutase Pmm1	2	12,80%
SPAC1782.09c	**Clp1**	Cdc14-related protein phosphatase Clp1/Flp1	2	4,28%
SPAC1786.01c	**Ptl2**	triacylglycerol lipase ptl2	2	4,60%
SPAC17C9.08	**Pnu1**	mitochondrial endodeoxyribonuclease Pnu1	2	9,63%
SPAC17G6.13	**Slt1**	Schizosaccharomyces specific protein Slt1	2	5,08%
SPAC1952.14c	**Mrpl25**	mitochondrial ribosomal protein subunit L25 (predicted)	2	17,20%
SPAC1B3.16c	**Vht1**	vitamin H transmembrane transporter Vht1	2	6,34%
SPAC1F5.03c	**Spac1F5.03C**	FAD-dependent oxidoreductase involved in late endosome to Golgi transport (predicted)	2	6,54%
SPAC1F7.03	**Pkd2**	TRP-like ion channel Pkd2	2	4,23%
SPAC1F7.07c	**Fip1**	iron permease Fip1	2	7,81%

SPAC20G8.04c	**Cir2**	mitochondrial electron transfer flavoprotein-ubiquinone oxidoreductase Cir2 (predicted)	2	6,96%
SPAC22A12.06c	**Spac22A12.06C**	serine hydrolase-like	2	6,99%
SPAC22E12.13c	**Rlp24**	ribosomal L24-like protein involved in ribosome biogenesis Rlp24 (predicted)	2	13,00%
SPAC23A1.03	**Apt1**	adenine phosphoribosyltransferase (APRT) (predicted)	2	13,80%
SPAC23A1.18c	**Mrp51**	mitochondrial ribosomal protein subunit L51-b (predicted)	2	15,20%
SPAC23D3.10c	**Eng2**	endo-1,3-beta-glucanase Eng2	2	4,67%
SPAC24C9.09	**Spac24C9.09**	mitochondrial threonine-tRNA ligase (predicted)	2	6,12%
SPAC26H5.09c	**Spac26H5.09C**	oxidoreductase involved in NADPH regeneration (predicted)	2	8,13%
SPAC27E2.10c	**Rfc3**	DNA replication factor C complex subunit Rfc3	2	8,77%
SPAC2F3.06c	**Kap104**	karyopherin Kap104	2	3,30%
SPAC2F7.11	**Nrd1**	RNA-binding protein Nrd1	2	6,43%
SPAC343.04c	**Gid7**	GID complex subunit Gid7 (predicted)	2	7,30%
SPAC3G9.16c	**Bet5**	TRAPP complex subunit Bet5 (predicted)	2	20,60%
SPAC4F10.20	**Grx1**	glutaredoxin Grx1	2	22,80%
SPAC4G9.08c	**Rpc2**	DNA-directed RNA polymerase III complex subunit Rpc2	2	2,49%
SPAC521.03	**Spac521.03**	short chain dehydrogenase (predicted)	2	12,00%
SPAC637.13c	**Slm1**	cytoskeletal signaling protein Slm1 (predicted)	2	9,04%
SPAC644.11c	**Pkp1**	mitochondrial pyruvate dehydrogenase (lipoamide) kinase Pkp1 (predicted)	2	8,94%
SPAC644.12	**Cdc5**	splicing factor, Prp19 complex subunit Cdc5	2	4,36%
SPAC664.06	**Rlp7**	ribosomal protein L7-like Rlp7 involved in ribosome biogenesis (predicted)	2	10,00%
SPAC694.05c	**Rps2502**	40S ribosomal protein S25 (predicted)	2	12,40%
SPAC6F12.14	**Cut23**	anaphase-promoting complex, TPR lobe subcomplex subunit Apc8	2	5,84%
SPAC6F6.10c	**Arc2**	ARP2/3 actin-organizing complex subunit Arc34	2	7,57%
SPAC6G10.08	**Idp1**	isocitrate dehydrogenase Idp1 (predicted)	2	6,15%

SPAC9.03c	**Brr2**	U5 snRNP complex subunit Brr2	2	1,29%
SPAPB1A11.04c	**Mca1**	transcription factor, zf-fungal binuclear cluster type Mca1 (predicted)	2	2,73%
SPBC106.09	**Cut4**	anaphase-promoting complex, platform subcomplex scaffold subunit Apc1	2	2,33%
SPBC115.01c	**Rrp46**	exosome subunit Rrp46	2	15,90%
SPBC119.09c	**Spbc119.09C**	ORMDL family protein (predicted)	2	18,30%
SPBC119.17	**Spbc119.17**	mitochondrial metalloendopeptidase (predicted)	2	3,23%
SPBC11G11.02c	**End3**	actin cortical patch component End3 (predicted)	2	12,00%
SPBC1215.02c	**Naa25**	NatB N-acetyltransferase complex regulatory subunit Naa25	2	3,95%
SPBC1271.07c	**Spbc1271.07C**	N-acetyltransferase (predicted)	2	16,00%
SPBC12C2.04	**Spbc12C2.04**	NAD binding dehydrogenase family protein	2	7,81%
SPBC12C2.08	**Dnm1**	mitochondrial dynamin family GTPase Dnm1	2	3,84%
SPBC13G1.13	**Tfb2**	transcription factor TFIIH complex subunit Tfb2	2	7,83%
SPBC146.13c	**Myo1**	myosin type I	2	2,63%
SPBC14C8.15	**Spbc14C8.15**	triglyceride lipase-cholesterol esterase (predicted)	2	6,96%
SPBC14F5.09c	**Ade8**	adenylosuccinate lyase Ade8	2	7,26%
SPBC15D4.14	**Taf73**	transcription factor TFIID complex subunit Taf5-like	2	4,21%
SPBC16A3.04	**Rsm25**	mitochondrial ribosomal protein subunit Rsm25 (predicted)	2	15,90%
SPBC16A3.05c	**Rae1**	RNA export factor, nucleoporin Rae1	2	9,09%
SPBC16C6.12c	**Las1**	Las1 pre-rRNA processing protein	2	8,30%
SPBC16D10.03	**Pgp2**	EKC/KEOPS complex ATPase subunit Pgp2	2	10,70%
SPBC1718.05	**Trs31**	TRAPP complex subunit Trs31 (predicted)	2	14,80%
SPBC1734.03	**Fol1**	trifunctional dihydropteroatesynthase/2-amino-4-hydroxy-6-hydro xymethyldihydropteridinediphosphokinase/dihydroneopterin aldolase Fol1 (predicted)	2	3,96%
SPBC1734.15	**Rsc4**	RSC complex subunit Rsc4	2	6,46%
SPBC17A3.02	**Spbc17A3.02**	conserved fungal protein	2	33,60%

SPBC17G9.08c	**Cnt5**	Centaurin Cnt5	2	3,33%
SPBC19C7.02	**Ubr1**	N-end-recognizing protein, UBR ubiquitin-protein ligase E3 Ubr1	2	1,33%
SPBC19C7.03	**Cyr1**	adenylate cyclase	2	2,66%
SPBC19F5.02c	**Utp4**	U3 snoRNP protein Utp4 (predicted)	2	4,37%
SPBC19F5.05c	**Ppp1**	pescadillo-family BRCT domain protein Ppp1 (predicted)	2	4,78%
SPBC1E8.03c	**Spbc1E8.03C**	conserved fungal protein	2	7,97%
SPBC211.01	**Rsm10**	mitochondrial ribosomal protein subunit S10 (predicted)	2	21,50%
SPBC211.03c	**Gea1**	guanyl-nucleotide exchange factor (predicted)	2	2,33%
SPBC23E6.07c	**Rfc1**	DNA replication factor C complex subunit Rfc1	2	2,57%
SPBC25H2.07	**Tif11**	translation initiation factor eIF1A	2	20,30%
SPBC29A3.01	**Ccc2**	copper transporting ATPase Ccc2 (predicted)	2	4,87%
SPBC29A3.07c	**Sap14**	U2 snRNP-associated protein SF3B14 Sap14	2	21,90%
SPBC29A3.09c	**Gcn20**	AAA family ATPase Gcn20 (predicted)	2	5,57%
SPBC31E1.02c	**Pmr1**	P-type ATPase, calcium transporting Pmr1	2	4,89%
SPBC31F10.07	**Lsb5**	cortical component Lsb5 (predicted)	2	11,20%
SPBC32F12.02	**Rec14**	Ski complex subunit Rec14	2	11,60%
SPBC336.02	**Spbc336.02**	18S rRNA dimethylase (predicted)	2	10,10%
SPBC3B9.03	**Srp101**	signal recognition particle receptor alpha subunit Srp101 (predicted)	2	6,22%
SPBC418.01c	**His4**	imidazoleglycerol-phosphate synthase (predicted)	2	6,65%
SPBC4C3.12	**43709**	forkhead transcription factor Sep1	2	5,13%
SPBC4F6.16c	**Ero11**	ER oxidoreductin Ero1a	2	8,99%
SPBC800.06	**Brx1**	ribosome biogenesis protein Brx1 (predicted)	2	8,14%
SPBC887.12	**Spbc887.12**	P-type ATPase (predicted)	2	3,26%
SPBC887.13c	**Cem1**	3-oxoacyl-[acyl-carrier-protein]-synthase condensing enzyme Cem1 (predicted)	2	8,22%

SPBC8D2.10c	**Rmt3**	type I ribosomal protein arginine N-methyltransferase Rmt3	2	5,89%
SPBC9B6.08	**Clc1**	clathrin light chain	2	10,00%
SPBP4H10.17c	**Spbp4H10.17C**	carboxyl methyl esterase (predicted)	2	7,33%
SPCC11E10.06c	**Elp4**	elongator complex subunit Elp4 (predicted)	2	8,31%
SPCC1450.04	**Tef5**	translation elongation factor EF-1 beta subunit, guanyl-nucleotide exchange factor (eEF1B)	2	14,00%
SPCC1672.07	**Spcc1672.07**	U3 snoRNP-associated protein Utp21 (predicted)	2	4,32%
SPCC1672.08c	**Tfa2**	transcription factor TFIIE beta subunit, TFIIEB, Tfa2	2	9,12%
SPCC24B10.17	**Emp24**	COPII-coated vesicle component Emp24 (predicted)	2	13,10%
SPCC306.03c	**Cnd2**	condensin complex non-SMC subunit Cnd2	2	4,31%
SPCC550.15c	**Spcc550.15C**	ribosome biogenesis protein (predicted)	2	6,70%
SPCC553.06	**Swp1**	oligosaccharyltransferase delta subunit Swp1 (predicted)	2	12,20%
SPCC576.01c	**Xan1**	alpha ketoglutarate dependent xanthine dioxygenase Xan1	2	7,51%
SPCC584.05	**Sec1**	SNARE binding protein Sec1 (predicted)	2	6,06%
SPCC594.02c	**Spcc594.02C**	conserved fungal protein	2	5,52%
SPCC5E4.06	**Smc6**	Smc5-6 complex SMC subunit Smc6	2	2,89%
SPCC622.10c	**Sec5**	exocyst complex subunit Sec5 (predicted)	2	4,54%
SPCC63.03	**Spcc63.03**	DNAJ domain protein, DNAJC11 family	2	4,41%
SPCC645.08c	**Snd1**	RNA-binding protein, involved in chromatin silencing by small RNA, Snd1	2	3,53%
SPCC895.07	**Alp14**	TOG/XMAP14 family protein Alp14	2	4,20%
SPCC965.06	**Osr2**	aldo-keto reductase (predicted)	2	10,50%
SPCP25A2.03	**Tho1**	THO complex subunit Tho1 (predicted)	2	3,59%